ABSTRACT

Title of Document:	HIV REVERSE TRANSCRIPTASE FIDELITY AND INHIBITION ARE MODULATED BY DIVALENT CATIONS IN A CONCENTRATION-DEPENDENT MANNER *IN VITRO*
	Vasudevan Achuthan, Doctor of Philosophy, 2016
Directed By:	Dr. Jeffrey J. DeStefano Professor Department of Cell Biology and Molecular Genetics

Human immunodeficiency virus (HIV) rapidly evolves through generation and selection of mutants that can escape drug therapy. This process is fueled, in part, by the presumably highly error prone polymerase reverse transcriptase (RT). Fidelity of polymerases can be influenced by cation co-factors. Physiologically, magnesium (Mg^{2+}) is used as a co-factor by RT to perform catalysis, however, alternative cations including manganese (Mn^{2+}), cobalt (Co^{2+}), and zinc (Zn^{2+}) can also be used. I demonstrate here that fidelity and inhibition of HIV RT can be influenced differently, *in vitro,* by divalent cations depending on their concentration. The reported mutation frequency for purified HIV RT *in vitro* is typically in the 10^{-4} range (per nucleotide addition), making the enzyme several-fold less accurate than most polymerases. Paradoxically, results examining HIV replication in cells indicate an error frequency that is ~10 times lower than the error rate obtained in the test tube. Here, I reconcile, at least in part, these discrepancies by showing that HIV RT fidelity *in vitro* is in the same range as cellular results, in physiological

concentrations of free Mg^{2+} (~0.25 mM). At low Mg^{2+}, mutation rates were 5-10 times lower compared to high Mg^{2+} conditions (5-10 mM). Alternative divalent cations also have a concentration-dependent effect on RT fidelity. Presumed promutagenic cations Mn^{2+} and Co^{2+} decreases the fidelity of RT only at elevated concentrations, and Zn^{2+}, when present in low concentration, increases the fidelity of HIV-1 RT by ~2.5 fold compared to Mg^{2+}.

HIV-1 and HIV-2 RT inhibition by nucleoside (NRTIs) and non-nucleoside RT inhibitors (NNRTIs) *in vitro* is also affected by the Mg^{2+} concentration. NRTIs lacking 3'-OH group inhibited both enzymes less efficiently in low Mg^{2+} than in high Mg^{2+}; whereas inhibition by the "translocation defective RT inhibitor", which retains the 3′-OH, was unaffected by Mg^{2+} concentration, suggesting that NRTIs with a 3′-OH group may be more potent than other NRTIs. In contrast, NNRTIs were more effective in low vs. high Mg^{2+} conditions. Overall, the studies presented reveal strategies for designing novel RT inhibitors and strongly emphasize the need for studying HIV RT and RT inhibitors in physiologically relevant low Mg^{2+} conditions.

HIV REVERSE TRANSCRIPTASE FIDELITY AND INHIBITION ARE MODULATED BY
DIVALENT CATIONS IN A CONCENTRATION-DEPENDENT MANNER *IN VITRO*

By

Vasudevan Achuthan

Dissertation submitted to the Faculty of the Graduate School of the

University of Maryland, College Park, in partial fulfillment
of the requirements for the degree of
Doctor of Philosophy
2016

Advisory Committee:

Professor Jeffrey J. DeStefano, Chair

Professor James N. Culver

Professor Richard C. Stewart

Professor Douglas K. Julin

Professor Siba K. Samal, Dean's Representative

Dedication

This dissertation is dedicated to my mother, father, brother, and sister whose unconditional love

made all of this possible; to friends who supported me through thick and thin.

Acknowledgements

I consider myself extremely fortunate to have one of the most rewarding and pleasant experiences anyone could hope to get in graduate school. It has been an incredible journey of learning to become not only a better scientist but a better person, and it is only fitting that I acknowledge some of the most wonderful people I have met in my life.

First and foremost, I would like to thank my advisor, Dr. Jeffrey DeStefano, for his encouragement, guidance, knowledge, and great support to help me grow as an independent researcher. I am truly inspired by his love for science and his incredible ability to keep going. I have been working in his lab through some of the more difficult financial times in his lab; and his strength, drive, belief, and composure to work through them and still continue to be himself are very important lessons for my life. Jeff is also an excellent scientist with an exceptional talent to focus on molecular details important for understanding significant biological problems. I am very thankful to him for teaching me how to do good science and enjoy myself in the process. I will miss working with him and discussing science, music, philosophy, and politics. Joining his lab is easily one of the best decisions I have made in my life.

I would like to thank my committee members, Drs. James Culver, Richard Stewart, Douglas Julin, and Siba Samal, for their time, feedback, encouragement, and guidance. I am very thankful to them for making time to meet me despite their busy schedules. Dr. Rick Stewart, especially, was very helpful with some critical experiments. I would also like to acknowledge Dr. Anne Simon for all the Virology group meetings, workshops, annual Virology retreat, and for the opportunity to do an internship at MedImmune, LLC. I would like to acknowledge Drs. Qing Zhu, Kelly Huang, Beth Kelly, and Jason Laliberte, for their valuable time, mentorship, and guidance during my internship at MedImmune. I would like to thank Dr. Qing Zhu for being very

patient in dealing with all the paperwork and making the internship happen; to Dr. Kelly Huang for making me part of her research group, spending her valuable time teaching me how science and administration works in a major biologics company, and for introducing me to lots of other scientists in the company. My career goal is to do pre-clinical research in a biologics company and the internship at MedImmune provided me a much-appreciated glimpse of working in a company and provided me valuable contacts for my future.

Next, I would like to thank each and every member of the DeStefano lab, starting with Megan Lai, who was very patient when training me during my rotation. Gauri Nair, for being a dear friend and a great mentor. My conversation with her when deciding on my PhD lab proved to be very useful when making my choice and she continues to be an excellent sounding board for my career aspirations with plenty of good suggestions. My lab sisters, Divya Gangaramani and Katherine Fenstermacher, for always looking out for me when I joined the lab and still always being available when I need them. Divya has been an excellent friend and has helped me get through some of the challenging phases of my life with her great suggestions and has always been a wonderful person to talk about life in general. Katherine has been extremely helpful with great tips to do science, images, presentations, and made the last few years in my lab extremely fun with her quirky jokes, pranks, and conversations about philosophy and politics. The ambience in the lab was one of the main reasons I chose to join the lab and am thankful for everything. Of course, I also have to thank my current lab mate Irani Ferreira, for her warmth, patience, eagerness to help me, for all the food, and for patiently listening to all my complaints about job hunting, thesis writing, and everything else in my final year of graduate school. Thank you for being an awesome friend and all your help. I am going to miss working with you a lot!

Table of contents

List of Tables

List of Figures

List of Abbreviations

-sssDNA   - Minus strand strong stop DNA

+sssDNA   - Plus strand strong stop DNA

AAV   -Adeno-associated virus

ADCC   -Antibody dependent cell-mediated cytotoxicity

AIDS   -Acquired Immune Deficiency Syndrome

AMV   -Avian myeloblastosis virus

APOBEC   -Apolipoprotein B mRNA editing enzyme, catalytic polypeptide-like

ARV   -Anti-retroviral

ART   -Highly active Anti-Retroviral Therapy

bNAb   -Broadly neutralizing antibody

BSA   -Bovine serum albumin

Co^{2+} -Cobalt

dNTPs   -Deoxyribonucleotide triphophates

ds   -Double-stranded

DTT   -Dithiothreitol

EDTA   -Ethylenediaminetetraacetic acid

ELISA   - Enzyme-linked immunosorbent assay

HIV   -Human Immunodeficiency Virus

HDAC   -Histone deacetylase

Kb   -Kilobase(s)

k_{cat} -Rate constant for enzyme kinetics

K_d -Dissociation constant

K_m -Michaelis-Menten constant, concentration of substrates when the reaction rate reaches half of V_{max}

kDa   -Kilo Daltons

LTR   -Long terminal repeat

Mg^{2+} -Magnesium

Mn^{2+}	-Manganese
MuLV	-Moloney murine leukemia virus
NC	-Nucleocapsid
Ni^{2+}	-Nickel
NNRTI	-Non-Nucleoside Reverse Transcriptase Inhibitors
NRTI	-Nucleoside Reverse Transcriptase Inhibitors
nt	-Nucleotide(s)
PCR	-Polymerase chain reaction
Pfu	-*Pyrococcus furiosus*
PNK	-Polynucleotide kinase
Pol	-Polymerase
PPT	-Polypurine tract
PR	-Protease
PT	-Primer-template
RNase H	-Ribonuclease H
RT	-Reverse Transcriptase
SIV	-Simian Immunodeficiency Virus
ss	-Single-stranded
Taq	-*Thermus aquaticus*
TALEN	- Transcription activator-like effector nucleases
V_{max}	-Michaelis-Menten constant, maximum rate obtained when all enzyme is bound to the substrate
ZFN	-Zinc-finger nucleases
Zn^{2+}	-Zinc

Chapter 1 : Human Immunodeficiency virus lifecycle and treatment options against AIDS

1.1 HIV & AIDS

1.1.1 General history and epidemiology

Human immunodeficiency virus (HIV), the causative agent of Acquired Immunodeficiency Syndrome (AIDS), is a lentivirus (*lenti*, "slow (growth)" in Latin) in the *Retroviridae* family. *Retroviridae* (retrovirus) family viruses, utilizing the polymerase activity of reverse transcriptase, converts viral RNA into DNA in a reverse flow of genetic information opposite to the central dogma of life. AIDS is caused by decimation of CD4^{+} T helper cells and macrophages in infected individuals. AIDS is currently defined by CD4^{+} T cell count dropping below 200 cells/μl along with positive indications for the presence of the virus such as a positive test for HIV antibodies or HIV RNA in the patient.

AIDS syndrome was first observed in the late 1970s [11-13] and was initially called as Gay Related Immune Deficiency (GRID) as it was seen only in the gay community. The condition was soon discovered in other patient populations such as blood transfusion recipients [14] and IV drug users [15], and was renamed as Acquired Immune Deficiency Syndrome (AIDS). HIV was first co-discovered by Françoise Barré-Sinoussi and Luc Montagnier lab groups in 1983. They named it human T cell lymphotropic virus III [16], and the virus was later renamed as the Human Immunodeficiency Virus.

AIDS is currently one of the leading causes of deaths among infectious diseases. By the end of 2014, approximately 36.9 million people globally were living with HIV. The total number of AIDS related deaths since HIV discovery is estimated to be ~33.5 million [17], with HIV

infections leading to ~ 1.2 million AIDS related deaths in the year of 2014 alone. As HIV is a sexually transmitted pathogen, high risk populations for HIV transmission include workers in the sex industry. Intravenous drug users who practice needle sharing and homosexual men in the USA remain a high risk group. HIV can also be transmitted through vertical transmission: HIV positive mothers can pass the disease to their newborn infants during childbirth or through breastfeeding.

1.1.2 HIV classification

HIV was derived from simian immunodeficiency virus (SIV), which is found naturally in more than 40 species of nonhuman primates in sub-Saharan Africa and infects many Old World primate species [18, 19]. HIV consists of two discrete viruses HIV-1 and HIV-2, sharing 50 - 60% nucleotide sequence identity between their genomes [20, 21]. HIV-1 is responsible for the majority of HIV infections worldwide and is divided into four groups based on four independent transmission events of SIV into humans: M (major), O (outlier), N (non-M, non-O), and P (Pending) [22]. Group O is thought to have originated by cross-species transmission of SIV from western lowland gorillas [23]. Group P viruses are more closely related to strains of SIVgor [22, 24], whereas groups M and N are closely related to strains of SIV from chimpanzees [22]. Group M is the major cause of the AIDS pandemic and has infected more than 40 million people [23]. Group M is further divided into ten subtypes (Fig. 1-1) [2]. Subtype C is the most prevalent subtype globally but the dominant subtype varies by country. Subtype B is predominant in Americas, Western Europe, and Australasia; whereas subtype C is the most dominant subtype in the high prevalence countries of Southern Africa and India. Although not as prevalent as group M, group O is estimated to have infected around 100,000 people and spreads epidemically in west central Africa [23]. Group N has been found in fewer than 20 individuals [25] and P viruses have

2

been found in only two individuals [22, 24]. HIV-2, which is far less pathogenic and less infectious than HIV-1, is likely derived from a zoonotic transmission of SIV from sooty mangabeys [26].
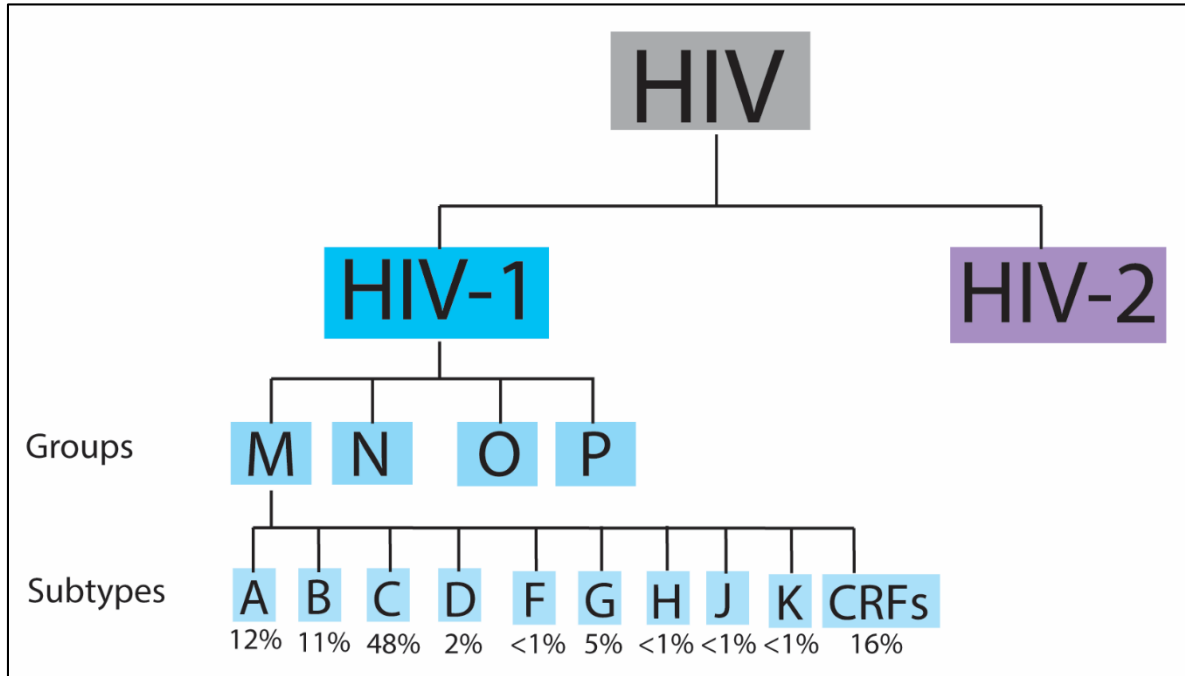
Figure 1-1. Classification of HIV. Group M, which is responsible for the majority of the AIDS epidemic, is divided into different subtypes. Circulating recombinant forms (CRFs) originate from recombination of two or more subtypes. Percentage of infections by each subtype is included. Figure modified from [2].

1.1.3 HIV clinical progression

HIV infection is characterized by gradual decrease in CD4$^+$ T cell levels, rising viral titers, immune dysregulation, and development of AIDS. Development of AIDS can occur about 8 to 12 years after initial infection with HIV and the process can be divided into four stages:

i. **Incubation period**: Although typical tests performed in healthcare industry to detect HIV cannot detect HIV infection during this stage, viral RNA and DNA might be identified by qPCR during this stage. This period lasts for two to four weeks.

ii. **Acute infection**: Acute infection lasts for a period of one to four weeks [27]. The virus begins to proliferate rapidly, which is accompanied by a concurrent drop in the level of circulating $CD4^+$ T cells in the blood: $CD4^+$ cells decrease from normal levels of ~ 1200 cells/µL to ~ 600 cells/µL [28]. Viral titers then begin to decrease due to the adaptive immune response mounted against the virus. $CD4^+$ T cell counts briefly recover during this stage to ~800 cells/µl. Infection can be detected from this point using the most common test for HIV detection (anti-capsid/p24 antibody ELISA). Flu-like symptoms and other symptoms including fever, malaise, swollen lymph nodes, pharyngitis, and oral sores may be observed during this stage. The patient is more infectious during this stage and capable of transmitting virus.

iii. **Latency stage**: Immune response in infected patients continues to suppress HIV titers in the blood during the latency period. This stage can last for a period of months to years, and long-term non-progressors (rare patients with a resistant genetic profile) as well as patients receiving antiretroviral treatment can maintain this stage indefinitely. The viral load remains low, despite ~10 billion virions being produced each day [29]. $CD4^+$ cell balance is maintained by an accelerated replenishment rate countering the virus-induced death. However, in normal patients without treatment, $CD4^+$ cells gradually decreases and the viral titers steadily increase.

iv. **AIDS:** Eventually the immune system collapses due to the exhaustion of the $CD4^+$ T cells. Appearance of various opportunistic infections, such as Kaposi's sarcoma, *Pneumocystic carinii* pneumonia, candidiasis, toxoplasma encephalitis, cytomegalovirus infections, Burkitt's lymphoma, B cell lymphomas and cervical cancer along with a highly decimated $CD4^+$ T cell count marks this stage. WHO

defines a patient with a CD4+ T cell count of less than 200/µL and the presence of indicator infections as having progressed to AIDS. Opportunistic infections are the most common cause of death for AIDS patients.

1.2 HIV lifecycle

1.2.1 Structure of HIV

HIV has a spherical structure with a diameter of about 80-100 nM (Fig. 1-2). HIV, like other retroviruses, contain a lipid based envelope derived from the host cell. The envelope of a mature virion contains the outer surface glycoproteins gp120 and transmembrane gp41 proteins [30]. Matrix proteins (MA, p17) form a layer immediately below the envelope (Fig. 1-2), below which a bullet-shaped core [31] made of the capsid protein (CA, p24) is present. Capsid contains two copies of the single-stranded RNA genome and important viral enzymes, accessory viral regulatory proteins (see Table 1-1 for more details), host-derived tRNALys3 primer, and other host derived proteins. Viral genomes are coated with the nucleocapsid protein (NC, p7), which also acts as a nucleic-acid chaperone aiding in destabilization of secondary structures of the genome, reverse transcription, recombination, and template annealing [32].
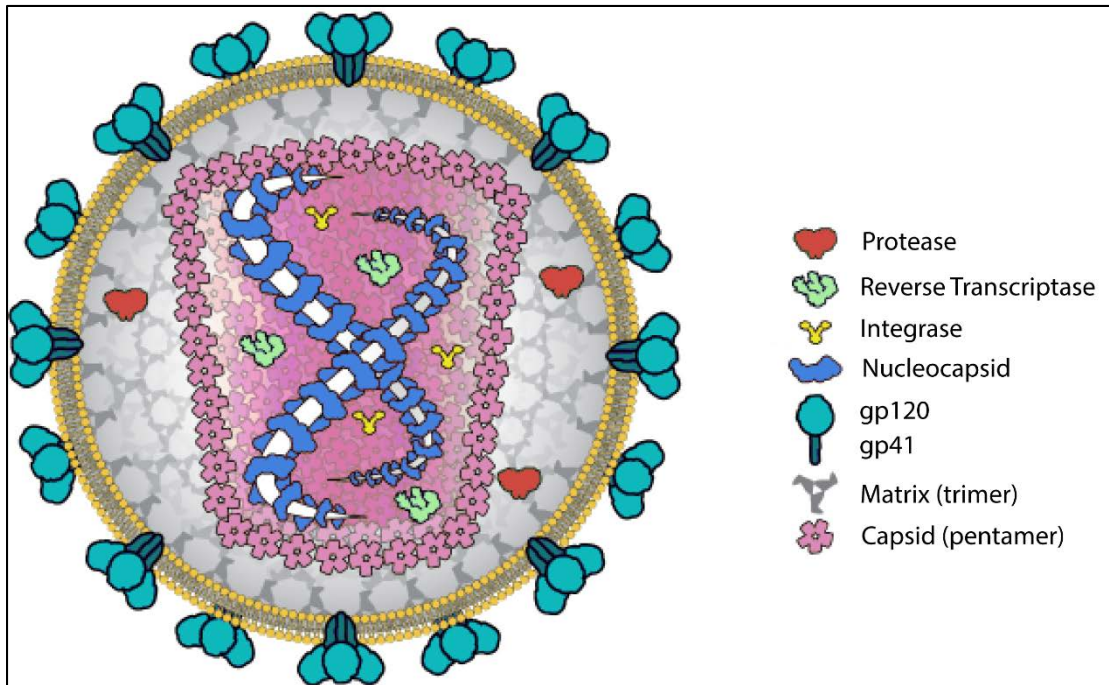
Figure 1-2: Structure of a mature HIV virion. Genomic RNA (white) is coated by nucleo-capsid protein, which is enclosed by a shell made by capsid protein. Other viral proteins are packaged within the virion. The virion is enclosed by a lipid membrane containing gp41 and gp120 trimers for attachment and entry into permissive cells. Adapted from [3].

1.2.2 HIV genome

Two synonymous copies of ~9.3 kb single stranded positive sense RNA, which form a diploid genome via non-covalent interactions at the 5′ end to form a dimer, gets packaged into the virion. As only one proviral double-stranded DNA is produced by the virus, HIV is considered to be a pseudo-diploid virus [33]. HIV-1 genome encodes for the canonical retroviral genes (*gag, pol,* and *env*), and other accessory proteins (Table 1-1) [7]. Env, which is produced from its own mRNA, is further processed into surface and transmembrane glycoproteins (gp120 and gp41,

respectively). Gag is further processed into other structural proteins (matrix, capsid, and nucleocapsid), while Pol is proteolytically cleaved into the three key enzymes: reverse transcriptase (RT), integrase (IN), and protease (PR). Individually spliced mRNAs code for other regulatory and accessory proteins (Fig. 1-3).

The genomic RNA also contain other features essential for viral replication. The genome is flanked at each end by a unique region (termed U5 or U3 based on the position at either the 5′ or 3′ ends of the genome, respectively) and a repeated region (R). U5 and U3 regions are duplicated to the opposite side of the genome during reverse transcription, creating a U3-R-U5 sequence called the Long Terminal Repeat (LTR) at each end of the proviral DNA (Fig. 1-5). LTRs are important for reverse transcription of the genome (section 1.3.1). The 5′-LTR contains the following important structural elements: a) the target sequence for viral transactivation (TAR), which binds Tat [34]; b) the primer-binding site (pbs), which binds the packaged host tRNA$_{lys}$ during the minus-strand synthesis [35]; c) the psi-packaging element involved in packaging the genome; and d) the dimer-initializing signal, necessary for dimerization and packaging of the two copies of the RNA genome [36]. Besides the LTR, the genome also contains other important structural elements:

- The Rev response element (RRE) capable of binding Rev [37].
- Two polypurine tracts (3′-PPT and central PPT), which act as primers for plus-strand DNA synthesis.
- A 3′ polyadenylation signal.
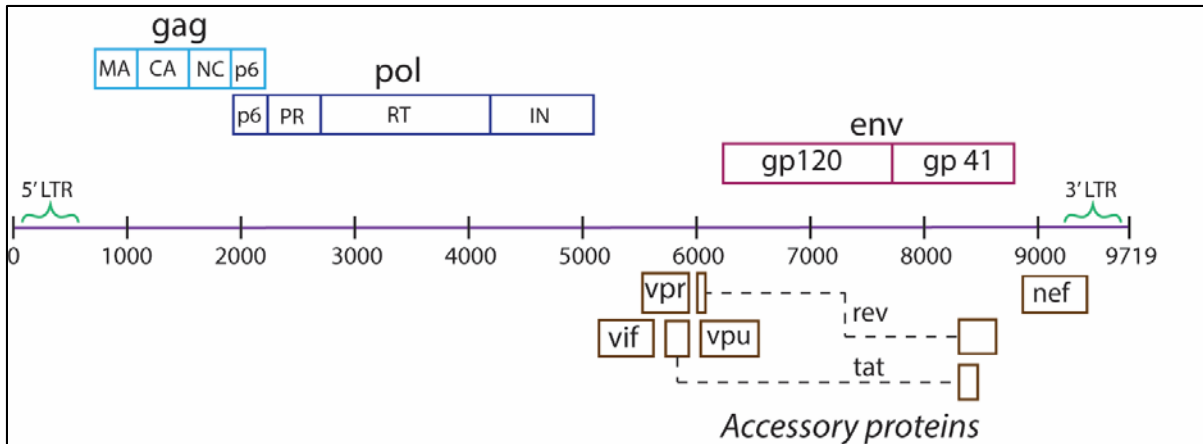
Figure 1-3: HIV-1 proviral DNA. The provirus DNA is shown as a single numbered line with a numbering scheme to facilitate identification of the location of proteins in HIV proviral DNA. This image represents a numbered set of proteins for HIV HXB2. Products derived from the polyproteins gag, pol, and env are described above the viral genome. Accessory proteins, some of which are multiply spliced variants, are described below the genome. Open reading frames of the proteins are described in rectangular boxes. The dotted lines represent different exons which are spliced together to make the mRNA of some proteins. For example, an exon starting at position 6045 and another exon beginning at position 8379 are spliced together to code for Rev. Adapted from [7] and [9].

Table 1-1: Functions of HIV proteins in HIV lifecycle. Adapted from [7]

Protein	Function in HIV replication
<u>Gag</u>	
Group-specific antigen	- precursor to matrix. capsid, nucleocapsid, & p6
Matrix, MA (p17^{Gag})	- involved in viral post-entry events - also targets Gag to the plasma membrane for viral assembly promoting Gag incorporation, while part of the Gag polyprotein
Capsid, CA (p24^{Gag})	- encapsulates genomic RNA - involved in assembly of the virion particles and hypothesized to play a role in integration of the proviral genome
Nucleocapsid, NC (p7^{Gag})	- performs nucleic acid chaperone activity - facilitates packaging of genomic RNA, reverse transcription, and recombination
p6^{Gag}	- incorporates Vpr into the virion and promotes virion budding. - a transframe version of p6 is also a part of Pol
<u>Pol</u>	
Polymerase	- polyprotein precursor to PR, RT, and IN
Protease, PR	- cleaves Gag and Gag-Pol polyproteins proteolytically into functional proteins completing the maturation of the virus
Reverse Transcriptase, RT	- performs RNA-dependent and DNA-dependent synthesis to convert the single stranded RNA to double stranded DNA.
Integrase, IN	- inserts proviral DNA covalently into the host genome
<u>Env</u>	
Envelope	- polyprotein precursor to gp120 and gp41
gp120	- host cell surface receptor binding CD4 and the chemokine receptor - facilitates attachment and entry
gp41	- fusion peptide induces fusion with the host membrane during entry
<u>Accessory proteins</u>	
Virion Infectivity Factor, Vif	- prevents incorporation of APOBEC3G/F into virion and mediates suppression of APOBEC3G/F
Viral Protein R, Vpr	- promotes proteosomal degradation of host restriction factors and induces G2/M cell-cycle arrest
trans-Activator of Transcription, Tat	- enhances transcription of viral RNA
Regulator of Expression of Virion Proteins, Rev	- increases nuclear export of unspliced genomic RNAs by preventing splicing
Viral Protein U, Vpu	- degrades newly synthesized CD4 - promotes viral release by blocking Tetherin.
Negative Factor, Nef	- downregulates CD4 from the cell by stripping CD4 from the surface

1.2.3 HIV infection cycle

The first step in the HIV lifecycle is entry of virus into the host cell (Fig. 1-4). HIV requires CD4 as a receptor, and can infect only CD4$^+$ cells such as T-cell lymphocytes and macrophages. HIV also requires a co-receptor in addition to the CD4 receptor for entry. Chemokine receptors CXCR4 and CCR5 are the most commonly used co-receptors. HIV-1 viruses which use CCR5 are considered R5-tropic, whereas viruses using CXCR4 are considered X4-tropic [38]. Dual-tropic X4R5 viruses capable of using both CCR5 and CXCR4 also exist. R5 and R5X4 HIV-1 viruses are usually transmitted better than X4 viruses [39], which do not predominate until late in infection [40-42]. Other minor co-receptors such as CCR3 and CCR2b can be used by some strains of HIV-1 for entry [43-46]. HIV-2, in addition to mainly using CCR5 and CXCR4 as co-receptors, can use many other minor co-receptors such as CCR4, CCR3, CCR2b, CCR1, BONZO and BOB [43]

Virions first bind to the target cell mediated through the viral envelope (Env) or host cell membrane proteins incorporated in the virion interacting with various cell attachment factors [47]. Env– mediated initial attachment can happen through non-specific interactions of Env with heparin sulfate proteoglycans [48] or specific interactions between Env and α4β7 integrin [48, 49] / dendritic cell-specific intercellular adhesion molecular 3-grabbing non-integrin (DC-SIGN) [50]. HIV attachment to the cell brings Env to close proximity of the CD4 receptor and binding of the viral envelope protein gp120 to the CD4 receptor is the next step. Engagement of CD4 results in conformational changes in gp120 leading to formation of a four-stranded β sheet [51, 52], enabling gp120 to bind to the co-receptor, which acts as the trigger activating the membrane fusion potential of Env. Co-receptor binding induces a series of conformational changes in gp41 [53], allowing the fusion peptides of each gp41 in the trimer to fold at a hinge region to form a six-helix bundle

[54, 55]. Formation of the six-helix bundle drives the fusion of viral and cellular membranes, as this step brings both membranes into close apposition (reviewed in [56]).

After fusion, capsid containing the RNA genome and viral proteins enters the cytoplasm. Coupling of uncoating and reverse transcription ensures gradual uncoating of the capsid as more of the single-stranded RNA genome gets converted into double stranded DNA [57]. Pre-integration complex containing the pro-viral DNA, RT, IN, and other accessory viral proteins is transported to the nuclear membrane, where it enters the nucleus through the nuclear pore complex [58]. The ability of lentiviruses to enter the nucleus through the nuclear pore complex enables lentiviruses to infect both dividing and non-dividing cells, unlike other retroviruses.

Once inside the nucleus, integrase (IN) facilitates integration of the provirus DNA into the host nucleus [59]. IN processes the viral DNA by removing the 5′- terminal two nucleotides and exposes the hydroxyl group on the terminal CA dinucleotide at 3′-end of each strand. The processed viral DNA gets inserted into host target DNA sequence and the gaps are then repaired by host cellular machinery [31]. Integration can occur at any location on the host genome but HIV-1 shows a preference for active transcription sites [60, 61]. More recently, it has been shown that specific integration sites play a critical role in clonal expansion and persistence of HIV-infected cells [62]. The inserted viral DNA remains stable as a provirus within the host cell.

After integration, HIV relies on host machinery to produce viral mRNA and genomic RNA for nascent viral particles. Initially, the 5′- LTR acts as weak promoter for RNA pol II [63] and export of multiply spliced viral mRNA is favored. Viral mRNAs gets processed in the same way as cellular mRNAs including 5′ capping, 3′ polyadenylation, and splicing [31], and viral protein synthesis occurs in the cytoplasm as the multiply spliced viral mRNAs are exported out of nucleus. These RNAs code for the Tat, Rev, and Nef proteins. As concentration of Rev increases in the

11

cytoplasm, more Rev is imported back into the nucleus and Rev favors export of unspliced full-length genomic RNA and singly spliced RNAs [64]. Rev binding to the RRE represses splicing, thereby facilitating export of the longer viral mRNAs. Tat is also imported into the nucleus and Tat increases the viral mRNA output by up-regulating transcription after binding to TAR [31]. Proteins expressed by *gag, pol, and env* are synthesized as polyproteins which are then processed by proteases (Fig. 1-3). Gag and Pol are processed by the virally encoded protease (PR), whereas Env is processed by cellular proteases such as furin to produce gp120 and gp41 [65]. The *gag-pol* region of the genome is transcribed as a single gene from unspliced RNA. 95% of translation of *gag-pol* leads to translation of the Gag protein product, however ~5-10% leads to production of Gag-Pol polyprotein due to ribosomes reading through the *gag* stop codon facilitated by a frameshift signal present in this region [64, 66]. The ratio of Gag: Gag-Pol proteins is carefully controlled by the frequency of programmed -1 frameshifting. Overexpression of Gag leads to non-infectious particles due to particles lacking viral enzymes [67, 68], whereas overexpression of Gag-pol inhibits assembly of structural proteins due to excess protease activity [69-71].

Two copies of viral genomic RNA dimerize using the dimer initiation signal (DIS) and gets packed into the viral particles via the NC portion of Gag biding at the Psi element of the genome. Viral genome along with other viral polyproteins are directed towards the lipid rafts in the host cell membrane [72]. Gag proteins multimerize at the cell surface through Gag-Gag interactions, and multimerization causes a curvature at the location. An increase in the curvature eventually leads to budding and release of the immature virion with the help of cellular endosomal sorting complexes required for transport (ESCRT) [73]. Overexpression of Gag alone, in the absence of genome and other viral proteins, can yield virus-like particles [74-76]. Maturation of

the immature virion occurs when the Gag and Gag-Pol polyproteins are processed by protease into capsid, matrix, nucleocapsid, and p6 proteins (from Gag) and RT, integrase, and protease enzymes (from Pol).
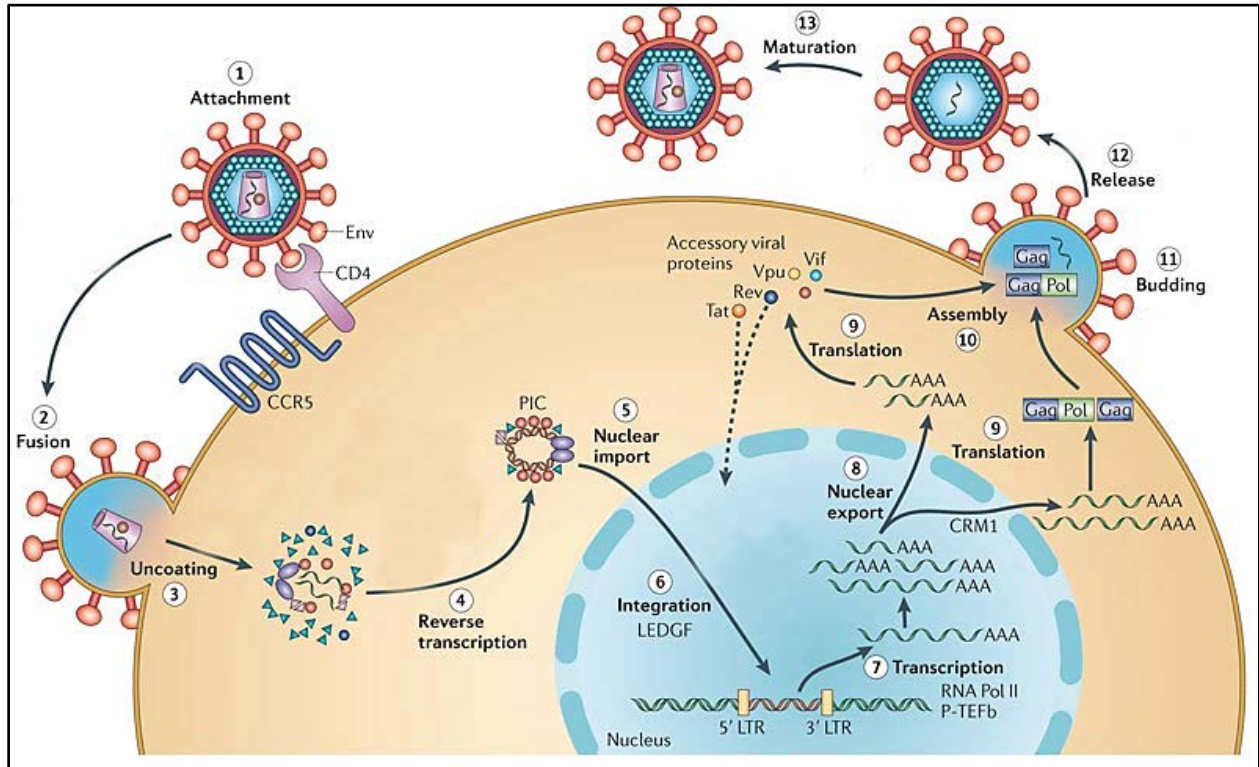
Figure 1-4: HIV-1 life cycle. HIV infects CD4+ cells such as T cells and macrophages. After attachment and entry, the single stranded RNA genome is reverse transcribed to double strand proviral DNA. Viral proteins and viral genomes are then synthesized by the host machinery for assembly into new virion particles. Figure adapted from [8].

1.3 Reverse Transcription

1.3.1 Process of reverse transcription

Reverse transcription of the single stranded RNA to the double stranded proviral DNA is carried out by the enzyme reverse transcriptase (RT), and it is a process heavily targeted in

antiretroviral therapy (Section 1.4.1). The complex process of reverse transcription occurs in the following steps [77].

1. RNA to DNA conversion begins with synthesis of the minus sense DNA strand. The packaged tRNA$_{Lys}$ binds at the primer binding site (PBS) located at the 5′ end of the genome, approximately 182 nucleotides downstream of the 5′ end (Fig. 1-5).

2. RT copies up to the 5′ R region of the genome, creating a minus sense strong-stop DNA (–sssDNA). During the synthesis of the –sssDNA, RT degrades the region of the RNA used as a template due to the RNase H activity of RT. The –sssDNA translocates to the 3′ R, making the first jump. –sssDNA synthesis proceeds upto the PBS site and the RNA strand is almost completely degraded during the process.

3. Two small portions of the RNA genome called the polypurine tract (PPT) are not degraded by RNase H activity during minus strand synthesis. HIV genome has two PPTs, one at the 3′ end (3′ PPT) and one near the center of the genome (cPPT). The "central DNA flap", formed because of the cPPT and central termination sequence (CTS), has been thought to aid nuclear import of the viral double-stranded DNA into the nucleus [78, 79]. However, it was recently shown that central DNA flap is not required for transport into nucleus, but the absence of the central flap reduces the efficiency of 2-LTR circle formation [80]. Plus sense DNA synthesis is initiated by RT using the 3′ PPT as a primer, and the +sssDNA is produced when RT terminates at the 19th nucleotide from the 3′ end of the tRNA primer, which is a modified base that cannot be copied by RT. When completing the synthesis of +sssDNA, the tRNA primer is removed from the 5′ end of the minus strand DNA by RNase H activity of RT.

4. The synthesized plus sense strong stop DNA then makes another strand jump, when the PBS of the minus strand DNA base pairs with the PBS of the +sssDNA and DNA synthesis proceeds using both minus and plus strands as templates (Fig. 1-5).

5. Long terminal repeats (LTR) are formed at the last stage, completing the double stranded proviral DNA. (Fig. 1-5).
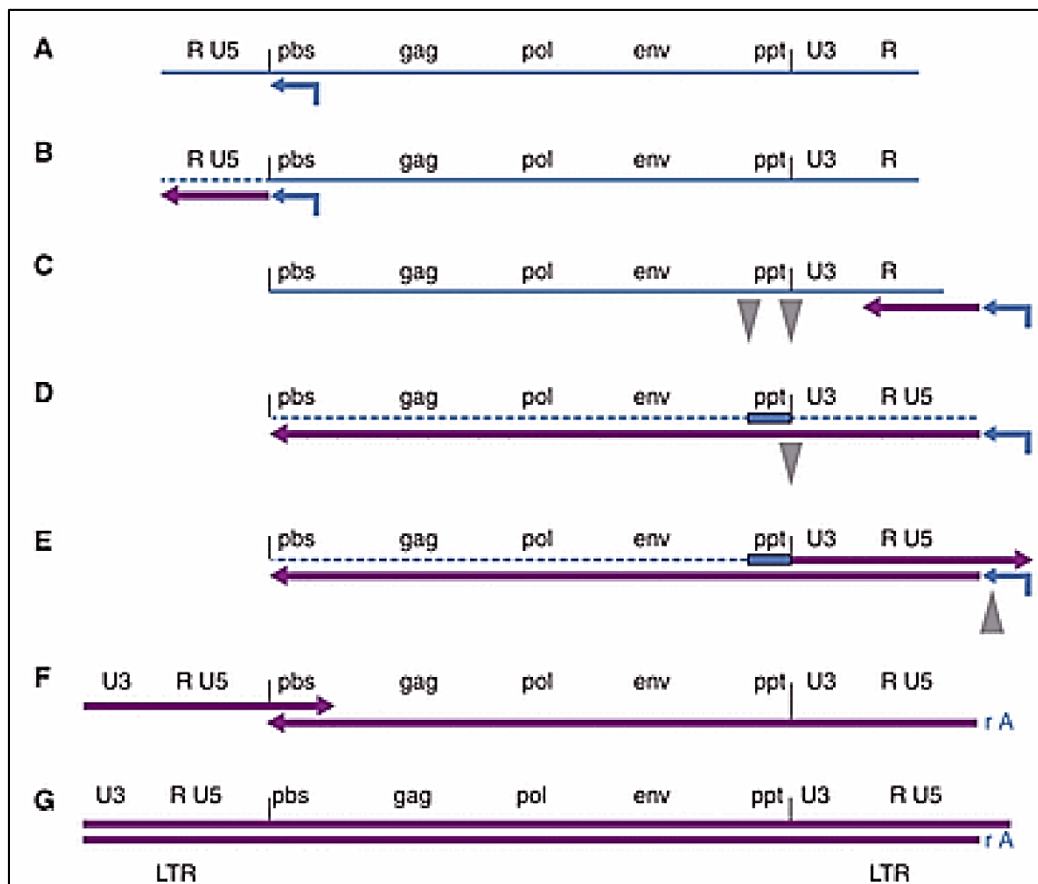
Figure 1-5: Reverse transcription process. Different steps of the reverse transcription process which converts the RNA genome into a double stranded DNA. The host cell tRNALys3 hybridizing to the PBS near the 5'end of the genome begins the process. Other steps are described in more detail in the text. HIV genomic RNA is shown as a blue line and the dotted blue lines represent the RNA strand degraded by RNase H domain of RT. The synthesized DNA strands are shown as violet lines. Figure adapted from [4].

1.3.2 Reverse Transcriptase

HIV reverse transcriptase can perform DNA- and RNA-dependent DNA polymerase activity as well as ribonuclease H (RNase H) activities [81]. HIV-1 RT, encoded by the *pol* gene, is a heterodimer consisting of a 66 kDa subunit (p66) and a catalytically inactive 51 kDa subunit (p51) [82] (Fig. 1-6). HIV-2 RT is a more stable heterodimer consisting of p68 and p55 subunits [83]. HIV protease converts a subset of the p66 and p68 subunits to the smaller p51 and p55 subunits, respectively. p66 and p68 contain the enzymatic domains whereas the catalytically inactive p51 and p55 subunits supports catalysis by facilitating interaction of the tRNA primer and the primer-template hybrid during reverse transcription and also by protecting and stabilizing the larger subunit [84, 85]. The polymerase domain, contained in the N terminus of p66 (HIV-1) and p68 (HIV-2) subunits, has a right-handed structure characteristic of other polymerases, and consists of three sub-domains: "fingers", "thumb", and "palm" subdomains encircling the catalytic active site [86]. The 'thumb' subdomain, along with 'fingers' and 'palm' subdomains, form a nucleic acid binding cleft which binds the template-primer hybrid [87]. The 'fingers' subdomain interacting with the incoming nucleotide is called the specificity domain due to its importance in the polymerase fidelity [88]. The single stranded 5′ extension of the template makes modest interactions with RT helping to position the end of the primer at the polymerase active site [77]. The RNase H domain is located at the C terminus of the larger subunit, and performs ribonuclease activity. The two active sites are separated by ~18 nucleotides of duplex nucleic acid [89, 90].

Divalent cations are essential co-factors for both polymerase and RNase H activities of RT [91, 92]. Under physiological conditions, Mg^{2+} presumably functions as the co-factor for both activities. The catalytic active site of HIV RT, similar to other DNA polymerases, contains three conserved aspartate residues (Asp-110, Asp-185, and Asp-186) which coordinate the binding of

two divalent cations (Fig. 1-6) (reviewed in [5]). Two Mg^{2+} ions participate in polymerization via

a universal "two metal ion" mechanism. One of the Mg^{2+} ions binds the incoming dNTP as a

divalent cation-dNTP complex, while the other metal ion activates the 3'OH on the primer as a

metal hydroxide (reviewed in [5]). Additionally, these cations are required to play other roles such

as stabilizing the structure and charge of the pentavalent transition state during catalysis and

assisting the leaving of the pyrophosphate after catalysis [93]. The number of Mg^{2+} ions bound at

the RNase H active site is unclear, as both one and two metal mechanisms have been proposed

(reviewed in [94]), although it is generally thought that the RNase H domain also binds two

divalent cations. Divalent cations are coordinated by the catalytic triad (Asp-443, Asp-498, and

Glu-478) at the RNase H active site of the enzyme [86].
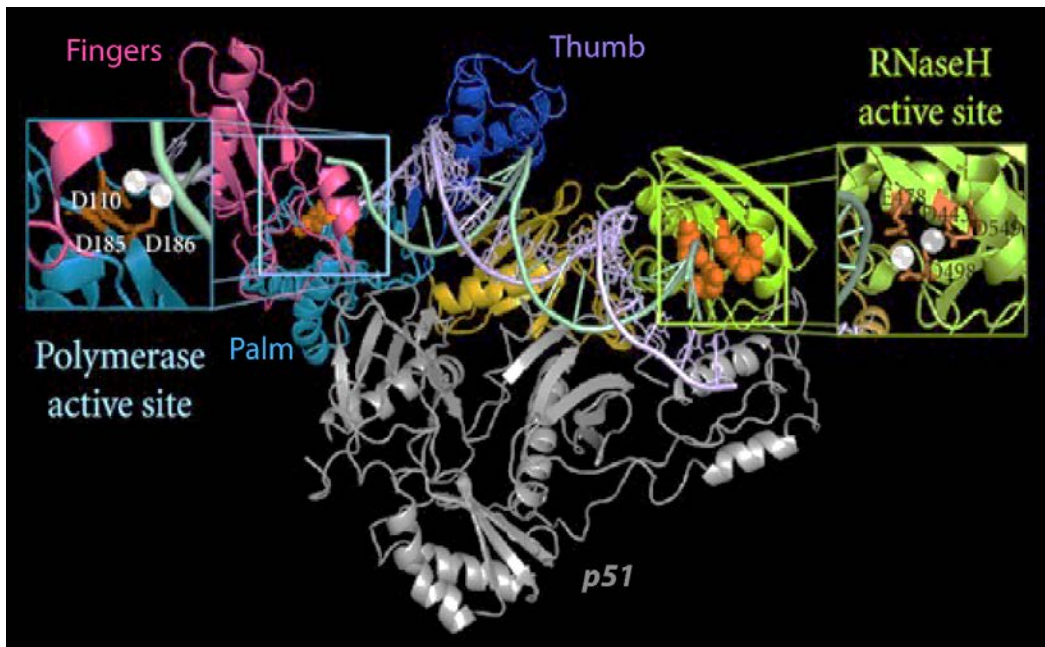
Figure 1-6: Structure of HIV-1 RT. Polymerase domain, resembling a right hand,
consists of fingers (magenta), palm (cyan), and thumb (blue) sub-domains. Palm
subdomain of p66 binds two divalent cations. The RNase H domain is located at
C-terminus of the p66 subunit, with the RNase H active site also binding divalent
cations. Adapted from [4].

1.3.3 Fidelity of reverse transcription

HIV-RT lacks the 3′-5′ exonuclease activity to excise the misincorporated nucleotides and lack of proofreading activity in RT makes it an error-prone polymerase compared to the cellular DNA polymerases [95]. The error rate of HIV-1 RT calculated from *in vitro* assays optimized for enzyme activity using the purified enzyme is ~1.6 x 10^{-4}, which is roughly 1 error per 6,000 incorporations [96, 97]. This error rate is greater than that of closely related avian myeloblastosis virus and Moloney murine leukemia virus reverse transcriptases – both RTs make ~1 error per 30,000 nucleotide incorporations *in vitro* [98, 99]. However, at physiologically relevant Mg^{2+} conditions (~0.25-0.5 mM free Mg^{2+}), which are much lower than concentrations used in optimized reactions (~5-10 mM), the error rate of HIV-1 RT is 1.3 x 10^{-5} or ~1 error per 77,000 incorporations (see Chapter 3 for details). Although this mutation frequency contributes to the genetic diversity of the virus, errors made by RT are not the only source of HIV diversity. The comparatively large number of infected cells and the rapid turnover of infected cells are the major reasons why the virus generates diversity so rapidly [100]. The capacity of HIV to diversify rapidly plays an important role in the ability of the virus to become resistant to antiretroviral drugs. The mutation rate for HIV-1 cellular replication is ~2 x 10^{-5} per nucleotide per replication cycle (about 1 error per 50,000 incorporations) [101-103]. This rate includes the errors made by RT and the cellular RNA polymerase RNA Pol II. Although the error rate of RNA Pol II and its contribution to the fidelity of HIV replication is not known, the errors made by RNA Pol II is unlikely to be higher than RT [104, 105].

In addition to the errors made by RT and RNA Pol II, additional cellular factors can affect the fidelity of reverse transcription process. Apoliporotein B editing complex-3 (APOBEC-3) proteins amplify the errors made by RT during reverse transcription process.

APOBEC-3s are cytidine deaminases packaged into the virions and modify the minus-strand DNA before the plus strand has been synthesized. APOBECs convert some of the Cs in the minus strand to Us and when the virus synthesizes the plus strand, it copies As over the converted Us. This leads to conversion of Gs to As (G to A hypermutation). HIV counteracts this protein using Vif, which interacts with the host machinery to degrade the APOBECs [106, 107]. RNA editing enzymes such as adenine deaminases that act on dsRNAs (ADARs) can also cause mutations in HIV-1 [103]. ADARs act by converting adenosines to inosines in double stranded RNAs and the HIV genome consists of several double-stranded regions such as RRE, TAR, and DIS which could act as potential ADARs substrates. ADAR-1 edits adenosines in the 5′ untranslated region (UTR) of HIV-1 genome [108]. Interestingly, ADAR-1 have also been reported to stimulate HIV-1 infection by enhancing the expression of HIV proteins through editing-independent mechanisms [108]. Uracil incorporation into the replicating DNA is another source of mutations in the HIV genome. Uracil can occur in DNA either by misincorporation of dUTP by RT or by spontaneous deamination of dCTP [109]. Uracil in DNA can be repaired by the enzyme uracil–DNA glycosylase (UNG). HIV-1 Vpr interacts with UNG and mediates packaging of UNG in the budding virion, which also facilitates HIV-1 replication in non-dividing cells by removing uracil bases during HIV-1 DNA synthesis [110]. A 4-fold increase in the rate of G-A transitions was observed in a single round of HIV replication in the absence of Vpr or with Vpr mutants not capable of interacting with UNG [111]. In addition, mistakes made during second strand synthesis could be subjected to the cellular proof-reading machinery [112]. This would be expected to result in up to 50% reduction in errors made on the plus-sense strand and if the mutation rate during the synthesis of both strands is assumed to be nearly equal, ~25% reduction in the overall mutation rate of reverse transcription. Tumor suppressor protein p53 has also been shown to improve the

accuracy of HIV reverse transcriptase *in vitro*. The misincorporation of non-complementary nucleotides as well as mispair extension by HIV-1 RT was decreased with both RNA/DNA and DNA/DNA template-primers in the presence of p53. There is also some conflicting evidence that HIV NC can affect fidelity by promoting extension of mismatches or correction of mismatches [113, 114]. However, previous studies using α-complementation assay showed no difference in fidelity in the presence or absence of NC [115]. In addition, other small cellular components may also influence the fidelity of RT. For example, polyamines, which are present at near millimolar levels in cells, have been reported to increase HIV RT fidelity [116]. Spermine, in particular, decreased the efficiency of mispair extension of RT by ~4-fold to ~18-fold, depending on the sequence.

1.3.4 Molecular basis of fidelity

Recent work has shown that substrate induced conformational changes in polymerases play a very important role in the specificity of the enzyme [88]. "Induced fit" of the correctly matched incoming dNTP governs the specificity of incorporation. The wrong substrate promotes substrate release, whereas the correct substrate induces a structure to facilitate catalysis. The correct base pairs fits snugly in the nascent base-pair–binding pocket without steric clashes, as the canonical Watson–Crick base pairs have similar geometries [117]. But mismatches with different geometries are predicted to have steric clashes in the binding pocket, affecting subsequent conformational changes in the enzyme required to set up the proper alignment for catalysis, and/or the rate of phosphodiester bond formation. According to the "induced fit" model, incorporation of a nucleotide happens through the following scheme (Fig. 1-7):

$$ED_n + dNTP \rightleftarrows ED_ndNTP \rightleftarrows FD_ndNTP \rightleftarrows FD_{n+1}PPi \longrightarrow ED_{n+1} + PPi$$

Figure 1-7: Reaction scheme for nucleotide incorporation by polymerases. Incoming nucleotide binds to the primer-template-enzyme complex in the open conformation (EDn), which undergoes a conformational change to the closed state (FDn). A chemical reaction incorporating the nucleotide and release of pyrophosphate follows the conformational change. Adapted from [5].

According to the reaction scheme, initial weak binding of the nucleotide to the 'open' conformation of the enzyme is followed by a fast conformational change in the enzyme. The binding of a nucleotide substrate to a polymerase induces a change in structure of the enzyme from an *open* state to a *closed* state and in the *closed* state, the substrate is surrounded by residues that promote catalysis [5]. The incoming dNTP is thought to initially bind the template nucleotide through hydrogen bonds between the two base pairs [118], which is followed by conformational change, chemical reaction, and release of the pyrophosphate. Analysis of conformational changes in T7 DNA polymerase by attaching a fluorophore to the fingers sub-domain of the polymerase revealed three different states of the enzyme: open, closed, and mismatch recognition site [119]. A correct base pair binding to the open E-DNA complex leads to the closed F-DNA complex, whereas an incorrect base pair led to a different conformation state (G-DNA complex) [119]. It has been postulated that the mismatch-recognition site misaligns the catalytic residues using the substrate-binding energy and promotes the release of mismatched nucleotides [5, 119]. In contrast, recognition of a correct base in the open state results in re-organization of the active site to hold the nucleotide tightly and promote catalysis [120]. This two-step nucleotide binding induced–fit mechanism holds true for HIV RT as well [121].

To understand the role of "induced fit" in fidelity, it is important to first understand the structure of a mismatched ternary complex with a polymerase. But the crystallization experiments for mismatched ternary complexes have not been easy and the molecular models of fidelity are mostly based on correct incorporations. Examinations of the protein conformational transitions by comparing the crystal structures of the open and closed states of HIV RT using Directional Milestoning (structural analysis) underscored the importance of substrate-induced conformational changes in the specificity of the enzyme [88]. Upon initial weak binding of the substrate, the enzyme undergoes a rapid conformational change to reach the transition state. At this state, rapid motions in the fingers subdomain (specificity domain) samples the bound nucleotide by probing for key interactions indicative of the correct substrate. A correctly matched substrate leads to the closed state favorable for catalysis, whereas a mismatched substrate facilitates the rapid opening of the specificity domain and release of the misaligned substrate. The bound nucleotide at the transition state does not trigger conformational changes through allosteric interactions, but instead captures the constellation of charged amino acid residues at the active site facilitating the rapid collapse to the closed state. Because this capture is dependent upon proper base pair geometry, the substrate induced conformational changes are important. Base pair geometry is dictated by base pair stacking and correct hydrogen bond interactions between the incoming nucleotide and the templating base [122].

Some error-prone polymerases do not undergo *open* to *closed* conformational changes, suggesting that the lack of substrate induced conformation changes could be a reason for their low fidelity. Low fidelity Y-family DNA polymerase DinB pre-exists in a closed conformation in the free form [123] and X family DNA polymerase Pol λ does not show significant conformational

changes in the ternary complex after binding the substrate for both match [124] and mismatch formation [125].

1.3.5 Genetic recombination

HIV packages two copies of RNA genome and undergoes frequent recombination between them, which is another source of the viral genetic diversity. Genetic recombination enhances the survival rate of the virus even if one of the RNA genome is severely mutated or damaged [33]. The two genomes may be genetically similar or vary among themselves. If recombination occurs between two identical RNA molecules, it would result in progeny virus almost identical to the parent virus (excluding mutations made by RT). However, if the two strands are different, the resulting progeny would differ from either of the genomes present in the parent virus, essentially producing a chimera of the parent genomes. Difference in the genetic make-up of the two strands may arise from mutations introduced by RNA polymerase II or RT during synthesis of the genomes or when two different viruses infect the same cell resulting in two different proviral insertions. Most recombination is thought to occur during synthesis of the first DNA strand by "copy-choice" recombination, which is strand transfer or template switching during synthesis. In copy-choice recombination, DNA synthesized on one RNA genome ("donor") switches to a homologous region on the packaged second RNA genome ("acceptor"), and DNA synthesis continues on the acceptor strand. Nascent DNA can also switch back and forth between the original donor and acceptor several times during replication (see below). Another proposed mechanism, which occurs with a lower frequency, occurs by "strand displacement-assimilation" during second strand DNA synthesis [126].

In addition to recombination which can occur at internal regions of the genome, two essential strand transfer events occur near the termini of the genome during HIV replication (see

section 1.3.1 for details). Internal strand transfer events contributing to recombination may occur randomly at any position on the viral genome, with the majority of internal strand transfers occurring between homologous regions of two genomic RNAs [33, 127]. In addition, non-homologous recombination has also been reported to occur at a lower rate (~2-3 orders of magnitude) than homologous recombination [127]. Genetic recombination, in addition to serving as a source of genetic diversity enabling the virus to stay ahead of the host immune response [128-130] and selection of drug resistant strains [131].

HIV recombination rates vary according to the host cell type. On average, 3-10 recombinations per replication cycle have been reported in T cells [132], and ~30 recombinations per cycle in macrophages (an average of one recombination per every 300 nucleotides) [133] were observed. Reports measuring the recombination rate of other retroviruses such as Moloney murine leukemia virus (MLV) are conflicting, with one report suggesting MLV recombines at a rate about 1/10 to 1/50 that of HIV [134] and another report suggesting that the recombination rates of MLV and HIV are similar [135]. However, due to other retroviruses not replicating as rapidly as HIV-1, the overall mutation rate of replication and recombination may not be as high as HIV-1 [77].

1.4 Treatment and efforts to cure HIV infection

1.4.1 Highly active antiretroviral therapy

Due to significant advances in the treatment of HIV-1 infections, the morbidity associated with HIV infection and AIDS has drastically reduced. The first HIV-1 specific antiviral drugs were administered as monotherapy in the early 1990s. But monotherapy just selected for drug-resistant strains, ultimately resulting in treatment failure. The advent of combinatorial

therapy, also known as highly active antiretroviral therapy (ART), played a very important role in reducing the mortality of HIV infections [136, 137]. ART dramatically suppresses viral replication and reduces the plasma load of HIV to below detection limits (<50 RNA copies / mL). This results in significant increase in the amounts of circulating $CD4^+$ T cells, with a consequent reconstitution of the immune system [138, 139]. With proper adherence, ART can tremendously increase the life expectancy of HIV infected individual by suppressing viral replication for decades. However, ART cannot cure HIV infection, with patients on ART required to be on lifelong therapy.

ART is successful because therapy using antiretroviral drugs targeted towards three or more distinct molecular viral targets preempts evolution of drug resistance. There are currently 26 Food and Drug Administration (FDA)–approved HIV drugs. These drugs are classified into six categories based on their molecular mechanism and viral target: 1) nucleoside analog reverse transcriptase inhibitors (NRTIs), 2) non-nucleoside reverse transcriptase inhibitors (NNRTIs), 3) integrase strand transfer inhibitors (INSTIs), 4) protease inhibitors (PIs), 5) fusion inhibitors, and 6) entry inhibitors. Additionally, FDA has also approved another class of HIV drugs called the pharmacokinetic enhancers (cobicistat), which is used to increase the efficacy of some protease inhibitors. Cobicistat does not directly inhibit HIV but interferes with breakdown of some PIs, making them more effective.

Nucleoside reverse transcriptase inhibitors (NRTIs)

NRTIs were the first class of HIV drugs to be approved by the FDA for HIV therapy. AZT, which is the most commonly known anti-retroviral drug, was the first approved drug for AIDS treatment [140]. All the currently approved NRTIs are analogues of natural nucleotides lacking a functional 3′- hydroxyl (OH) group at the sugar moiety. After getting incorporated into the replicating strand by RT, they prevent formation of the phosphodiester bond with the next

incoming nucleotide and thereby resulting in chain termination. Chain termination can occur during RNA-dependent or DNA-dependent synthesis, inhibiting synthesis of either minus strand or plus strand proviral DNA [141-143]. Currently, seven NRTIs are approved by the FDA: abacavir (ABC), didanosine (ddI), emtricitabine (FTC), lamivudine (3TC), stavudine (d4T), zidovudine (AZT), and tenofovir disoprovil formulate (TDF). NRTIs are administered as prodrugs, which after entering into the host cell must be phosphorylated by cellular kinases to have an antiviral effect [144].

Treatment with these drugs often results in selection of HIV-1 and HIV-2 strains with reduced susceptibility. Two mechanisms exist for resistance to NRTIs through development of mutations in RT during treatment. Treatment with AZT and d4T predominately selects for a class of mutations called thymidine analog mutations (TAMs) [145, 146]. TAMs promote ATP dependent pyrophosphorolysis of the inhibitor, which is the removal of NRTIs from the 3′ end of the nascent chain using ATP as a pyrophosphate donor [147, 148]. This pathway is called as the excision mechanism. The exclusion mechanism is the second mechanism, in which the selected mutations increase the ability of drug-resistant mutant RTs to discriminate against NRTIs, thereby reducing the incorporation of NRTI into the nascent chain. HIV-1 RT uses exclusion mechanism against NRTIs such as 3TC, FTC, ABC, ddC, ddI, and Tenofovir through selection of K65R and M184V/I mutations, among others [149-152].

HIV-1 and HIV-2 develop different mechanisms of resistance against some NRTIs. HIV-1, with a better ATP binding pocket than HIV-2 RT, uses the excision mechanism to generate resistance against AZT, which is the ATP-dependent removal of chain terminators; whereas HIV-2 uses the exclusion mechanism, which is increased discrimination against the chain terminators [153, 154]. Treatment of HIV-2 infected patients with AZT selects mutations at the

Q151 position (usually Q151M; although Q151I and Q151L have been reported), increasing the ability of HIV-2 RT to discriminate against AZT. Similarly, treatment of HIV-2 with FTC selected M184V/I, TFV selected K65R and Y115F mutations associated with exclusion mechanisms [154, 155].

Non-nucleoside reverse transcriptase inhibitors (NNRTIs)

There are currently five NNRTIs approved for treatment of HIV-1 infections (Table 1-2). HIV-2 and other lentiviruses such as simian immunodeficiency virus are not inhibited by NNRTIs, as these viruses are inherently resistant to most NNRTIs [86, 156]. HIV-1 group O is also intrinsically resistant to NNRTIs [157]. NNRTIs inhibit other groups of HIV-1 RT, non-competitively, by binding to a hydrophobic pocket proximal to the active site and changing the spatial conformation of the substrate-binding site resulting in decreased polymerase activity. The NNRTI pocket consist of hydrophobic residues (Y181, Y188, F227, W229, and Y232) and hydrophilic residues such as K101, K103, S105, D192, and E224 (in the p66 subunit of HIV-1 RT) and E138 of the p51 subunit of HIV-1 RT [158]. The NNRTI pocket gets formed in HIV-1 RT only in the presence of NNRTIs, with the hydrophobic and hydrophilic residues coming together to make the NNRTI binding pocket [158, 159].

NNRTI resistance results from amino acid substitutions in the NNRTI-binding pocket of RT, the most common NNRTI mutations being K103N and Y181C [160, 161]. NNRTI associated drug resistance mutations usually results only in a minor loss of replicative fitness [162, 163] compared to the significant reductions in replication fitness associated with NRTI resistance mutations. Therefore, NNRTIs have a lower genetic barrier to resistance, which contributes to the stable transmission of NNRTI-resistant HIV-1 in the population.

Integrase strand transfer inhibitors (INSTIs)

Three INSTIs have been currently approved for therapy (Table 1-2). INSTIs have higher efficacy, better safety, and tolerability profiles than other HIV drugs. Four out of five recommended treatment regimens for ART-naïve patients are INSTI-based regimens, as they contain at least one INSTI among the recommended drugs in the treatment regimen. All approved integrase inhibitors target the strand transfer reaction and hence are called integrase strand transfer inhibitors. INSTIs specifically affect the strand-transfer reaction by binding to the complex between integrase and viral DNA in the integrase active site [164]. INSTIs have a broad spectrum of antiviral activity, as inhibition of all HIV-1 subtypes, HIV-2, and other retroviruses such as XMRV is observed using INSTIs [165-167].

Mutations associated with INSTI resistance almost always map to the active site of the integrase, resulting in deleterious effects on integrase function translating to very poor replicative capacity [168]. Resistance to raltegravir, in clinical studies, is associated with three primary mutations at integrase: Y143, N155, and Q148 [169], which are commonly seen in association with secondary mutations. Due to higher impact on replicative fitness, INSTIs have a higher genetic barrier to resistance.

Protease inhibitors (PIs)

Protease inhibitors targeting HIV protease also form a major component of the ART treatment regimens, with eight HIV drugs approved for therapy (Table 1-2). PIs inhibit the catalytic function of protease, thereby preventing proteolytic cleavage of HIV polyproteins. This prevents maturation of the released virions. There are differences in susceptibility to protease inhibitors between HIV-1 and HIV-2. Out of the approved PIs, Darunavir, lopinavir, and saquinavir appear to be more active against HIV-2 than other PIs [170-172]. HIV-2 and SIV are

28

naturally resistant to amprenavir [157], whereas all eight approved PIs show good inhibition profiles against HIV-1.

Resistance to PIs is associated with mutations clustering at the substrate/ inhibitor binding site near the active site of protease (e.g. D103N, G48V, V82A) [173]. These mutations are usually associated with deleterious effects on the replicative fitness of the virus [173], and secondary mutations usually arise in the eight major protease cleavage sites of the substrates [174]. Cleavage site mutants compensate for the loss in the catalytic efficiency of the PI-resistant mutant proteases by acting as better substrates.

Fusion inhibitors

Enfuvirtide (ENF) is the only fusion inhibitor currently approved for therapy. ENF is a peptide-based inhibitor blocking the formation of six-helix bundle in the fusion protein gp41 [175], which is a very important step in the fusion of viral and cellular membranes (Section 1.2.3). HIV-2 is intrinsically resistant to ENF due to high genetic diversity in the HR1 and HR2 domains of gp41 between HIV-1 and HIV-2 [176].

Mutations to ENF result in reduced replication capacity because mutations which reduce ENF binding also reduce the formation of the six-helix bundle [177]. Adaptation to ENF has resulted in viruses that require enfuvirtide for fusion [178]. Susceptibility to ENF is also limited by the time between CD4 binding and six-helix bundle formation, and any decrease in the rate of the entry process increases susceptibility to ENF [179]. ENF is therefore synergistic to compounds inhibiting CD4 or co-receptor engagement.

Entry inhibitors

Entry inhibitors are CCR5 antagonists binding to hydrophobic pockets in the transmembrane helices of CCR5 [180]. Maraviroc (MVC) is the only approved FDA entry inhibitor for HIV-1 treatment. MVC is not effective against X4 tropic viruses, as the target is CCR5. HIV-2 has been shown to be affected by MVC [181]; however as there are no approved assays to determine HIV-2 co-receptor tropism and as HIV-2 can use other co-receptors (see section 1.2.3), MVC is not included in treatment regimens for HIV-2 infections. MVC binding to CCR5 alters the conformation of its extracellular loop and thereby prevents interaction with gp120 [180].

Susceptibility to entry inhibitors can be affected by cell type, cellular activation state, and number of virus replication cycles [182]. Different primary HIV-1 isolates show different sensitivities to entry inhibitors [183]. Tropism switching, where treatment of R5 tropic viruses with entry inhibitors could lead to selection of X4 tropic viruses, is a major concern with the use of entry inhibitors [184].

Table 1-2: List of FDA-approved HIV medicines

Drugs	Common name (acronyms)
Nucleoside Reverse Transcriptase Inhibitors (NRTIS)	• Abacavir (ABC) • Didanosine (ddI) • Emtricitabine (FTC) • Lamivudine (3TC) • Stavudine (d4T) • Tenofovir disoproxil fumarate (TDF) • Zidovudine (AZT)
Non-Nucleoside Reverse Transcriptase Inhibitors (NNRTIs)	• Delavirdine (DLV) • Efavirenz (EFV) • Etravirine (ETV) • Nevirapine (NVP) • Rilpivirine (RPV)
Integrase strand transfer Inhibitors (INSTIs)	• Dolutegravir (DTG) • Elvitegravir (ETG) • Raltegravir (RTG)
Protease Inhibitors (PIs)	• Atazanavir (ATV) • Darunavir (DRV) • Fosamprenavir (FPV) • Indinavir (IDV) • Nelfinavir (NFV) • Ritonavir (RTV) • Saquinavir (SQV) • Tipranavir (TPV)
Fusion Inhibitor	• Enfuvirtide (T-20)
Entry Inhibitor	• Maraviroc (MVC)

1.4.2 Complications in ART therapy

ART dramatically increases the life expectancy of HIV infected individuals by suppressing viral loads as long as patients continue to be on treatment. However, ART cannot eliminate the infection and does not offer a cure, which is a major disadvantage of ART. The virus continues to persist dormant in the so-called latent reservoirs and can drive infection once treatment is stopped or when latently infected cells are activated [185, 186]. The effect of therapy can also be minimalized by non-adherence, poor drug tolerability, and interactions of antiretroviral drugs with

other medications which may decrease drug efficacy. In addition, ARVs are associated with severe side effects. Anemia, nausea, vomiting, hypersensitivity reactions, peripheral neuropathy headache, diarrhea, depression, insomnia, and pancreatitis are some of the common adverse reactions which can decrease the quality of life for patients on therapy. Long term complications such as cardiovascular disease, liver and renal failure, neurocognitive dysfunction, and HIV-associated malignancies can develop in HIV infected patients living on therapy [187-189].

Drug resistance is another major complication accompanying the treatment regimens, as each ARV is associated with drug-resistance (section 1.4.1). It is common for patients in developed countries to have their baseline resistance measured before initiation of the treatment regimen to determine their susceptibility to specific ARVs. It is also recommended to continuously monitor the CD4 viral load and the viral titer values during treatment. Increase in viral titers during treatment suggests emergence of resistance to the existing treatment regimen, requiring resampling the existing quasispecies and adjustment of the treatment regimen based on resistance. In rare cases where the resistance profile in the patients cannot be treated with ART, salvage therapy (ART + additional drug combination) is used as a final line of defense.

Another important factor in treatment of HIV infections is *when* to initiate therapy. Without treatment, most patients will eventually develop immunosuppression and progress to AIDS. But the side effects associated with many ARVs, cost, and lifestyle changes can unfortunately discourage compliance with treatment, and the timing of therapy initiation is important. The current treatment guideline 'treat early-treat hard' [190], is based on observations that untreated HIV infections can lead to development of non-AIDS-defining complications such as cardiovascular disease, liver disease, neurologic complications, and malignancies combined with the fact that newer ART regimens are better tolerated and more effective than the past

regimens. Current treatment guidelines are linked with strong recommendations to begin therapy for patients with CD4 count < 350 cells/mm and moderate recommendations for CD4 counts between 350–500 cells/mm as well as for patients with CD4 counts >500 cells/mm [191]. Continuous evolution of the virus, development of drug resistance, and other concerns discussed here highlight the need for development of new HIV treatment options.

1.4.3. Novel HIV treatment strategies

Several number of novel treatment strategies, which might have potential advantages over conventional drugs, and could add to the repertoire of available therapy choices are currently being investigated. Due to serious limitations associated with currently existing ARVs (section 1.3.2), it is imperative to continue to develop novel strategies with better efficacy and tolerability profiles. Protein-based inhibitors, nucleic acid-based inhibitors, and gene therapy approaches targeting viral and cellular targets are under investigation. Both viral and host cellular factors important for HIV infection are currently being investigated, as inhibitors targeting viral factors can be designed with higher specificity whereas inhibitors targeting cellular factors are less prone to mutational escape. Some examples of novel treatment strategies are discussed below.

Protein-based inhibitors

Protein-based inhibitors include dominant negative inhibitors, intrabodies, intrakines, and novel fusion inhibitors. Dominant negative inhibitors are mutant viral proteins which can be used as antiviral inhibitors. A mutant form of HIV Rev called M10 was the first protein used in gene therapy trial for HIV treatments [192], but Rev M10 only had a modest survival advantage. Rev M10 works by blocking the export of singly spliced and unspliced HIV RNA from the nucleus to the cytoplasm. Intrabodies and intrakines are novel protein-based inhibitors currently under investigation. Intrabodies are intracellular antibodies, typically single-chain Fv fragments and

intrakines are intracellular chemokines [193]. Binding of intrabodies and intrakines to their intracellular targets leads to intracellular degradation. CCR5 and CXCR4 co-receptors are major targets of intrabody and intrakine development [194], and intrabodies against several viral targets such as gp120 [195], Tat [196], and Rev [197] have been developed. A host restriction factor Tripartite motif-containing protein 5 (TRIM 5- α) which acts by binding and degradation of viral capsids is also examined as another protein-based inhibitor. Although HIV capsid proteins have evolved to escape binding by TRIM 5-α, TRIM 5- α from a non-permissive primate species inhibits HIV replication *in vitro* [198]. A major limitation with all the novel protein-based approaches, in addition for the need to maintain sufficient levels of expression, is avoiding immunogenicity *in vivo*.

Nucleic acid-based inhibitors

Nucleic acid-based inhibitors do not typically elicit adaptive immune responses unlike protein-based inhibitors but they suffer from potential off-target toxicity due to innate immune responses. Antisense RNAs, aptamers, decoys, ribozymes, and short hairpin RNAs (shRNAs) are some examples of nucleic acid-based HIV inhibitors currently being investigated. Antisense RNA transgenes work by blocking HIV replication through pairing with HIV transcripts and making nonfunctional duplexes. Patients infused with autologous CD4 cells genetically engineered to express antisense RNA to HIV *env* [199] were followed in a clinical trial recently [200]. While the antisense RNA was successful in decreasing the viral loads in the majority of the treated patients (88%) even after discontinuing ARV therapy, the exact mechanism by which antisense RNAs inhibited HIV replication was not conclusive [200]. RNA decoys are short RNA oligonucleotide sequences targeting structurally important elements in the HIV genome. RNA decoys for the TAR sequence inhibit Tat binding to the authentic TAR [201] and RRE decoys

preventing Rev binding to the viral RRE [202]. RNA decoys, however, proved to be insufficient for antiviral activity in a clinical trial [203]. Ribozymes are antisense RNAs which are also capable of enzymatically cleaving their targets. Ribozyme-based antivirals targeting U5 region of LTR, *tat*, and *rev* genes were tested in clinical trials [204, 205], but showed no significant anti-viral effects. RNA interference (RNAi) targeting HIV-encoded mRNAs were also evaluated and RNAi approaches have been shown to have antiviral activity pre-clinically in cell lines [206]. Aptamers are RNA and DNA sequences that based on their secondary/tertiary structure or sequence bind tightly to target proteins and inhibit them. Several effective aptamers against HIV proteins in gene therapy settings have been characterized, although no aptamers have been tested in clinical trials for HIV infections. RNA pseudoknot-type structure aptamers [207], single stranded DNA aptamers [208, 209] and DNA loopback aptamers [210, 211] against HIV RT are very effective in inhibiting RT primer-template extension *in vitro* [212].

Gene therapy strategies targeting CCR5

Resistance to HIV infections in people homozygous for a mutant form of the CCR5 (CCR5Δ32) was first observed in the late 1990s [213]. This observation along with the fact that individuals with this mutation do not present CCR5 on the cell surface but remain healthy has provided impetus for development of novel strategies targeting CCR5 expression. Gene therapy approaches targeting CCR5 expression are developed with a goal of mimicking the CCR5Δ32 phenotype. Gene therapy vectors expressing small interfering RNA (siRNA) [214] or ribozymes [215] against CCR5 (modification of CCR5 at RNA level) and CCR5-targeted intrabodies [215] and intrakines [216] (modifying CCR5 at protein level) have been developed. Transduction of CD34$^+$ hematopoietic stem cells (HSCs) with lentiviral vectors expressing anti-CCR5 shRNAs conferred resistance to HIV infections to macrophages [217] and provided *in vivo* protection

against infection in the bone marrow/liver/thymus (BLT) model [218]. AIDS patients who develop lymphomas represent a unique cohort of patients who could be used to test the efficacy of the gene therapy approaches, as their HSCs are harvested before chemotherapy and would require autologous HSC transplants.

Gene-editing strategies to disrupt CCR5

Gene editing strategies to achieve permanent CCR5 gene disruption were explored more recently due to the theoretical oncologic potential of lentiviral gene therapy vectors. Zinc finger nucleases (ZFNs) are engineered fusion proteins containing a DNA-binding zinc finger protein and an endonuclease domain of a type-1 restriction enzyme. Zinc finger proteins are domains of several zinc finger peptides with sequence-specific DNA binding properties. The binding specificity of zinc finger peptides can be modified by altering the contact amino acid residues at the tip of each zinc finger peptide. ZFNs act as restriction enzymes cutting both strands of DNA at the bound target sequence. The cleaved sequence is repaired in mammalian cells by nonhomologous end-joining (NHEJ) pathway, which typically generates a series of mutations at the breaking site resulting in disruption of the open reading frame [219]. ZFNs targeting CCR5 and CXCR4 are evaluated in preclinical and clinical settings as HIV therapeutics [219]. ZFNs led to disruption of ~ 50% of CCR5 alleles in primary CD4$^+$ cells preclinically, generating HIV-resistant CD4$^+$ cells [220]. HIV-resistant CD4$^+$ cells expanded stably resulting in enrichment of ZFN-generated CCR5-modified cells. ZFN-treated HSPCs retained the ability to engraft NOD/SCID/IL2r gamma (null) mice, and upon HIV challenge selected for CCR5-modifed cells and the serum HIV-1 levels were controlled efficiently in mice which received the ZFN-treated HSPCs [221].

Clustered regularly interspaced palindromic repeats (CRISPR)/Cas9 gene editing system was also investigated as a tool for gene editing and gene regulation. CRISPR/Cas9 system is comprised of a single or multiple chimeric guide RNAs along with Cas9 nuclease. The guide RNA binds to the target, which is then recognized and cleaved by the Cas9 nuclease. Using dual gRNAs against CCR5, 27% of the human induced pluripotent stem cells (iPSCs) demonstrated CCR5 editing showing a biallelic gene alteration frequency of 41%, and the macrophages from CCR5-edited iPSCs were resistant to R5 tropic virus challenge [222].

Transcription activator-like effectors nucleases (TALENs) are another gene editing system used to edit the CCR5 gene. TALENs are fusion proteins consisting of DNA binding domains and nucleases. TALENs can edit the CCR5 gene in up to 45% of the transfected cells with less toxicity compared to ZFNs [223], as TALENs recognize one nucleotide instead of three resulting in better specificity [224]. CCR5-edited T cells using TALENs were resistant to R5-tropic HIV infection in a pre-clinical study [225].

Latency reversing agents

HIV latently persisting in reservoirs during treatment is a major problem impeding the cure of HIV infections. Several novel latency reversing agents (LRAs) are currently being investigated in an approach termed as "shock and kill" strategy. The idea is to activate dormant viruses either by directly activating viral replication using LRAs or indirectly activating the immune system, and then purging the reactivated viral replication using ARVs. Histone deacetylase inhibitors (HDACi) like valproic acid had a limited impact on reducing the size of the latent reservoir [226]. But more promising results were recently obtained using other HDACi such as suberoylanilide hydroxamic acid (SAHA/vorinostat) and panobinostat [227].

1.4.4 Recent progress towards HIV-1 vaccine development

Only one curious documented case of curing HIV infection exists in the entire history of treating HIV infections. The patient famously termed "Berlin patient" was cured of HIV infection following an allogenic bone marrow transplant from a donor with CCR5Δ32 mutations [228]. After transplantation with CCR5Δ32 mutated bone marrow, ART was discontinued and no HIV was detected in the plasma and peripheral CD4 cells even after three and half years in the absence of ART [229]. Low frequency of CCR5Δ32 homozygotes in the general population combined with the low feasibility and logistics of performing transplantation makes this less likely to cure HIV and it is imperative to continue to research ways of developing vaccines to cure HIV infection. Despite 30 years of research in the HIV-1 vaccine field, there is no available vaccine. Recombinant adenovirus based vaccines expressing Gag, Pol, and Nef were tested in clinical trials by Merck and National Institutes of Health (NIH) [230, 231]. Although the NIH vaccine elicited T-cell and antibody responses against Env, it failed to show efficacy against HIV-1 acquisition [232]. The second trial using Merck recombinant adenovirus type 5 not only failed to show efficacy but also appeared to enhance infection in seropositive vaccinees [233]. However, there have been several recent advances in basic and translational sciences towards the quest for developing an effective HIV-1 vaccine. A new set of recent pre-clinical studies has demonstrated that replicating cytomegalovirus vectors expressing simian immunodeficiency virus (SIV) antigens could eradicate SIV infection in 50% of rhesus-macaques challenged with SIV [234]. It was also recently shown that cytotoxic T lymphocyte response against sub-dominant Gag epitopes eliminated target cells infected with virus from the latent reservoir [231]. Analysis of an HIV-1 vaccine trial using the RV144 canarypox-prime gp120 protein carried out in Thailand, from 2003 to 2006, also gave promising insights for future vaccine development [235]. An immune correlates study from that

trial showed that IgG responses to the second variable region in Env correlated with decreased HIV transmission, but IgA responses correlated with decreased HIV-1 vaccine efficacy [236]. It was later discovered that the IgA response to gp120 blocked IgG mediated antibody dependent cell-mediated cytotoxicity (ADCC), leading to lower efficacy of the vaccine [237]. New vaccine candidates are engineered to increase the breadth of IgG ADCC activity and to optimize the profile of the induced antibody subclass (IgG3) [238]. Progress has also been reported in attempts to overcome HIV-1 diversity impeding vaccine development through introduction of *in-silico* designed vaccines [239]. The *in-silico* designed immunogens are constructed to increase the coverage across $CD4^+$ and $CD8^+$ T-cell epitopes and clinical trials are currently ongoing with some of the *in-silico* designed vaccines. No current vaccine candidates have been able to induce high levels of HIV-1 broadly neutralizing antibodies (bNAbs) even though HIV-1 Env possess conserved regions to which neutralizing antibodies can bind [240]. It is now clear that bnAbs share unique characteristics such as: high levels of somatic hypermutation [241], autoreactivity for host molecules, and longer heavy chain complementarity determining region 3 sequences [240]. B-cell lineage immunogen design [242] is a new strategy proposed to overcome the difficulty in the development of bNAbs based on these studies, which may provide better efficacy of the developed vaccine candidates. High throughput screening of sera of HIV infected patients who remain healthy (elite neutralizers) has resulted in identification of new bNAbs with better potency. Passive immunization through injection of the broadly neutralizing monoclonal antibodies has conferred protection against simian human immunodeficiency virus (SHIV) challenges in monkeys [243-245]. PGT121, one of the recently identified bnAbs, conferred protection against SHIV in monkeys at significantly lower serum concentrations (1.8 μg/mL) [246]. Although these studies demonstrate the potential for passive immunization, injecting antibodies every few weeks

cannot be used as a viable treatment option. Recent strategies of antibody gene transfer by means of expressing bNAbs using adeno-associated viral (AAV) vectors as an alternative to passive immunization is also actively investigated (for review, see [247]). Once administered, the antibody gene directs endogenous expression of the antibody molecule inside the host negating the need for repeated injection. Another advantage to the gene transfer approach is that it bypasses adaptive immune response as success is not dependent on the design of immunogen. This approach, also called as vectored immunoprophylaxis, was used to express the native bNAbs such as 2G12, 4E10, and VRC01 using recombinant adeno associated virus (rAAV) vectors in mice and expression levels greater than 100 μg/mL was observed for more than 12 months [248]. The authors also showed that these rAAV vectors can provide protection against HIV challenges in humanized mice models. An ongoing phase I clinical trial testing the safety, tolerability, and immunogenicity of rAAV vectors expressing the bNAb PG9 should give more information on the feasibility of antibody gene transfer techniques.

Despite these advances, there are still number of roadblocks preventing the progress of HIV-1 vaccine candidates. However, all the advances discussed above are recent and there is still hope of overcoming these challenges. Challenges associated with development of vaccines also highlight the need to continually research the possibilities of obtaining a cure from HIV infection using antiretroviral drugs, if possible.

1.5 Concluding remarks

The contribution of RT fidelity to evolution of the virus makes it a topic of immense significance. HIV RT is also a very important target for antiretroviral therapy, with 12 out of the 26 approved ARVs targeting RT and several novel antiretrovirals being developed against RT

(section 1.4.1). In this study, I will address the ability of divalent cations to profoundly alter the fidelity of HIV RT in a concentration-dependent manner. I will also investigate the effect of the physiologically relevant divalent cation concentration on the inhibitor potency of nucleoside and non-nucleoside RT inhibitors. Results presented here establish conditions which might yield more accurate assessment of different biochemical properties of RT and efficiency of RT inhibitors. Results presented here also provide an important contribution to the "Rational drug design" strategy by highlighting key RT-inhibitor interactions which may improve the potency of the inhibitors in cellular conditions. In addition, the work presented here will show that alternative divalent cations, presumed to be pro-mutagenic, do not decrease the fidelity of HIV-1 RT at concentrations optimal for RT activity.

Chapter 2 : Alternative divalent cations (Zn^{2+}, Co^{2+}, and Mn^{2+}) are not mutagenic at conditions optimal for reverse transcriptase activity

2.1 Introduction

Divalent cations are essential co-factors for polymerase catalysis and the RNase H activity of reverse transcriptase (RT) (section 1.3.2) [91, 249]. Under physiological conditions, Mg^{2+} functions as the co-factor for both activities. In addition to Mg^{2+}, RT *in vitro* can use alternative divalent cations such as manganese (Mn^{2+}), copper (Cu^{2+}), cobalt (Co^{2+}) and zonc (Zn^{2+}) for polymerase activity [250]. These cations are important to many cellular processes and are tightly regulated. The total concentration of Zn^{2+} in cells is ~0.1-0.5 mM [251-254] while the total concentration of Mn^{2+} in red blood cells is ~2.5- 3 µM [255, 256], and Co^{2+} in the serum is in the low µM range [257]. The available free concentration of all these cations is kept extremely low by cellular mechanisms (Chapter 5) [258, 259].

Zn^{2+} is a potent inhibitor of several viral polymerases [260-264] and Zn^{2+}, in addition to Mn^{2+}, has been shown to inhibit Mg^{2+}-dependent HIV RT activity *in vitro* in work from our lab and others [250, 265-267]. Other groups have demonstrated that Zn^{2+}-based drugs can inhibit HIV spread in animal models [268-273]. Zn^{2+} is an active ingredient of topical solutions under study for the treatment of HIV [271, 272] and herpes simplex, an infection that can increase HIV transmission [274-279]. Zn^{2+} has been investigated in several past and current HIV therapeutic trials [280], and is a proposed treatment for rhinovirus infections [281, 282]. Therefore, understanding how Zn^{2+} and other divalent cations affect different properties of RT is potentially important for future drug development.

One of the most notable effects of alternative divalent cations on polymerases is alteration of polymerase fidelity. Mn^{2+}, Co^{2+}, and Ni^{2+} have all been shown to dramatically decrease the fidelity of DNA synthesis by several human, bacterial, and viral polymerases including HIV RT [283-289]. Mn^{2+} and Co^{2+} decreased the fidelity of avian myeoblastosis virus (AMV) RT and human DNA polymerase I in a concentration-dependent manner [286]. Increased error frequency in presence of Mn^{2+} has also been observed *in vitro* with HIV RT [289], *Escherichia coli* DNA polymerase I [290], phage T4 DNA polymerase [291], DNA polymerases α and β [292], and *Taq* polymerase [293]. Most of these experiments were performed using concentrations of divalent cation higher than those required for maximal enzyme activity. However, physiological Mg^{2+} concentrations, which are lower than the high concentration typically used to optimize enzyme kinetics *in vitro*, can increase RT fidelity (Chapter 3) [10].

Given the potential of Zn^{2+}-based compounds as novel drugs against HIV and the vast amount of literature on alternative cations like Mn^{2+} and Co^{2+} being pro-mutagenic, it is important to investigate the fidelity of HIV RT with each of these cations. Although Mn^{2+} and Co^{2+} were previously demonstrated to support RT catalysis, a recent publication from our lab [266] was the first to show that Zn^{2+}, a potent polymerase inhibitor, can also support polymerase catalysis [261]. Therefore, I wanted to look more closely at how this previously untested divalent cation affects RT fidelity. A better understanding of the fidelity of RT with these alternative cations could also be important for modulating the accuracy of RT-PCR reactions. Mn^{2+} is already being used in PCR reactions to generate random mutations [293]. In this chapter, I show that under optimal extension conditions, Zn^{2+} increases the fidelity of RT, a previously unprecedented observation of an alternative cation for a polymerase. I also show that presumed pro-mutagenic cations, such as Mn^{2+} and Co^{2+}, are not mutagenic with HIV RT at concentrations optimal for dNTP catalysis. The

potential mechanisms by which Zn^{2+} enhance fidelity as well as the reason for the concentration-dependence of mutagenesis is discussed in this chapter.

2.2 Materials and Methods

2.2.1 Materials

Calf intestinal alkaline phosphatase (CIP), T3 RNA polymerase, "High Fidelity" (PvuII and EcoRI) and other restriction enzymes, T4 polynucleotide kinase (PNK), and MuLV RT were from New England Biolabs. DNase (deoxyribonuclease)-free RNase (ribonuclease), ribonucleotides, and deoxyribonucleotides were obtained from Roche. RNase free-DNase I was from United States Biochemical. Rapid DNA ligation kit, RNasin (RNase inhibitor), and the phiX174 HinfI digest DNA ladder was from Promega. Radiolabeled compounds were from PerkinElmer. *Pfu* DNA polymerase was from Stratagene. DNA oligonucleotides were from Integrated DNA Technologies. G-25 spin columns were from Harvard Apparatus. RNeasy RNA purification and the Plasmid DNA Miniprep kits were from Qiagen. X-gal was from Denville Scientific, Inc. IPTG and media were from Gibco, Life Technologies. All other chemicals were obtained from Fisher Scientific, VWR, or Sigma. HIV RT (from HXB2 strain) was prepared as described [294]. The HIV RT clone was a generous gift from Dr. Michael Parniak (University of Pittsburgh). This enzyme is a non-tagged heterodimer consisting of equal proportions of p66 and p51 subunits. Aliquots of HIV RT were stored frozen at -80°C and fresh aliquots were used for each experiment.

2.2.2 Methods

Polyacrylamide gel electrophoresis. Denaturing polyacrylamide gels (6, 8, and 16% w/v), native polyacrylamide gels (15% w/v), and 0.7% agarose gels were prepared and run as described [295].

Preparation of RNA for the PCR-based *lacZα*-complementation fidelity assay and RNA-DNA hybridization. Transcripts (~760 nucleotides (nts)) were prepared with T3 RNA polymerase and hybrids were prepared at a 2:1 5' ^{32}P-labeled primer: template ratio as previously described [296].

Primer extension reactions for the PCR-based *lacZα*-complementation fidelity assay. For RNA-directed DNA synthesis, the ~760 nt RNA template was hybridized to a radiolabeled 25 nt DNA primer (5'-GCGGGCCTCTTCGCTATTACGCCAG-3'). Full extension produced a 199 nt final product (see Fig. 2-2A). The long template was used to make it easier to separate DNA synthesis products from the RNA template on a denaturing polyacrylamide-urea gel (see below). The primer-template complex was pre-incubated in 48 μl of buffer (see below) for 3 min at 37°C. The reaction was initiated by addition of 2 μl of 5 μM HIV RT in 50 mM Tris-HCl pH 8, 80 mM KCl, 1 mM DTT and 10 % glycerol and incubation was continued for 30 min for Mg^{2+}, 1 hour for Mn^{2+} and Co^{2+}, and 3 hours for Zn^{2+}. Different time points were used to assure that all the reactions were essentially complete with each cation. The final concentration of reaction components were 200 nM HIV RT, 25 nM template, 50 nM primer, 50 mM Tris-HCl, 80 mM KCl, 1 mM DTT, 0.4% glycerol and 0.4 units/μl RNasin along with different concentrations of salts. A final concentration of 100 μM dNTPs was used along with one of the following divalent cation: 2 mM MgCl$_2$, 0.25 mM CoCl$_2$, 0.4 mM ZnCl$_2$. The final pH of the reactions was 7.7. After incubations, 1 μl of DNase-free RNase was added and the sample was heated to 65°C for 5 min. Typically two reactions for each condition were combined and material was recovered by standard phenol: chloroform extraction and ethanol precipitation. Pellets were resuspended in 20 μl of 10 mM Tris-HCl (pH 7) and 2X loading buffer (90% formamide, 10 mM EDTA (pH 8), 0.25% each bromophenol blue and xylene cyanol) and products were analyzed by gel electrophoresis on 6%

polyacrylamide-urea gels (19:1 acrylamide: bis-acrylamide). Fully extended 199 nt DNA was located using a phosphoimager (Fujifilm FLA5100), and recovered by the crush and soak method [295] in 500 µl of elution buffer containing 10 mM Tris-HCl (pH 7). After overnight elution, this material was passed through a 0.45 µm syringe filter and recovered by ethanol precipitation after addition of 10% volume 3M sodium acetate (pH 7) and 50 µg of glycogen. After centrifugation, the pellets were vigorously washed with 500 µl of 70% ethanol to remove any traces of EDTA that may have carried over from the gel and potentially interfere with the second round of synthesis. The recovered DNA was hybridized to another 20 nt radiolabeled DNA primer (5'-AGGATCCCCGGGTACCGAGC-3') with 10-fold greater specific activity than the primer used for round one, and a second round of DNA synthesis was performed as described above except the reaction volume was 25 µl. Conditions for the cation, dNTPs, and pH were identical in the RNA- and DNA-templated reactions. Reactions were terminated with an equal volume of 2X loading buffer and products were gel purified as described above but on an 8% gel. The gel was run far enough to efficiently separate the 199 nt templates from the 162 nt full extension product of round 2.

Polymerase chain reaction (PCR) for the PCR-based *lacZα*-complementation fidelity assay. The round two DNA (50% of recovered material) produced above by reverse transcription was amplified by PCR using the following primers: 5'-GCGGGCCTCTTCGCTATTACGCCAG-3' and 5'- AGGATCCCCGGGTACCGAGC -3'. Reactions were performed and processed as previously described except that restriction digestion was done with 30 units each of "High Fidelity" EcoRI and PvuII in 50 µl of NEB buffer 3 for 2 hours at 37°C [296].

Preparation of vector for PCR-based *lacZα*-complementation fidelity assay. Thirty µg of the plasmid pBSΔPvuII$_{1146}$ [115] was double-digested with 50 units each of "High

Fidelity" EcoRI and PvuII in 100 µl using the supplied buffer and protocol. After 3 hours, DNA was recovered by phenol-chloroform extraction and ethanol precipitation then treated with 20 units of CIP for 2 hours at 37°C in 100 µl of the supplied NEB restriction digest buffer 3. Dephosphorylated vector was recovered by phenol-chloroform extraction followed by ethanol precipitation and quantified using absorbance at 260 nm. The quality of the vectors for the fidelity assay was assessed in two ways: (a) ligation (see below) of the vector preparation in the absence of insert; and (b) re-ligation of the vector preparation and PvuII-EcoRI cleaved fragment (recovered from agarose gels after cleavage of pBSΔPvuII$_{1146}$ but before dephosphorylation as described above). Vectors from (a) that did not produce any white or faint blue colonies and very few blue colonies in the complementation assay (see below), and those producing colony mutant frequencies of less than ~0.003 (1 white or faint blue colony in ~333 total) in (b) were used in the fidelity assays.

Ligation of PCR fragments into vectors and transformation for the PCR-based lacZα-complementation fidelity assay. The cleaved vector (50 ng, ~0.025 pmol) and insert fragments (0.05 pmol) were ligated at a 1:2 (vector: insert) molar ratio using a rapid DNA ligation kit. Ligation and transformation of *E. coli* GC5 bacteria were carried out as previously described [296]. White or faint blue colonies were scored as harboring mutations while blue colonies were non-mutated. Any colonies that were questionable with respect to either being faint blue or blue were picked and replated with an approximately equal amount of blue colony stock. Observing the faint blue colony in a background of blue colonies made it easy to determine if the colony was faint blue rather than blue.

Gapped plasmid-based based *lacZα*-complementation fidelity assay. The gapped version of the plasmid pSJ2 was prepared as described [297]. One nM of the gapped plasmid was

filled by 100 nM RT at 37°C in 20 µl of buffer containing 50 mM Tris-HCl, 80 mM KCl, 1 mM DTT, 2 µg of bovine serum albumin, 100 µM dNTPs, and varying concentrations of different cations. The reaction pH was 7.7. Reactions with 2 mM Mg^{2+}, 0.25 mM Mn^{2+}, 6 mM Mn^{2+}, 0.4 mM Co^{2+}, and 6 mM Co^{2+} were carried out for 30 min while reactions with 0.4 mM Zn^{2+} were performed overnight. Reactions were terminated by heating at 65°C for 15 min. After confirming complete extension by restriction digestion analysis (see [297]), ~1 µl of the remaining original mixture was transformed into *E.coli* GC5 cells. The colony mutant frequency (CMF) was determined using blue-white screening as described above.

Running-start misincorporation assays. The approach used for these assays was based on previous results [298]. Reactions were performed as above using the same template but with a primer (5'- GAAATTAACCCTCACTAAAGGGAAC -3') (Fig. 2-4A) which does not have the last five nts at the 3' end and has 5 additional bases at the 5' end. Reactions with 2 mM Mg^{2+} and 0.4 mM Zn^{2+} were performed for 3 min and 30 min respectively at 37°C. The nt directed by the homopolymeric T run on the template running (dATP) was kept at a constant saturating concentration (55 µM) and the nt to be misinserted (for example, dTTP for measuring C-T misinsertion kinetics) was added at increasing concentrations in these reactions. The reaction pH was 7.7. Reactions were initiated by adding 2 µl of HIV RT (final concentration of 2 nM for Mg^{2+} reactions and 8 nM for Zn^{2+} reactions) and terminated by adding 2X loading buffer. The reactions were then electrophoresed on 16% denaturing polyacrylamide gels, dried, and imaged using a Fujifilm FLA5100 phosphoimager. Steady-state kinetic parameters K_m, and V_{max} were then calculated as described below. The amount of free cation in each reaction was adjusted according to the dNTP concentration because dNTPs are the major chelators of Mg^{2+} or Zn^{2+} in the reactions. The concentration of free cation was calculated using the formula:

$$[MD] = 0.5(M_t + D_t + K_d) - 0.5((M_t + D_t + K_d)^2 - 4M_tD_t)^{0.5}$$

Where M_t, D_t, and [MD] represent the concentration of total Mg^{2+} or Zn^{2+}, total dNTP, and Mg^{2+} or Zn^{2+} bound to the dNTPs, respectively. The equilibrium dissociation constant (K_d) for dNTP with Mg^{2+} as well as Zn^{2+}, Co^{2+} and Mn^{2+} was assumed to be the same as that of ATP with Mg^{2+}, ($K_d = 89.1$ x 10^{-6} M) [299]. This assumption leads to an approximate value for the free concentration of these cations in reactions.

Mismatched primer extension assays. The approach used for these assays was based on previous results [300]. The template (5'-GGGCGAATTTAG(G/C)TTTT GTTCCCTTTAAGGGTT AATTTCGAGCTTGG-3') used in these assays was a modified version of the template originally described in [301]. The underlined nts in parentheses indicate that templates with either a G or C at this position were used. The DNA primer (5'-TAACCCTCACTAAAGGGAACAAAAX-3') used in the assays was 5' radiolabeled and hybridized to the template at a 1:1 ratio. The "X" at the 3' end of the primer denotes either G, A, T, or C (Fig. 2-4). Matched or mismatched primer templates (14 nM final) were incubated for 3 min at 37°C in 10.5 ul of buffer containing 50 mM Tris-HCl, 1 mM dithiothreitol, 80 mM KCl with either 2 mM $MgCl_2$ or 0.4 mM $ZnCl_2$ and increasing concentrations of the next correct dNTP substrate (dCTP for this template). The reaction pH was 7.7. Reactions were initiated by adding 2 µl of HIV RT (final concentration of 2 nM for Mg^{2+} reactions and 8 nM for Zn^{2+} reactions) and terminated by adding 2X loading buffer. All reactions involving matched primer-templates were carried out for 2 min with 2 mM Mg^{2+} and for 30 min with 0.4 mM Zn^{2+}. Reactions with mismatched primer-templates at 2 mM Mg^{2+} or 0.4 mM Zn^{2+} were carried out for 5 min and 30 min respectively. The reactions were then electrophoresed on 16% denaturing polyacrylamide

gels, dried, and imaged using a Fujifilm FLA5100 phosphoimager. Steady-state kinetic parameters K_m, and V_{max} were then calculated as described below. The amount of free cation in each reaction was adjusted according to the dNTP concentration as described above.

Velocity measurements and calculation of V_{max} and K_m for steady-state assays. Velocity measurement and calculation of V_{max} and K_m were conducted as described previously for mismatch extension [300] and running-start assays [298].

Calculation of extension rates for RNA-directed DNA synthesis in the PCR-based fidelity assay. Extension rate determinations for DNA synthesis on the 760 nt RNA template for various cations were performed as described previously [266]. Briefly, the maximal extension rate was determined by calculating the length of the longest product on 8% polyacrylamide-urea gels (19:1 acrylamide: bis-acrylamide) in reactions that had not proceeded to the end of the template (l). The primer length was then subtracted (20 nt) and the maximum extension rate was calculated using the formula: $\frac{(l-20)}{t}$,where t is the reaction time in seconds. The average extension rate was calculated by taking into account the length and the relative intensity of all extension products in a time point. Average extension rate was estimated by calculating the size in nts of each band on the gel (s) and subtracting the primer length (20 nt), then using the imager to determine the relative proportion (with the total being set to 1) of the total extended primers to which each band corresponded (y). The band's contribution to the average extension rate can be represented by the following equation: $(s - 20) * y$. The average extension rate can then be calculated using the following expression:

$$\frac{\Sigma\,[(s - 20) * y]}{t}$$

Where t is the reaction time in seconds. Time points in which none of the extension products had reached the end of the template were chosen for the calculation of the maximal and the average extension rate. For example, time points of 30 s or 1 min were chosen for 0.4 mM Mn^{2+} and 0.4 mM Zn^{2+} reactions (see Fig. 2-1).

2.3 Results

2.3.1 Estimation of average and maximal extension rates of RT synthesis under the alternative divalent cations

Optimal extension conditions for HIV RT with Mg^{2+}, Mn^{2+}, Co^{2+}, and Zn^{2+} in presence of 100 µM dNTPs were determined on a 425 nt RNA template derived from the *gag-pol* region of the HIV genome (as described in [266]). Optimal extension for each cation in the presence of 100 µM of each dNTP was observed at the following concentrations: 2 mM Mg^{2+}, 0.4 mM Zn^{2+}, 0.4 mM Mn^{2+}, and 0.25 mM Co^{2+}. Since a total concentration of 400 µM total nts (100 µM each) was used in the assays, the free concentration of each cation for optimal extension was ~1.6 mM for Mg^{2+}, 0.15 mM for Zn^{2+}, 0.15 mM for Mn^{2+}, and 0.07 mM for Co^{2+}. Note that all 3 alternative cations showed maximal activity at much lower concentrations than Mg^{2+}. This suggests that these alternative cations bind more tightly to RT than the physiological cation. Interestingly, we also found that Cu^{2+} supported RT catalysis but optimum extension occurred at a higher concentration of 3 mM (data not shown). Average and maximum extension rates were then calculated as described in section 2.2.2 using the RNA template used for round 1 synthesis of the PCR-based *lacZα*-complementation fidelity assay. As expected, the rate of synthesis was fastest using Mg^{2+} and slowest with Zn^{2+} (Fig. 2-1 and Table 2-1). An average extension rate of 1.8 ± 0.48 nts/s and a maximal extension rate of 7.4 ± 1.9 nts/s was observed with 2 mM Mg^{2+}, whereas with 0.4 mM

Zn^{2+}, extension rates were 0.03 ± 0.02 nts/s and 0.19 ± 0.10 nts/s, respectively. Both 0.4 mM Mn^{2+} and 0.25 mM Co^{2+} decreased both the average and maximal rate of extension as well (Table 2-1).
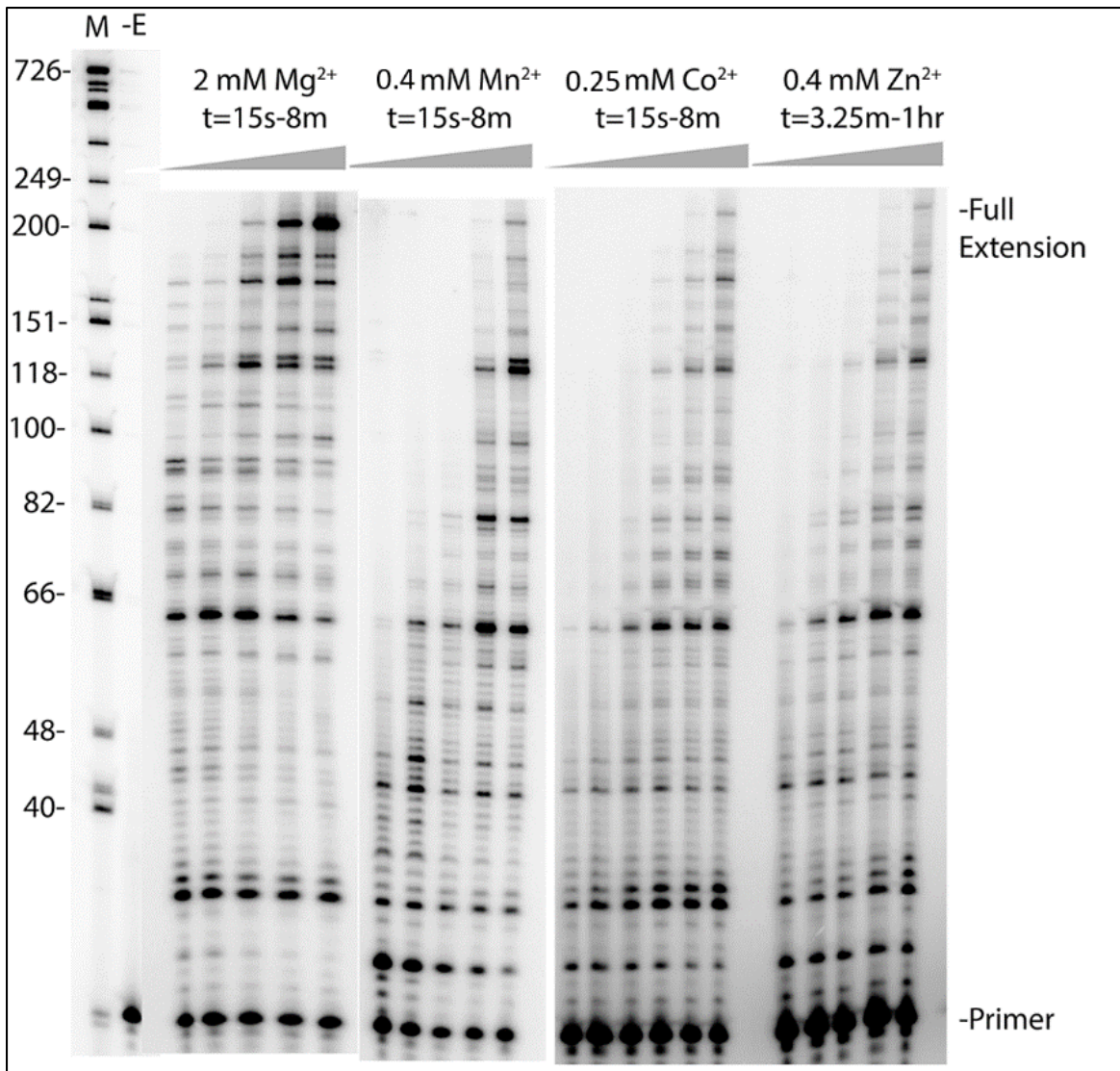
Figure 2-1: Time course of HIV RT synthesis on the ~760 nt RNA template used in the PCR-based α-complementation assay. Shown is an autoradiogram with extension of a 20 nt 5' P-32 end-labeled DNA primer on the RNA template used for round 1 synthesis by HIV RT (see Fig. 2-2). Full extension of the primer resulted in a 199 nt product. A DNA ladder with nt size positions is shown on the left. Concentrations of the cations and dNTPs are indicated above the lanes. Reactions were performed for (1-r) 15 s, 30 s, 1 min, 2 min, 4 min, or 8 min with Mg^{2+}, Mn^{2+}, and Co^{2+}, and 3.25 min, 7.5 min, 15 min, 30 min, and 1 hour with Zn^{2+}. A minus enzyme control (-E) is also shown. Refer to section 2.2.2 for details.

Table 2-1: Synthesis rate on the RNA template for the PCR-based α-complementation fidelity assay at different cation concentrations

Cation	[a]Optimal concentration mM	[b]Maximal extension rate nts /sec	[b]Average extension rate nts/sec
Mg^{2+}	2 (1.6)	7.4 ± 1.9	1.8 ± 0.5
Mn^{2+}	0.4 (0.15)	1.2 ± 0.3	0.48 ± 0.09
Co^{2+}	0.25 (0.07)	1.1 ± 0.1	0.23 ± 0.05
Zn^{2+}	0.4 (0.15)	0.19 ± 0.10	0.03 ± 0.02

[a]The concentration of free cation is shown in parenthesis. Free cation concentration for Mg^{2+} was calculated as described in materials and methods using the dissociation constant for Mg^{2+} and ATP. Free concentrations for alternative cations (Mn^{2+}, Co^{2+}, and Zn^{2+}) were approximately using the dissociation constant for Mg^{2+} and ATP.

[b]Values are averages from 3 experiments ± standard deviation. Rates were calculated as described in materials and methods.

2.3.2 HIV RT shows greater fidelity with Zn^{2+} in the PCR-based and plasmid-based lacZα-complementation fidelity assays

The PCR-based assay was a modified version of an assay used previously to examine the fidelity of poliovirus 3Dpol [296, 302] (Fig. 2-2). The 115 nt region screened for mutations is shown in Fig. 2-2C. The assay is capable of detecting all frameshift mutations and several substitutions (see legend) in this region [6]. The assay essentially mimics the reverse transcription process since both RNA- and DNA-directed RT synthesis steps are performed. Most of the possible background mutations can be accounted for by performing a control in which plasmid DNA is PCR amplified to produce an insert identical to those produced in the complete assay. These inserts should comprise all error sources except the errors derived from HIV RT and T3 RNA polymerase. An average background colony mutant frequency (CMF, number of white or faint blue colonies divided by total colonies) of 0.0019±0.0014 was obtained (Table 2-2). This

corresponds to 1 white or faint blue colony in every ~500 colonies. Further details of this assay

are discussed in section 3.3.1.
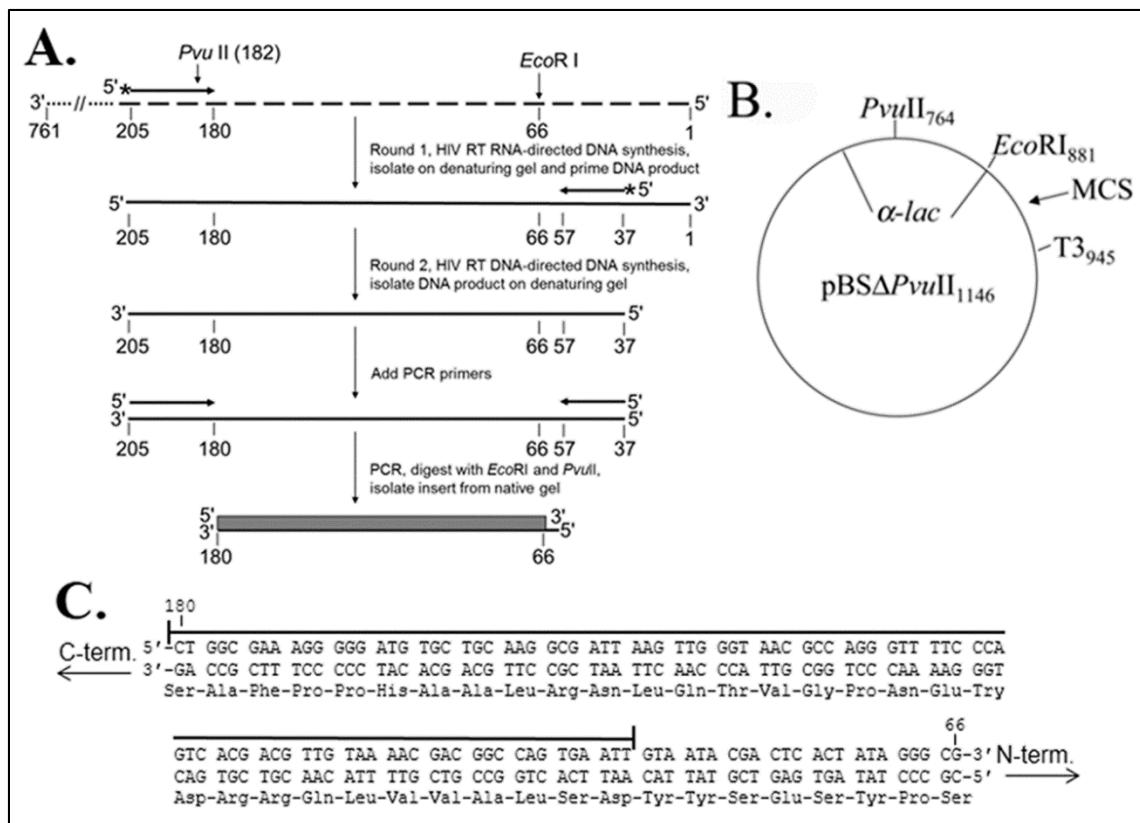
Figure 2-2: PCR-based *lacZα*-complementation system. (A) An overview of the procedure used to assess polymerase fidelity is presented. RNA is represented by broken lines and DNA is represented by solid line. Primers have arrowheads at the 3' end. The ~760 nt template RNA used as the initial template for HIV RT RNA-directed DNA synthesis is shown at the top with the 3' and 5' ends indicated. The positions of PvuII and EcoRI restriction sites are indicated for reference to the vector. The filled box at the bottom of the figure is the 115 base region of the *lacZα* gene that was scored in the assay. Details for specific steps are provided in section 2.2.2. (B) Plasmid pBSM13ΔPvuII$_{1146}$, is shown. Relevant sites on the plasmid are indicated and numbering is based on the parent plasmid (pBSM13+ (Stratagene)). (C) The nt and amino acid sequence for the 115 base region of the *lacZα* gene that was scored in the assay is shown. Both strands of the DNA plasmid are shown since HIV RT synthesis was performed in both directions (Fig. 2-2A). A line is drawn above the 92 nts that are in the detectable area for substitution mutations while frameshifts can be detected over the entire 115 nt region. Based on a previous cataloging of mutations in this gene [6], the assay can detect 116 different substitutions (33.6% of the 345 possible substitutions in the 115 nt sequence) and 100% of the frameshift mutations.

Using 2 mM Mg^{2+}, a CMF value of 0.006 (about 1 mutant colony in every 167 total) was obtained after background subtraction (Table 2-2). Results using Co^{2+} were similar to Mg^{2+} while Zn^{2+} increased fidelity about 2.5-fold (with high statistical significance). Although Co^{2+} is reported to be mutagenic, its effect on the mutation rate of polymerases is concentration-dependent [286, 288, 292]. For example, the error frequency of avian myeloblastosis virus (AMV) RT increased from about 1 error per 1680 nt additions with Mg^{2+} to 1 error per 1100 nt addition with activating concentrations of Co^{2+} (1 mM), but increased further to 1 error per 200 nt addition when excess amounts of Co^{2+} were used (5 mM) [286]. Only 0.07 mM free Co^{2+} was used in these assays and it is possible that Co^{2+} does not have a profound impact on fidelity at this concentration. This was further tested in the gapped plasmid assay described below.

Table 2-2: Colony Mutation Frequencies in PCR-based $lacZ\alpha$-complementation assay

[a]Exp#	[b]Bkg (CMF x 10^{-3})	2 mM $MgCl_2$ [c]1.6 mM free (CMF x 10^{-3})	0.4 mM $ZnCl_2$ 0.15 mM free (CMF x 10^{-3})	0.25 mM $CoCl_2$ 0.07 mM free (CMF x 10^{-3})
[d]1	4/1205 3.3	10/960 10(6.7)	7/1328 5.3(2.0)	
2	3/1726 1.7	13/1826 7.1 (5.4)	5/1315 3.8 (2.1)	16/1639 9.8 (8.1)
3	1/1577 0.6	13/1899 6.8 (6.2)	6/2195 2.7 (2.1)	11/1520 7.2 (6.6)
4	7/2942 2.4	26/3318 7.8 (5.4)	18/2977 6.0 (3.6)	
[e]Avg. ±S.D.	1.9±1.4	7.9±1.4 (5.9±0.6)	4.5±1.5 (2.5±0.8)	8.5±1.8 (7.4±1.1)
[f]P-value			4.4×10^{-4}	0.098
[g]Relative Fidelity		1.0	2.4	0.8
[h]Tukey HSD		P<0.01 (Zn^{2+}) P- N.S. (Co^{2+})	P<0.01 (Mg^{2+}) P<0.01 (Co^{2+})	P<0.01 (Zn^{2+}) P- N.S. (Mg^{2+})

[a]Independent experiments performed at different times. In typical experiments, 1000-3500 colonies were scored for each condition.

[b]In background assays, plasmid pBSM13ΔPVUII (Fig, 2-2B) was used as a template in PCR reactions to generate the insert that was scored in the assays. Numbers shown are the "colony mutation frequency" (CMF) defined as white + faint blue colonies divided by total colonies. Refer to section 2.2.2 for details.

[c]Free cation concentration under each condition was calculated as described in materials and methods using the dissociation constant for Mg^{2+} and ATP.

[d]Numbers shown on top are: (white + faint blue colonies)/total colonies. The bottom number is the colony mutation frequency (CMF) (see b above) for experiments under the listed condition. The CMF minus the background frequency from column two is in parentheses.

[e]Averages ± standard deviations from the experiments in the column are shown.

[f]Values were calculated using a standard Student's t-test and the background subtracted values from each condition. All values were compared to the 2 mM Mg^{2+} condition.

[g]All values are relative to the 2 mM $MgCl_2$ average CMF-Bkg. value (0.0059). The 0.0059 value was divided by the average CMF-Bkg. value for each condition to determine relative fidelity. Higher numbers indicate greater fidelity.

[h]In order to address the effect of comparing multiple sample conditions on statistical significance, ANOVA analysis coupled with a Tukey's honest significance of difference (Tukey HSD) test were conducted using the background subtracted values from all samples and the calculator available online from Statistica: http://statistica.mooo.com/OneWay_Anova_with_TukeyHSD. The cation in parenthesis is being compared to the one listed in the column. N.S.- Not Significant.

A second gapped plasmid-based *lacZα*-complementation fidelity assay, similar to the phage-based *lacZα* gap-filling assay, was performed to further confirm results obtained from the PCR-based assay. The gap filled by the polymerase is in a plasmid construct, which after fill in, is directly transformed into bacteria. Bacterial colonies rather than phage plaques are scored by blue-white screening in this assay. This assay screens a large region (288 nts) of the *lacZα* gene including the promoter sequence and it avoids the enzymatic (T3 RNA polymerase and *Pfu* polymerase) background issues of the PCR-based assay. The results (Table 2-3) were in strong agreement with the PCR-based assay (Table 2-2). In this assay, HIV RT was modestly more accurate with Mg^{2+} than with 0.25 mM Co^{2+}, while Zn^{2+} once again resulted in ~2.5–fold greater fidelity than Mg^{2+}. Interestingly, Mn^{2+}, a known pro-mutagenic cation for several polymerases including HIV RT [289], was comparable to Mg^{2+} in the assays when used at its optimal concentration (0.4 mM total and 0.15 mM free). However, both Co^{2+} and Mn^{2+} were highly mutagenic when used at 6 mM, an amount which is in the same range shown by others to decrease the fidelity of several polymerases *in vitro* [285-289, 303]. There was a ~25-fold decrease in fidelity with 6 mM Mn^{2+} compared to 0.4 mM Mn^{2+}. Similarly, a ~7-fold decrease in fidelity was observed with 6 mM vs. 0.25 mM Co^{2+}. Both cations also showed severely inhibited polymerase activity at the 6 mM concentration, while Zn^{2+} incorporates just a few nts even after prolonged incubation at high concentrations (see [250], results with Co^{2+} here were similar to those shown with Mn^{2+} in this report). Overall, the results from both the PCR-based and gapped plasmid-based *lacZα*-complementation fidelity assays show that the fidelity of RT increases with Zn^{2+} and presumed pro-mutagenic cations do not modify RT's error rate significantly when used at low concentrations optimal for catalysis.

Table 2-3: Colony mutant frequencies in plasmid –based *lacZα*-complementation assay

[a]Exp#	[b]Bkg (CMF x 10^{-3})	2 mM $MgCl_2$ [c]1.6 mM free (CMF x 10^{-3})	0.4 mM $MnCl_2$ 0.15 mM free (CMF x 10^{-3})	6 mM $MnCl_2$ 5.6 mM free (CMF x 10^{-3})	0.25 mM $CoCl_2$ 0.07 mM free (CMF x 10^{-3})	6 mM $CoCl_2$ 5.6 mM free (CMF x 10^{-3})	0.4 mM $ZnCl_2$ 0.15 mM free (CMF x 10^{-3})
[d]1	4/1893	11/1395	10/1297				10/2993
	2.1	7.9(5.8)	7.7(5.6)				3.3(1.2)
2	2/1246	8/1176	7/1067		10/1054		5/1301
	1.6	6.8(5.2)	6.6(5.0)		9.5(7.9)		3.8(2.2)
3	3/3456	10/1755	10/2145		16/1389		14/3799
	0.9	5.7(4.8)	4.7(3.8)		12(11.1)		3.7(2.8)
4	4/1250	10/1192	11/1257		12/1007		
	3.2	8.4(5.2)	8.8(5.6)		12(8.8)		
5	3/3113			160/1823	14/1324	101/1084	
	0.96			88(87)	11(10)	93(92)	
6	7/5866			249/1286		90/1850	
	1.2			194(193)		49(48)	
7	3/2682			375/2740		119/2503	
	1.1			137(136)		48(47)	
[e]Avg.±S.D.	1.6±0.8	7.2±1.7 (5.3±0.4)	7.4±1.8 (5.7±1.6)	140±53 (139±53)	11.1±1.2 (9.5±1.4)	63±26 (62±26)	3.6±0.3 (2.1±0.8)
[f]Statistics (see legend)			0.63	0.0034	0.0012	0.0059	0.00097
[g]Relative Fidelity		1	0.93	0.038	0.56	0.085	2.5

[a]Independent experiments performed at different times.

[b]In background assays, the gapped plasmid was transformed into the bacteria allowing the bacterial polymerases to fill in the gap. Numbers shown are the "colony mutant frequency" (CMF) defined as white + faint blue colonies divided by total colonies. Refer to sections 2.2.2 and 2.3.2 for details.

[c]Free cation concentration under each condition was calculated as described in materials and methods using the dissociation constant for Mg^{2+} and ATP.

[d]Numbers shown on top are: (white + faint blue colonies)/total colonies. The bottom number is the colony mutant frequency (CMF) (see b above) for experiments under the listed condition. The CMF minus the background frequency from column two is in parentheses.

[e]Averages ± standard deviations from the experiments in the column are shown. Values in parentheses are after background subtraction.

[f]P-values shown were calculated using a standard Student's t-test and the background subtracted values from each condition. All values were compared to the 2 mM $MgCl_2$ condition. In order to address the effect of comparing multiple sample conditions on statistical significance, ANOVA analysis coupled with a Tukey's honest significance of difference (Tukey HSD) test were conducted using the background subtracted values from samples and the calculator available online from Statistica: http://statistica.mooo.com/OneWay_Anova_with_TukeyHSD. The 6 mM $MnCl_2$ and $CoCl_2$ conditions were excluded from the analysis as their dramatically different magnitudes compared to other values complicates the analysis. Tukey analysis indicated highly significant differences (P<0.01) for all conditions tested except 2 mM $MgCl_2$ vs. 0.4 mM $MnCl_2$, which was not significant, consistent with the insignificant P value (0.63) from the Student's t-test.

[g]All values are relative to the 2 mM Mg^{2+} average CMF-Bkg. value (0.0053). The 0.0053 value was divided by the average CMF-Bkg. value for each condition to determine relative fidelity. Higher numbers indicate greater fidelity.

2.3.3 Estimation of mutation frequency from CMF and sequencing data

An estimate of the base misincorporation frequency can be made from the CMFs in Table 2-1 and the sequencing results in Fig. 2-3 as described before [10]. In experiments with Mg^{2+}, ~41% (17/42) of recovered mutations, after excluding the background mutations, were insertions or deletions (indels), and ~59% (25/42) substitutions. Using a 33.6% detection rate for substitutions and 100% detection rate for indels in this region (see Fig. 2-2C and accompanying legend) and a CMF of 0.0059 (from Table 2-2), the mutation frequency for Mg^{2+} was 5.6 x 10^{-5}, or ~1 error per 18,000 incorporations ((0.0059 x 0.41)/230 = 1.1 x 10^{-5} for indels, and ((0.0059 x 0.59)/230)/0.336 = 4.5 x 10^{-5} for substitutions, total is 5.6 x 10^{-5} for both (see Fig. 2-3 legend for further details)). Synthesis with Zn^{2+} resulted in a higher ratio of indels vs. substitution: indels ~63% (26/41), and ~37% substitutions (15/41) were obtained. With a CMF of 0.0025 (Table 2-2), a mutation frequency of 1.9 x 10^{-5} or ~ 1 error per 53,000 incorporations was obtained for experiments with Zn^{2+}. This value is near the rate of ~1 error per 77,000 incorporations that was observed with more physiological (0.25 mM), though sub-optimal Mg^{2+} concentrations [250].
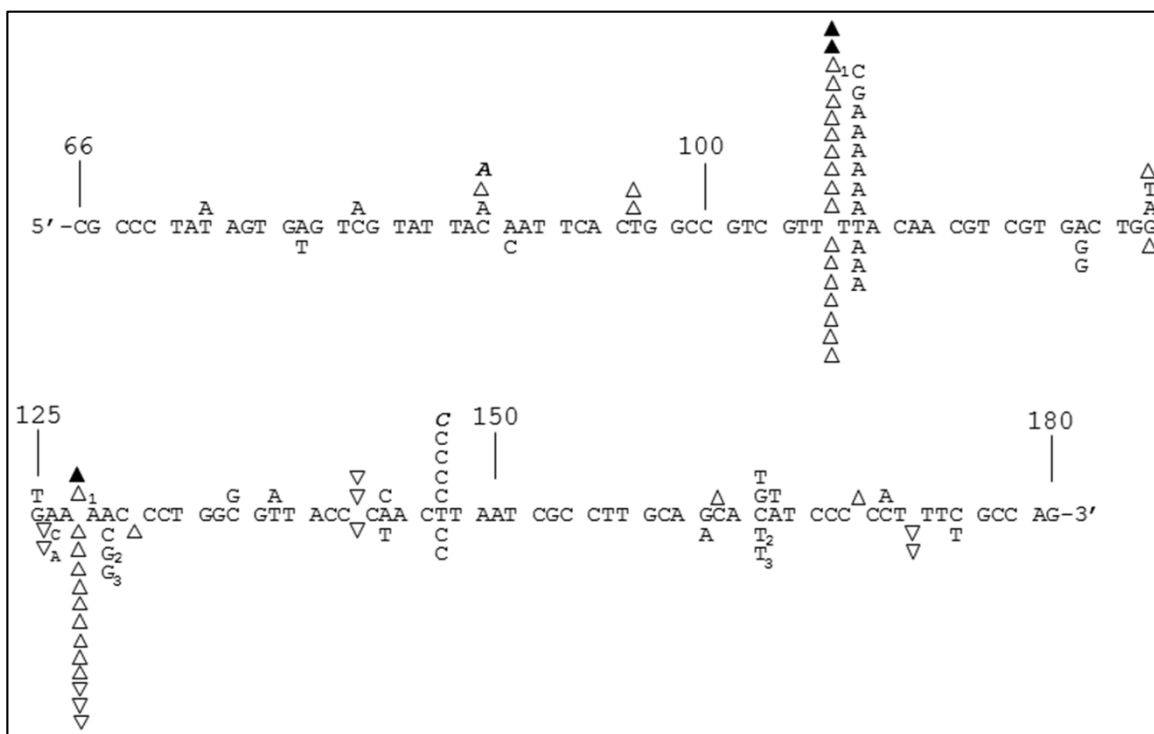
Figure 2-3: DNA sequence analysis from the PCR-based *lacZα*-complementation fidelity assay. The 115 base region analyzed for mutations is shown. The coding strand for *lacZα* is shown in the 5′-3' direction (bottom strand in Fig. 2-2C). Numbering is as shown in Fig. 2-2C. Deletions are shown as regular triangles, insertions are shown as downward triangles with the inserted base shown adjacent to the downward triangle, unless it was the same as the base in a nt run, and base substitutions are shown directly above or below the sequence. Substitutions shown correspond to the recovered sequence for the coding strand; however, these mutations could have occurred during synthesis of the non-coding strand as well (i.e. a C to A change shown here could have resulted from a C to A change during synthesis of the coding strand or a G to T during synthesis of the non-coding strand) (see Fig. 2-2). Mutations recovered from HIV RT with 2 mM Mg^{2+}, and mutations from background controls are shown above the sequence as open triangles and normal text or filled triangles and bold italicized text, respectively. Mutations from HIV RT at 0.4 mM Zn^{2+} are shown below the sequence. Individual sequence clones which had multiple mutations (more than one mutation event) are marked with subscripts adjacent to the mutations. Several clones with deletions (either single or multiple deletions) at positions 181-183, just outside of the scored region were also recovered (not shown). This was the dominant mutation type recovered in background controls (19 out of 24 total sequences) and probably resulted from improper ligation events or damaged plasmid vectors (see **[10]**).

It is also possible to estimate the mutation frequency using the plasmid-based assay results (Table 2-3). As no sequencing data were acquired, a combined error rate for both substitutions and indels can be estimated using the formula: $ER = \frac{CMF}{D \times P}$, where ER is the error rate, CMF is the Colony Mutant Frequency (from Table 2-3), D is the total number of detectable sites for plasmid pSJ2 which is 448, P is the expression frequency of the plasmid which equals 0.444 [297]. The calculations yield a mutation rate of 2.7 x 10^{-5} for 2 mM Mg^{2+} and 1.1 x 10^{-5} for Zn^{2+}. A mutation rate of 2.9 x 10^{-5} for 0.4 mM Mn^{2+} vs. 7.0 x 10^{-4} for 6 mM Mn^{2+} (~24-fold increase) and 4.8 x10^{-5} for 0.25 mM Co^{2+} vs. 3.1 x 10^{-4} for 6 mM Co^{2+} (~7-fold increase) was obtained. Both the PCR-based and plasmid-based assays showed a comparable fidelity increase (~2.5-fold) for Zn^{2+} vs. Mg^{2+}, although the calculated mutation frequency were modestly lower in the plasmid-based assay.

2.3.4 Analysis of fidelity by steady-state kinetics also demonstrates higher fidelity with Zn^{2+}

Kinetic assays have been used by many groups as a reliable way to estimate polymerase fidelity by insertion of specific nt mismatches or extension of specific mismatched primer termini (reviewed in [98, 304, 305]). Although pre-steady-state assays are more useful for understanding kinetic parameters of misincorporation, steady-state assays are much simpler to perform and typically yield results that are broadly similar to results with pre-steady-state assays [98]. Mismatched primer extension and running-start assays using the sequences shown in Fig. 2-4 were performed with constant concentrations of free cation of 0.4 mM Zn^{2+} or 2 mM Mg^{2+}. Note that reactions with each cation were performed using different enzyme concentrations and time points (see section 2.2.2). This was necessary as catalysis with Zn^{2+} is much slower than with Mg^{2+} yielding negligible levels of extension with the conditions used for Mg^{2+}. The results with Zn^{2+} were seemingly consistent with steady-state conditions as the reactions were conducted over a

prolonged period (30 min) and the ratio of unextended to extended primers remained high (i.e. the substrate was not significantly depleted). However, it is possible that these reactions may to some extent reflect pre-steady-state conditions since RT-primer-template complexes are extremely stable in Zn^{2+} while catalysis is slow [266]. Because of these constraints, a direct comparison of the kinetic and equilibrium constants between the two cations cannot be made. However, the fidelity with Zn^{2+} relative to that with Mg^{2+} can still be estimated by comparing misinsertion ratios calculated for particular mismatches with each cation. The running-start assays performed here test RT's ability to misincorporate at a template C or G residue (depending on the sequence) after a "running-start" on a run of T's immediately downstream of the primer 3' terminus. Experiments were analyzed on denaturing polyacrylamide-urea gels (Fig. 2-4B). Statistically relevant (based on P-values) increase in fidelity was observed for all mismatches with Zn^{2+} (Table 2-4). The misinsertion ratio for the G.A mismatch, which is a difficult mismatch to make [10], could not be evaluated with Zn^{2+} as no incorporation was detected (data not shown). In general, there was a ~4-fold to 8-fold increase in fidelity for different mismatches in Zn^{2+} compared to Mg^{2+}.

Figure 2-4: Sequences used in mismatched primer extension and running-start misincorporation assays and examples of analysis. (A) The sequence of the DNA used in each assay type is shown. The underlined nts show the only differences between the two templates. Only one primer was used in the running-start assays and it terminated at the 3' C nt before the dashes. The four dashes indicate the 4 A nts that must be incorporated before RT incorporates the target nt (denoted by X or Y). (B) Running-start misincorporation of C.T base pair at 2 mM Mg^{2+} or 0.4 mM Zn^{2+}. Reactions were performed on the primer-template shown in panel A for the indicated time with a final free concentration of 2 mM Mg^{2+} or 0.4 mM Zn^{2+} (adjusted according to the total concentration of dNTPs in each reaction using the K_d value of Mg^{2+} and ATP). A fixed concentration of dATP = 55 µM was used in all running-start reactions for elongation of the primer to the target site. The concentration of the target nt (dTTP for C.T insertion) in each lane was from l-r: 400, 630, 1380, 2610, and 3660 µM. For other base pair misinsertions noted in the Table 2-4, the target nt was changed according to the desired misinsertion. (C) Extension of a mismatched primer-template with a C.T 3' terminus, using 2 mM Mg^{2+} and 0.4 mM Zn^{2+}. Reactions were performed on the primer-template shown in panel A for the indicated time with the same free cation concentration as above. The concentration of the next correct nt (dCTP) in each lane was from l-r: 50, 100, 200, 400, 630, 1200 and 1870 µM. -E lane corresponds to no enzyme added.

63

Table 2-4: Running-start misincorporation assay of various mismatches with Mg^{2+} or Zn^{2+}

[a]Cation	[b]Base pair	[c]$V_{max,rel}$	[d]K_m μM	V_{max}/K_m μM^{-1}	[e]Misinsertion ratio, f_{ins}	[f]Relative Fidelity	[g]P-value
[h]Mg^{2+}	C.G	2.9 ± 1.1	0.68 ± 0.33	4.3 ± 1.3	1		
	G.C	1.4 ± 0.26	1.2 ± 0.64	1.2 ± 0.6	1		
	C.T	0.55 ± 0.14	1863 ± 670	2.9 (±0.33) x 10^{-4}	6.7 (± 2.6) x 10^{-5}		
	C.A	0.50 ± 0.06	825 ± 217	6.1 (± 1.1) x 10^{-4}	1.4 (± 0.3) x 10^{-4}		
	C.C	0.09 ± 0.07	312 ± 166	2.9 (± 0.8) x 10^{-4}	6.7 (± 1.9) x 10^{-5}		
	G.T	0.36 ± 0.16	242 ± 50	1.5 (± 0.9) x10^{-3}	1.3 (± 0.8) x10^{-3}		
	G.A	0.38 ± 0.11	1515 ± 85	2.5 (± 0.6) x 10^{-4}	2.1 (± 0.5) x 10^{-4}		
Zn^{2+}	C.G	8.2 ± 5.5	0.19 ± 0.09	43 ± 11	1		
	G.C	5.8 ± 5.1	5.1 ± 4.7	1.3 ± 0.6	1		
	C.T	0.19 ± 0.07	244 ± 102	7.8 (±0.97) x 10^{-4}	1.8 (± 0.8) x 10^{-5}	3.7	0.028
	C.A	0.55 ± 0.33	518 ± 43	1.1 (± 0.6) x 10^{-3}	2.5 (± 1.6) x 10^{-5}	5.6	0.0023
	C.C	0.05 ± 0.01	224 ± 104	2.2 (± 1.4) x 10^{-4}	5.1 (± 5.6) x 10^{-6}	13.1	0.029
	G.T	0.2 ± 0.08	914 ± 378	2.2 (± 0.7) x 10^{-4}	1.6 (± 0.6) x 10^{-4}	8.1	0.038
	G.A			N.D.			

[a]The extension reactions were carried as described in Materials and Methods using either 2 mM free Mg^{2+} or 0.4 mM free Zn^{2+}. Free cation concentration was calculated as described in materials and methods using the dissociation constant for Mg^{2+} and ATP. All values are averages from at least 3 experiments ± standard deviation.

[b]Refer to the running-start sequences in Fig. 2-4. The particular mismatch that was measured after incorporation of a run of A's over a run of T's on the template is shown in the column

[c]$V_{max,rel} = I_i/I_{i-1}$ where I_i is the sum of band intensities at the target site and beyond, I_{i-1} is the intensity of the band prior to the target band. See materials and methods for a description.

[d]Refers to the K_m of the nucleotide being incorporated at the target site (e.g. dGTP for C.G and dATP for C.A).

[e]f_{ins} is the ratio of $\{V_{max}/K_m \ (mismatch)\}/\{V_{max}/K_m \ (match)\}$.

[f]Fidelity values for misincorporation in Zn^{2+} are relative to the same mismatch using Mg^{2+}. Determinations were made by dividing the misinsertion ratio in Mg^{2+} by the ratio in Zn^{2+}. Higher values indicate greater fidelity.

[g]Values were calculated using a standard Student's t-test. Misinsertion ratio values from experiments in Zn^{2+} were compared against the Mg^{2+} condition for the same misincorporation.

[h]Values for Mg^{2+} were taken from Chapter 3 (33).

The ability of RT to extend primers with mismatched 3' termini in Mg^{2+} or Zn^{2+} was also evaluated (Fig. 2-4C). Extension was more difficult with Zn^{2+} and the magnitude of difference was dependent on the particular mismatch (Table 2-5). Fidelity increased between ~3- fold to

5- fold for C.T, C.A, and C.C mismatches, however the G.T mismatch showed a statistically

insignificant (P-value of 0.375) change in fidelity. Consistent with results in the running-start

reaction, no extension of the G.A mismatched primer was detected with Zn^{2+}. Overall, results

from running-start and mismatch extension assays are in strong agreement with the *lacZα-*

complementation assays showing that fidelity with HIV RT improves in Zn^{2+}.

[a]Cation	[b]Base pair at the 3' end	[c]V_{max} %/min	[d]K_m µM	V_{max}/K_m	[e]Standard extension efficiency, f_{ext}	[f]Relative Fidelity	[g]P-value
	C.G	21.4 ± 2.0	0.37 ± 0.13	57.8 ± 19.2	1		
	G.C	39.9 ± 14.5	0.27 ± 0.13	147.8 ± 40.6	1		
[h]Mg^{2+}	C.T	22.5 ± 2.1	396 ± 28	5.7 (± 0.9) x 10^{-2}	9.9 (± 1.7) x 10^{-4}		
	C.A	11.1 ± 2.9	445 ± 188	2.5 (± 0. 57) x 10^{-2}	4.3 (± 0.94) x 10^{-4}		
	C.C	0.70 ± 0.29	77 ± 14	9.1 (± 2.2) x 10^{-3}	1.6 (± 0.38) x 10^{-4}		
	G.T	18.6 ± 3.3	157 ± 44	0.12 ± 0.03	8.1 (± 2.5) x10^{-4}		
	G.A	0.95 ± 0.04	196 ± 50	4.8 (± 1.6) x 10^{-3}	3.2 (± 1.0) x 10^{-5}		
	C.G	0.62 ± 0.23	0.04 ± 0.01	15.5 ± 5.8	1	1	
	G.C	0.39 ± 0.10	0.04 ± 0.01	9.8 ± 1.9	1	1	
Zn^{2+}	C.T	2.9 ± 1.0	591 ± 63	4.9 (± 2. 3) x 10^{-3}	3.2 (± 1.6) x 10^{-4}	3.1	0.026
	C.A	3.3 ± 1.0	1240 ± 186	2.7 (± 1.3) x 10^{-3}	1.7 (±0.75) x 10^{-4}	2.5	0.029
	C.C	0.50 ± 0.14	914 ± 457	5.4 (± 4.6) x 10^{-4}	3.5 (± 3.4) x 10^{-5}	4.6	0.023
	G.T	6.8 ± 1.8	1223 ± 568	5.6 (± 2.8) x 10^{-3}	5.7 (± 3.2) x 10^{-4}	1.4	0.375
	G.A			N.D.			

Table 2-5. Mismatched primer extension with Mg^{2+} or Zn^{2+}

[a]The extension reactions were carried out in either 2 mM fee Mg^{2+} or 0.4 mM free Zn^{2+}. Free cation concentration was calculated as described in materials and methods using the dissociation constant for Mg^{2+} and ATP. All values are averages from at least 3 experiments ± standard deviation.

[b]Refer to the mismatch extension sequences in Fig. 2-4. In this assay primers with a matched C.G or a mismatched C.T, C.A, or C.C at the 3' end were extended on one sequence. A second sequence with a matched G.C or mismatched G.T or G.A was also used.

[c]V_{max} is the maximum velocity of extending each primer- template hybrid. See materials and methods for a description.

[d]Refers to the K_m of the next correct nucleotide being added (i.e. dCTP for C.G, C.T, C.A, and C.C or dGTP for G.C, G.T, and G.A extensions).

[e]f_{ext} is the ratio of {V_{max}/K_m (mismatch)}/{V_{max}/K_m (match)}.

[f]Fidelity values for misextension in Zn^{2+} are relative to the same mismatch using Mg^{2+}. Determinations were made by dividing the standard extension efficiency in Mg^{2+} by the same parameter in Zn^{2+}. Higher values indicate greater fidelity.

[g]Values were calculated using a standard Student's t-test. Standard extension efficiency values from experiments in Zn^{2+} were compared against the Mg^{2+} condition for the same mismatch.

[h]Values for Mg^{2+} were taken from Chapter 3 (33).

2.4 Discussion

The results presented in this chapter show that using concentrations optimized for catalysis, Zn^{2+} increases the fidelity of HIV-RT approximately 2-fold to 3-fold when compared to the physiological cation Mg^{2+}. Mn^{2+} and Co^{2+} decreased the fidelity of RT at high concentrations; but at optimal concentrations these effects were almost completely mitigated. For Zn^{2+}, misincorporation (as determined by running-start assays) and mismatch extension (as determined with mismatched primer-templates) were both influenced, suggesting that both steps involved in fidelity could be affected by Zn^{2+}.

There may be several possible mechanisms by which Zn^{2+} alters fidelity. The geometry supported by different cations in the active site of polymerases has been proposed to affect fidelity. Magnesium supports tetrahedral symmetry at the active site, whereas Mn^{2+} accommodates square planar, octahedral, and tetrahedral symmetries (reviewed in [5]). The ability of Mn^{2+} to accommodate more than one type of symmetry may increase the reaction rate of misaligned substrates and hence decrease the fidelity of polymerization. It is important to note that although results presented here indicate Mn^{2+} is not highly mutagenic at optimal concentrations, this may not be the case for other polymerases. Crystal structures of polymerases with Zn^{2+} in the active site are not available, but Zn^{2+} has been crystallized in a distorted tetrahedral symmetry in erythrocyte carbonic-anhydrase [306], as well as in a near tetrahedral geometry in Zn^{2+} superoxide dismutase [307]. It is possible that Zn^{2+} supports a different geometry than Mg^{2+} in the active site and promotes a configuration of the amino acid residues which may be better suited to discriminate against misaligned substrates.

Results showed that the fidelity of HIV RT with Mn^{2+} and Co^{2+} was concentration-dependent, as I observed previously for Mg^{2+} [10]. Although Mn^{2+} is generally considered to be

pro-mutagenic [5], the error frequency for several DNA polymerases usually increased as the Mn^{2+} concentration increased [303]. In one report, *E. coli* DNA polymerase I and mammalian DNA polymerase β both showed relatively high fidelity when lower concentrations (below ~100 µM) of Mn^{2+} were used, whereas higher concentrations lead to greater mutagenesis. The high concentrations correlated with Mn^{2+} binding to the single stranded template and possibly to secondary binding sites on the polymerase, raising the possibility that these factors promote the lower fidelity observed at high Mn^{2+} concentrations [308]. In this regard, *E. coli* DNA polymerase I has been reported to have as many as 21 Mn^{2+} binding sites on a single molecule but just a single high affinity binding site [309]. The effect, if any, of binding at the secondary sites is unknown. Still, when compared to Mg^{2+}, careful analysis with other polymerases has suggested that Mn^{2+} is promutagenic over a range of concentrations [310]. Differences between our results and these may stem from intrinsic differences in the enzymes or the different nucleic acid substrate used (many of the former experiments used homopolymers). Also, unlike RT, most DNA polymerases have intrinsic exonuclease activity. El-Deiry *et al.* [310] found that *E. coli* DNA polymerase I demonstrated a significant reduction in 3' to 5' exonuclease proofreading activity in the presence of Mn^{2+}. This effect exacerbated the accelerated misincorporation with Mn^{2+} which was observed.

It is also possible that Zn^{2+} affects the rate of conformational change in the enzyme and this leads to an alteration in fidelity. Catalysis with Zn^{2+} is extremely slow (Table 1 and [266]) even though the complex between the enzyme and primer-template is over 100 times more stable than with Mg^{2+} [266]. This indicates that one or more of the steps in catalysis is slow. Conformational transition of the protein after binding the substrate has a significant contribution to the ability of RT to add the correct substrate (section 1.3.4) [311]. Upon binding the substrate in Mg^{2+}, the enzyme undergoes a conformational change to reach the transition state. A correctly

matched nt then leads to tight binding and alignment of catalytic residues to promote catalysis, whereas a mismatched nt does not induce the tight binding state, thereby facilitating the rapid opening of the specificity domain and release of the misaligned substrate [311]. The conformational change in the specificity subdomain (fingers subdomain) of the polymerase plays a key role in determining the enzyme fidelity, and it will be interesting to investigate if the modified catalysis with Zn^{2+} affects either the conformational change or the rate of conformational change in a way which might increase the specificity. Consistent with the model of slower catalysis promoting higher fidelity, suboptimal Mg^{2+} concentrations also enhanced fidelity [10]. The observed enhancement was similar to what was observed with Zn^{2+} as it resulted mostly due to a decrease in substitutions rather than insertion and deletion errors. Since insertions and deletions often result from primer-template slippage mechanisms, this suggests that both low Mg^{2+} and Zn^{2+} induce higher fidelity by intrinsically affecting RT catalysis rather than altering primer-template properties. It is possible that lowering the Zn^{2+} concentration to suboptimal levels could also alter fidelity, however, catalysis dramatically declines as the concentration of Zn^{2+} is either lowered or increased [266], making it difficult to test this possibility.

As was noted in section 2.1, the level of available Zn^{2+} and other divalent cations such as Mn^{2+} or Co^{2+} are kept extremely low in cells. Also, it is highly unlikely that these cations could support HIV replication. Although we show the alternative cations can support RT synthesis, the rate of nucleotide catalysis ranged from significantly reduced for Mn^{2+} and Co^{2+}, to essentially negligible for Zn^{2+} (Table 2-1).

Finally, the possibly of using supplements or natural minerals including Zn^{2+} to treat HIV infection must be approached with caution. Low µM concentrations of Zn^{2+}, which can inhibit HIV RT [266], are still ~2–3 orders of magnitude greater than the level of free available Zn^{2+} in

cells. Low µM concentrations of free Zn^{2+} in cells could have profound effects on the transcription of specific genes and the oxidation state of cells. Nevertheless, Zn^{2+} as a constituent of cation based compounds like topical ointments for treating HIV infection still holds promise.

2.5 Concluding remarks

From the results in this chapter, it is clear that DNA synthesis by HIV RT in Zn^{2+} is slow but highly accurate. It was even more accurate than with the physiologically relevant cation Mg^{2+}, when both were used at optimal concentrations. Other presumably pro-mutagenic cations (Mn^{2+} and Co^{2+}) showed fidelity levels that were comparable to Mg^{2+} under optimal conditions, while they were highly mutagenic when used at very high concentrations. This suggests that catalysis with these alternative cations is not intrinsically mutagenic and the observed mutagenicity in previous reports, may result from other mechanisms that could occur at high concentrations (section 2.4) that warrants further investigation.

2.6 Contributions

This chapter was published on May 3, 2015 in the journal "BMC Biochemistry" (DOI: 10.1186/s12858-015-0041-x) with myself (VA) and Jeffrey. J. DeStefano (JD) as authors [312]. I conducted all of the plasmid-based fidelity assays, all of the steady-state assays, and some of the PCR-based fidelity assays. JD conducted some of the PCR-based fidelity assays. Both authors participated in design of the experiments. Both authors read and approved the final manuscript.

Chapter 3 : HIV Reverse Transcriptase displays dramatically higher fidelity using physiological magnesium conditions *in vitro*

3.1 Introduction

Reverse transcriptase (RT), the DNA polymerase of retroviruses, is a key target for highly active antiretroviral therapy (ART) directed against HIV (for a recent review see [313]). The enzyme is a heterodimer with p66 and p51 subunits and like other RTs, possesses both DNA polymerase and ribonuclease H (RNase H) activity (Section 1.3.2) [81]. Both activities are divalent cation-dependent and the polymerase active site contains two divalent cation binding sites. Models for one or two cation binding sites have also been proposed for RNase H [5, 94, 314-318].

Much of what is known about the biochemical properties of HIV RT is based on *in vitro* assays with Mg^{2+} (~5-10 mM) and dNTP (25-100 μM) concentrations optimized for enzyme activity, which are much greater than the available levels in cells. Estimates for free Mg^{2+} concentrations in cells vary considerably from less than 0.25 mM to as high as about 2 mM [319-323]. However, results indicate that free Mg^{2+} concentrations are low in the brain (0.21–0.24 mM) [324], and most relevantly, in human lymphocytes (~0.25 mM), which are one of the main HIV-1 targets [322, 325]. Likewise, deoxy ribonucleotide triphosphate concentrations are also relatively low (5 μM in T cells [326, 327]).

Like other biochemical properties, RT fidelity has typically been examined using conditions optimized for polymerase activity and with *lacZα*-complementation assays [6] or steady-state and pre-steady-state misincorporation and mismatch extension assays (reviewed in [98]). Magnesium concentrations of 5-10 mM (or greater) are often used in these assays. Fidelity measured *in vitro* [96, 98, 104, 105, 328-333] is typically ~5-10-fold lower than the cellular fidelity

[95, 103, 334]. Explanations for this greater fidelity in cells range from cellular or viral proteins (in addition to RT) that participate in reverse transcription, small molecule components in cells, or special conditions in the virion, but the actual cause has remained unknown, as have other effects that the cell environment may have on the reverse transcription process (see [112] for a discussion of this topic). Interestingly, HIV RT displays lower fidelity *in vitro* than other reverse transcriptases (e.g. Moloney murine leukemia virus (MuLV) and avian myeloblastosis virus (AMV)) yet cellular fidelity for these viruses is comparable [98, 99]. In this chapter, I use Mg^{2+} concentrations ranging from 0.25 to 6 mM in both *lacZα*-complementation and steady-state misincorporation or mismatch extension assays. In both assay types, HIV RT fidelity was several-fold higher with low, more physiological Mg^{2+} (0.25 mM). In contrast to HIV RT, the fidelity of MuLV RT was not sensitive to Mg^{2+} concentrations and was approximately equal to that of HIV RT when assayed using more physiological conditions. These results suggest that the higher fidelity of HIV during cellular infection *vs.* classical *in vitro* fidelity assays is due, at least in part, to the lower Mg^{2+} concentration in cells. They also challenge the notion that HIV RT has relatively low fidelity in comparison to other RTs, and that RT infidelity allows HIV to evolve faster than other viruses.

3.2 Materials and Methods

3.2.1 Materials

Calf intestinal alkaline phosphatase (CIP), T3 RNA polymerase, "High Fidelity" (PvuII and EcoRI) and other restriction enzymes, T4 polynucleotide kinase (PNK), and MuLV RT were from New England Biolabs. DNase (deoxyribonuclease)-free RNase (ribonuclease), ribonucleotides, and deoxiribonucleotides were obtained from Roche. RNase free-DNase I was from United Stated Biochemical. Rapid DNA ligation kit, RNasin (RNase inhibitor), and the

phiX174 HinfI digest DNA ladder was from Promega. Radiolabeled compounds were from PerkinElmer. *Pfu* DNA polymerase was from Stratagene. DNA oligonucleotides were from Integrated DNA Technologies. G-25 spin columns were from Harvard Apparatus. RNeasy RNA purification and the Plasmid DNA Miniprep kits were from Qiagen. X-gal was from Denville Scientific, Inc. IPTG and media were from Gibco, Life Technologies. All other chemicals were obtained from Fisher Scientific, VWR, or Sigma. HIV RT (from HXB2 strain) was prepared as described [294]. The HIV RT clone was a generous gift from Dr. Michael Parniak (University of Pittsburgh). Aliquots of HIV-RT were stored frozen at -80°C and fresh aliquots were used for each experiment.

3.2.2 Methods

Polyacrylamide gel electrophoresis. Denaturing polyacrylamide gels (6, 8, and 16% w/v), native polyacrylamide gels (15% w/v), and 0.7% agarose gels were prepared and run as described in Chapter 2.2.2.

Preparation of RNA for the PCR-based *lacZα*-complementation fidelity assay and RNA-DNA and RNA-DNA hybridization. Transcripts (~760 nucleotides) were prepared with T3 RNA polymerase and hybrids were prepared at a 2:1 5' ^{32}P-labeled primer: template ratio as previously described [296].

Primer extension reactions for the PCR-based *lacZα*-complementation fidelity assay. For RNA-directed DNA synthesis, the ~760 nucleotide RNA template was hybridized to a radiolabeled 25 nucleotide DNA primer (5'-GCGGGCCTCTTCGCTATTACGCCAG-3'). Full extension produced a 199 nucleotide final product (see Figs. 2-2). The primer-template complex was pre-incubated in 48 µl of buffer (see below) for 3 min at 37°C. The reaction was initiated by addition

of 2 μl of 5 μM HIV RT in 50 mM Tris-HCl, 80 mM KCl, 1 mM DTT and 10 % glycerol and incubation was continued for 30 min. The final concentration of reaction components were 200 nM HIV RT (or MuLV RT), 25 nM template, 50 nM primer, 50 mM Tris-HCl, 80 mM KCl, 1 mM DTT, 0.4% glycerol and 0.4 units/μl RNasin. Concentrations of $MgCl_2$ (0.25, 2, or 6 mM) and dNTPs (5 or 100 μM each) were as indicated in the text and figure legends. The final pH of the reactions was either 7.7 unless otherwise indicated. After incubations, 1 μl of DNase-free RNase was added and the sample was heated to 65°C for 5 min. Typically two reactions for each condition were combined and material was recovered by standard phenol: chloroform extraction and ethanol precipitation. Pellets were resuspended in 20 μl of 10 mM Tris-HCl (pH 7) and 2X loading buffer (90% formamide, 10 mM EDTA (pH 8), 0.25% each bromophenol blue and xylene cyanol) and products were analyzed by gel electrophoresed on 6% polyacrylamide-urea gels (19:1 acrylamide: bis-acrylamide). Fully extended 199 nucleotide DNA was located using a phosphoimager (Fujifilm FLA5100), and recovered by the crush and soak method [295] in 500 μl of elution buffer containing 10 mM Tris-HCl (pH 7). After overnight elution, this material was passed through a 0.45 μm syringe filter and recovered by ethanol precipitation after addition of 10% volume 3M NaOAc (pH 7) and 50 μg of glycogen. After centrifugation the pellets were vigorously washed with 500 μl of 70% ethanol to remove any traces of EDTA that may have carried over from the gel and potentially interfered with the second round of synthesis. The recovered DNA was hybridized to another 20 nucleotide radiolabeled DNA primer (5'-AGGATCCCCGGGTACCGAGC-3') with 10-fold greater specific activity than the primer used for round one, and a second round of DNA synthesis was performed as described above except the reaction volume was 25 μl. Conditions for $MgCl_2$, dNTPs, and pH were identical in the RNA- and DNA-templated reactions. Reactions were terminated with an equal volume of 2X loading buffer

and products were gel purified as described above but on an 8% gel. The gel was run far enough to efficiently separate the 199 nucleotide templates from the 162 nucleotide full extension product of round 2.

Polymerase chain reaction (PCR) for the PCR-based *lacZα*-complementation fidelity assay. The round two DNA (50% of recovered material) produced above by reverse transcription was amplified by PCR using the following primers: 5'-GCGGGCCTCTTCGCTATTACGCCAG-3' and 5'- AGGATCCCCGGGTACCGAGC -3'. Reactions were performed and processed as previously described except that restriction digestion was with 30 units each of "High Fidelity" EcoRI and PvuII in 50 µl of NEB buffer 3 for 2 hours at 37°C [296].

Preparation of vector for PCR-based *lacZα*-complementation fidelity assay. Thirty µg of the plasmid pBSΔPvuII$_{1146}$ [115] was double-digested with 50 units each of "High Fidelity" EcoRI and PvuII in 100 µl using the supplied buffer and protocol. After 3 hours, DNA was recovered by phenol-chloroform extraction, ethanol precipitation, and then treated with 20 units of CIP for 2 hours at 37°C in 100 µl of the supplied NEB restriction digest buffer 3. Dephosphorylated vector was recovered by phenol-chloroform extraction, ethanol precipitation, and quantified using absorbance at 260 nm. The quality of the vectors for the fidelity assay was assessed in two ways: (a) ligation (see below) of the vector preparation in the absence of insert; and (b) re-ligation of the vector preparation and PvuII-EcoRI cleaved fragment (recovered from agarose gels after cleavage of pBSΔPvuII$_{1146}$ but before dephosphorylation as described above). Vectors from (a) that did not produce any white or faint blue colonies and very few blue colonies in the complementation assay (see below), and those producing colony mutation frequencies of less than ~0.003 (1 white or faint blue colony in ~333 total) in b were used in the fidelity assays.

74

Ligation of PCR fragments into vectors and transformation for the PCR-based lacZα-complementation fidelity assay. The cleaved vector (50 ng, ~0.025 picomoles) and insert fragments (0.05 picomoles) were ligated at a 1:2 (vector:insert) molar ratio using a rapid DNA ligation kit. Ligation and transformation of *E. coli* GC5 bacteria were carried out as previously described [296]. White or faint blue colonies were scored as harboring mutations while blue colonies were non-mutated. Any colonies that were questionable with respect to either being faint blue or blue were pick and replated with and approximately equal amount of blue colony stock. Observing the faint blue colony in a background of blue colonies made it easy to determine if the colony was faint blue rather than blue.

Gapped plasmid-based based *lacZα*-complementation fidelity assay. The gapped version of the plasmid pSJ2 was prepared as described [297]. One nM of the gapped plasmid was filled by 100 nM RT at 37°C in 20 µl of buffer containing 50 mM Tris-HCl, 80 mM KCl, 1 mM DTT, 2 µg of bovine serum albumin, and varying concentrations of dNTPs and $MgCl_2$ (as indicated in legends). The reaction pH was 7.7. Reactions with 2 mM Mg^{2+} (100 µM or 5 µM dNTPs) were carried out for 30 min and reactions with 0.25 mM Mg^{2+} were performed for 4 hours. Reactions were terminated by heating at 65°C for 15 min. After confirming complete extension by restriction digestion analysis (see [297]), ~1 µl of the remaining original mixture was transformed into *E.coli* GC5 cells. The colony mutation frequency (CMF) was determined using blue-white screening as described above.

Mismatched primer extension assays. The approach used for these assays was based on previous results [300]. The template (5'-GGGCGAATTTAG(G/C)TTTTGTTCCCTTTAAGGG TTAATTTCGAGCTTGG-3') used in these assays was a modified version of the template originally described in [301]. The underlined nts in parentheses indicate that templates with either

a G or C at this position were used. The DNA primer
(5'-TAACCCTCACTAAAGGGAACAAAAX-3') used in the assays was 5' radiolabeled and
hybridized to the template at a 1:1 ratio as described above. The "X" at the 3' end of the primer
denotes either G, A, T, or C (see Fig. 2-4). Matched or mismatched primer templates (14 nM final)
were incubated for 3 min at 37°C in 10.5 ul of buffer containing 50 mM Tris-HCl, 1 mM
dithiothreitol, 80 mM KCl, varying concentrations of $MgCl_2$, and increasing concentrations of the
next correct dNTP substrate (dCTP for this template). The reaction pH was 7.7. Reactions were
initiated by adding 2 µl of HIV RT (2 nM final concentration) and terminated by adding 2X loading
buffer. All reactions involving matched primer-templates were carried out for 2 min. Reactions
with mismatched primer-templates were carried out for 5 min (0.5, 1, 2, and 6 mM free Mg^{2+}
reactions). At 0.25 mM Mg^{2+}, mismatched primer-templates with a C.C or G.A were extended for
20 min and all other mismatches were extended for 15 min. The reactions were then
electrophoresed on 16% denaturing polyacrylamide gels, dried, and imaged using a Fujifilm
FLA5100 phosphoimager. Steady-state kinetic parameters K_m, and V_{max} were then calculated as
described below. The amount of free Mg^{2+} in each reaction was adjusted according to the dNTP
concentration because dNTPs are the major chelators of Mg^{2+} in the reactions. The concentration
of free Mg^{2+} was calculated using the formula:

$$[MD] = 0.5(M_t + D_t + K_d) - 0.5((M_t + D_t + K_d)^2 - 4M_tD_t)^{0.5}$$

Where M_t, D_t, and [MD] represent the concentration of total Mg^{2+}, total dNTP, and Mg^{2+} bound to the dNTPs, respectively. The equilibrium dissociation constant (K_d) for dNTP and Mg^{2+} was assumed to be the same as that of ATP, (K_d= 8.9 x 10^{-6} M).

Running-start misincorporation assays. The approach used for these assays was based on previous results [298]. Reactions were performed as above using the same template but with a primer (5'- GAAATTAACCCTCACTAAAGGGAAC -3') (Fig. 2-4) which does not have the last five nts at the 3' end and has 5 additional bases at the 5' end. Unlike mismatch extension assays, all reactions were performed for 3 min at 37°C. The nucleotide directed by the homopolymeric T run on the template running (dATP) was kept at a constant saturating concentration (55 μM) and the nucleotide to be misinserted (for example, dTTP for measuring C-T misinsertion kinetics) was added at increasing concentrations in these reactions. Reactions were resolved and processed as described above.

Velocity measurements and calculation of V_{max} and K_m for steady-state assays and calculation of extension rates for RNA-directed DNA synthesis in the PCR-based fidelity assay. Velocity measurement and calculation of V_{max} and K_m were conducted as described previously for mismatch extension [300] and running-start assays [298]. Extension rate determinations for DNA synthesis on the 760 nucleotide RNA template were performed as described previously [266].

3.3 Results

3.3.1 HIV RT shows greater fidelity with low Mg^{2+} in the PCR-based and plasmid-based

***lacZα*-complementation fidelity assays.**

Both PCR and plasmid-based *lacZα*-complementation assays were used to measure the fidelity of HIV RT. The PCR-based assay was a modified version of an assay used previously to examine the fidelity of poliovirus 3Dpol [296, 302] (refer to Fig. 2-2). The 115 nucleotide region screened for mutations is shown in Fig. 2-2C. All frameshift mutations and several substitutions (see legend) in this region can be detected in the assay [6]. The assay essentially mimics the reverse transcription process since both RNA- and DNA-directed RT synthesis steps are performed. As two rounds of synthesis are performed over the same 115 nucleotide region, the assay actually scores 230 total nts. Although there are several steps where background mutations can be introduced, most of the background can be accounted for by performing a control in which plasmid DNA is PCR amplified to produce an insert identical to those produced in the complete assay. These inserts should comprise all error sources except the errors derived from HIV RT and T3 RNA polymerase. In our assays, an average background colony mutation frequency (CMF, number of white or faint blue colonies divided by total colonies) of 0.0021 ± 0.0008 was obtained for the 16 experiments performed (Table 3-1). This corresponds to 1 white or faint blue colony in every ~500 colonies. This background is higher than some phage-based assays [6, 104, 105] but comparable to others [335, 336].

In the PCR-based assay, *in vitro* conditions that maximize RT activity (6 mM total Mg^{2+}/100 µM dNTPs) consistently showed the highest CMF with about 1 in every 120 colonies (CMF of 0.0083 after background subtraction) showing mutations (Table 3-1). Decreasing the total Mg^{2+} concentration to 2 mM produced a modest (less than 2-fold) decrease in CMF at both

100 µM and the more physiological 5 µM dNTP concentration (Section 3.1), indicating a small increase in fidelity. However, statistical analysis (p-values in Table 3-1) suggested there was not a reliably significant difference between results at 2 mM and 6 mM Mg^{2+}. The 2 mM Mg^{2+} results also suggest that the total dNTP concentration in the reactions is not a major determinant of fidelity as there was no difference in CMFs between the 5 and 100 µM conditions. In contrast, a highly significant (p=0.003) increase in fidelity of about 5-fold over 6 mM reactions was observed with 0.25 mM total Mg^{2+} and 5 µM dNTP. Reactions with 0.25 mM total Mg^{2+} and 100 µM dNTPs produced about a 9-fold increase in fidelity. Note that with this condition, free Mg^{2+} in the reactions was only 0.07 mM. However, the CMFs were on average, less than twice the assay background. Hence, although it is tempting to attribute the further increased fidelity to the very low Mg^{2+} concentration (0.07 mM) in these reactions, assay limitations preclude this conclusion. Overall the results show that low concentrations of free Mg^{2+} (~0.25 mM) reported in lymphocytes (section 3.1) dramatically increase the fidelity of HIV RT.

Other retroviral reverse transcriptases including MuLV RT, have been reported to have higher fidelity than HIV RT (sections 3.1 and 3.4) *in vitro*. The fidelity of MuLV RT was tested in the PCR-based assay with the 6 mM total Mg^{2+}/100 µM dNTP or 0.25 mM total Mg^{2+}/5 µM dNTP conditions. Consistent with previous results, MuLV RT was ~3-fold more accurate than HIV RT with the higher Mg^{2+} concentration commonly used in *in vitro* reactions (Table 3-1). However, unlike HIV RT, there was no improvement in fidelity with the low Mg^{2+} condition. Under this condition, the fidelity of the two RTs was essentially the same.

Table 3-1. Colony mutation frequencies for various Mg^{2+} and dNTP concentrations in PCR-based *lacZα*-complementation assay

[a]Exp#	[b,c]Bkg (CMF x 10^{-3})	[c]6 mM $MgCl_2$ 5.6 mM free 100 µM dNTPs (CMF x 10^{-3}) HIV RT	[c]2 mM $MgCl_2$ 1.98 mM free 5 µM dNTPs (CMF x 10^{-3}) HIV RT	[c]2 mM $MgCl_2$ 1.6 mM free 100 µM dNTPs (CMF x 10^{-3}) HIV RT	[c]0.25 mM $MgCl_2$ 0.24 mM free 5 µM dNTPs (CMF x 10^{-3}) HIV RT	[c]0.25 mM $MgCl_2$ 0.07 mM free 100 µM dNTPs (CMF x 10^{-3}) HIV RT	[c,d]6 mM $MgCl_2$ 5.6 mM free 100 µM dNTPs (CMF x 10^{-3}) MuLV RT	[c,d]0.25 mM $MgCl_2$ 0.24 mM free 5 µM dNTPs (CMF x 10^{-3}) MuLV RT
1	6/4150 1.4	32/3637 8.8 (7.4)						
2	6/4600 1.3	37/4281 6.9 (5.6)						
3	5/1967 2.5	27/1961 14 (12)						
4	13/4560 2.9	51/4583 11 (8.1)						
5	4/5714 0.7				30/10362 2.9 (2.2)			
6	24/8276 2.9				12/2597 4.6 (1.7)			
7	2/1153 1.7		16/2137 7.4 (5.7)		6/2164 2.7 (1.0)			
8	4/4565 0.8		38/8050 4.7 (3.9)		30/10362 2.8 (2.0)			
9	5/1605 3.0		10/1041 9.6 (6.6)	13/1354 9.6 (6.6)				
10	7/2942 2.4			26/3318 7.8 (5.4)		13/3585 3.6 (1.2)		
11	6/2036 2.9			10/1358 6.4 (3.5)		5/1310 3.8 (0.9)		
12	13/3691 3.5			20/2224 8.9 (5.5)		6/1503 4.0 (0.5)		
13	6/2608 2.3			16/1639 9.8 (7.5)				
14	6/2998 2.0						5/1323 3.8 (1.8)	8/1622 4.9 (2.9)
15	7/2464 2.8						23/3720 6.2 (3.4)	20/3402 5.9 (3.1)
16	4/2611 1.5						7/1800 3.9 (2.4)	9/2255 4.0 (2.5)
[e]Avg. ±S.D.	2.1± 0.8	10±3.1 (8.3±2.7)	7.2±2.4 (5.4±1.3)	8.5±1 (5.7±1.5)	3.3±0.9 (1.7±0.5)	3.8±0.2 (0.9±0.4)	4.9±0.9 (2.5±0.8)	4.9±1.0 (2.8±0.3)
[f]p-value			0.157	0.110	0.003	0.006	0.017	0.019
[g]Rel. Fidelity		1	1.5	1.5	4.9	9.2*	3.3	3.0

[a]Independent experiments performed at different times. In typical experiments, 1500-3500 colonies were scored for each condition.

[b]In background assays, plasmid pBSM13ΔPVUII (Fig, 2-2B) was used as a template in PCR reactions to generate the insert that was scored in the assays. See the Results section for a discussion of the background calculation. Numbers shown are the "colony mutation frequency" (CMF) defined as white + faint blue colonies divided by total colonies. Refer to section 3.2.2 for details.

[c](White + faint blue)/Total colonies is shown on top while the colony mutation frequency for experiments under the listed condition are shown below. This frequency minus the background frequency from column two is in parentheses.

[d]Assays were performed with MuLV RT from New England Biolabs. All other reactions were with HIV RT.

[e]Averages ± standard deviations from the experiments in the column are shown.

[f]Values were calculated using a standard Student's t-test and the background subtracted values from each condition. All values were scored against the 6 mM Mg^{2+} 100 µM dNTP condition.

[g]Relative Fidelity, all values are relative to the 6 mM Mg^{2+} 100 µM dNTP average CMF-Bkg. value (8.3 x 10^{-3}). The 0.0083 value was divided by the average CMF-Bkg. value for each condition to determine relative CMF. Higher numbers indicate greater fidelity.

*CMF values for this condition were on average less than 2 times the background. Hence the values are near the limits of this assay with respect to quantitative reliability.

To further confirm results with the PCR-based assay, a second gapped plasmid-based *lacZα*-complementation fidelity assay was performed. This assay is similar to the phage-based *lacZα* gap-filling assay, except that the gap filled by the polymerase is in a plasmid construct. After filling, the plasmid is directly transformed into bacteria, and bacterial colonies rather than phage plaques are scored by blue-white screening [297]. Like most phage-based assays, the assay screens a large region (288 nts) of the *lacZα* gene, including the promoter sequence. Although this assay does not mimic all the steps or reverse transcription, it avoids the enzymatic (T3 RNA polymerase and *Pfu* polymerase) background issues of the PCR-based assay. The results (Table 3-2) were in strong agreement with the PCR-based assay (Table 3-1). Fidelity was lowest with 6 mM (5.6 mM free) Mg^{2+}, improved about 2-fold between 1.98 and 0.6 mM free Mg^{2+}, and improved dramatically (~7-fold) under more physiological conditions (0.24 mM free Mg^{2+}/5 μM dNTPs). Once again, results from the plasmid based *lacZα*-complementation assay are in agreement with the PCR-based assay and the fidelity of RT is considerably high under physiological Mg^{2+} concentrations.

Table 3-2. Colony mutation frequencies for various Mg²⁺ and dNTP concentrations in plasmid-based *lacZα*-complementation assay

[a]Total Mg²⁺ (free Mg²⁺) mM	Total dNTPs µM	White & Faint blue colonies	Total Colonies	[c]Colony Mutation Frequency (CMF) x 10⁻³	[c]CMF-Bkg. x 10⁻³	[d]Relative Fidelity	[e]p-value
[b]Background		17	10138	1.7	--		
6 (5.6)	100	71	4328	16	14	1	
2 (1.98)	5	27	2866	9.4	7.7	1.9	0.0066
2 (1.6)	100	117	12602	9.3	7.6	1.9	<0.0001
1.5 (1.1)	100	51	5983	8.5	6.8	2.1	<0.0001
1 (0.6)	100	54	6492	8.3	6.6	2.1	<0.0001
0.25 (0.24)	5	19	5195	3.7	2.0	7.0	<0.0001

[a]Free Mg²⁺ was calculated as described in materials and methods using the dissociation constant for Mg²⁺ and ATP.

[b]Background was determined by transfecting plasmids with unfilled gaps into bacterial. Numbers shown are the "colony mutation frequency" (CMF) defined as white + faint blue colonies divided by total colonies. Refer to section 3.2.2 for details.

[c]Numbers shown are the colony mutation frequency as described above. The frequency minus the background frequency from the first row (see "b" above) is shown in the column marked CMF-Bkg.

[d]All values are relative to the 6 mM Mg²⁺ 100 µM dNTP CMF-Bkg. value (0.014). The 0.014 value was divided by the CMF-Bkg. value for each condition to determine relative CMF. Higher numbers indicate greater fidelity.

[e]Values were calculated using a Chi square analysis after performing the background correction by subtracting (0.0017 x total colonies) from the white and faint blue colonies for each condition. All values were scored against the 6 mM Mg²⁺ 100 µM dNTP condition.

3.3.2 Estimation of mutation frequency from CMF and sequencing data.

For the PCR-based assay, an estimate of the base misincorporation frequency can be made from the CMFs in Table 3-1 and the sequencing results in Fig. 3-1. Calculations depend on the proportion of errors that were deletions or insertions (indels) *vs.* substitutions, and whether a particular substitution error produces a white or faint blue phenotype. Indels result in frameshift mutations that are always detected as white or faint blue colonies. In contrast, less than half of the substitutions made in the assay result in a mutant phenotype [6]. Sequencing of mutant colonies from experimental controls showed that 19/24 (~79%) had deletion mutations near the PvuII site (Fig. 2-2), probably resulting from inaccurate cleavage or ligation errors. Since the Pfu PCR step is the only polymerase step in the controls, if mutations made during plasmid amplification in the bacteria are ignored, then only 5/24 errors (21%) in the controls resulted from Pfu during PCR. This translates to a Pfu-derived CMF of ~0.0021 (the average CMF value for the control assays in Table 3-1) x 0.21 or 0.0004 which is one Pfu-derived error per 2500 colonies (note that this

estimation is a rough approximate as it is based on only 5 recovered mutation). This is consistent with a mutation rate for Pfu in the ~1-2 x 10^{-6} range reported by others (see example calculation below) [337]. The fact that background mutations were mostly ligation errors outside the region scored for mutations, made it relatively easy to distinguish mutations resulting from HIV RT (or T3 RNA polymerase (see section 3.4)) in the experimental sequences. Excluding these background mutations, in experiments with 6 mM Mg^{2+}/100 µM dNTPs, ~28% (7/25) of recovered mutations were indels and ~72% (18/25) substitutions. This was similar to proportions determined in this laboratory under comparable conditions [115], although there has been significant variation depending on particular investigators and version of the *lacZα*-complementation assay used [104, 105, 328, 331, 338-340]. The assay used here included 230 nts (115 from each round of RT synthesis) of the *lacZα* gene (see Fig. 2-2). Based on the proportion of substitutions to indels from Fig. 3-1, the average CMF of 0.0083 from Table 3-1, and using a 33.6% detection rate for substitutions in this region (see Fig. 2-2C and accompanying legend), the mutation frequency for the 6 mM Mg^{2+}/100 µM dNTP condition would be 8.3 x 10^{-5}, or ~1 error per 12,000 incorporations ((0.0083 x 0.35)/230 = 1.3 x 10^{-5} for indels, and ((0.0083 x 0.65)/230)/0.336 = 7.0 x 10^{-5} for substitutions, total is 8.3 x 10^{-5} for both. Some mutations (4 in the 6 mM condition and 6 in the 0.25 mM condition) were recovered as part of compound mutations as indicated in Fig. 3-1. For calculation purposes, these were counted as a single substitution if they were recovered with another substitution and were counted only in the indel category if they were recovered with a deletion or insertion. Using this approach, for calculation purposes with 6 mM Mg^{2+} and 100 µM dNTPs, 7/20 (35%) and 13/20 (65%) of the mutations were indels or substitutions, respectively.

For the more physiological condition of 0.25 mM Mg^{2+}/5 µM dNTPs, the average CMF from Table 3-1 was 0.0017. Results showed a greater proportion of indels with ~59% (63/106),

and ~41% substitutions (43/106). The same approach yields a mutation frequency of 1.3×10^{-5}, or ~1 error per 77,000 incorporations. This number suggests a fidelity for RT *in vitro* that is similar to replication in cells [95, 103, 112, 334]. Note that the stated proportions of indels *vs.* substitutions underrepresents RT's propensity for making substitutions as only about 1/3 (see above) of the possible substitutions are detectable. Also note that the calculations for error frequency would include error contributions from T3 RNA polymerase (see above), so the actual mutation frequency for HIV RT may be somewhat lower (section 3.4).

Figure 3-1: DNA sequence analysis from the PCR-based *lacZα*-complementation fidelity assay. The 115 base region analyzed for mutations is shown (see Fig. 2-2). The coding strand for *lacZα* is shown in the 5′-3′ direction (bottom strand in Fig. 2-2C). Numbering is as shown in Fig. 2-2C. Deletions are shown as regular triangles, insertions are shown as downward triangles with the inserted base shown adjacent to the downward triangle, unless it was same as the base in a nucleotide run, and base substitutions are shown directly above or below the sequence. Substitutions shown correspond to the recovered sequence for the coding strand; however, these mutations could have occurred during synthesis of the non-coding strand as well (i.e. a C to A change shown here could have resulted from a C to A change during synthesis of the coding strand or a G to T during synthesis of the non-coding strand) (Fig. 2-2). Mutations recovered from HIV RT at 6 mM Mg^{2+} and 100 μM dNTPs, and mutations from background controls are shown above the sequence as open triangles and normal text or filled triangles and bold italicized text, respectively. Mutations from HIV RT at 0.25 mM Mg^{2+} and 5 μM dNTPs are shown below the sequence. Individual sequence clones which had multiple mutations (more than one mutation event) are marked with subscripts adjacent to the mutations. Several clones with deletions (either single or multiple deletions) at positions 181-183, just outside of the scored region were also recovered (not shown). This was the dominant mutation type recovered in background controls (19 out of 24 total sequences) and probably resulted from improper ligation events or damaged plasmid vectors (see Results). Two out of 22 HIV RT-derived sequences at 6 mM Mg^{2+} and 62 out of 162 HIV RT-derived sequences at 0.25 mM Mg^{2+} also had these deletions.

It is also possible to estimate the mutation frequency using the plasmid-based assay results (Table 3-2). As no sequencing data were acquired, it is only possible to obtain a combined error rate for both substitutions and indels. These calculations yield a mutation rate of 7.1 x 10^{-5} for

85

6 mM Mg^{2+}/100 μM dNTPs and 1.0 x 10^{-5} for 0.25 mM Mg^{2+}/5 μM dNTPs (see Ref. [297] for

calculation details). These figures are in strong agreement with those calculated from the PCR-

based assay.

3.3.3 Analysis of fidelity by steady-state kinetics also demonstrates higher fidelity with low Mg^{2+}.

Kinetic assays have been used by many groups as a reliable way to estimate polymerase

fidelity (reviewed in [98, 304, 305]). A major strength of this approach is the ability to analyze

individual types of misincorporations, and also the extension of primers with mismatches at the 3'

end. One drawback is that these assays are typically performed with just a small set of sequences,

so the effect of sequence context on fidelity is limited [341]. In addition, high non-physiological

concentrations of some nucleotides are required to force measurable misincorporation or mismatch

extension in the time scale of the assay. Therefore the assays are non-physiological with respect

to dNTP concentrations, however, physiological levels of Mg^{2+} can be evaluated. We performed

both mismatched primer extension and running-start assays using the constructs shown in

Fig. 2-4A, which we have used previously in fidelity assays [301]. The running-start assays test

RT's ability to misincorporate at a template C or G residue (depending on construct) after a

"running-start" on a run of T's immediately downstream of the primer 3' terminus. Assays shown

in Table 3-3 evaluated these reactions at different concentrations of free Mg^{2+}. Since large

amounts of nucleotides are often added to these types of reactions to force misincorporation,

concentrations of total Mg^{2+} were altered as described in Section 3.2.2 to obtain the desired free

Mg^{2+} concentration. Misincorporation ratios and relative fidelity (compared to the 6 mM free

Mg^{2+} condition which showed the lowest fidelity) were determined by comparing the rate of

misincorporating an A nucleotide, to the rate of adding the correct G nucleotide opposite a C in

the template. Experiments were analyzed on denaturing PAGE gels (Fig. 3-2A). Similar to what was observed in the *lacZα*-complementation assays, fidelity increased modestly between 6 and 0.5 mM Mg^{2+}, reaching almost 3-fold greater by 0.5 mM. Statistical analysis indicated fidelity values for 2 and 1 mM Mg^{2+} were not statistically different compared to the 6 mM Mg^{2+} condition. A large increase to ~7-fold greater fidelity was observed at 0.25 mM Mg^{2+}.
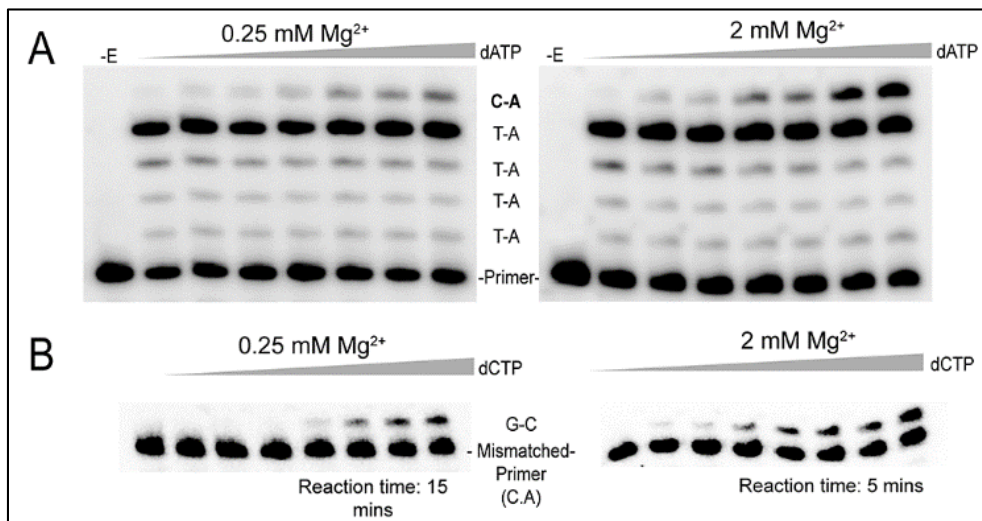
Figure 3-2: Representative experiments for running-start misincorporation and mismatch extension assays. (A) Running-start misincorporation of C.A base pair at 0.25 and 2 mM Mg^{2+}. Reactions were performed on the primer-template shown in Fig. 2-4A for 3 minutes with a final free Mg^{2+} concentration of 0.25 or 2 mM (adjusted according to the total concentration of dNTPs in each reaction using the K_d values of Mg^{2+} and ATP). A fixed concentration of dATP = 55 µM was used in all running-start reactions for elongation of the primer to the target site. The concentration of the target nucleotide (dATP for C.A insertion) in each lane was from l-r: 0, 400, 630, 1380, 2610, and 3660 µM. For other base pair misinsertions noted in the Table 4, the target nucleotide was changed according to the desired misinsertion. -E lane corresponds to no enzyme added. (B) Extension of a mismatched primer-template with a C.A 3′ terminus, using 0.25 and 2 mM Mg^{2+}. Reactions were performed on the primer-template shown in Fig. 2-4B for the indicated time with a final free Mg^{2+} concentration of 0.25 or 2 mM (adjusted as described above). The concentration of the next correct nucleotide (dCTP) in each lane was from l-r: 0, 50, 100, 200, 400, 630, 1200 and 1870 µM. All mismatched primer- templates were extended for 5 minutes at 2 mM Mg^{2+} whereas in 0.25 mM Mg^{2+}, primer -template constructs with a 3' temini of C.C and G.A were extended for 20 minutes and all other mismatched primer-templates were extended for 15 minutes.

Table 3-3: Running-start misincorporation assay with various Mg^{2+} concentrations

[a]Base pair	[b][Mg^{2+}] mM	[c]$V_{max,rel}$	[d]K_m μM	[e]V_{max}/K_m μM^{-1}	[f]Misinsertion ratio, f_{ins}	[g]Rel. Fidelity	[h]p-value
	6	1.5 ± 0.3	0.16 ± 0.06	9.4 ± 1.7	1		
	2	2.9 ± 1.1	0.68 ± 0.33	4.3 ± 1.3	1		
C.G	1	3.1 ± 1.9	0.82 ± 0.43	3.8 ± 0.4	1		
	0.5	2.3 ± 1.1	0.72 ± 0.27	3.2 ± 0.8	1		
	0.25	3.5 ± 2.6	1.3 ± 0.32	2.7 ± 1.8	1		
	6	0.47 ± 0.10	282 ± 24	1.7 (± 0.5) x 10^{-3}	1.8 (± 0.5) x 10^{-4}	1	
	2	0.50 ± 0.06	825 ± 217	6.1 (± 1.1) x 10^{-4}	1.5 (± 0.3) x 10^{-4}	1.2	0.50
C.A	1	0.41 ± 0.06	1025 ± 189	4.0 (± 0.5) x 10^{-4}	1.1 (± 0.1) x 10^{-4}	1.6	0.13
	0.5	0.46 ± 0.06	1841 ± 143	2.5 (± 0.2) x 10^{-4}	7.8 (± 0.7) x 10^{-5}	2.3	0.061
	0.25	0.31 ± 0.14	4574 ± 1221	6.8 (± 2.9) x 10^{-5}	2.5 (± 0.8) x 10^{-5}	7.2	0.00079

[a]Refer to the running-start constructs in Fig. 2-4A. In this assay incorporation of a correct G residue at a template C was compared to incorporation of an incorrect A residue at this same position. All assay included saturating concentrations of dATP to produce a "running-start" over the 4 template T nucleotides that preceded the C.

[b]The concentration of free Mg^{2+} in the reactions is shown. Free Mg^{2+} was calculated as described in materials and methods using the dissociation constant for Mg^{2+} and ATP.

[c]$V_{max,rel} = I_i/I_{i-1}$ where I_i is the sum of band intensities at the target site and beyond, I_{i-1} is the intensity of the band prior to the target band. See materials and methods for a description. Values are averages from at least 3 experiments ± standard deviation.

[d]Refers to the K$_m$ of the nucleotide being incorporated at the target site (dGTP for C.G and dATP for C.A). Values are averages from at least 3 experiments ± standard deviation.

[e]Values are averages from at least 3 experiments ± standard deviation.

[f]f_{ins} is the ratio of $\{V_{max}/K_m \ (mismatch)\}/\{V_{max}/K_m \ (match)\}$ at each Mg^{2+} concentration respectively. Values are averages from at least 3 experiments ± standard deviation.

[g]Values are relative to the 6 mM Mg^{2+} condition. Determinations were made by dividing the misinsertion ratio at 6 mM by the ratios at the other Mg^{2+} concentrations. Higher values indicate greater fidelity.

[h]Values were calculated using a standard Student's t-test. All values were scored against the 6 mM Mg^{2+} condition.

In a second running-start analysis, different mismatches opposite a C or G in the template strand were measured at 2 mM and 0.25 mM free Mg^{2+} (Table 3-4). A pronounced increase in fidelity was observed at the lower concentration for all mismatches, with the exception of G.A. Two mismatch types (C.T, C.C) showed a 2-fold increases in fidelity (note that "Relative Fidelity" in this table is relative to the 2 mM Mg^{2+} reactions rather than 6 mM as was done in Table 3-3), while two other (C.A and G.T) showed ~6-fold greater fidelity with lower Mg^{2+}. In general, fidelity differences were greater for mismatches that tend to be easier for polymerases to make (e.g. C.A and G.T), and lesser for those that are more difficult to make (e.g. C.T, C.C, and G.A).

Table 3-4: Running-start misincorporation assay of various mismatches at 0.25 mM or 2 mM Mg^{2+}

[a]Base pair	[b][Mg^{2+}] mM	[c]$V_{max,rel}$	[d]K_m μM	[e]V_{max}/K_m μM^{-1}	[f]Misinsertion ratio, f_{ins}	[g]Rel. Fidelity	[h]p-value
C.G	2	2.9 ± 1.1	0.68 ± 0.33	4.3 ± 1.3	1		
	0.25	3.5 ± 2.6	1.3 ± 0.32	2.7 ± 1.8	1		
G.C	2	1.4 ± 0.26	1.2 ± 0.64	1.2 ± 0.6	1		
	0.25	3.0 ± 0.96	3.4 ± 1.66	0.9 ± 0.5	1		
C.T	2	0.55 ± 0.14	1863 ± 670	2.9 (±0.33) x 10^{-4}	6.7 (± 2.6) x 10^{-5}	1	0.014
	0.25	0.18 ± 0.06	2004 ± 582	8.9 (± 3.8) x 10^{-5}	3.3 (± 0.8) x 10^{-5}	2.0	
C.A	2	0.50 ± 0.06	825 ± 217	6.1 (± 1.1) x 10^{-4}	1.5 (± 0.3) x 10^{-4}	1	4.7 x 10^{-5}
	0.25	0.31 ± 0.14	4574 ± 1221	6.8 (± 2.9) x 10^{-5}	2.5 (± 0.8) x 10^{-5}	6	
C.C	2	0.09 ± 0.07	312 ± 166	2.9 (± 0.8) x 10^{-4}	6.7 (± 1.9) x 10^{-5}	1	0.040
	0.25	0.24 ± 0.11	2666 ± 478	9.0 (± 2.8) x 10^{-5}	3.3 (± 0.9) x 10^{-5}	2.0	
G.T	2	0.36 ± 0.16	242 ± 50	1.5 (± 0.9) x10^{-3}	1.3 (± 0.8) x10^{-3}	1	0.065
	0.25	0.29 ± 0.05	1488 ± 628	1.9 (± 0.7) x 10^{-4}	2.1 (± 0.8) x 10^{-4}	6.2	
G.A	2	0.38 ± 0.11	1515 ± 85	2.5 (± 0.6) x 10^{-4}	2.1 (± 0.5) x 10^{-4}	1	0.25
	0.25	0.14 ± 0.06	427 ± 23	3.3 (± 2.5) x 10^{-4}	3.7 (± 1.5) x 10^{-4}	0.6	

[a]Refer to the running-start constructs in Fig. 2-4. The particular mismatch that was measured after incorporation of a run of A's over a run of T's on the template is shown in the column.

[b]The concentration of free Mg^{2+} in the reactions is shown. Free Mg^{2+} was calculated as described in materials and methods using the dissociation constant for Mg^{2+} and ATP.

[c]$V_{max,rel} = I_i/I_{i-1}$ where I_i is the sum of band intensities at the target site and beyond, I_{i-1} is the intensity of the band prior to the target band. See materials and methods for a description. Values are averages from at least 3 experiments ± standard deviation.

[d]Refers to the K_m of the nucleotide being incorporated at the target site (dGTP for C.G and dATP for C.A). Values are averages from at least 3 experiments ± standard deviation.

[e]Values are averages from at least 3 experiments ± standard deviation.

[f]f_{ins} is the ratio of $\{V_{max}/K_m\ (mismatch)\}/\{V_{max}/K_m\ (match)\}$ at each Mg^{2+} concentration respectively. Values are averages from at least 3 experiments ± standard deviation.

[g] Relative fidelity values are relative to the 2 mM condition for each mismatch type. Determinations were made by dividing the misinsertion ratio at 2 mM by the ratio at 0.25 mM. Higher values indicate greater fidelity. Values are averages from at least 3 experiments ± standard deviation.

[h]Values were calculated using a standard Student's t-test. Misinsertion ratio values from experiments at 0.25 mM Mg^{2+} were compared against the 2 mM Mg^{2+} condition listed above for each mismatch type.

A second set of assays was used to examine the ability of RT to extend primers with mismatched 3' termini (Fig. 2-4B). Table 3-5 shows results from extension reactions with a C.A mismatch at various Mg^{2+} concentrations. The results were similar to the running-start results with the C.A misincorporation (Table 3-3). Extension of the mismatch was more difficult as the concentration of Mg^{2+} decreased, but there was not a significant difference in comparison to the 6 mM Mg^{2+} result until the Mg^{2+} was lowered to 0.5 mM (as indicated by p-values).

Table 3-5: Extension of C.A mismatched primer-template with various Mg^{2+} concentrations

[a]Base pair 3' end	[b][Mg^{2+}] mM	[c]V_{max} %/min	[d]K_m μM	[e]V_{max}/K_m	[f]Standard extension efficiency, f_{ext}	[g] Rel. Fidelity	[h]p-value
	6	36.4 ± 7.7	0.61 ± 0.10	59.7 ± 12.7	1		
	2	21.4 ± 2.0	0.37 ± 0.13	57.8 ± 19.2	1		
C.G	1	23.8 ± 3.6	0.44 ± 0. 08	54.1 ± 5.0	1		
	0.5	23.2 ± 3.1	0.42 ± 0.07	55.2 ± 2.8	1		
	0.25	24.1 ± 10.8	0.41 ± 0.01	58.8 ± 28.1	1		
	6	9.6 ± 3.6	204 ± 122	4.7 (± 0.14) x 10^{-2}	7.8 (± 0.15) x 10^{-4}	1	
	2	11.1 ± 2.9	445 ± 188	2.5 (± 0. 57) x 10^{-2}	4.3 (± 0.94) x 10^{-4}	1.8	0.10
C.A	1	11.2 ± 4.0	507 ± 194	2.2 (± 0.57) x 10^{-2}	4.0 (± 0.10) x 10^{-4}	2.0	0.11
	0.5	4.4 ± 1.4	311 ± 153	1.4 (± 0.3) x 10^{-2}	2.5 (± 0.71) x 10^{-4}	3.1	0.055
	0.25	4.4 ± 3.9	1546 ± 714	2.8 (± 1.9) x 10^{-3}	4.8 (±3.4) x 10^{-5}	16.3	0.0067

[a]Refer to the mismatch extension constructs in Fig. 2-4. In this assay primers with a matched C.G or a mismatched C.A at the 3' end were extended.

[b]The concentration of free Mg^{2+} in the reactions is shown. Free Mg^{2+} was calculated as described in materials and methods using the dissociation constant for Mg^{2+} and ATP.

[c]V_{max} is the maximum velocity of extending each primer- template construct. See materials and methods for a description. Values are averages from at least 3 experiments ± standard deviation

[d]Refers to the K_m of the next correct nucleotide being added (dCTP for C.G and C.A extension). Values are averages from at least 3 experiments ± standard deviation

[e]Values are averages from at least 3 experiments ± standard deviation .

[f]f_{ext} is the ratio of $\{V_{max}/K_m\ (mismatch)\}/\{V_{max}/K_m\ (match)\}$ at each Mg^{2+} concentration respectively. Values are averages from at least 3 experiments ± standard deviation.

[g]Values are relative to the 6 mM condition. Determinations were made by dividing the standard extension efficiency at 6 mM Mg^{2+} by this same value at other Mg^{2+} concentrations. Higher values indicate greater fidelity.

[h]Values were calculated using a standard Student's t-test. All values were scored against the 6 mM Mg^{2+} condition.

Extension of several mismatch types was also examined at 0.25 mM and 2 mM Mg^{2+}. Once again, extension was more difficult with lower Mg^{2+} and the magnitude of difference was dependent on the particular mismatch (Table 3-6). Small but insignificant differences were observed for G.A and G.T, while C.C, C.T, and C.A mismatches showed more significant difference. In this regard, the mismatch extension assays differed from the misincorporation assays in that there was not a clear trend for Mg^{2+} showing a greater effect with mismatches that are easier to make.

Table 3-6: Mismatched primer extension at 0.25 or 2 mM Mg^{2+}

[a]Base pair at the 3' end	[b][Mg^{2+}] mM	[c]V_{max} %/min	[d]K_m µM	[e]V_{max}/K_m	[f]Standard extension efficiency, f_{ext}	[g]Rel. Fidelity	[h]p-value
C.G	2	21.4 ± 2.0	0.37 ± 0.13	57.8 ± 19.2	1		
	0.25	24.1 ± 10.8	0.41 ± 0.01	58.8 ± 28.1	1		
G.C	2	39.9 ± 14.5	0.27 ± 0.13	147.8 ± 40.6	1		
	0.25	18.7 ± 3.7	0.14 ± 0.03	133.6 ± 14.3	1		
C.T	2	21.2 ± 2.7	500 ± 181	4.2 (± 1.8) x 10^{-2}	7.3 (± 3.3) x 10^{-4}	1	0.013
	0.25	3.1 ± 0.42	748 ± 57	4.1 (± 0. 59) x 10^{-3}	7.1 (± 1.0) x 10^{-5}	10	
C.A	2	11.1 ± 2.9	445 ± 188	2.5 (± 0. 57) x 10^{-2}	4.3 (± 0.94) x 10^{-4}	1	5.2 x 10^{-5}
	0.25	4.4 ± 3.9	1546 ± 714	2.8 (± 1.9) x 10^{-3}	4.8 (±3.4) x 10^{-5}	8.9	
C.C	2	0.70 ± 0.29	77 ± 14	9.1 (± 2.2) x 10^{-3}	1.6 (± 0.38) x 10^{-4}	1	0.027
	0.25	0.20 ± 0.01	61 ± 34	3.3 (± 2.1) x 10^{-3}	5.6 (± 3.6) x 10^{-5}	2.9	
G.T	2	18.6 ± 3.3	157 ± 44	0.12 ± 0.03	8.1 (± 2.5) x10^{-4}	1	0.13
	0.25	8.6 ± 1.5	120 ± 6	7 .2 (± 1.4) x 10^{-2}	5.4 (± 1.1) x 10^{-4}	1.5	
G.A	2	0.95 ± 0.04	196 ± 50	4.8 (± 1.6) x 10^{-3}	3.2 (± 1.0) x 10^{-5}	1	0.23
	0.25	0.50 ± 0.30	169 ± 13	2.9 (± 1.6) x 10^{-3}	2.2 (± 1.3) x 10^{-5}	1.5	

[a]Refer to the mismatch extension constructs in Fig. 2-4. In this assay primers with a matched C.G or a mismatched C.T, C.A, or C.C at the 3' end were extended on one construct. A second construct with a matched G.C or mismatched G.T or G.A was also used.

[b]The concentration of free Mg^{2+} in the reactions is shown. Free Mg^{2+} was calculated as described in materials and methods using the dissociation constant for Mg^{2+} and ATP.

[c]V_{max} is the maximum velocity of extending each primer- template construct. See materials and methods for a description. Values are averages from at least 3 experiments ± standard deviation.

[d]Refers to the K_m of the next correct nucleotide being added (dCTP for C.G, C.T, C.A, and C.C or dGTP for G.C, G.T, and G.A extensions). Values are averages from at least 3 experiments ± standard deviation.

[e]Values are averages from at least 3 experiments ± standard deviation.

[f]f_{ext} is the ratio of $\{V_{max}/K_m\ (mismatch)\}/\{V_{max}/K_m\ (match)\}$ at each Mg^{2+} concentration respectively. Values are averages from at least 3 experiments ± standard deviation.

[g]Values are relative to the 2 mM condition. Determinations were made by dividing the standard extension efficiency at 2 mM Mg^{2+} by the extension efficiency at 0.25 mM Mg^{2+}. Higher values indicate greater fidelity.

[h]Values were calculated using a standard Student's t-test. Misinsertion ratio values from experiments at 0.25 mM Mg^{2+} were compared against the 2 mM Mg^{2+} condition listed above for each mismatch type.

Overall, results from running-start and mismatch extension assays are in strong agreement with the *lacZα*-complementation assays in showing that fidelity improves at lower Mg^{2+} concentrations, and is higher at the proposed physiological levels in lymphocytes [322, 325]. Both misincorporation (as determined by running-start assays) and mismatch extension (as determined with mismatched primer-templates) are influenced, suggesting that both steps involved in fidelity are affected by Mg^{2+} concentrations.

3.4 Discussion

The results demonstrate that the fidelity of HIV RT can be dramatically changed over just a small range of Mg^{2+} concentrations. Using concentrations optimized for RT catalysis (2-6 mM) resulted in about 5- to 7-fold lower fidelity than with concentrations closely mimicking free Mg^{2+} in lymphocytes (~0.25 mM) (Tables 3-1 and 3-2). Fidelity assays, including both steady-state and *lacZα*-complementation assays, showed only modestly lower fidelity with 6 mM *vs.* 2 mM or even 0.5 mM (in steady-state assays) Mg^{2+} (Tables 3-1, 3-2, 3-3, and 3-5). In contrast, a dramatic increase in fidelity was observed at 0.25 mM Mg^{2+}. This may mean that HIV RT fidelity is only modestly sensitive to Mg^{2+} concentrations above 0.5 mM Mg^{2+}.

Significant changes in fidelity in response to Mg^{2+} concentrations have also been demonstrated for *Taq* polymerase [342]. Results showed that fidelity was highest when the concentrations of total dNTPs and Mg^{2+} were equal. When Mg^{2+} was present in excess, fidelity decreased by an order of magnitude or more for some mutation types. Like HIV RT (Tables 3-4 and 3-6), the enhanced fidelity with *Taq* resulted from both a lowered misincorporation rate, and lowered ability to extend mismatched primer-templates. Importantly, the higher fidelity for *Taq* observed under these conditions, also resulted in a reduced rate of synthesis [342]. This is why PCR reactions are typically performed with Mg^{2+} in excess over dNTPs. Interestingly, both Vent

and *Pfu*, thermostable polymerases with proof-reading activity, showed reduced fidelity with low Mg^{2+} concentrations [337]. Therefore, higher fidelity with lower Mg^{2+} does not appear to be a general property of all polymerases. This was also the case with MuLV RT where fidelity was unaffected in high vs. low Mg^{2+} (Table 3-1). In addition to Mg^{2+}, other experiments have shown that non-physiological acidic pH (~5-6.5) can improve the fidelity for several polymerases, including HIV RT [343, 344]. For HIV RT, enhanced fidelity at a lower pH seemed to result mostly from an inability to extend mismatched primer-templates rather than a lowered rate of misincorporation. Our experiments were conducted at pH 7.7 which is slightly higher than normal physiological cytosolic pH (~7.2). However, we also tested the 2 mM Mg^{2+}/100 μM dNTP and 0.25 mM Mg^{2+}/5 μM dNTP conditions at pH 7.1 and found that the pH did not significantly alter fidelity (data not shown). These experiments suggest that RT fidelity is not particularly sensitive to pH within this limited near-physiological range.

The reason why lower Mg^{2+} concentrations increase HIV RT (or *Taq*) fidelity remains to be determined. Reverse transcriptase has at least 3-4 binding sites for divalent cations, 2 in the polymerase active site and 1-2 in the RNase H active site (see section 3.1). It is possible that more sites exist. For example, *E. coli* polymerase I may have as many as 21 divalent cation binding sites and the roles, if any, for those sites not involved in catalysis are unknown [309]. Analysis of retrotransposon RTs suggests that the two binding sites in the polymerase active site domain have vastly different affinities for Mn^{2+} and Mg^{2+}, and occupation of one *vs.* two sites and interactions between the sites can significantly alter RT enzymatic properties [267, 345]. Nucleic acid binding titrations of HIV RT also suggest two or more binding states that are dependent on the concentration of Mg^{2+} [346]. The results presented here are, at least in principle, consistent with RT binding sites that have broadly different affinities for Mg^{2+} controlling fidelity. All the assays

(Tables 3-1 to 3-6) showed a modest effect on fidelity between ~1-6 mM Mg^{2+}, and a much more significant change at low Mg^{2+} concentrations. This suggests that a high affinity binding site which is fully occupied at the higher Mg^{2+} levels may enhance fidelity upon titration. Interplay between this site and lower affinity site(s) may also effect fidelity as was proposed for altering other properties for retrotransposon RTs [267, 345]. It is also conceivable that divalent cation binding in the RNase H site could influence fidelity, as active site mutations in this domain that eliminate RNase H activity can effect fidelity [347]. Finally, the progressive reduction in enzyme efficiency as represented by V_{max}/K_m values in Tables 3-3 and 3-5 as the Mg^{2+} concentration is gradually reduced suggests that the increased fidelity may be a function of the lower velocity of the reaction, which increases the residence time on each template base and therefore affords better discrimination. We are pursuing further experiments with the hope of uncovering further mechanistic details for these observations.

Sequencing results indicated that the proportion of indels vs. substitutions increased in the 0.25 mM vs. 6 mM Mg^{2+} conditions (Fig. 3-1). A significant decrease in substitutions would be predicted based on the running-start assay results (Tables 3-3 and 3-4), so it is possible that low Mg^{2+} increases fidelity mainly by lowering substitutions rather than altering indel rates. The spectrum of mutations obtained with low Mg^{2+} showed both differences and similarities from what has been observed in cells over a similar region of the *lacZα* gene. In the cellular experiments, the ratio of substitutions to indels was skewed toward the former, with a high proportion of G to A mutations [95, 103, 334]. This mutation type along with T to A were the most common substitutions observed in the current work with each comprising 9 of 43 total substitutions. However, the frequency of G to A mutations is still significantly greater in the cellular assays than our assays (see below). The two main hotspots for indels in our assays with low Mg^{2+} (Fig. 3-1)

also matched indel hotspots observed in cellular assays from other groups [95, 110, 334]. There are also differences even between cellular experiments, with one group calculating a much lower rate for the proportion of frameshifts to total recovered mutations than was determined by others (~5% vs. >25%) [95, 103]. A recent report found that although the HIV mutation rate for different cell types was near constant, the spectrum of mutations observed was significantly different [348]. This suggests there may be several factors determining the reverse transcription mutation spectrum including cell type, RT subtype, and the particular assay system used to score mutations. A future goal is to obtain a much larger mutational spectrum dataset *in vitro* that will allow a more comprehensive comparison between mutations made by RT *in vitro* and those made during reverse transcription and replication in cells.

Comparing cellular and in vitro mutation spectrums is complicated by several factors. In the *in vitro* assays performed here or in other reports using an RNA template, T3 or a comparable RNA polymerase is used to make the RNA template. Like the RNA polymerase II enzyme in cells that synthesizes the HIV genome, the error spectrum of T3 and other phage polymerase is unknown. Contributions to the sequence profile from this enzyme are likely small in the 6 mM Mg^{2+} conditions, for which the CMFs were far above the assay background (Table 6), but more significant with 0.25 mM Mg^{2+}. Pfu polymerase, used in the PCR step, has very high fidelity (mutation rate of ~1-2 x 10^{-6} [337]), so its contribution at both Mg^{2+} conditions would be small as was demonstrated (see 3.3). As mentioned in 1.3.3, additional cellular factors can also affect the fidelity of reverse transcription process and it is impossible to mimic the effects of the cellular proteins in a test tube.

Interestingly, results suggest that suboptimal Mg^{2+} concentrations, though modestly decreasing RT's catalytic activity, actually improve DNA synthesis efficiency. Using an *in vitro*

system with a DNA primer and RNA template to mimic the synthesis of strong-stop minus strand DNA (-sssDNA), lower Mg^{2+} levels (~0.1 mM) yielded significantly higher quantities of -sssDNA than reactions performed in higher concentrations (2-6 mM) [299]. The authors suggest that stabilization of some template secondary structures by higher Mg^{2+} leads to more RT pausing. The paused complexes are susceptible to more extensive RNase H cleavage that can destabilize the nascent DNA-RNA template interaction, leading to dissociated "dead-end" DNA synthesis products and "stalled" RT complexes. We conducted similar experiments on the RNA template used for the PCR-based fidelity assay. At physiological dNTP concentrations (5 μM) reactions were modestly more efficient with lower Mg^{2+}, showing a decrease in some pause sites and increase in fully extended products (Fig. 3-3).

3.5 Contributions

This chapter was published on August 2014 in the vol. 88 no. 15 issue of the journal "Journal of Virology" (DOI: 10.1186/s12858-015-0041-x) with myself (VA), Brian. J. Keith (BK), Bernard. A. Connolly (BC), and Jeffrey. J. DeStefano (JD) as authors [10]. I conducted all of the plasmid-based fidelity assays, all of the steady-state assays, and some of the PCR-based fidelity assays. JD conducted some of the PCR-based fidelity assays. BK and BC provided critical reagents for the plasmid-based fidelity assays. VA and JD participated in design of the experiments. VA, BC, and JD critically reviewed the manuscript and all authors approved the final manuscript.
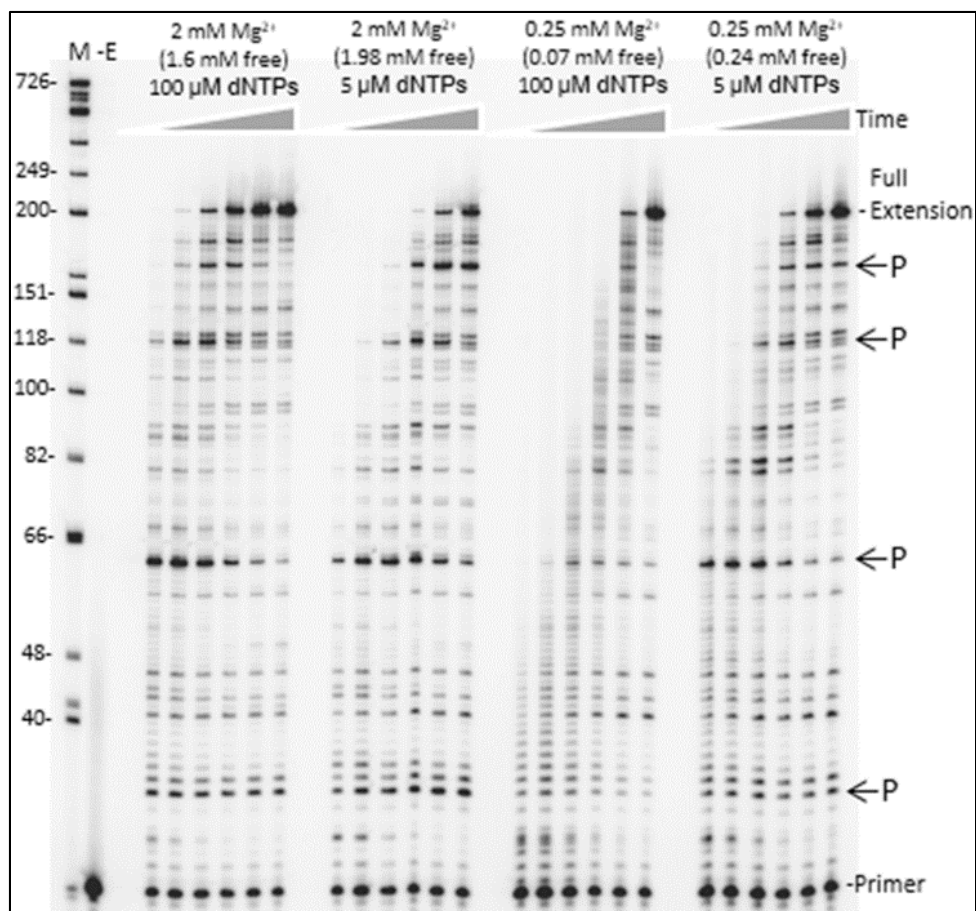
Figure 3-3: Time course of HIV RT synthesis on the ~760 nucleotide RNA template used in the PCR-based α-complementation assay. Shown is an autoradiogram with extension of a 20 nucleotide 5' P-32 end-labeled DNA primer on the RNA template used for round 1 synthesis by HIV RT (see Fig. 2-2). Full extension of the primer resulted in a 199 nucleotide product. A DNA ladder with nucleotide size positions is shown on the left. Concentrations of total and free Mg^{2+} and dNTPs are indicated above each lane. Positions of some prominent DNA synthesis pause sites (P) are indicated on the right. Reactions were performed for (1-r) 15s, 30s, 1m, 2m, 4m, or 8m at each condition. A minus enzyme control (-E) is also shown. Refer to 3.2.2 for details.

Results presented here indicate that the low free Mg^{2+} levels in lymphocytes leads to an increase in HIV RT fidelity, perhaps by several-fold. This brings the fidelity determined *in vitro* in line with that observed in cell culture, both having mutation rates in the ~1-3 x 10^{-5} range [95,

103, 334]. It also brings HIV RT fidelity *in vitro* in the range of the *in vitro* fidelity of other RTs (20). Interestingly, although the fidelity of several RTs (e.g. AMV and MuLV RTs) is reported to be greater than HIV RT *in vitro*, cell culture analysis suggests similar fidelities for the viruses [112]. The cellular results are much more consistent with the findings in this report that show MuLV and HIV RTs have similar fidelity under more physiological conditions (Table 3-1). Although it is not clear why HIV RT fidelity is sensitive to Mg^{2+} levels while MuLV RT is not, HIV RT has a much lower K_m for dNTPs than MuLV RT, a property that allows HIV to replicate in macrophages where the concentration of dNTPs is extremely low [326]. As dNTPs bind in conjunction with Mg^{2+}, this suggests that one or more of the cation binding sites on these enzyme have significantly different properties.

Finally, it could be argued that the concentration of free Mg^{2+} in lymphocytes may fluctuate (e.g. during the cell cycle as nucleotide pools change), and the 0.25 mM level quoted here is based on limited data. Therefore, the level could be higher or even lower, and more work would be required to unequivocally determine the free Mg^{2+} concentration in lymphocytes under different conditions. Although this is true, results presented here for fidelity, and from others for RNA-directed DNA synthesis [299], show that *in vitro* conditions using low Mg^{2+} concentrations yield results that are more consistent with those determined or predicted in cells. This consistency represents a strong argument for those conditions more closely matching cellular conditions, at least for replication in rapidly dividing culture cells.

Chapter 4 : Physiological Mg^{2+} conditions *in vitro* significantly alters the inhibition of HIV-1 and HIV-2 Reverse Transcriptase by nucleoside and non-nucleoside inhibitors

4.1 Introduction

Highly active antiretroviral therapy (ART), since its introduction in the early nineties (1990), has changed HIV from a death sentence to a manageable, though lifelong, condition (section 1.4). However, issues concerning drug resistance, side-effects of the drugs, availability, cost, and delivery infrastructure still remain major concerns, highlighting the need for development of new drugs with better efficacy (see section 1.4.3). A better understanding of the efficacy, interactions between drug and drug-target, and mechanism of action of the existing anti-HIV drugs is pivotal for designing novel drugs. Reverse transcriptase (RT), the DNA polymerase of HIV, is one of the main targets for ART [313]. Nucleoside reverse transcriptase inhibitors (NRTIs) and non-nucleoside reverse transcriptase inhibitors (NNRTIs) targeting RT are heavily used in the ART therapy (section 1.4.1 and [349, 350]).

HIV RT polymerase and RNase H activities, on homopolymeric templates, were found to be optimal at 3-8 mM and 4-12 mM Mg^{2+} respectively [351-354], hence most *in vitro* assays use high Mg^{2+} levels. Studies examining the mechanism of action and resistance against NRTIs and NNRTIs are also usually studied in *in vitro* reactions with optimal, ~5-8 mM Mg^{2+} [355-360]. However, the concentration of free Mg^{2+} in lymphocytes is only ~0.25-0.50 mM, despite higher concentrations (~10 mM) of total cellular Mg^{2+} [322, 325]. The concentration of available Mg^{2+} can have profound effects on the properties of HIV RT. At physiological Mg^{2+} concentrations,

though primer extension is modestly slower, the fidelity of HIV-1 RT is increased several-fold and thereby bringing the *in vitro* error rate of HIV-1 RT close to the cellular estimates of reverse transcription fidelity (Chapter 3) [10]. RNA-directed ssDNA synthesis reactions performed with HIV-1 RT also led to more efficient ssDNA synthesis with less polymerase pausing, and lowered RNase H cleavage in low Mg^{2+} levels [299]. These results at suboptimal Mg^{2+} concentrations, suggest that although RT's catalytic activity is modestly decreased, the DNA synthesis efficiency and fidelity are improved, and indicate that interactions between RT and RT inhibitors could also be affected by Mg^{2+} concentration.

Previous experiments showed that low Mg^{2+} concentrations increased the ability of HIV-1 RT to unblock primers with 3′AZT and decreased the sensitivity of HIV-1 RT for AZTTP and other NRTIs [299]. The authors suggested that the observed effects may be due to a combination of diminished RNase H activity at low Mg^{2+} and altered interactions with NRTIs, although the exact mechanism was not investigated. Potency of the NNRTIs, which form a very critical component of the ART regime, in physiologically relevant low Mg^{2+} concentrations is largely unknown. Determining the underlying mechanism for the observed Mg^{2+} sensitivity of NRTIs and the effect of physiological Mg^{2+} levels on NNRTIs may lead to a better understanding of how these inhibitors function in cells. Examination of HIV-2 RT could help shed light on this subject as, despite showing significant amino acid sequence homology to HIV-1 RT, this enzyme demonstrates marked differences in inhibition by RT inhibitors. HIV-2 RT is structurally different at the "NNRTI pocket" [83] compared to HIV-1 RT, and is not inhibited by most NNRTIs [361]. This fact, along with the resistance shown by HIV-2 against HIV-1 protease and fusion inhibitors has led to limited treatment options against HIV-2 infections [362].

Here, I show that low Mg^{2+} conditions dramatically alter RT's susceptibility to NRTIs and NNRTIs: HIV-1 and HIV-2 RT discriminate against NRTIs with modified 3′- hydroxyl (-OH) groups better at physiologically relevant low Mg^{2+} concentrations compared to optimized *in vitro* conditions. In experiments conducted on a DNA template, NRTIs with 3′- azido (AZT), 3′- thiol (3TC), and 3′- dideoxy (ddC, ddG) groups showed an ~4 to 5-fold decrease in inhibition at low Mg^{2+} (0.25 mM) compared to elevated Mg^{2+} concentrations (6 mM). However, a novel class of NRTIs referred to as translocation-defective RT inhibitors (represented by EfdATP), which has a 3′-OH group, inhibited both HIV-1 and HIV-2 RT with similar efficiency at both low and high Mg^{2+} concentrations. Steady-state kinetic analyses revealed that a lower k_{cat} as well as a higher K_m for the 3′-OH-modified NRTIs resulted in decreased potency of these inhibitors against HIV-1 and HIV-2 RT in low vs. high Mg^{2+} conditions. In contrast, NNRTIs inhibited HIV-1 RT ~4-fold better in low Mg^{2+} vs. high Mg^{2+} concentrations, suggesting that Mg^{2+} also affects the interactions between NNRTI and "NNRTI pocket" of HIV-1 RT. Several drug-resistant HIV-1 RT mutants were also examined and showed similar trends. This chapter, in addition to highlighting the need for studying RT inhibitors in physiologically relevant Mg^{2+} concentrations, also lends insight into ***"Rational Drug Design"*** strategies by implicating interactions between the dNTP 3′-OH group and RT in stabilizing binding interactions. Future inhibitors that either retain or mimic this group (structurally/chemically) may be more effective and more difficult to overcome through development of resistance.

4.2 Materials and Methods

4.2.1 Materials

Calf intestinal alkaline phosphatase (CIP), T3 RNA polymerase, "High Fidelity" (PvuII and EcoRI) and other restriction enzymes, T4 polynucleotide kinase (PNK), and MuLV RT were from New England Biolabs. DNase (deoxyribonuclease)-free RNase (ribonuclease), ribonucleotides, and deoxyribonucleotides were obtained from Roche. RNase free-DNase I was from United States Biochemical. Rapid DNA ligation kit, RNasin (RNase inhibitor), and the phiX174 HinfI digest DNA ladder was from Promega. Radiolabeled compounds were from PerkinElmer. *Pfu* DNA polymerase was from Stratagene. Exonuclease-free Klenow fragment of *E. coli* DNA polymerase I was from United States Biological. DNA oligonucleotides were from Integrated DNA Technologies. G-25 spin columns were from Harvard Apparatus. RNeasy RNA purification and the Plasmid DNA Miniprep kits were from Qiagen. X-gal was from Denville Scientific, Inc. Isopropyl-D-thiogalactopyranoside (IPTG) and media were from Gibco, Life Technologies. AZTTP, ddCTP, and ddGTP were obtained from Perkin Elmer and United States Biologicals. Nevirapine (NVP) and Efavirenz (EFV) were obtained from the NIH AIDS Research and Reference Reagent Program. All other chemicals were obtained from Fisher Scientific, VWR, or Sigma.

4.2.2 Methods

Preparation of enzymes. The clones (pRT66 and pRT51) for HIV-1 RT were a generous gift from Dr. Michael Parniak (Professor Emeritus, University of Pittsburgh) [363]. All the wild type and the mutant proteins of HIV-1 RT were derived from the HXB2 strain. Wild type HIV-1 RT was prepared as described [294]. This enzyme is a non-tagged heterodimer consisting of equal proportions of p66 and p51 subunits. After induction with IPTG, the two plasmids express the p66

and p51 subunits. Bacterial cells individually expressing the p66 and p51 subunits were harvested by centrifugation at 4000 rpm for 30 min. The cell pellet was weighed and stored at -80°C. Cell pellets of both the subunits were mixed and resuspended in the buffer A (50mM Tris–HCl, pH 7.9, 60mM NaCl, 10% glycerol, and 1mM of 2-mercaptoethanol). The cell suspension was sonicated and the debris was removed by ultracentrifugation. The clarified lysate was purified through the Q-Sepharose column followed by the RESOURCE S column. Non-tagged recombinant forms of HIV-1 reverse transcriptases with the mutations D67N, K70R, T215F, K219Q and K65R were provided generously by Dr. Michael Parniak [363, 364].

The plasmid clones for the HIV-1 mutant RT with the K103N mutation and the HIV-2 RT were provided as a gift by Dr. Stephen Hughes (National Cancer Institute). HIV-2 RT was derived from the strain ROD (GenBank accession no. HIV2ROD). After induction with IPTG, these plasmids express the His-tagged version of the respective RT along with the protease (PR). Approximately half of the RT in the bacteria is converted into the small subunit by PR [365]. Both the HIV-1 K103N and HIV-2 RTs were purified in the same manner, as described in [365], but with a small modification. The order of the purification columns were reversed. The bacterial cell lysates were first purified through a Q-Sepharose column. RTs, bound to the Q-sepharose column, were eluted and then purified through a nickel-nitrilotriacetic acid (Ni-NTA) metal affinity column. Aliquots of HIV RT were stored frozen at -80°C and fresh aliquots were used for each experiment.

5'end-labeling of primers. Reactions for labeling various primers were done in a 50-µl volume of the reaction buffer [70mM Tris-HCl (pH = 7.6), 10mM $MgCl_2$, 5mM dithiothreitol (DTT)] containing 50 pmol of the oligo, 5 µL of γ-^{32}P ATP (3,000 Ci/mmol, 10 mCi/mL), and 10 units of T4 polynucleotide kinase. The reaction mixture was incubated for 60 minutes at 37°C,

and then the PNK was heat inactivated for 15 minutes at 70°C. The material was then run through a Sephadex G-25 spin column.

Nucleic Acid Hybridization. Primer–template hybrids were prepared by mixing the template and end-labeled DNA primer at the mentioned ratio in buffer containing 50mMTris-HCl (pH 8), 80mMKCl, and 1mM dithiothreitol (DTT). The mixtures were heated to 65 °C for 5 min and then cooled slowly to room temperature.

Polyacrylamide gel electrophoresis. Denaturing polyacrylamide gels (6, 8, and 16% w/v), native polyacrylamide gels (15% w/v), and 0.7% agarose gels were prepared and run as described [295].

Primer extension reactions. Radiolabeled primer extension reactions were performed to study the inhibition of extension by NRTIs and NNRTIs. For each reaction, 15 nM of the radiolabeled primer (5′-TTGTTGTCTCTTCCCCAAAC-3′) was hybridized with 22.5 nM of the template (5′- TGGCCTTCCCACAAGGGAAGGCCAGGGAATTTTCTTCAGAGCAGACCAG AGCCAACAGCCCCACCAGAAGAGAGCTTCAGGTTTGGGGAAGAGACAACAA- 3′) at a ratio of 1:1.5. Hybrids (Fig. 4-1) were pre-incubated for 3 minutes at 37°C in 8.5 µl of reaction buffer (50 mM Tris-HCl, 1 mM DTT, and 80 mM KCl) along with 6 mM or 0.25 mM free Mg^{2+}, 5 µM dNTPs, and varying concentrations of the NRTIs (as mentioned in the figure legend). Extension was initiated by adding 4 µl of recombinant RTs (final concentration of 100 nM at similar activities of primer extension). After 30 minutes of extension, the reactions were terminated by adding 12.5 µl of the 2X loading dye (90% formamide, 10 mM EDTA (pH 8.0), and 0.025% bromophenol blue and xylene cyanol). NNRTIs were dissolved in 50% dimethyl sulfoxide (DMSO). For primer extension reactions with NNRTIs, RTs were pre-incubated with the NNRTI at room temperature for 10 minutes before extension of the hybrids was initiated. Samples were

then resolved on 8% denaturing urea gel, dried, and imaged using a Fujifilm FLA-5100 or FLA-7000. Since dNTPs and the NRTIs are the major chelators of the divalent cations in these reactions, the amount of free Mg^{2+} in each reaction was adjusted according to the total dNTP and the inhibitor concentration. The approximate concentration of free Mg^{2+} was calculated using the formula:

$$[MD] = 0.5(M_t + D_t + K_d) - 0.5((M_t + D_t + K_d)^2 - 4M_t D_t)^{0.5}$$

Where M_t, D_t, and [MD] represent the concentration of total Mg^{2+} or Zn^{2+}, total dNTP, and Mg^{2+} or Zn^{2+} bound to the dNTPs, respectively. The equilibrium dissociation constant (K_d) for dNTP with Mg^{2+} was assumed to be the same as that of ATP with Mg^{2+}, (K_d= 89.1 x 10^{-6} M) [299]. This assumption leads to an approximate value for the free concentration of Mg^{2+} in reactions.

Primer rescue assay. Primer rescue experiments were conducted according to previously published results [360]. Unlabeled AZTMP-terminated primer was first prepared by incubating 200 pmol of the primer (5′- CTACTAGTTTTCTCCATCTAGACGATACCAGA-3′) with 100 μM AZTTP and 45 units of terminal transferase. AZTMP-terminated primer was then 5′-labeled as described above. The labeled primer was then run on a 15% denaturing gel to isolate the primers with the AZTMP at the 3′ end. 5 nM of the gel purified primer was annealed with 20 nM of the template (5′GAGTGCTGAGGTCTTCATTCTGGTATCGTCTAGATGGAGAAAACTAGT AG-3′). The hybrid was incubated with 200 nM HIV-1 RT or AZTres RT (at similar activities of primer extension), 0.25 or 6 mM free Mg^{2+} (Mg^{2+} adjusted according to the concentration of ATP), and varying concentrations of ATP, as indicated, in 10 µl of buffer containing 50 mM Tris-HCl, 1 mM DTT, and 80 mM KCl for 30 min at 37°C. The reaction was terminated by heating at 90°C for 5 min. The total free Mg^{2+} in 0.25 mM Mg^{2+} reactions was adjusted to 6 mM before proceeding to the next step. The samples were placed on ice for 5 min, followed by addition of 3.5 µl of the same reaction buffer containing exonuclease-free Klenow fragment of *E. coli* DNA polymerase I

(0.1 units/µl) and 100 µM dNTPs. The samples were incubated at 37°C for 30 min. The reaction was terminated by addition of the loading dye and the samples were separated by electrophoresis on a 12% denaturing gel.

Single nucleotide incorporation assay. These assays were performed as described in [326]. Four different 19-mer DNA templates containing sequence variations (**N**) at the 5′ end nucleotide (5′-**N**TGGCGCCCGAACAGGGAC-3′) and a 5′ end labeled 18-mer DNA primer (5′-GTCCCTGTTCGGGCGCCA-3′) was used for the assay (Fig. 4-1). The nucleotide at the 5′end of the primer determines the dNTP or the NRTI to be measured. Primer- template hybrids were generated by mixing the radiolabeled primer and template in the ratio of 1:1, as described above, in the reaction buffer (50 mM Tris-HCl, 1 mM DTT, 80 mM KCl, and 0.1 mg/ml BSA). The primer-template hybrids (10 nM) were pre-incubated in 8 µl of the reaction buffer along with 5 µM $(dT)_{20}$ and 0.25 or 6 mM free Mg^{2+} (Mg^{2+} adjusted according to the concentration of the nucleotide or the NRTI) at 37°C for 3 minutes. Reactions were initiated by adding 2 µl of RT proteins (at similar activities of primer extension) (0.8 or 1.6 nM according to the template) and the reaction was incubated at 37 °C for different times (in order to make sure > 60 % of the primers are extended at the highest nucleotide concentration) according to the enzyme and the nucleotide to be incorporated. HIV-1 RT reactions were done for the following times: dATP and EfdATP reactions for 2 minutes (6 mM Mg^{2+}) and 4 minutes (0.25 mM Mg^{2+}); dCTP and ddCTP reactions for 2 and 4 minutes, respectively, at 6 mM Mg^{2+}, 4 and 30 minutes, respectively, at 0.25 mM Mg^{2+}; dTTP and AZTTP reactions for 4 minutes at 6 mM Mg^{2+}, 10 and 30 minutes, respectively, at 0.25 mM Mg^{2+}. HIV-2 RT reactions were done for the following times: dATP and EfdATP reactions for 2 minutes (6 mM Mg^{2+}) and 4 minutes (0.25 mM Mg^{2+}); dCTP and ddCTP reactions for 4 minutes at 6 mM Mg^{2+}, 10 and 30 minutes, respectively, at 0.25 mM Mg^{2+}; dTTP and AZTTP

reactions for 2 minutes (6 mM Mg^{2+}), 10 and 30 minutes, respectively, at 0.25 mM Mg^{2+}. Reactions measuring dTTP and AZTTP incorporation by AZTr RT were performed for 4 and 10 minutes at 0.25 mM Mg^{2+} and 2 minutes at 6 mM Mg^{2+}. dCTP and ddCTP reactions by K65R RT were performed for 2 and 4 minutes at 6 mM Mg^{2+} and 10 and 30 minutes at 0.25 mM Mg^{2+}. Reactions were terminated with 10 µl of the loading dye and the products were resolved on a 15% denaturing gel. The percent of primer extension in each reaction was calculated by determining the ratio of extended *vs.* total (extended and unextended) primers. The calculated percentage of primer extension was plotted against the concentration of the measured nucleotide or the NRTI. Steady-state constants k_{cat} and K_d were then calculated by standard curve-fitting using the Sigmaplot 10.0 software.

Assays to determine half maximal inhibitory concentration (IC_{50}). The template which was extended by HIV-1 RT with maximum efficiency (5′T) in the previous experiment (Table 4-1) was chosen for this assay. These assays were performed as stated in [366]. The levels of catalysis by recombinant HIV-1 and HIV-1 K103N RT enzymes were determined by measuring the percentage of extension of the labeled hybrid in the presence of different amounts of NNRTIs. The NNRTI compound to be evaluated, (NVP), was serially diluted in 50% DMSO. The reaction mixtures containing 150 nM labeled primer-template, 100 µM dATP, 0.25 mM or 6 mM free Mg^{2+} (adjusted according to the concentration of dATP), and 5% DMSO was pre-incubated at 37°C for 3 minutes in a total volume of 8.5 µl of the reaction buffer (see above). 25 nM of the wild type HIV-1 or K103N RT (at similar activities of primer extension) was pre-incubated with different dilutions of NVP (as mentioned in the figure legends) for 10 minutes at room temperature. Reaction was then initiated by adding the NVP-RT mix to the primer-template hybrid. After 3 minutes of extension, the reactions were stopped by adding 12.5 µl of the 2X loading dye and the

samples were resolved in a 15% denaturing polyacrylamide-7M urea gel. The percentage of primer extension at each concentration of NVP was determined. The IC_{50} value was determined by plotting the percentage of primer extension relative to the logarithm of the inhibitor concentration. A 4-parameter logistic equation was used for curve-fitting with SigmaPlot 10.0 software to obtain IC_{50} for Nevirapine at different conditions.

4.3 Results

4.3.1 Low Mg^{2+} conditions decrease the inhibitory effect of NRTIs lacking a 3′-OH group.

I first tested the influence of the free Mg^{2+} concentration on NRTI inhibition of DNA-dependent DNA synthesis by HIV-1 and HIV-2 RT. A 100 nucleotide-region from the HIV *gag* gene hybridized to a ^{32}P labeled 20 nucleotide primer (Fig. 4-1) was used for ssDNA synthesis at different Mg^{2+} concentrations in the presence of the following triphosphorylated NRTIs (all of which lack a 3′-OH group): zidovudine (AZTTP), zalcitabine (ddCTP), ddGTP, and lamivudine (3TCTP) (Fig. 4-2). These NRTIs compete with cellular dNTPs as substrate for HIV RT and induce chain termination after getting incorporated into the elongating DNA [367]. Inhibition of HIV-1 RT DNA synthesis by these NRTIs was highly Mg^{2+}-dependent. In the experiment shown in Fig. 4-3, the amount of total dNTPs was constant (5 µM each) and the amount of NRTI inhibitor was chosen such that little or no full-length DNA synthesis product was observed at the highest Mg^{2+} concentration used (6 mM free Mg^{2+}). A pronounced decrease in inhibition of DNA synthesis was observed as the concentration of Mg^{2+} was decreased. This was evident from an increase in the amount of fully extended products and a decrease in the intensity of NRTI-terminated products. The presence of weak (hydrogen, ddCTP and ddGTP), moderate (thiol, 3TCTP) or stronger (azido, AZTTP) electronegative groups at the 3′-position of the analogue did not affect the general trend of Mg^{2+}-dependent decrease in inhibition.

The common theme of the inhibitors tested above is the lack of a 3' hydroxyl group (Fig. 4-2). To examine the role of the 3' hydroxyl in stabilizing nucleotide binding at low Mg^{2+} concentrations, another type of NRTI referred to as "translocation defective RT inhibitor" [368, 369] was tested. This new class of drugs (represented by EfdATP) has been shown to inhibit HIV replication at low concentrations with very low toxicity and is highly effective in protecting humanized mice from HIV infections [370]. Translocation inhibitors, despite retaining the 3′ hydroxyl group, inhibit RT by multiple mechanisms [369]. EfdA, stabilizes the enzyme in the pre-translocation site preventing the enzyme from translocating to the next site on the template [371], primarily acting as a chain terminator by blocking RT translocation. In some cases, EfdA functions as a delayed chain terminator allowing incorporation of an additional dNTP before blocking DNA synthesis. EFdA-TP can also be more efficiently misincorporated than dATP by RT, leading to mismatched primers which are extremely hard to extend and are protected from excision [369]. Unlike other NRTIs, chain termination by EFdATP was essentially unaffected by Mg^{2+} concentration (Fig. 4-3). Both the amount of full-length products and the intensities of the EfdA-terminated products were similar at all tested Mg^{2+} concentrations. In addition to supporting the idea that a 3' hydroxyl group is important for stabilizing binding at low Mg^{2+} concentrations, this finding also provides insight for the high efficacy of translocation inhibitors in cell culture. EFdA inhibited HIV-1 replication in activated peripheral blood mononuclear cells with an EC_{50} of 0.05 nM [371].

```
A
  1       20                              100
  |       |                               |

  3'————————————————————————————————5'

B
      ACCGCGGGCTTGTCCCTG-5'
5'- NTGGCGCCCGAACAGGGAC -3'

N= A, T, G, or C (as shown in Tables)
```

Figure 4-1: Schematic representation of the primer-template hybrids used to monitor RT inhibition. A) Primer-template hybrids used in primer extension assays. Numbers indicate size in nts. Primers labeled at 5′-end were hybridized to the 100 nt DNA from the HIV gag region of the genome (nts 1647-1746 of HXB2) and reactions were performed with 5 µM dNTPs and the indicated amount of NRTIs or NNRTIs with increasing concentrations of MgCl$_2$. B) Primer-template constructs used in the steady-state assays. The sequence of the DNA constructs used in the steady-state assay is shown. Different templates with a different nucleotide at the 5′ end (N) and a common primer was used in these assays. Reactions were performed with different nucleotides or the corresponding analogues for times indicated in the table legend.

Figure 4-2: Structures of HIV RT inhibitors used in the study. All nucleoside RT inhibitors except EfdA are analogues of natural dNTPs, with a modified 3′ group. EfdA has modifications in other side chain positions but retain a functional 3′-OH group. Non-nucleoside RT inhibitors are not nucleoside analogues and have a completely different structure. Figure adapted from [1].
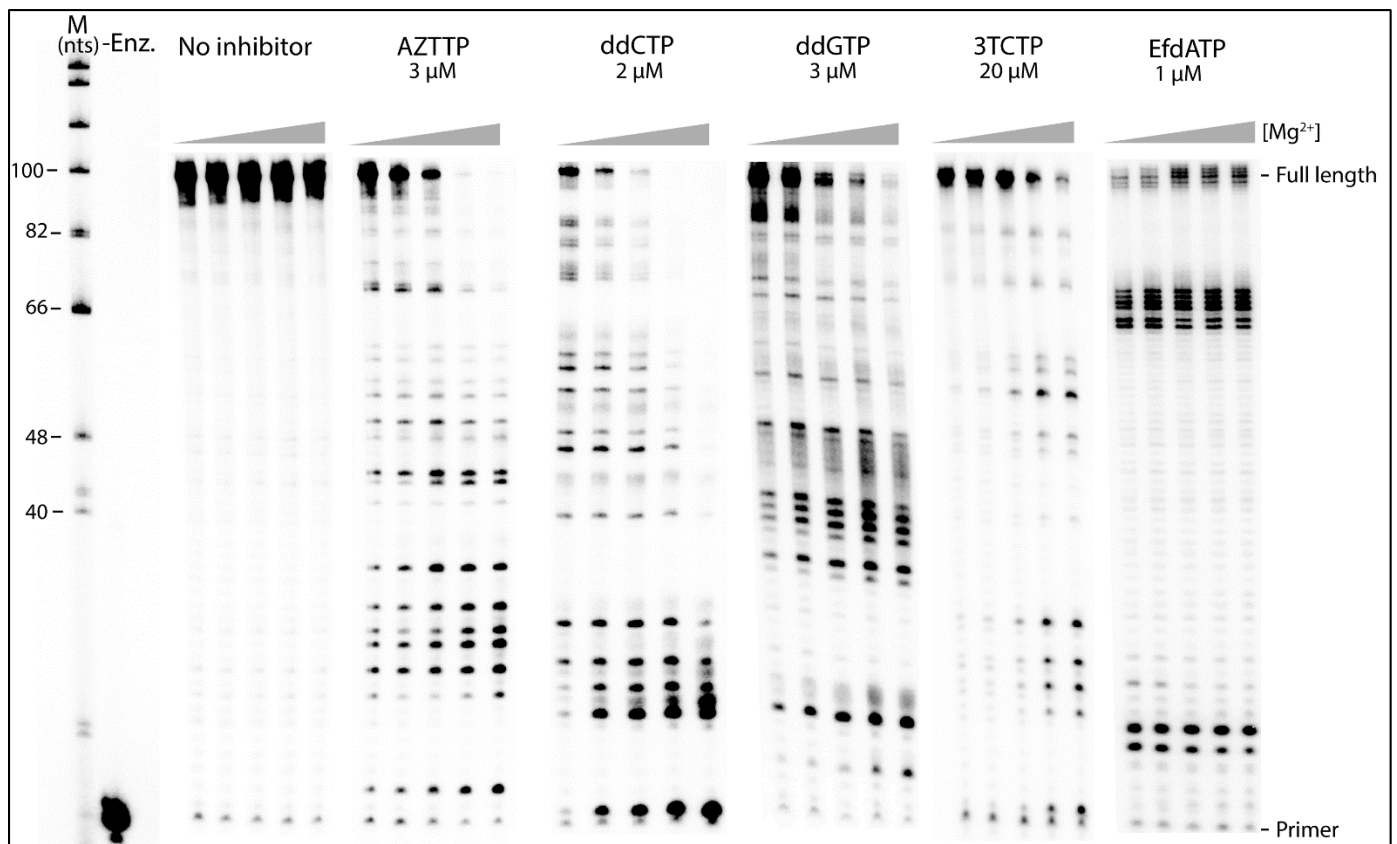
Figure 4-3: HIV-1 RT shows lower inhibition by NRTIs lacking a 3′-OH group at lower Mg²⁺ concentrations. Extension with 100 nM wild type HIV-1 RT was monitored with increasing concentrations of Mg²⁺ (l-r) 0.25, 0.5, 1, 3, and 6 mM and 5 μM dNTP for 30 min along with the indicated concentrations of the NRTI. M represents size marker in nts . -Enz. represents reactions in the absence of enzyme. Decrease in the total amount of fully extended products along with a corresponding increase in the intensity of premature termination products was observed for AZTTP, ddCTP, ddGTP, and 3TCTP, when Mg²⁺ was increased. EfdATP inhibition was however not altered by Mg²⁺ levels.

I then examined if inhibition of HIV-2 RT by NRTIs varies depending on the concentration of Mg^{2+}. Though HIV-1 and HIV-2 RTs have similar polymerase activity [372, 373], there are notable differences with some biochemical properties. HIV-2 RT is less processive than HIV-1 RT [365, 373, 374], and this effect is enhanced under reduced dNTP pools [365]. RNase H activity of HIV-2 RT is about ten-fold lower than that of HIV-1 RT [372]. There are also some reported differences in the susceptibility to zidovudine [375] and HIV-2 RT is not inhibited by 1st generation NNRTIs [376]. However, inhibition of HIV-2 RT DNA synthesis by the NRTIs tested above showed a very similar trend in comparison to HIV-1 RT with lower Mg^{2+} concentrations (Fig. 4-4). The levels of the various NRTIs required to observe little or no inhibition at the highest Mg^{2+} concentration were also similar, although HIV-2 RT was less sensitive than HIV-1 RT to 3TCTP. EfdATP displayed potent inhibition of HIV-2 RT suggesting that it may also be effective in treating HIV-2 infections. Thus, inhibition of HIV-1 and HIV-2 RT DNA synthesis by NRTIs lacking a 3′-OH group is reduced at more physiological Mg^{2+} levels, suggesting that both RTs discriminate against these analogues with better efficiency under these conditions.
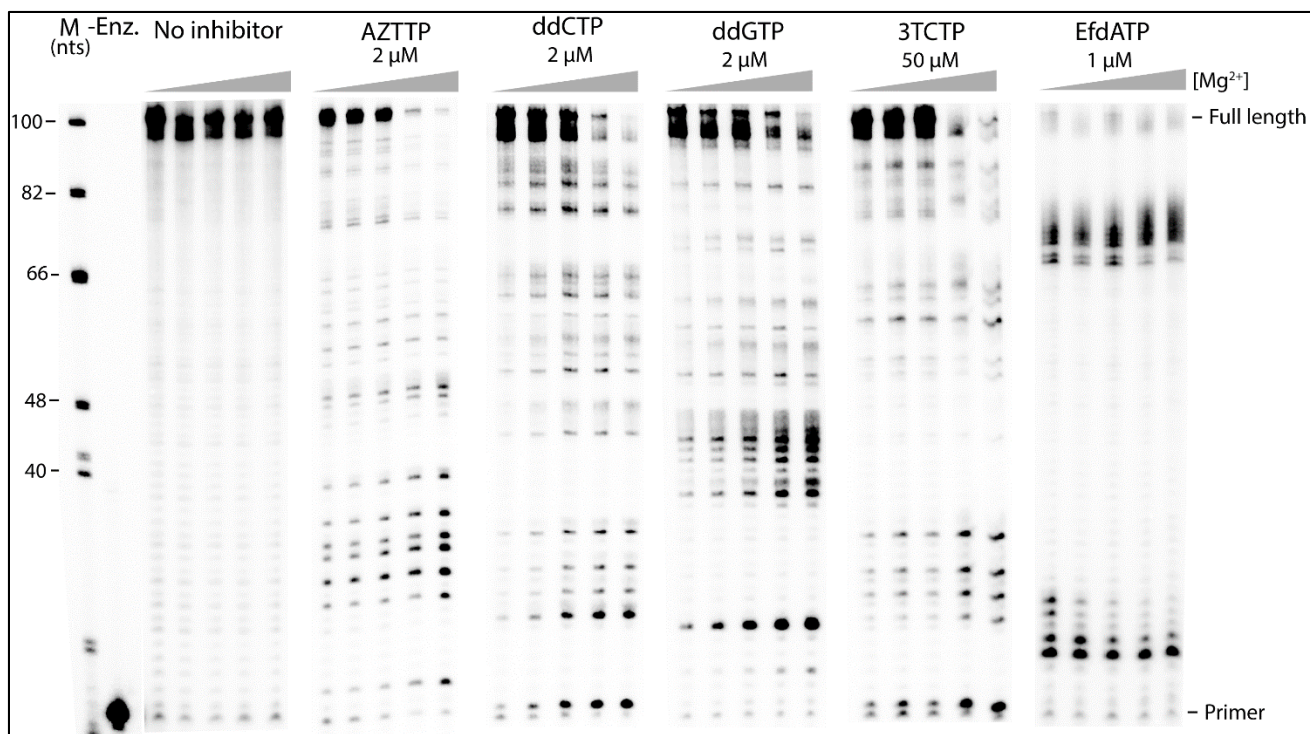
Figure 4-4: HIV-2 RT also shows lower inhibition by NRTIs lacking a 3′-OH group at lower Mg^{2+} concentrations. Primer extension reactions were performed with 100 nM wild type HIV-2 RT, increasing concentrations of Mg^{2+} (l-r) 0.25, 0.5, 1, 3, and 6 mM, 5 µM dNTPs, and the indicated concentrations of the NRTIs for 30 min. -Enz.is reaction with no enzyme. A similar inhibition profile to that of HIV-1 RT was observed for AZTTP, ddCTP, ddGTP, 3TCTP, and EfdATP.

4.3.2 Steady-state kinetic analyses reveal lower affinity as well as slower kinetics of NRTIs lacking a 3′-OH group for HIV-1 and HIV-2 RT.

To further examine the mechanism for decreased NRTI sensitivity with low Mg^{2+}, the V$_{max}$, K$_m$, and k_{cat} for incorporation of AZTTP, ddCTP, and EFdATP by HIV-1 RT was determined using a steady-state assay that examines incorporation of a single nucleotide on a short template (Fig. 4-1,Table 4-1) [326]. The efficiency of incorporation (as judged by k_{cat}/K$_m$) of both the natural substrates (dTTP, dCTP, and dATP) and nucleotide-analogue inhibitors (AZTTP, ddCTP, and EfdATP) was calculated at 6 mM and 0.25 mM free Mg^{2+}. Efficiency of incorporation of the natural substrates decreased when using the lower Mg^{2+} condition (e.g. 4.1-fold for dATP,

Table 4-1), consistent with the decreased extension rate observed at the low Mg^{2+} condition [10]. However, the efficiency of nucleotide analogue inhibitors lacking a 3′-OH group decreased to a much greater extent with 0.25 mM Mg^{2+} (e.g 19-fold for AZTTP). The results with dCTP and ddCTP at 6 mM and 0.25 mM Mg^{2+} also displayed a similar pattern (Table 4-1). This results in AZTTP and ddCTP being less competitive vs. the natural nucleotide with low Mg^{2+}. Lower affinity for AZTTP and ddCTP (higher K_m values compared to the natural substrate at 0.25 mM Mg^{2+}) as well as intrinsically slower kinetics for AZTTP and ddCTP (lower k_{cat} values at 0.25 mM Mg^{2+}) contributed to the observed results. In contrast, a comparable decrease in efficiency was observed at 0.25 mM Mg^{2+} for both dATP and EFdATP (3.3- and 4.3-fold, respectively), consistent with the fact that EfdATP inhibition is unaffected by Mg^{2+} concentrations (Fig. 4-3).

HIV-2 RT, indeed, showed a very similar decrease in efficiency of incorporation of nucleotide analogue inhibitors without a 3′-OH group at low Mg^{2+} conditions (Fig. 4-4). The decrease in efficiency of the natural substrates at 0.25 mM Mg^{2+} (8-fold and 2.2-fold for dTTP and dCTP, respectively) was completely overshadowed by a more dramatic decrease in the efficiency of AZTTP (34-fold) and ddCTP (22-fold). With HIV-2 RT, slower kinetics (i.e. a lower k_{cat}) for AZTTP and ddCTP incorporation was most responsible for the observed results (Table 4-2). The decrease in efficiency observed at 0.25 mM vs. 6 mM Mg^{2+} for dATP and EFdATP were equivalent (5.2-fold and 6.1-fold, respectively). These results are consistent with EFdATP maintaining potent inhibition against both HIV-1 and HIV-2 RTs with low Mg^{2+} (Figs. 4-3 and 4-4).

116

Table 4-1: V$_{max}$, K$_m$, and *k$_{cat}$* determinations for TTP and AZTTP, dCTP and ddCP, or dATP and EFdATP at different Mg^{2+} concentrations using HIV-1 RT

[a]Condition	V$_{max}$ (nM/min)	[b]*k$_{cat}$* (min^{-1})	K$_m$ (µM)	*k$_{cat/}$* K$_m$ [c](fold decrease)	[d]p value
6 mM Mg^{2+} dTTP	1.1 ± 0.1	1.3 ± 0.09	2.3 ± 0.2	0.57	-
0.25 mM Mg^{2+} dTTP	0.65 ± 0.07	0.81 ± 0.09	5.7 ± 0.7	0.14 (4.1)	<0.001
6 mM Mg^{2+} AZTTP	0.95 ± 0.08	1.2 ± 0.09	2.3 ± 0.4	0.52	-
0.25 mM Mg^{2+} AZTTP	0.26 ± 0.01	0.32 ± 0.01	12 ± 1	0.027 (19)	<0.001
6 mM Mg^{2+} dCTP	2.1 ± 0.1	1.0 ± 0.1	1.3 ± 0.4	0.77	-
0.25 mM Mg^{2+} dCTP	1.4 ± 0.1	0.68 ± 0.03	3.9 ± 1.7	0.17 (4.5)	0.05
6 mM Mg^{2+} ddCTP	1.4 ± 0.2	0.72 ± 0.08	5.0 ± 0.3	0.14	-
0.25 mM Mg^{2+} ddCTP	0.23 ± 0.05	0.12 ± 0.03	12.5 ± 3.5	0.01 (18)	< 0.001
6 mM Mg^{2+} dATP	2.1 ± 0.2	2.6 ± 0.3	2.2 ± 0.8	1.2	-
0.25 mM Mg^{2+} dATP	0.72 ± 0.08	0.90 ± 0.09	2.5 ± 1.1	0.36 (3.3)	0.1
6 mM Mg^{2+} EFdATP	0.72 ± 0.02	0.90 ± 0.01	1.1 ± 0.1	0.82	-
0.25 mM Mg^{2+} EFdATP	0.53 ± 0.27	0.66 ± 0.35	3.5 ± 2.2	0.19(4.3)	0.1

(HIV-1 RT)

a- Assays were conducted with a 20 nucleotide template and 19 nucleotide 5' end labeled primer as described [326]. The single template-directed nucleotide was a T opposite an A, a C opposite a G, or an A opposite a T for AZT, ddCTP, and EFdATP, respectively. All assay used 0.8 nM RT. Results were ave. of 3 exp. ± S.D.
b- *k$_{cat}$* was calculated by dividing V$_{max}$ by the enzyme concentration (0.8 nM).
c- Fold decrease in enzyme efficiency (as judged by *k$_{cat/}$* K$_m$) compared to the 6 mM result (number above) with the same nucleotide or inhibitor.
d- Values were calculated using a standard Student's t-test.

Table 4-2: V$_{max}$, K$_m$, and *k$_{cat}$* determinations for TTP and AZTTP, dCTP and ddCP, or dATP and EFdATP at different Mg^{2+} concentrations using HIV-2 RT

[a]Condition	V$_{max}$ (nM/min)	[b]*k$_{cat}$* (min^{-1})	K$_m$ (µM)	*k$_{cat/}$* K$_m$ [c](fold decrease)	[d]p value
6 mM Mg^{2+} dTTP	0.48 ± 0.07	1.2 ± 0.19	3 ± 0.99	0.40	-
0.25 mM Mg^{2+} dTTP	0.25 ± 0.09	0.31 ± 0.11	6.1 ± 1.1	0.05 (8)	0.001
6 mM Mg^{2+} AZTTP	0.82 ± 0.45	1.5 ± 0.44	4.4 ± 1.8	0.34	-
0.25 mM Mg^{2+} AZTTP	0.05 ± 0.03	0.07 ± 0.04	7.2 ± 1.5	0.01 (34)	0.001
6 mM Mg^{2+} dCTP	1.2 ± 0.23	0.78 ± 0.15	6.9 ± 2	0.11	-
0.25 mM Mg^{2+} dCTP	0.42 ± 0.02	0.26 ± 0.01	5.3 ± 2.4	0.05 (2.2)	0.01
6 mM Mg^{2+} ddCTP	0.99 ± 0.63	0.62 ± 0.39	5.1 ± 2.3	0.12	-
0.25 mM Mg^{2+} ddCTP	0.09 ± 0.07	0.06 ± 0.01	9.7 ± 2.3	0.006 (20)	0.01
6 mM Mg^{2+} dATP	1.6 ± 0.28	1.99 ± 0.35	3.5 ± 0.43	0.57	-
0.25 mM Mg^{2+} dATP	0.45 ± 0.19	0.56 ± 0.24	5.3 ± 3.1	0.11 (5.2)	0.005
6 mM Mg^{2+} EfdATP	1.2 ± 0.43	1.9 ± 0.35	0.76 ± 0.25	0.54	-
0.25 mM Mg^{2+} EfdATP	0.29 ± 0.02	0.18 ± 0.01	1.4 ± 0.38	0.13 (6.1)	0.03

(HIV-2 RT)

a- Assays were conducted with a 20 nucleotide template and 19 nucleotide 5' end labeled primer as described [326]. The single template-directed nucleotide was a T opposite an A, a C opposite a G, or an A opposite a T for AZT, ddCTP, and EFdATP, respectively. All assay used 0.4, 0.8, 1.6 nM RT. Results were ave. of 3 exp. ± S.D.
b- *k$_{cat}$* was calculated by dividing V$_{max}$ by the enzyme concentration.
c- Fold decrease in enzyme efficiency (as judged by *k$_{cat/}$* K$_m$) compared to the 6 mM result (number above) with the same nucleotide or inhibitor.
d- Values were calculated using a standard Student's t-test.

4.3.3 Mg^{2+} conditions do not affect the ATP-dependent rescue efficiency of AZT-terminated primers.

Next, I examined if the concentration of Mg^{2+} impacts the ability of HIV-1 and HIV-2 RT to excise the AZTTP by reversing the polymerization reaction using a pyrophosphate donor [148, 360]. HIV-1 RT *in vitro* can use inorganic phosphate, pyrophosphate, or ATP as a pyrophosphate donor, but physiologically uses ATP [148, 360, 377, 378]. The most common form of HIV-1 resistance to AZT is enhancing the ATP-mediated excision activity [378]. The primer rescue assay [360] was used to measure ATP-dependent removal of AZT terminated primers. Previous experiments on a RNA template indicated that low Mg^{2+} concentrations led to an increase in the ability to unblock primers with 3′ AZT [299]. The authors suggested that the reduced RNase H activity at low Mg^{2+} would allow more time for unblocking before RNase H activity degraded the RNA to the point where the primer dissociated from the template. Experiments shown here on a DNA template showed that the unblocking activity of HIV-1 and HIV-2 RT was not affected by the concentration of Mg^{2+} (Fig. 4-5), supporting the idea that diminished RNase H activity may be the reason for the previously observed results [299]. HIV-2 RT showed much lower ability than HIV-1 RT to unblock AZT-terminated primers, at both high and low Mg^{2+} (Fig. 4-5), as has been shown previously [359]. In contrast to HIV-1 RT, HIV-2 RT primarily develops resistance against AZT by selecting for the Q151M mutation [154], thereby increasing the ability of HIV-2 RT to discriminate against the analogue [359]. The results presented here suggest that the Mg^{2+} concentration has no significant effect on the ATP-dependent unblocking activity of HIV RT.
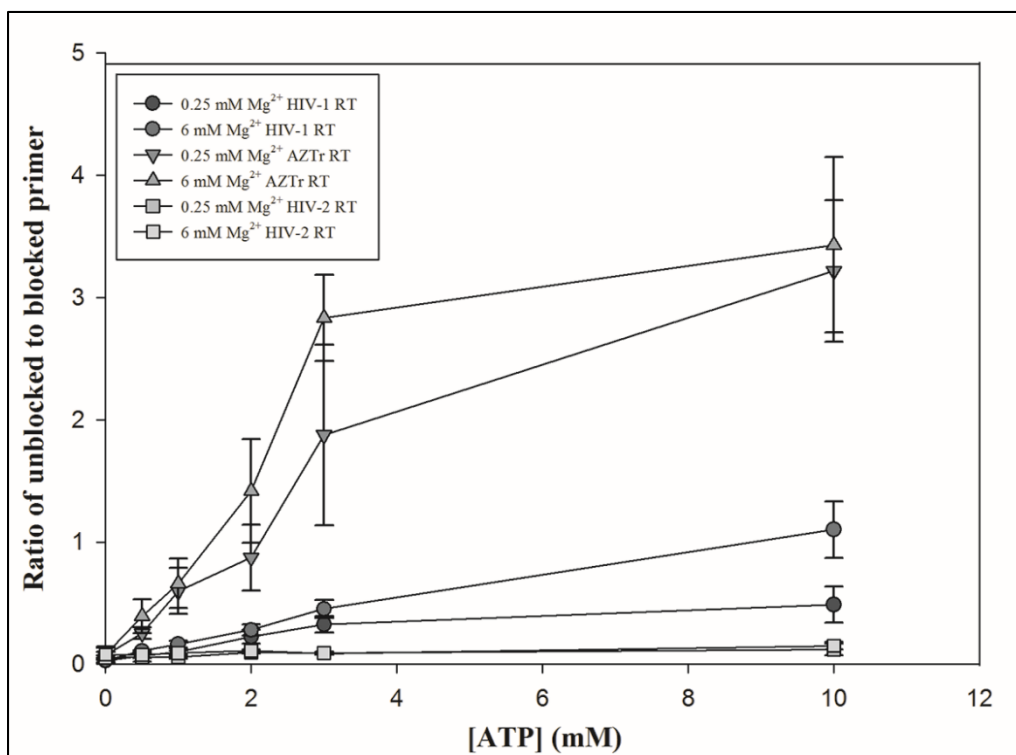
Figure 4-5: ATP-dependent unblocking of chain-terminated primer by different RTs was not affected by Mg²⁺ concentrations. Primer unblocking experiments were performed using the primer-rescue assay described in section 4.2.2. Primer unblocking activity by HIV-1, HIV-2, and the AZTr RT was similar in both 0.25 and 6 mM Mg²⁺. As expected, the unblocking efficiency of different RTs was in the following order: HIV-1 AZTr > HIV-1 > HIV-2.

4.3.4 NNRTIs are more effective against HIV-1 RT at low Mg²⁺ conditions.

Non-nucleoside reverse transcriptase inhibitors are non-competitive inhibitors, which bind at a hydrophobic site in the p66 subunit of the heterodimer [379]. NNRTIs bind very close to the polymerase active site, at ~10 Å from the active site [380], and inhibit the enzyme by slowing the rate of catalysis [381]. In the experiment monitoring inhibition of RT synthesis by NNRTIs at different Mg²⁺ concentrations, the amount of NNRTI inhibitor was chosen such that little or no full-length DNA synthesis product was observed at the lowest rather than highest (as in the NRTI experiments) Mg²⁺ concentration used (0.25 mM free Mg²⁺). Interestingly, first generation

(Nevirapine (NVP) and Efavirenz (EFV)) and second generation (Rilpivirine (RPV)) NNRTIs were more potent in inhibiting HIV-1 RT at low Mg^{2+} concentrations than at high Mg^{2+} (Fig. 4-6). A decrease in the amount of fully extended products and an increase in the intensity of premature termination products was observed with decreasing Mg^{2+} levels. The half-maximal inhibitory values (IC_{50}) of NVP at 6 mM and 0.25 mM Mg^{2+} were also measured (Table 4-3). Consistent with the above results, there was a ~4-fold decrease in the IC_{50} value of NVP at 0.25 mM Mg^{2+}, confirming the increased potency of NVP at the lower Mg^{2+} condition. These results suggest that NNRTIs may be more potent in cells than would be predicted from commonly used *in vitro* RT assays and that Mg^{2+} affects the interactions between NNRTI and the NNRTI binding pocket of the enzyme in an inverse manner compared to that of NRTIs. Consistent with the published data, HIV-2 RT was not inhibited by these first generation NNRTIs in any of the tested Mg^{2+} conditions (Fig. 4-6 and data not shown). HIV-2 RT, with positional changes of conserved residues and significant side-chain differences compared to HIV-1 RT [83], does not bind these NNRTIs. Second-generation NNRTIs have several advantages over the first generation NNRTIs such as improved tolerability profile and better genetic barrier of resistance compared to efavirenz and efficiently inhibits HIV-1 RT resistant to the first generation NNRTIs [382]. RPV also showed a similar pattern of inhibition against HIV-1 RT, with better inhibition observed at lower Mg^{2+} concentrations compared to high Mg^{2+} (Fig. 4-6).
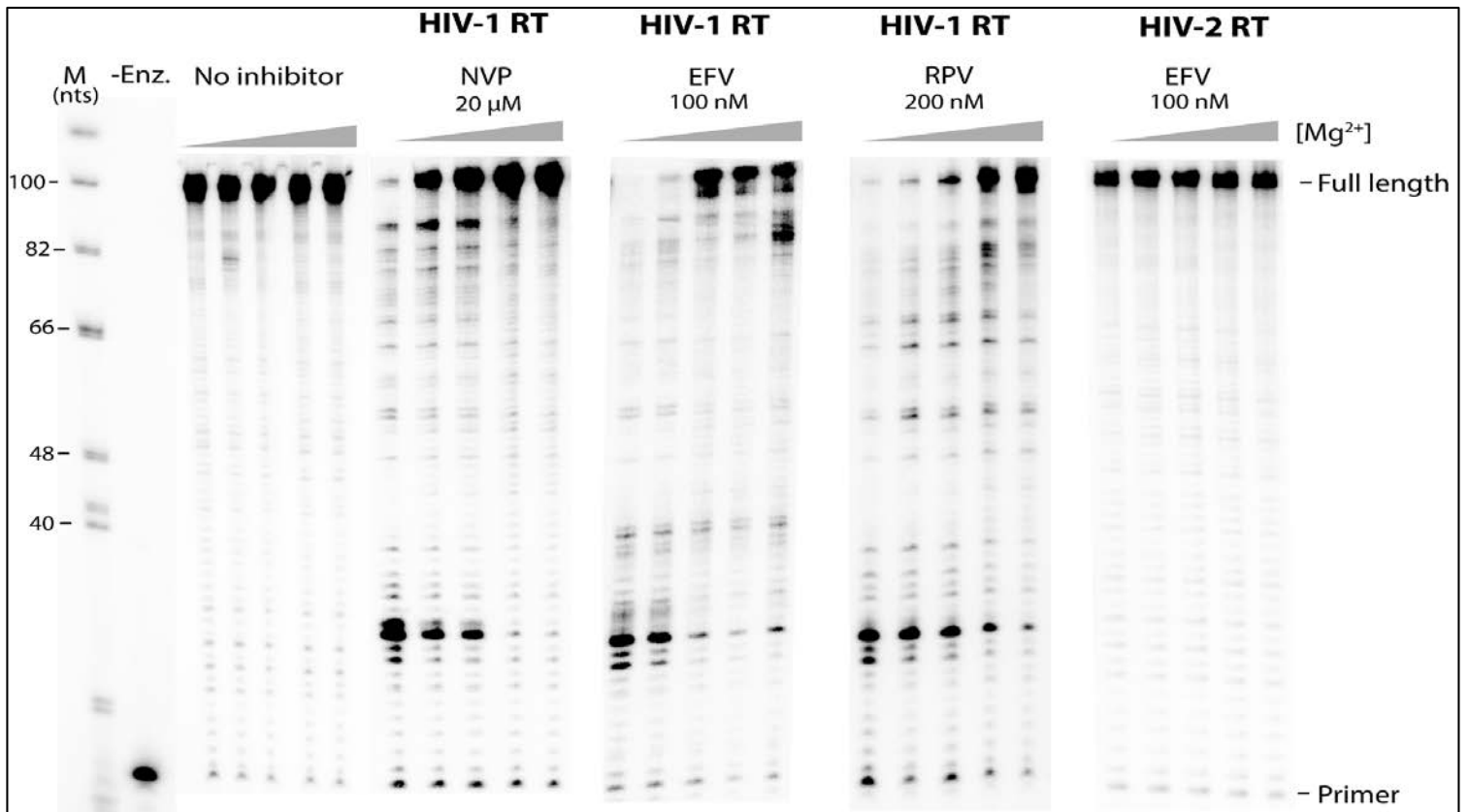
Figure 4-6: HIV-1 RT is inhibited by NNRTIs better at lower Mg^{2+} concentrations. Primer extension reactions were performed with 100 nM wild type HIV-1 RT or HIV-2 RT, 5 μM dNTPs, the indicated concentrations of the NNRTIs, and increasing concentrations of Mg^{2+} (l-r) 0.25, 0.5, 1, 3, and 6 mM for 30 minutes. M and -Enz. are same as other primer-extension images. Increase in the total amount of fully extended products by HIV-1 RT was observed for NVP, EFV, and RPV, when Mg^{2+} was increased. HIV-2 RT was not inhibited by EFV

Table 4-3: IC$_{50}$ determinations for NVP with WT HIV-1 and HIV-1 K103 N RT at 0.25 and 6 mM Mg^{2+}

	[a]Condition	[b]IC$_{50}$ (μM)	[c]Fold decrease [d](p value)
HIV-1 RT	6 mM Mg^{2+}	16 ± 0.47	-
	0.25 mM Mg^{2+}	4.3 ± 0.69	3.7 (<0.00001)
K103N RT	6 mM Mg^{2+}	49 ± 4.7	-
	0.25 mM Mg^{2+}	14 ± 2.6	3.5 (0.0003)

a- Assays were done as described in section 4.2.2. The single template-directed nucleotide used in this assay was a dATP opposite T (5'T template). All assays used 25 nM RT.

b- Half-maximal inhibitory values (IC$_{50}$) were calculated, as described in Materials and Methods, from the relationship between the concentration of nevirapine and percent of inhibition achieved at the particular inhibitor concentration. Results were ave. of 3 exp. ± S.D.

c- Fold decrease in IC$_{50}$ values compared to the 6 mM result (number above) with the same RT. Lower IC$_{50}$ value at 0.25 mM Mg^{2+} confirms better inhibition with the lower Mg^{2+}.

d- Values were calculated using a standard Student *t* test.

4.3.5 Drug-resistant HIV-1 RTs are also sensitive to changes in Mg^{2+} concentration.

HIV-1 RT develops resistance against NRTIs primarily by two mechanisms: increased exclusion by discriminating against the NRTIs and ATP-dependent primer unblocking by excision of the incorporated NRTI. NRTI drugs such as Zalcitabine, Lamivudine (3TC), dideoxyinosine, and Stavudine (d4T) selects for mutations in RT which confers resistance through the exclusion mechanism via K65R and other mutations [383-386]. Resistance to the thymidine analog class of NRTIs such as 3'-azido-3'-deoxythymidine (AZT) is conferred by facilitating excision of the incorporated AZTMP from the growing chain of DNA through thymidine analog mutations (TAM) such as the K70R and the T215F mutations [145, 378]. Since wild type HIV-1 RT showed increased exclusion of NRTIs in low Mg^{2+} conditions (Fig. 4-3), exclusion by HIV-1 drug-resistant RTs was tested in different Mg^{2+} conditions. HIV-1 RTs with a K65R mutation (referred to as

RT^{K65R}) or D67N, K70R, T215F, and K219Q mutations (referred to as AZTr RT) were used to check the impact of Mg^{2+} concentrations on the exclusion of ddCTP and AZT, respectively. Inhibition of RTK65R by ddCTP showed a similar Mg^{2+}-dependent pattern to that of wild type HIV-1 RT. An increase in fully extended products and a decrease in the intensity of NRTI-terminated products was observed with decreasing Mg^{2+}. As expected, a higher concentration of ddCTP was required to observe a level of inhibition comparable to wild-type HIV-1 with RT^{K65R} (Fig. 4-7). When the assay was performed with the same level of ddCTP that was used with wild-type RT, although the effects of Mg^{2+} were still evident, incorporation of ddCTP (judging from the presence and intensity of premature termination sites) was greatly reduced. Steady-state kinetic analysis were consistent with RT^{K65R} excluding ddCTP more effectively in low Mg^{2+} (Table 4-4). Overall, the results were consistent with the K65R mutation conferring greater resistance to ddCTP but retaining sensitivity to Mg^{2+}. Further, they suggest that RT^{K65R} is more effective in the low Mg^{2+} conditions present in cells (see section 4.1) compared to the high conditions used in typical in vitro drug assays.

Similar to RT^{K65R}, AZTr RT also remained sensitive to changes in Mg^{2+}, showing greater exclusion of AZTTP as Mg^{2+} was decreased (Fig. 4-7). Profiles observed with AZTr were similar to wild-type, as both enzymes had similar efficiency incorporating AZTTP (Fig. 4-7 and Table 4-4). As stated above, AZTr RT primarily confers resistance against AZT through the excision pathway. As was the case with HIV-1 and HIV-2 wild type RTs, Mg^{2+} did not have a significant effect on the unblocking activity of AZTr RT, although this activity was higher with AZTr RT than wild-type enzymes as expected (Fig. 4-7).

HIV-1 RT resistance against NNRTIs develops through mutations in the NNRTI binding pocket of the enzyme. Lys103Asn (K103N) mutation is 10- fold to 100-fold more resistant than

123

wild type HIV-1 to most NNRTIs including nevirapine, efavirenz, and TIBO [387-389]. K103N

RT was evaluated to see if Mg^{2+} affects the mutated NNRTI binding pocket in a similar manner to

the wild type enzyme. K103N, as expected, was more resistant than wild type RT to NVP, and

showed a similar pattern of increased sensitivity against NVP at low Mg^{2+} compared to the high

Mg^{2+} condition (Fig. 4-7). IC_{50} values decreased ~4-fold at low Mg^{2+} conditions compared to the

high Mg^{2+} (Table 4-3). This shows that K103N RT, although resistant to NVP, may not be as

resistant as suggested by the previous *in vitro* experiments at the elevated Mg^{2+} concentrations.

Overall, the results highlight the need for the use of physiological Mg^{2+} conditions when

studying the RT inhibitors. Elevated Mg^{2+} concentrations compromise RT's ability to discriminate

against the modified 3′-OH group of the incoming nucleotide and weakens the binding of NNRTI

to the NNRTI binding pocket. Our results also suggest that optimized *in vitro* conditions may have

misrepresented the magnitude of resistance developed by the resistant mutants.
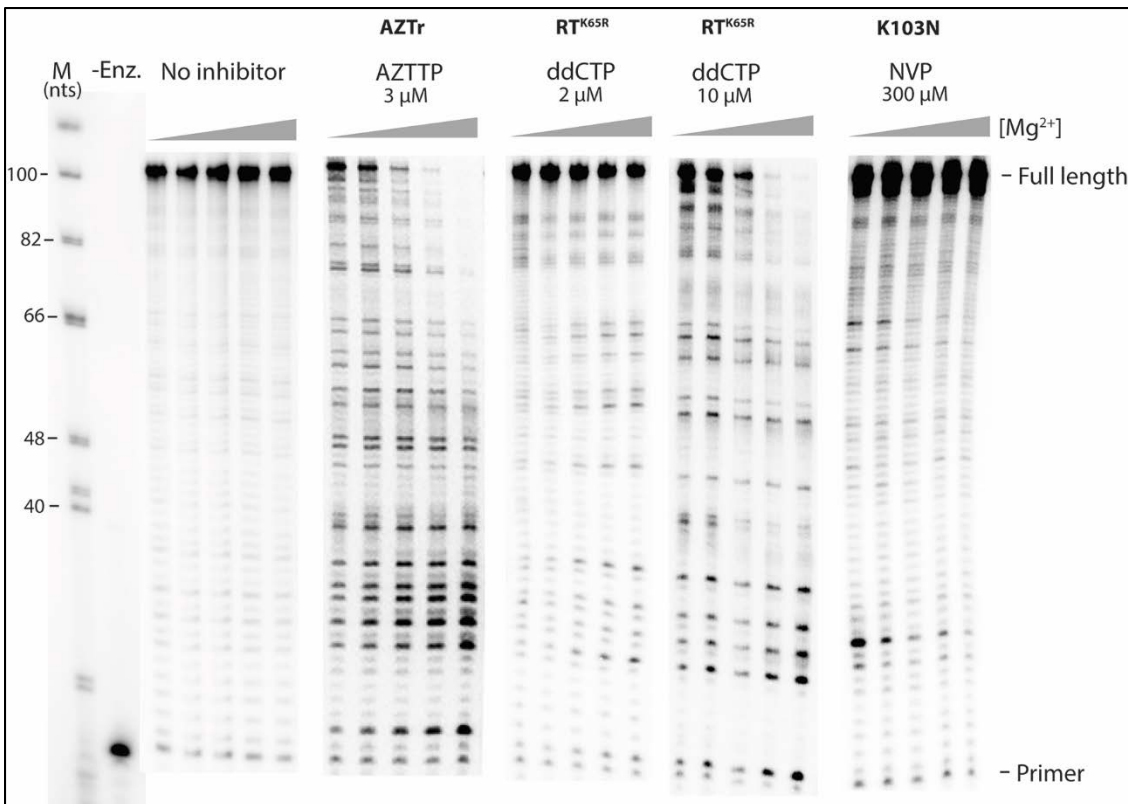
Figure 4-7: HIV-1 drug resistant mutant RTs also show Mg^{2+}- dependent sensitivity to NRTIs and NNRTIs. Primer extension reactions, performed in the same conditions as of Fig. 4-2, with 100 nM of the indicated drug resistant RT are shown. Increasing concentrations of Mg^{2+} (l-r) are 0.25, 0.5, 1, 3, and 6 mM. M and -Enz. are same as other primer-extension images. The inhibition profiles for AZTr RT was very similar to HIV-1 RT. K65R and K103N RTs also showed similar Mg^{2+}- dependent inhibition to HIV-1 RT, but only at higher concentrations of the inhibitor.

Table 4-4: V$_{max}$, K$_m$, and k_{cat} determinations for TTP and AZTTP incorporation by AZTr RT; dCTP and ddCTP by RT^{K65R} at 6 mM and 0.25 mM Mg^{2+}

	[a]Condition	V$_{max}$ (nM/min)	[b]k_{cat} (min^{-1})	K$_m$ (μM)	$k_{cat/}$K$_m$ [c](fold decrease)	[d]p value
AZTr RT	6 mM Mg^{2+} dTTP	1.6 ± 0.2	1.6 ± 0.2	4.8 ± 0.49	0.33	-
	0.25 mM Mg^{2+} dTTP	0.55 ± 0.22	0.55 ± 0.22	2.2 ± 1	0.25 (1.3)	0.05
	6 mM Mg^{2+} AZTTP	1.3 ± 0.01	1.3 ± 0.01	5.2 ± 0.98	0.25	-
	0.25 mM Mg^{2+} AZTTP	0.32 ± 0.05	0.32 ± 0.05	5.5 ± 1.8	0.06 (4.2)	0.009
RT^{K65R}	6 mM Mg^{2+} dCTP	1.5 ± 0.36	0.75 ± 0.18	1.6 ± 0.52	0.59	-
	0.25 mM Mg^{2+} dCTP	0.24± 0.02	0.12 ± 0.01	1.0 ± 0.37	0.15 (5.2)	0.007
	6 mM Mg^{2+} ddCTP	1.1 ± 0.08	0.53 ± 0.04	6.2 ± 0.3	0.08	-
	0.25 mM Mg^{2+} ddCTP	0.07 ± 0.04	0.03 ± 0.02	9.1 ± 0.5	0.003 (27)	<0.001

a- Assays were conducted with a 20 nucleotide template and 19 nucleotide 5' end labeled primer as described in section 4.2.2. The single template-directed nucleotide was a T opposite an A, a C opposite a G for AZT and ddCTP respectively. All assay used 0.8 or 1.6 nM RT. Results were ave. of 3 exp. ± S.D.
b- k_{cat} was calculated by dividing V$_{max}$ by the enzyme concentration.
c- Fold decrease in enzyme efficiency (as judged by $k_{cat/}$K$_m$) compared to the 6 mM result (number above) with the same nucleotide or inhibitor.
d- p values were calculated using a standard student's t test for $k_{cat/}$K$_m$ values between 0.25 and 6 mM Mg^{2+}.

4.4 Discussion

In this chapter, I show that elevated Mg^{2+} conditions in *in vitro* reactions misrepresent the potency of RT inhibitors. When studied in lower, more physiological Mg^{2+} conditions, some NRTIs show less inhibition, whereas some NNRTIs show greater inhibition than in high Mg^{2+} conditions typically used *in vitro* (see Tables 4-1 and 4-2 and Figs. 4-3 and 4-4). The results presented with EfdATP also highlight that the 3' hydroxyl group is more important for stabilizing binding of NRTIs at low Mg^{2+} concentrations, and the elevated Mg^{2+} conditions underrepresents the significance of the interaction between the 3′-OH group and RT. Of course, inhibition of reverse transcription by NRTIs and NNRTIs in cellular conditions might be affected by cellular and/or viral proteins involved in the reverse transcription complex, as well as other cell factors not included in our studies.

Steady-state analyses at high (6 mM) and low (0.25 mM) Mg^{2+} revealed that both dNTP and NRTI incorporation was less efficient (as judged by k_{cat}/K$_m$) in low Mg^{2+} (Tables 4-1 and

4-2). This is consistent with RT showing higher catalytic activity with high Mg^{2+} concentrations [10, 299]. The magnitude of the decrease in efficiency, however, was typically several-fold greater for NRTIs without 3′-OH groups, resulting in less efficient incorporation of these NRTIs in primer extension reactions as the concentration of Mg^{2+} is decreased. Discretion is advised when using steady-state kinetic analyses to quantify the inhibition of HIV-1 or HIV-2 RTs by NRTIs. The efficiency of incorporating nucleotides and NRTIs is sequence-dependent [390] and the kinetic assays presented here using a specific sequence and incorporation at the end of the template may not fully reflect the efficiency of RT to incorporate the nucleoside analog and dNTPs at other sequences or template locations. However, the kinetic assays were in general agreement with the assays that measure incorporation over several different sites (like those in Figs. 4-3 and 4-4), which provide a better qualitative representation of viral genome replication.

Studies comparing the different analogs of EfdA also highlighted the contribution of the 3′-OH group for the potency of EfdA inhibiting HIV infection [371]. EfdA inhibited HIV-1 replication in phytohemagglutinin-activated PBMCs with an EC_{50} value of 0.05 nM, whereas EfddA, the analog of EfdA lacking the 3′-OH group, had an EC_{50} value of 570 nM [371]. EfdATP, after incorporation into the growing DNA strand, locks the enzyme in the pre-translocation (N site), thereby preventing the binding of the next correct nucleotide. HIV-1 RT is able to unblock the EfdA-terminated primers locked at the N site efficiently, however facile reincorporation of EfdATP due to the 3′-OH and the 4′-ethynyl groups maintains the potency of inhibition [371]. The stabilizing effect of the 3′-OH group of EfdA is strongly reflected in our kinetic and primer extension experiments.

The results presented in this chapter agree with the mechanism proposed by Goldschmidt *et. al.* to explain the increased discrimination against NNRTIs at the low Mg^{2+} concentration [299].

Crystal structures of RT with the primer-template complex [391] show that three networks of interactions maintain the deoxyribose and phosphate parts of the dNTP: i) side chains of D113, Y115, F116 and Q151 and the main chain of D113 and Y115 with the 3′-OH group of the dNTP. ii) side chains of R72 (with the β phosphate) and K65 (with the γ phosphate) with the convex face of the triphosphate group [391]. iii) a non-bridging oxygen, on the concave face, from each phosphates of the triphosphate with a Mg^{2+} ion; while the α phosphate also interacts with the second Mg^{2+} ion. The authors suggested that RT can function with reasonable efficiency when one of the three interaction sets are perturbed but simultaneous perturbations of two networks results in a more pronounced reduction in efficiency. The results in this chapter show that at low Mg^{2+} conditions, destabilizing both the Mg^{2+} network and the 3′-OH network results in poor incorporation efficiency for NRTIs without 3′-OH. Whereas, destabilizing either the Mg^{2+} network alone (EfdATP at low Mg^{2+}) or the 3′-OH network alone (AZT and ddCTP at high Mg^{2+}) result in a less severe decrease in efficiency. In addition, our kinetic analyses suggests that the altered conformation affects mostly the ddNTP catalysis step (as judged by a decrease in k_{cat}), although binding (as judged by an increase in K_m) is also affected to a lesser extent.

The results with NNRTIs are consistent with experiments showing that the binding of some NNRTIs (O-TIBO and Cl-TIBO) to HIV-1 RT is better with no Mg^{2+} as opposed to high Mg^{2+} levels (10 mM) [381]. The authors hypothesized that Mg^{2+} interactions with the active site aspartate residues may impede the binding of NNRTIs to the "NNRTI pocket" of RT. NNRTIs bind HIV-1 RT near the polymerase active site [369] containing the conserved aspartate residues (D110, D185, D186), which interact with two Mg^{2+} ions during catalysis [391] . In fact, the structural mechanism for the inhibition of HIV-1 RT by NNRTIs is through distortion of the active site aspartates [392]. When possible interplay between the catalytic active site and the NNRTI site

was examined, the binding affinities of the NNRTIs in the presence of Mg^{2+} decreased [381]. Equilibrium dissociation constant values (K_D) of O-TIBO and Cl-TIBO, in the presence of 10 mM Mg^{2+}, increased 3.5-fold and 6-fold compared to the K_D values in the absence of Mg^{2+}. It is plausible that interactions between Mg^{2+} ions and the aspartate residues hinder the binding of NNRTIs, while once the inhibitor is bound, the dissociation rate is governed by its intrinsic affinity for RT [381]. The authors could not detect a similar Mg^{2+}-dependent change in the K_D of NVP but our results suggest that NVP and EFV may be affected by the high Mg^{2+} conditions similarly. Increased binding affinity may explain the observed increase in potency of NNRTI in the low Mg^{2+} condition (Fig. 4-6 and Table 4-3).

4.5 Concluding remarks

The results presented here demonstrate that interactions between NRTIs and NNRTIs are highly dependent on Mg^{2+} conditions and are misrepresented by results of experiments performed using conditions at which HIV-RT shows maximum catalytic activity. For NRTIs, the lack of a 3′-OH seem to play an important role, as the NRTI translocation inhibitor EfdA containing a 3′-OH group was unaffected by Mg^{2+} concentration. The results could have potential implications for computer aided drug design strategies, especially for quantitative structure activity relationship studies (QSAR). Several strategies such as QSAR, molecular docking, and virtual screening against HIV RT are currently being undertaken in an attempt to develop novel HIV small-molecule inhibitors [393]. The results also strongly emphasize the need to use physiological amounts of free Mg^{2+} when studying future RT inhibitors.

4.6 Contributions

The experiments in this chapter were performed by me (VA) in collaboration with Stefan. S. Sarafianos (SS) and Jeffrey. J. DeStefano (JD). I conducted all of the primer-extension assays, primer-rescue assays, assays to determine half-maximal inhibitory concentrations and most of the steady-state single nucleotide incorporation assays. JD conducted some of the single-nucleotide incorporation assays. SS provided critical reagents for the primer extension assays. VA and JD participated in design of the experiments. VA, SS, and JD critically reviewed the interpretation and discussion of the results. This chapter will be submitted to the journal "Retrovirology" for publication.

Chapter 5 : General Discussion

Nucleic acid polymerases have probably been the most heavily studied of all enzymes. Their biological role — to faithfully copy the genetic material — is a function necessary for continuous cell division of unicellular and multicellular organisms. Pols, perhaps more than any other proteins, are responsible for the remarkable diversity and development of complex organisms. Despite the remarkable fidelity of the overall process, errors made by pols serve as one of the major driving forces for generating diversity. Several important techniques like PCR, RT-PCR, cloning, and other molecular biology techniques heavily employ pols. The importance of these enzymes explains why they have been so heavily studied. Despite thousands of reports describing mechanistic details of nucleotide incorporation, our understanding of pols is not complete. Fidelity, substrate recognition, processivity (avg. number of nts added in a single binding event between pol and the primer-template) of pols, and how these properties relate to the enzyme function continue to be heavily investigated.

HIV RT is known for uncommonly low fidelity with a mutation rate in *in vitro* assays several-fold higher than other RTs (Section 1.3.3). In Chapter 2, I show that the fidelity of RT can be influenced by alternative divalent cations in different ways. Previously, it has been found that alternative divalent cations such as manganese (Mn^{2+}) and cobalt (Co^{2+}) can decrease the fidelity of HIV RT, consistent with the notion that these cations are promutagenic. However, I show that the promutagenic cations are mutagenic only at extremely high concentrations. I also show strong data indicating that HIV RT has higher fidelity in the presence of zinc (Zn^{2+}), the first clear demonstration that an alternative divalent cation can enhance fidelity. Alpha complementation assays, performed with cation conditions optimized for nucleotide catalysis, show that the fidelity of DNA synthesis by HIV-1 RT is approximately 2.5 fold greater in Zn^{2+} when compared to Mg^{2+}.

Consistent with this, in steady-state assays RT extended primers with mismatched 3' nucleotides poorly, and inserted incorrect nucleotides less efficiently using Zn^{2+} than Mg^{2+}. Mn^{2+} and Co^{2+}, indeed, decreased the fidelity of RT at highly elevated concentrations (6 mM), in agreement with previous literature. However, the fidelity of HIV RT with Mn^{2+} and Co^{2+} remains similar to Mg^{2+} at lower concentrations that are optimal for catalysis. This challenges the notion that alternative cations capable of supporting polymerase catalysis are inherently mutagenic, and the observed effects in previous reports may result from other mechanisms discussed in section 2.4. It remains to be investigated if Zn^{2+} can be used to improve the fidelity of commercially available RT PCR reactions. Although Zn^{2+} slows down the catalysis rate of HIV RT, doping RT PCR reactions with small amounts of Zn^{2+} may result in an increase in fidelity without compromising too much on the catalysis rate. Experiments measuring the fidelity of HIV RT in different Mg^{2+}-Zn^{2+} combinations will be interesting to pursue.

Alternative divalent cations may not have a big impact on the fidelity of HIV reverse transcription in cells, due to the tight regulation of their physiological concentration. The availability of divalent cations in cells is carefully controlled by a combination of ion transporters, cation binding proteins, and sequestration within specific cell organelles. Tight regulation is needed because some of the divalent cations have the ability to inhibit or alter the activity of several enzymes. Zinc, which is a component of several zinc finger containing enzymes, is important for several processes in the cells [251, 394, 395]. The concentration of available free Zn^{2+} is in the low nM range despite a total concentration of ~0.1-0.5 mM in cells [251, 282, 396, 397], whereas a total of ~2.5- 3 μM Mn^{2+} is present in red blood cells [255, 256] and Co^{2+} is present in the low μM range in serum [257] . Zn^{2+} is a potent inhibitor of many enzymes including several cell enzymes, viral polymerases, and TY1 RTs [260-264]. The mechanism by which Zn^{2+} inhibits HIV

RT was recently solved [266]. Zinc induces the formation of a "dead-end" RT-Zn^{2+}-(primer-template) complex since it ties up RT- potentially for hours - in a complex that is from a kinetic perspective, minimally productive. It will be interesting to check which particular step of the catalysis is affected by Zn^{2+} to result in an increase in fidelity of HIV RT. Crystal structures of polymerase ternary complexes with Zn^{2+} in the polymerase active site may give us a better understanding of the mechanism of polymerase function and fidelity with Zn^{2+}. It is also possible to investigate if Zn^{2+} prevents transition between the different catalytic states by examining the $k_{on/off}$ rates using the ^{65}Zn isotope to determine which cation is occupying the enzyme's metal ion binding sites under various catalytic states. Zn^{2+} could also restrict enzyme catalysis due to an allosteric effect by binding on sites other than the active site on the enzyme. It is possible to verify if this is the case by performing the $k_{on/off}$ rate determination experiments using the ^{65}Zn isotope.

In Chapter 3, I showed that physiological concentration of Mg^{2+} increased the fidelity of HIV RT in the test tube to the levels observed in cells. These "cellular conditions", though suboptimal with respect to RT catalytic activity, produce optimal DNA synthesis with respect to production of long DNA products. Therefore, it is conceivable that HIV RT has evolved to function with optimal efficiency under these conditions despite modestly lowered catalytic activity and that the conditions used in previous experiments lead to misrepresentation of RT's fidelity. Understanding RT's fidelity and other biochemical properties at a mechanistic level using conditions that represent the cellular environment will allow an accurate assessment of the effect of drug-resistance mutations on enzyme activity and function. This is especially relevant given accumulating evidence suggesting that viruses survive near the edge with respect to fidelity, sacrificing accuracy for the enhancement of genetic diversity [398-408]. The possibility of

exploiting this to push viruses over the edge is the basis for lethal mutagenesis, an idea under intensive study [399, 401-403, 409-413].

However, it is challenging to directly relate the results observed *in vitro* to the properties of RT in cells. It is not possible to completely mimic every effect of cellular conditions on the properties of RT in a test tube. Several additional cellular factors play a role in the fidelity of reverse transcription and it is not possible to include all the cellular factors in an *in vitro* reaction. It will be interesting, however, to see if we can mimic the small molecule milieu of the cell in an *in vitro* reaction. This can be achieved either by looking at the literature and adding physiological levels (levels present in the cytoplasm of lymphocytes) of the relevant small molecules such as dNTPs, rNTPs, Mg^{2+}, polyamines, amino acids, NAD+ and related compounds, glutathione, and monovalent cations like K^+, Na^+, and Cl^-. An alternative to reconstituting small molecule milieu *in vitro* is to develop a minimally-invasive protocol for extracting the small molecular fraction from cells, which can then be used to perform cell-free assays of reverse transcription. Our lab is investigating both these strategies to create an *in vitro* system which is more representative of the small molecule environment present inside the cells. These experiments to test potential effects of other cellular small molecule components in addition to dNTPs and Mg^{2+} will help us identify if other small molecules have a significant impact on the behavior of HIV RT. Developing an *in vitro* assay which better represents the small molecule environment present in cells might also be useful for assaying future RT inhibitors and the drug-resistant mutants (see below).

Although the effects seen on HIV RT fidelity by decreasing Mg^{2+} concentration in *in vitro* reactions are dramatic, it remains to be seen if fidelity can be modulated in cellular reactions by modulating the intracellular concentration of free Mg^{2+}. Intracellular concentration of free Mg^{2+} can be increased. Previous results indicate that incubating cultured cells in elevated Mg^{2+} medium

can increase the level of free Mg^{2+} in the cells [414]. It will be interesting to check the fidelity of reverse transcription in cells incubated with different concentration of Mg^{2+}. A vector-based *lacZα*-complementation-based system which can be used to measure the fidelity of reverse transcription in cells has been developed by others [103]. This system has already been used to determine the fidelity of HIV replication in cells and to catalog the types of mutations made by wild type and drug-resistant HIV RTs [103, 415]. In Chapter 3, most of the ~6-fold improvement in fidelity occurred below 0.5 mM Mg^{2+} as there was only about a 2-fold improvement from 6 mM to 0.5 mM. This suggests that the effect of Mg^{2+} on fidelity can be tested in HIV infected cells. Though obtainable increases in cellular free Mg^{2+} may be modest (up to about 1 mM [414]), the *in vitro* fidelity results imply that this increase will have a pronounced effect on the fidelity of reverse transcription.

Efficiency of RT inhibitors in *in vitro* reactions is also dependent on the amount of free Mg^{2+} in the reaction (Chapter 4). NRTIs lacking the 3′-OH group inhibited RT with less efficiency *in vitro* in low Mg^{2+} than in high Mg^{2+}. Steady-state kinetic analyses revealed that the reduced inhibition by NRTIs lacking the 3′-OH in low Mg^{2+} resulted from less efficient incorporation of these analogues under these conditions. In contrast, EFdATP was incorporated with similar efficiency to its analogue dATP at low Mg^{2+} concentration. NNRTIs, on the other hand, displayed better inhibition efficiency in low Mg^{2+} compared to high Mg^{2+}. Drug-resistant HIV-1 RT mutants also displayed the Mg^{2+}- dependent difference in susceptibility to NRTIs and NNRTIs – although the overall resistance pattern shown by the drug resistant mutants remained similar, the magnitude of resistance was misrepresented using high Mg^{2+} conditions. It is interesting to speculate that it is possible that NRTI drug resistant mutants work globally by weakening the 3′-OH network interactions (Section 4.4) via selecting for mutations in HIV RT, which might allow RT to

discriminate against NRTIs better. Testing different drug resistant mutant RTs in low Mg^{2+} conditions might give us important clues to suggest if this hypothesis holds true.

The results presented in Chapter 4 also highlight the importance of 3′- OH group for incorporation by HIV RT. Previous experiments looking at these inhibitors may have overlooked the functional importance of this group because all NRTIs get incorporated by HIV RT with reasonably good efficiency, when high Mg^{2+} concentrations are available. This is an important finding relevant to the rational drug design strategy, where new drugs or modifications of existing drugs are created based on structural, biochemical, and computational information. Designing future RT inhibitors which can mimic the 3′- OH structurally or functionally might confer beneficial advantages over the existing antiviral drugs. Comparison of the existing NNRTIs for efficiency in low Mg^{2+} conditions *in vitro* might lead to identification of functional groups required for efficient inhibition.

Similar to the experiments monitoring the fidelity of HIV replication in cells incubated with different Mg^{2+}, it will also be interesting to check the susceptibility of wild-type and drug-resistant viruses to NRTIs and NNRTIs in elevated intracellular Mg^{2+} concentration. If the *in vitro* observations made in Chapter 4 hold true, wild type and drug resistant viruses will show greater susceptibility to NRTIs without 3′-OH and lesser susceptibility to NNRTIs when Mg^{2+} levels are raised. It is important to evaluate the results from these experiments with considerable caution, as changes in the concentration of Mg^{2+} in cells could also affect other cellular or viral proteins, which in turn might have a direct or indirect effect on reverse transcription.

Overall, this work has uncovered novel ways in which divalent cations affect the property and behavior of HIV RT *in vitro.* Interestingly, fidelity of both HIV-1 RT (Chapter 3) and HIV-2 RT (unpublished data) increases by decreasing the concentration of Mg^{2+} in *in vitro* reactions, whereas the fidelity of the related avian myeloblastosis virus (AMV) and murine leukemia virus (MuLV) RTs is not affected by changing the concentration of Mg^{2+}. The fidelity of HIV RT, thus, is comparable to AMV and MuLV RT when compared in physiologically relevant concentration of Mg^{2+}. The results presented here challenge the notion that HIV RT is exceptionally error prone and underscores the importance of using physiologically relevant low levels of Mg^{2+} when studying other properties of wild type and mutant HIV RTs in the future. The work also highlights the need for testing the efficiency of future RT drugs *in vitro* in low Mg^{2+} concentration, and more importantly indicates that designing future NRTIs which can mimic the function of an –OH group at the 3′ position may yield more potent NRTIs.

Appendix I: Establishing optimal growth conditions of a chronic persistent virus: Lymphocytic Choriomeningitis Virus – Clone 13.

AI.1 Introduction

In the context of chronic infections such as HIV, where the virus persists in the body (Section 1.1.3), T cell dynamics play an important role. During HIV infection, the viral titers rise rapidly during the initial phase of the infection along with a concurrent depletion of CD4+ T cells [416]. But the immune system recovers briefly with the appearance of HIV specific CD8+ T cells, and this partial retaliation of the immune system results in a decline in viremia. Usually, this decline in viremia plateaus and the virus establishes latent reservoirs and enters the chronic phase of infection (Section 1.1.3). The chronic phase of HIV infection is also associated with the depletion of the CD4 T cell pool. Eventually, critical populations of effector CD4+ T-cell population decline, as CD4+ T cell homeostasis fails, below the level necessary to prevent opportunistic infections. CD4+ T cells are required for optimal CD8 responses, as CD4 T cells perform multiple helper functions that play a central role to the overall immune responses. Some of the helper functions include activating professional antigen-presenting cells such as dendritic cells, guiding naïve T cells to the sites of priming and activated T cells to the site of infection by secreting chemokines and cytokines, and producing cytokines such as IL-2 and IL-21 which can support CD8+ T cells [417-420]. Loss of CD4+ T cells during the course of an infection probably feedbacks on the CD8+ T cells response as well, rendering them less effective [421, 422]. The primary role of CD8+ T cells is to identify and eliminate infected cells in response to an infection. When CD8+ T cells encounter foreign antigen, they undergo marked proliferation and kill the infected cell that expresses the target antigen [423]. During chronic and persistent viral infections

such, the large and persistent viral load during the entire course of the infection cycle results in exhaustion of CD8+ T cells as well. HIV is unique among other chronic viral infections in that in addition to CD8 T cell exhaustion, CD4 depletion also contributes to weakening the immune response.

Lymphocytic choriomeningitis virus (LCMV) is a common infection in mice, best known for its application in immunological studies. Several key concepts such as Major Histocompatibility Complex (MHC) restriction, persistent infections, T cell memory, and T cell exhaustion emerged using LCMV studies (reviewed in [424]). LCMV- clone 13 (LCMV-13) and LCMV Armstrong are two most commonly used strains of LCMV. LCMV Armstrong is the original strain of LCMV discovered by Charles Armstrong, while studying epidemic encephalitis. LCMV Armstrong strain induces a robust cytotoxic T lymphocyte (CTL) response in the host and is subsequently cleared rapidly by the host, resulting in an acute infection. However, LCMV-clone 13 (LCMV-13) is associated with functional impairment, T cell exhaustion, deletion of viral specific CD8+ T cell responses, and can persist in the host organism indefinitely, causing a chronic infections. LCMV-13 is an excellent model to study T cell exhaustion in chronic infections and remains an active platform for biological research. Immune studies using LCMV offer benefits such as defined immune-dominant and subdominant epitopes and defined tetramers for enumeration of virus-specific T cell populations [424]. LCMV-13 infection model can be used to study CD4+ and CD8+ T cell exhaustion, which occurs in human chronic infections such as HIV, hepatitis B virus, and hepatitis C virus. Studying T cell exhaustion using LCMV-13 *vs.* HIV also has an added advantage in that LCMV is a natural mice infection and hence there are excellent animal models established for LCMV infections.

Both LCMV and HIV produce a significant amount of defective interfering (DI) particles during replication. DI particles are spontaneously generated virus particles in which a critical portion of the viral genome is lost or damaged due to error prone replication or genome not getting packed inside the virus particle. HIV and LCMV have a particularly high ratio of DI particles to infectious virus particle, which is a very common problem associated with propagation of both viruses. It is important to get an efficient infectious titer of LCMV for performing experiments with the animal models. LCMV particles are extremely labile and temperature sensitive and the amount of DI particles in the seed stock can dramatically decrease the infectious titer value. Therefore, it is important to establish the appropriate multiplicity of infection and harvest time point that will yield optimal infectious titer values of LCMV. LCMV infectious particles can be tittered using a plaque assay; however, LCMV shows poor cytopathic effects requiring lengthy periods of incubation to observe plaques and poor visualization. I attempted to establish the optimum growth conditions to generate useful and reportedly typical infectious particle count (~1 x10^8 PFU/ml) of both LCMV-13 and LCMV Armstrong and optimize the plaque assay for visualizing LCMV plaques. The experience obtained by propagating LCMV would also be useful in performing the experiments monitoring the fidelity and inhibition of HIV in cells with higher intracellular Mg^{2+} (Chapter 5).

AI.2 Materials

Baby hamster kidney cell, line 21 (BHK-21), Vero cells (African green monkey kidney cells), T175 tissue culture flasks, 6-well Petri plates, 48-well microtiter plates, Agarose, 0.5% neutral red solution.

BHK propagation media: Dulbecco's high glucose minimal essential medium (500 ml), 10 ml 200 mM glutamine, 50 ml heat-inactivated fetal bovine serum, 5 ml pen/strep solution.

Vero cell propagation medium: Eagle minimal essential medium (500 ml), 5 ml 200 mM Glutamine, 50 ml heat inactivated fetal bovine serum, 5 ml pen/strep solution.

LCMV plaque assay medium: 250 ml 2X Eagle minimal essential medium without phenol red, 5 ml 200 mM glutamine, 25 ml heat inactivated fetal bovine serum, 5 ml pen/strep solution.

AI.3 Results

AI.3.1 Optimizing plaque assay to monitor LCMV plaques.

Historically, LCMV was assayed by a lethal dose assay in mice. Although the assay is very sensitive, as little as one plaque forming unit (PFU) of virus could kill an intracerebrally inoculated mice, the assay is very expensive and time consuming. Therefore, the plaque assay for these studies was performed according to [425]. Plaque assay on Vero cell monolayers has been the most commonly used technique to assay LCMV. LCMV plaque assay was performed according to the following procedure.

1. Vero cells were seeded onto six-well Petri plates, at a density of 5×10^5 cells/ml on the day before infections.
2. The next day the monolayers were ~80% confluent. The medium was replaced with 1 ml of fresh Vero propagation medium.
3. A series of 10-fold dilutions of the stock virus sample were prepared in 48-well microtiter plates by serially transferring 20 μl of the inoculum to 180 μl medium, changing pipet tips after each transfer.
4. 100 μl of the dilution was added to the Vero cell monolayers.
5. The plates were incubated at 37°C for 60-90 minutes in a 5% carbon dioxide incubator, with occasional rocking every 20-30 minutes.

6. Agarose overlay was prepared by combining equal volumes of 2x plaque assay medium with recently boiled 1% agarose solution. The agarose solution was maintained in a 50°C water bath for at least 10 minutes.

7. The medium in the wells of the 6 well plate was removed and ~4 ml agarose overlay was added to each well. The agarose overlay was allowed to solidify for 15 minutes in room temperature and then placed in the incubator.

8. The plates were incubated for 4 days at 37°C in 5% CO_2 incubator.

9. On the fourth day, plates were stained with 1.5 ml of a 1:20 dilution of 0.5 % neutral red solution made up in 1:1 2x plaque assay medium and 1% agarose.

10. The plates were incubated overnight at 37°C in 5% CO_2 and the plaques were visible for a period of 48 hours after staining.

Both LCMV Armstrong and LCMV-13 strains were assayed using the above procedure. LCMV Armstrong formed bigger plaques which were visualized more easily using the neutral red staining procedure compared to the plaques formed by LCMV-13 (Fig. AI-1). Four stocks for LCMV, two for each strain were available (LCMV-13 and LCMV Armstrong harvested after infection with MOI of 0.1 and 0.5 at 48 hours), and all four stocks were assayed (Table AI-1). Infectious titer values obtained for LCMV Armstrong (Plaque forming units /ml; PFU/ml) were within the optimal range for *in vivo* studies while the titer values obtained for LCMV-13 were low (Table AI-1). It is possible that the original stock used to grow up the LCMV-13 stocks had a high amount of DI particles, and so an experiment to monitor growth kinetics of the LCMV-13 stocks at different multiplicity of infection was next performed.
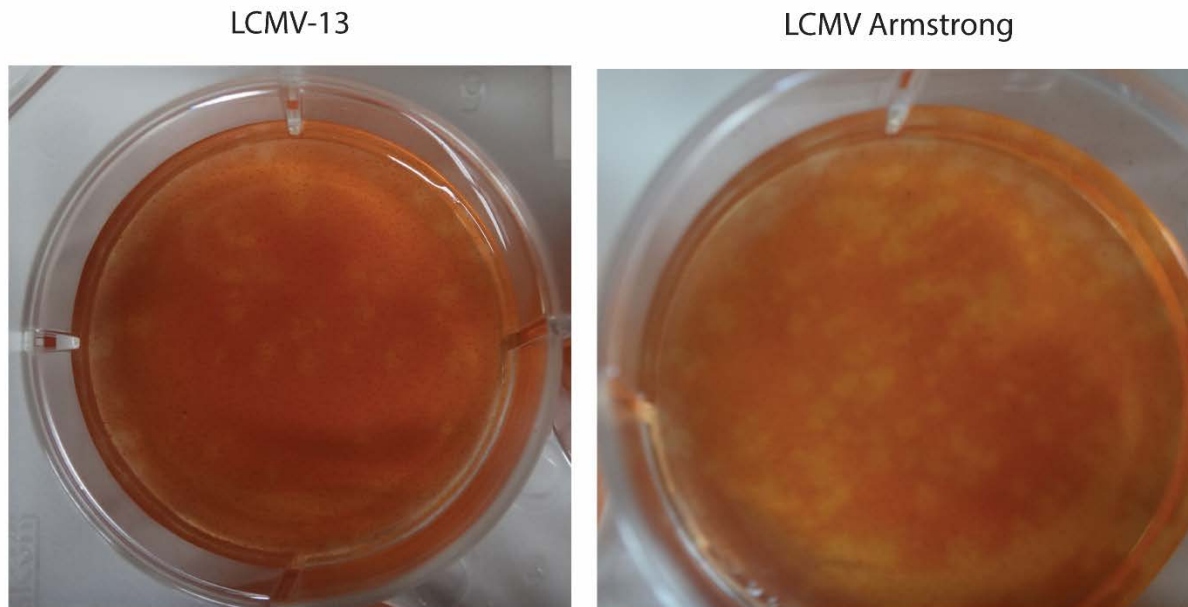
Figure AI-0-1. Plaques obtained from plaque assay of LCMV-13 and LCMV Armstrong.
Plaques are visualized as circular unstained clearing of monolayers, whereas the live cells are
stained by the neutral red stain. LCMV Armstrong plaques are bigger in size and visualized
better using neutral red stain.

**Table AI-1. Titer values of the stock LCMV-13 and LCMV Armstrong
aliquots**

LCMV strain	MOI	Average Titer (PFU/ml)
LCMV 13	0.1	2×10^7
LCMV 13	0.5	8×10^6
LCMV Armstrong	0.1	2×10^7
LCMV Armstrong	0.5	6×10^8

AI.3.2 Establishing optimum growth conditions for LCMV-13 to obtain a higher infectious titer.

LCMV can be propagated in a wide variety of cell lines as the LCMV alpha-dystroglycan receptor is a ubiquitous protein which enables the virus to grow in multiple cell lines. Baby hamster kidney cells, specifically BHK21 cells, are known to produce high titers of LCMV. Usually, desirable titers can be obtained at 48 hours post infection by inoculating monolayers with an MOI of 0.03-0.1 PFU/ cell or using a lower MOI of infection and longer incubation (72 hours). LCMV 13 was propagated at MOIs of 0.01, 0.05 and 0.1 and virus was harvested at 48 and 72 hours post infection. LCMV was propagated according to the following procedure [425].

1. Approximately 5×10^6 BHK-21 cells were seeded onto T175 flasks a day prior to infection.

2. When the flasks were ~ 75% confluent, culture fluid was decanted and the 3 ml virus inoculum was added to the flasks. Assuming 2×10^7 cells/flask during the infection, the flasks were infected with volumes of the LCMV 13 stock corresponding to MOI of 0.01, 0.05, and 0.1. The flasks were incubated at 37°C in 5% CO_2 incubator for one hour with rocking every 10-15 minutes.

3. After 1 hour, 37 ml of medium was added to the flasks and were incubated for 3 days.

4. At 48 hours post infection, the virus-containing cell culture fluid was obtained by decanting ~10 ml of the culture fluid and pelleting cells away by centrifuging at 1200 RPM for 10 minutes at 4° C.

5. The virus samples were aliquoted on ice and snap frozen on dry ice and ethanol. The frozen aliquots were then stored at -80° C.

6. The procedure was repeated in 72 hours.

7. Aliquoted samples were assayed using the plaque assay, as described above.

The best titers of LCMV-13 were generated using a MOI of 0.1 and harvesting virus at 48 hours post infection. (Table AI-2). The LCMV-13 viral stocks obtained using MOI of 0.05 and 0.1 and rescued after 48 and 72 hours post infection, can be used in *in vivo* studies. Infections using a lower MOI confers the advantage of diluting the DI particles out, giving the infectious LCMV particles a better chance to replicate and yield a better infectious titer.

Table AI-2. LCMV-13 titer values at different MOI and time of infection

MOI	Rescue time point	Average Titer (PFU/ml)
0.01	48 hours	3×10^7
	72 hours	1×10^7
0.05	48 hours	1×10^7
	72 hours	1×10^8
0.1	48 hours	1.3×10^9
	72 hours	9×10^8

AI.4 Concluding remarks

Optimal titer values for LCMV-13 can be obtained using a MOI of 0.1 and by rescuing viruses at 48 hours post infection. Growth conditions of LCMV likely depend on the nature of the seeding stock (the infectious titer of the seeding stock), where the optimal MOI and rescue time point may differ accordingly. The results of these experiments are key for building capabilities to study T cell exhaustion using the LCMV mouse model of chronic viral infection.

AI.5 Contributions

The experiments in this chapter were performed by me (VA) in collaboration with Kelly Huang (KH) as part of my curricular practical training (CPT) at MedImmune, LLC. I conducted all the plaque assays and the experiment to monitor the LCMV virus growth dynamics. VA and KH participated in design of the experiments. VA and KH critically reviewed the interpretation and discussion of the results.

Bibliography

1. Singh K, Flores JA, Kirby KA, Neogi U, Sonnerborg A, Hachiya A, Das K, Arnold E, McArthur C, Parniak M, Sarafianos SG: **Drug resistance in non-B subtype HIV-1: impact of HIV-1 reverse transcriptase inhibitors.** *Viruses* 2014, **6:**3535-3562.
2. AVERT: **HIV types, subtypes groups and strains.** 2011.
3. Fenstermacher K: **The mature HIV virion. figshare.** 2013.
4. Esposito F, Corona A, Tramontano E: **HIV-1 Reverse Transcriptase Still Remains a New Drug Target: Structure, Function, Classical Inhibitors, and New Inhibitors with Innovative Mechanisms of Actions.** *Mol. Biol. Int.* 2012, **2012:**586401.
5. Johnson KA: **The kinetic and chemical mechanism of high-fidelity DNA polymerases.** *Biochem. Biophys. Acta* 2010, **1804:**1041-1048.
6. Boyer JC, Bebenek K, Kunkel T, A: **Analyzing the fidelity of reverse transcription and transcription.** *Methods in Enzymology* 1996, **275:**523-537.
7. Swanson CM, Malim MH: **SnapShot: HIV-1 proteins.** *Cell* 2008, **133:**742, 742 e741.
8. Engelman A, Cherepanov P: **The structural biology of HIV-1: mechanistic and therapeutic insights.** *Nat. Rev. Microbiol.* 2012, **10:**279-290.
9. Korber TB, Foley TB, Kuiken LC, Pillai KS, Sodroski GJ: **Numbering Positions in HIV Relative to HXB2CG.** *Human Retroviruses and AIDS* 1998.
10. Achuthan V, Keith BJ, Connolly BA, DeStefano JJ: **Human Immunodeficiency Virus Reverse Transcriptase Displays Dramatically Higher Fidelity under Physiological Magnesium Conditions In Vitro.** *J. Virol.* 2014, **88:**8514-8527.
11. Gottlieb MS: **Pneumocystis pneumonia--Los Angeles.** 1981.
12. Am J Public Health 96 d: 2006.
13. (CDC). CfDC: **Kaposi's sarcoma and Pneumocystis pneumonia among homosexual men--New York City and California. MMWR Morb. Mortal. Wkly. Rep. .** *30* 1982**:**305-308.
14. Centers for Disease Control (CDC). 31 --: **Update on acquired immune deficiency syndrome (163) among patients with hemophilia A. MMWR Morb. Mortal. Wkly. Rep.** 1982, **31:**644-646-652.
15. Masur H, Michelis, M. A., Greene, J. B., Onorato, I., Stouwe, R. A., Holzman, R. S., Wormser, G., Brettman, L., Lange, M., Murray, H. W. & Cunningham-Rundles, S. : **An outbreak of community-acquired Pneumocystis carinii pneumonia: initial manifestation of cellular immune dysfunction.** *N. Engl. J. Med.* 1981, **305:**1431–1438.
16. Gallo RC, Salahuddin SZ, Popovic M, Shearer GM, Kaplan M, Haynes BF, Palker TJ, Redfield R, Oleske J, Safai B, et al.: **Frequent detection and isolation of cytopathic retroviruses (HTLV-III) from patients with AIDS and at risk for AIDS.** *Science* 1984, **224:**500-503.
17. UNAIDS: **Global AIDS Response Progress Reporting 2015.** 2015.
18. Sharp PM, Hahn BH: **Origins of HIV and the AIDS pandemic.** *Cold Spring Harb. Perspect. Med.* 2011, **1:**a006841.
19. Locatelli S, Peeters M: **Cross-species transmission of simian retroviruses: how and why they could lead to the emergence of new diseases in the human population.** *AIDS* 2012, **26:**659-673.

20. Guyader M, Emerman M, Sonigo P, Clavel F, Montagnier L, Alizon M: **Genome organization and transactivation of the human immunodeficiency virus type 2.** *Nature* 1987, **326:**662-669.

21. Ntemgwa ML, d'Aquin Toni T, Brenner BG, Camacho RJ, Wainberg MA: **Antiretroviral drug resistance in human immunodeficiency virus type 2.** *Antimicrobial agents and chemotherapy* 2009, **53:**3611-3619.

22. Plantier JC, Leoz M, Dickerson JE, De Oliveira F, Cordonnier F, Lemee V, Damond F, Robertson DL, Simon F: **A new human immunodeficiency virus derived from gorillas.** *Nat. Med.* 2009, **15:**871-872.

23. D'Arc M, Ayouba A, Esteban A, Learn GH, Boue V, Liegeois F, Etienne L, Tagg N, Leendertz FH, Boesch C, et al: **Origin of the HIV-1 group O epidemic in western lowland gorillas.** *Proc. Natl. Acad. Sci. U S A* 2015, **112:**E1343-1352.

24. Vallari A, Holzmayer V, Harris B, Yamaguchi J, Ngansop C, Makamche F, Mbanya D, Kaptue L, Ndembi N, Gurtler L, et al: **Confirmation of putative HIV-1 group P in Cameroon.** *J. Virol.* 2011, **85:**1403-1407.

25. Delaugerre C, De Oliveira F, Lascoux-Combe C, Plantier JC, Simon F: **HIV-1 group N: travelling beyond Cameroon.** *Lancet* 2011, **378:**1894.

26. Sharp PMH, B. H. : **Origins of HIV and the AIDS pandemic.** *Cold Spring Harb. Perspect. Med. 1, a006841* 2011.

27. Kahn JO, Walker BD: **Acute human immunodeficiency virus type 1 infection.** *N. Engl. J. Med.* 1998, **339:**33-39.

28. Grossman Z, M. Meier-Schellersheim, W. E. Paul, and L. J. Picker.: **Pathogenesis of HIV infection: what the virus spares is as important as what it destroys.** *Nat. Med.* 2006, **12:**282-295.

29. Perelson AS, Neumann AU, Markowitz M, Leonard JM, Ho DD: **HIV-1 dynamics in vivo: virion clearance rate, infected cell life-span, and viral generation time.** *Science* 1996, **271:**1582-1586.

30. Barin F, McLane MF, Allan JS, Lee TH, Groopman JE, Essex M: **Virus envelope protein of HTLV-III represents major target antigen for antibodies in AIDS patients.** *Science* 1985, **228:**1094-1096.

31. Coffin JM, Hughes SH, Varmus HE: *Retroviruses.* Cold Spring Harbor, NY: Cold Spring Harbor Laboratory Press; 1997.

32. Levin JG, Guo J, Rouzina I, Musier-Forsyth K: **Nucleic Acid chaperone activity of HIV-1 nucleocapsid protein: critical role in reverse transcription and molecular mechanism.** *Prog Nucleic Acids Res. Mol. Biol.* 2005, **80:**217-286.

33. Hu W-S, Temin HM: **Genetic consequences of packaging two RNA genomes in one retroviral particle: pseudodiploidy and high rate of genetic recombination.** *Proc. Natl. Acad. Sci.* 1990, **87:**1556-1560.

34. Bannwarth S, Gatignol A: **HIV-1 TAR RNA: the target of molecular interactions between the virus and its host.** *Curr. HIV Res.* 2005, **3:**61-71.

35. Beerens N, Groot F, Berkhout B: **Initiation of HIV-1 reverse transcription is regulated by a primer activation signal.** *J. Biol. Chem.* 2001, **276:**31247-31256.

36. Moore MD, Fu W, Nikolaitchik O, Chen J, Ptak RG, Hu WS: **Dimer initiation signal of human immunodeficiency virus type 1: its role in partner selection during RNA copackaging and its effects on recombination.** *J. Virol.* 2007, **81:**4002-4011.

37. Fernandes J, Jayaraman B, Frankel A: **The HIV-1 Rev response element: an RNA scaffold that directs the cooperative assembly of a homo-oligomeric ribonucleoprotein complex.** *RNA Biol.* 2012, **9:**6-11.

38. Berger EA, Doms RW, Fenyo EM, Korber BT, Littman DR, Moore JP, Sattentau QJ, Schuitemaker H, Sodroski J, Weiss RA: **A new classification for HIV-1.** *Nature* 1998, **391:**240.

39. Keele BF, Giorgi EE, Salazar-Gonzalez JF, Decker JM, Pham KT, Salazar MG, Sun C, Grayson T, Wang S, Li H, et al: **Identification and characterization of transmitted and early founder virus envelopes in primary HIV-1 infection.** *Proc. Natl. Acad. Sci. U. S. A.* 2008, **105:**7552-7557.

40. Tersmette M, Gruters RA, de Wolf F, de Goede RE, Lange JM, Schellekens PT, Goudsmit J, Huisman HG, Miedema F: **Evidence for a role of virulent human immunodeficiency virus (HIV) variants in the pathogenesis of acquired immunodeficiency syndrome: studies on sequential HIV isolates.** *J. Virol.* 1989, **63:**2118-2125.

41. Schuitemaker H, Koot M, Kootstra NA, Dercksen MW, de Goede RE, van Steenwijk RP, Lange JM, Schattenkerk JK, Miedema F, Tersmette M: **Biological phenotype of human immunodeficiency virus type 1 clones at different stages of infection: progression of disease is associated with a shift from monocytotropic to T-cell-tropic virus population.** *J. Virol.* 1992, **66:**1354-1360.

42. Connor RI, Sheridan KE, Ceradini D, Choe S, Landau NR: **Change in coreceptor use correlates with disease progression in HIV-1--infected individuals.** *J. Exp. Med.* 1997, **185:**621-628.

43. Owen SM, Ellenberger D, Rayfield M, Wiktor S, Michel P, Grieco MH, Gao F, Hahn BH, Lal RB: **Genetically divergent strains of human immunodeficiency virus type 2 use multiple coreceptors for viral entry.** *J. Virol.* 1998, **72:**5425-5432.

44. Choe H, Farzan M, Sun Y, Sullivan N, Rollins B, Ponath PD, Wu L, Mackay CR, LaRosa G, Newman W, et al: **The beta-chemokine receptors CCR3 and CCR5 facilitate infection by primary HIV-1 isolates.** *Cell* 1996, **85:**1135-1148.

45. Dittmar MT, McKnight A, Simmons G, Clapham PR, Weiss RA, Simmonds P: **HIV-1 tropism and co-receptor use.** *Nature* 1997, **385:**495-496.

46. Doranz BJ, Rucker J, Yi Y, Smyth RJ, Samson M, Peiper SC, Parmentier M, Collman RG, Doms RW: **A dual-tropic primary HIV-1 isolate that uses fusin and the beta-chemokine receptors CKR-5, CKR-3, and CKR-2b as fusion cofactors.** *Cell* 1996, **85:**1149-1158.

47. Wilen CB, Tilton JC, Doms RW: **HIV: cell binding and entry.** *Cold Spring Harb. Perspect. Med.* 2012, **2**.

48. Bleichner G, Monsallier JF: **[Cardio-circulatory arrest].** *Nouv. Presse Med.* 1975, **4:**1435-1438.

49. Cicala C, Martinelli E, McNally JP, Goode DJ, Gopaul R, Hiatt J, Jelicic K, Kottilil S, Macleod K, O'Shea A, et al: **The integrin alpha4beta7 forms a complex with cell-surface CD4 and defines a T-cell subset that is highly susceptible to infection by HIV-1.** *Proc. Natl. Acad. Sci. U. S. A.* 2009, **106:**20877-20882.

50. Geijtenbeek TB, Kwon DS, Torensma R, van Vliet SJ, van Duijnhoven GC, Middel J, Cornelissen IL, Nottet HS, KewalRamani VN, Littman DR, et al: **DC-SIGN, a dendritic cell-specific HIV-1-binding protein that enhances trans-infection of T cells.** *Cell* 2000, **100:**587-597.

51. Kwong PD, Wyatt R, Robinson J, Sweet RW, Sodroski J, Hendrickson WA: **Structure of an HIV gp120 envelope glycoprotein in complex with the CD4 receptor and a neutralizing human antibody.** *Nature* 1998, **393:**648-659.

52. Chen B, Vogan EM, Gong H, Skehel JJ, Wiley DC, Harrison SC: **Structure of an unliganded simian immunodeficiency virus gp120 core.** *Nature* 2005, **433:**834-841.

53. Sattentau QJ, Moore JP, Vignaux F, Traincard F, Poignard P: **Conformational changes induced in the envelope glycoproteins of the human and simian immunodeficiency viruses by soluble receptor binding.** *J. Virol.* 1993, **67:**7383-7393.

54. Chan DC, Fass D, Berger JM, Kim PS: **Core structure of gp41 from the HIV envelope glycoprotein.** *Cell* 1997, **89:**263-273.

55. Weissenhorn W, Dessen A, Harrison SC, Skehel JJ, Wiley DC: **Atomic structure of the ectodomain from HIV-1 gp41.** *Nature* 1997, **387:**426-430.

56. Melikyan GB: **Common principles and intermediates of viral protein-mediated fusion: the HIV-1 paradigm.** *Retrovirology* 2008, **5:**111.

57. Warrilow D, Tachedjian G, Harrich D: **Maturation of the HIV reverse transcription complex: putting the jigsaw together.** *Rev. Med. Virol.* 2009, **19:**324-337.

58. Arhel N: **Revisiting HIV-1 uncoating.** *Retrovirology* 2010, **7:**96.

59. Brown PO, Bowerman B, Varmus HE, Bishop JM: **Retroviral integration: structure of the initial covalent product and its precursor, and a role for the viral IN protein.** *Proc. Natl. Acad. Sci. U. S. A.* 1989, **86:**2525-2529.

60. Schroder AR, Shinn P, Chen H, Berry C, Ecker JR, Bushman F: **HIV-1 integration in the human genome favors active genes and local hotspots.** *Cell* 2002, **110:**521-529.

61. Craigie R: **HIV integrase, a brief overview from chemistry to therapeutics.** *J. Biol. Chem.* 2001, **276:**23213-23216.

62. Maldarelli F, Wu X, Su L, Simonetti FR, Shao W, Hill S, Spindler J, Ferris AL, Mellors JW, Kearney MF, et al: **HIV latency. Specific HIV integration sites are linked to clonal expansion and persistence of infected cells.** *Science* 2014, **345:**179-183.

63. Rampalli S, Kulkarni A, Kumar P, Mogare D, Galande S, Mitra D, Chattopadhyay S: **Stimulation of Tat-independent transcriptional processivity from the HIV-1 LTR promoter by matrix attachment regions.** *Nucleic Acids Res.* 2003, **31:**3248-3256.

64. Jacks T, Madhani HD, Masiarz FR, Varmus HE: **Signals for ribosomal frameshifting in the Rous sarcoma virus gag-pol region.** *Cell* 1988, **55:**447-458.

65. Hallenberger S, Bosch V, Angliker H, Shaw E, Klenk HD, Garten W: **Inhibition of furin-mediated cleavage activation of HIV-1 glycoprotein gp160.** *Nature* 1992, **360:**358-361.

66. Brierley I, Dos Ramos FJ: **Programmed ribosomal frameshifting in HIV-1 and the SARS-CoV.** *Virus Res.* 2006, **119:**29-42.

67. Cen S, Guo F, Niu M, Saadatmand J, Deflassieux J, Kleiman L: **The interaction between HIV-1 Gag and APOBEC3G.** *J. Biol. Chem.* 2004.

68. Dinman JD, Richter S, Plant EP, Taylor RC, Hammell AB, Rana TM: **The frameshift signal of HIV-1 involves a potential intramolecular triplex RNA structure.** *Proc. Natl. Acad. Sci. U. S. A.* 2002, **99:**5331-5336.

69. Park J, Morrow CD: **Overexpression of the gag-pol precursor from human immunodeficiency virus type 1 proviral genomes results in efficient proteolytic processing in the absence of virion production.** *J. Virol.* 1991, **65:**5111-5117.

70. Karacostas V, Wolffe EJ, Nagashima K, Gonda MA, Moss B: **Overexpression of the HIV-1 gag-pol polyprotein results in intracellular activation of HIV-1 protease and inhibition of assembly and budding of virus-like particles.** *Virology* 1993, **193:**661-671.

71. Cherry E, Liang C, Rong L, Quan Y, Inouye P, Li X, Morin N, Kotler M, Wainberg MA: **Characterization of human immunodeficiency virus type-1 (HIV-1) particles that express protease-reverse transcriptase fusion proteins.** *J. Mol. Biol.* 1998, **284:**43-56.

72. Waheed AA, Ablan SD, Mankowski MK, Cummins JE, Ptak RG, Schaffner CP, Freed EO: **Inhibition of HIV-1 replication by amphotericin B methyl ester: selection for resistant variants.** *J. Biol. Chem.* 2006, **281:**28699-28711.

73. Demirov DGaEOF: **Retrovirus budding.** *Virus. Res.* 2004, **406:**87-102.

74. Wills JW, Craven RC: **Form, function, and use of retroviral gag proteins.** *AIDS* 1991, **5:**639-654.

75. Swanstrom R, Wills JW: **Synthesis, Assembly, and Processing of Viral Proteins.** 1997.

76. Vogt VM: **Retroviral Virions and Genomes.** 1997.

77. Hu WS, Hughes SH: **HIV-1 reverse transcription.** *Cold Spring Harb. Perspect. Med.* 2012, **2**.

78. Ao Z, Yao X, Cohen EA: **Assessment of the role of the central DNA flap in human immunodeficiency virus type 1 replication by using a single-cycle replication system.** *J. Virol.* 2004, **78:**3170-3177.

79. Zennou V, Petit C, Guetard D, Nerhbass U, Montagnier L, Charneau P: **HIV-1 genome nuclear import is mediated by a central DNA flap.** *Cell* 2000, **101:**173-185.

80. Burdick RC, Hu WS, Pathak VK: **Nuclear import of APOBEC3F-labeled HIV-1 preintegration complexes.** *Proc. Natl. Acad. Sci. U. S. A.* 2013, **110:**E4780-4789.

81. Telesnitsky A, Goff SP: *Reverse Transcriptase.* Cold Spring Harbor, N. Y.: Cold Spring Harbor Laboratory Press; 1993.

82. Abram ME, Sarafianos SG, Parniak MA: **The mutation T477A in HIV-1 reverse transcriptase (RT) restores normal proteolytic processing of RT in virus with Gag-Pol mutated in the p51-RNH cleavage site.** *Retrovirology* 2010, **7:**6.

83. Ren J, Bird LE, Chamberlain PP, Stewart-Jones GB, Stuart DI, Stammers DK: **Structure of HIV-2 reverse transcriptase at 2.35-A resolution and the mechanism of resistance to non-nucleoside inhibitors.** *Proc. Natl. Acad. Sci. U. S. A.* 2002, **99:**14410-14415.

84. Tasara T, Amacker M, Hubscher U: **Intramolecular chimeras of the p51 subunit between HIV-1 and FIV reverse transcriptases suggest a stabilizing function for the p66 subunit in the heterodimeric enzyme.** *Biochemistry* 1999, **38:**1633-1642.

85. Harris. D. RL, H. S. Misra, P. K. Pandey, and V. N. Pandey: **The p51 subunit of human immunodeficiency virus type 1 reverse transcriptase is essential in loading the p66 subunit on the template.** *Biochemistry* 1998, **37:**5903-5908.

86. Kohlstaedt LA, Wang J, Friedman JM, Rice PA, Steitz TA: **Crystal structure at 3.5 A resolution of HIV-1 reverse transcriptase complexed with an inhibitor.** *Science* 1992, **256:**1783-1790.

87. Chiba J, Yamaguchi A, Suzuki Y, Nakano M, Zhu W, Ohba H, Saito A, Shinagawa H, Yamakawa Y, Kobayashi T, Kurata T: **A novel neutralization epitope on the 'thumb' subdomain of human immunodeficiency virus type 1 reverse transcriptase revealed by a monoclonal antibody.** *J. Gen. Virol.* 1996, **77 (Pt 12):**2921-2929.

88. Kirmizialtin S, Nguyen V, Johnson KA, Elber R: **How conformational dynamics of DNA polymerase select correct substrates: experiments and simulations.** *Structure* 2012, **20:**618-627.

89. Sarafianos SG, Das K, Tantillo C, Clark AD, Jr., Ding J, Whitcomb JM, Boyer PL, Hughes SH, Arnold E: **Crystal structure of HIV-1 reverse transcriptase in complex with a polypurine tract RNA:DNA.** *Embo J.* 2001, **20:**1449-1461.

90. Schatz O, Mous J, Le Grice SF: **HIV-1 RT-associated ribonuclease H displays both endonuclease and 3'----5' exonuclease activity.** *Embo J.* 1990, **9:**1171-1176.

91. Herschhorn A, Hizi A: **Retroviral reverse transcriptases.** *Cell Mol. Life Sci.* 2010, **67:**2717-2747.

92. Goff SP: **Retroviral reverse transcriptase: synthesis, structure and function.** *Acquired Immune Deficiency Syndromes* 1990, **3:**817-831.

93. Steitz TA: **A mechanism for all polymerases.** *Nature* 1998, **391:**231-232.

94. Schultz SJ, Champoux JJ: **RNase H activity: structure, specificity, and function in reverse transcription.** *Virus Res.* 2008, **134:**86-103.

95. Mansky LM, Temin HM: **Lower *in vivo* mutation rate of human immunodeficiency virus type 1 than that predicted from the fidelity of purified reverse transcriptase.** *J. Virol.* 1995, **69:**5087-5094.

96. Preston BD, Poiesz BJ, Loeb LA: **Fidelity of HIV-1 reverse transcriptase.** *Science* 1988, **242:**1168-1171.

97. Bebenek K, Abbotts J, Roberts JD, Wilson SH, Kunkel TA: **Specificity and mechanism of error-prone replication by human immunodeficiency virus-1 reverse transcriptase.** *J. Biol. Chem.* 1989, **264:**16948-16956.

98. Menendez-Arias L: **Mutation rates and intrinsic fidelity of retroviral reverse transcriptases.** *Viruses* 2009, **1:**1137-1165.

99. Sanjuan R, Nebot MR, Chirico N, Mansky LM, Belshaw R: **Viral mutation rates.** *J. Virol.* 2010, **84:**9733-9748.

100. Coffin JM: **HIV population dynamics in vivo: implications for genetic variation, pathogenesis, and therapy.** *Science* 1995, **267:**483-489.

101. Pathak VK, Temin HM: **Broad spectrum of in vivo forward mutations, hypermutations, and mutational hotspots in a retroviral shuttle vector after a single replication cycle: deletions and deletions with insertions.** *Proc. Natl. Acad. Sci. U. S. A.* 1990, **87:**6024-6028.

102. Pathak VK, Temin HM: **Broad spectrum of in vivo forward mutations, hypermutations, and mutational hotspots in a retroviral shuttle vector after a single replication cycle: substitutions, frameshifts, and hypermutations.** *Proc. Natl. Acad. Sci. U. S. A.* 1990, **87:**6019-6023.

103. Abram ME, Ferris AL, Shao W, Alvord WG, Hughes SH: **Nature, position, and frequency of mutations made in a single cycle of HIV-1 replication.** *J. Virol.* 2010, **84:**9864-9878.

104. Boyer JC, Bebenek K, Kunkel TA: **Unequal human immunodeficiency virus type 1 reverse transcriptase error rates with RNA and DNA templates.** *Proc. Natl. Acad. Sci. U. S. A.* 1992, **89:**6919-6923.

105. Ji JP, Loeb LA: **Fidelity of HIV-1 reverse transcriptase copying RNA in vitro.** *Biochemistry* 1992, **31:**954-958.

106. Russell RA, Pathak VK: **Identification of two distinct human immunodeficiency virus type 1 Vif determinants critical for interactions with human APOBEC3G and APOBEC3F.** *J. Virol.* 2007, **81:**8201-8210.

107. Fang L, Landau NR: **Analysis of Vif-induced APOBEC3G degradation using an alpha-complementation assay.** *Virology* 2007, **359:**162-169.

108. Doria M, Neri F, Gallo A, Farace MG, Michienzi A: **Editing of HIV-1 RNA by the double-stranded RNA deaminase ADAR1 stimulates viral infection.** *Nucleic Acids Res.* 2009, **37:**5848-5858.

109. Sousa MM, Krokan HE, Slupphaug G: **DNA-uracil and human pathology.** *Mol. Aspects. Med.* 2007, **28:**276-306.

110. Mansky LM, Preveral S, Selig L, Benarous R, Benichou S: **The interaction of vpr with uracil DNA glycosylase modulates the human immunodeficiency virus type 1 In vivo mutation rate.** *J. Virol.* 2000, **74:**7039-7047.

111. Guenzel CA, Herate C, Le Rouzic E, Maidou-Peindara P, Sadler HA, Rouyez MC, Mansky LM, Benichou S: **Recruitment of the nuclear form of uracil DNA glycosylase into virus particles participates in the full infectivity of HIV-1.** *J. Virol.* 2012, **86:**2533-2544.

112. Hu W-S, Hughes SH: **HIV-1 reverse transcription.** In *HIV From Biology to Prevention and Treatment.* Edited by Bushman FD, Nabel GJ, Swanstrom R. Cold Spring Harbor Cold Spring Harbor Laboratory Press; 2012: 37-58

113. Bampi C, Bibillo A, Wendeler M, Divita G, Gorelick RJ, Le Grice SF, Darlix JL: **Nucleotide excision repair and template-independent addition by HIV-1 reverse transcriptase in the presence of nucleocapsid protein.** *The Journal of biological chemistry* 2006, **281:**11736-11743.

114. Lapadat-Tapolsky M, Gabus C, Rau M, Darlix JL: **Possible roles of HIV-1 nucleocapsid protein in the specificity of proviral DNA synthesis and in its variability.** *J. Mol. Biol.* 1997, **268:**250-260.

115. DeStefano J, Ghosh J, Prasad B, Raja A: **High fidelity of internal strand transfer catalyzed by human immunodeficiency virus reverse transcriptase.** *J. Biol. Chem.* 1998, **273:**1483-1489.

116. Bakhanashvili M, Novitsky E, Levy I, Rahav G: **The fidelity of DNA synthesis by human immunodeficiency virus type 1 reverse transcriptase increases in the presence of polyamines.** *FEBS Lett.* 2005, **579:**1435-1440.

117. Kunkel TA: **Evolving views of DNA replication (in)fidelity.** *Cold Spring Harb Symp Quant. Biol.* 2009, **74:**91-101.

118. Wu WJ, Su MI, Wu JL, Kumar S, Lim LH, Wang CW, Nelissen FH, Chen MC, Doreleijers JF, Wijmenga SS, Tsai MD: **How a low-fidelity DNA polymerase chooses non-Watson-Crick from Watson-Crick incorporation.** *J. Am. Chem. Soc.* 2014, **136:**4927-4937.

119. Tsai YC, Johnson KA: **A new paradigm for DNA polymerase specificity.** *Biochemistry* 2006, **45:**9675-9687.

120. Johnson KA: **Role of induced fit in enzyme specificity: a molecular forward/reverse switch.** *J. Biol. Chem.* 2008, **283:**26297-26301.

121. Kellinger MW, Johnson KA: **Role of induced fit in limiting discrimination against AZT by HIV reverse transcriptase.** *Biochemistry* 2011, **50:**5008-5015.

122. Lee HR, Helquist SA, Kool ET, Johnson KA: **Importance of hydrogen bonding for efficiency and specificity of the human mitochondrial DNA polymerase.** *J. Biol. Chem.* 2008, **283:**14402-14410.

123. Zhou BL, Pata JD, Steitz TA: **Crystal structure of a DinB lesion bypass DNA polymerase catalytic fragment reveals a classic polymerase catalytic domain.** *Mol. Cell* 2001, **8:**427-437.
124. Garcia-Diaz M, Bebenek K, Krahn JM, Kunkel TA, Pedersen LC: **A closed conformation for the Pol lambda catalytic cycle.** *Nat. Struct. Mol. Biol.* 2005, **12:**97-98.
125. Bebenek K, Pedersen LC, Kunkel TA: **Replication infidelity via a mismatch with Watson-Crick geometry.** *Proc. Natl. Acad. Sci. U. S. A.* 2011, **108:**1862-1867.
126. Hunter E: **The mechanism for genetic recombination in the avian retroviruses.** *Curr. Top Microbiol. Immunol.* 1978, **79:**295-309.
127. Zhang J, Temin HM: **Rate and mechanism of nonhomologous recombination during a single cycle of retroviral replication.** *Science* 1993, **259:**234-238.
128. Hu WS, Temin HM: **Retroviral recombination and reverse transcription.** *Science* 1990, **250:**1227-1233.
129. Katz RA, Skalka AM: **Generation of diversity in retroviruses.** *Annu. Rev. Genet.* 1990, **24:**409-445.
130. Temin HM: **Retrovirus variation and reverse transcription: abnormal strand transfers result in retrovirus genetic variation.** *Proc. Natl. Acad. Sci. U. S. A.* 1993, **90:**6900-6903.
131. Coffin JM: **Structure, replication, and recombination of retrovirus genomes: some unifying hypotheses.** *Journal of General Virology* 1979, **42:**1-26.
132. Zhuang J, Jetzt AE, Sun G, Yu H, Klarmann G, Ron Y, Preston BD, Dougherty JP: **Human immunodeficiency virus type 1 recombination: rate, fidelity, and putative hot spots.** *J. Virol.* 2002, **76:**11273-11282.
133. Levy DN, Aldrovandi GM, Kutsch O, Shaw GM: **Dynamics of HIV-1 recombination in its natural target cells.** *Proc. Natl. Acad. Sci. U. S. A.* 2004, **101:**4204-4209.
134. Onafuwa A, An W, Robson ND, Telesnitsky A: **Human Immunodeficiency Virus Type 1 Genetic Recombination Is More Frequent Than That of Moloney Murine Leukemia Virus despite Similar Template Switching Rates.** *J. Virol.* 2003, **77:**4577-4587.
135. Zhuang J, Mukherjee S, Ron Y, Dougherty JP: **High rate of genetic recombination in murine leukemia virus: implications for influencing proviral ploidy.** *J. Virol.* 2006, **80:**6706-6711.
136. Collier AC, Coombs RW, Schoenfeld DA, Bassett RL, Timpone J, Baruch A, Jones M, Facey K, Whitacre C, McAuliffe VJ, et al: **Treatment of human immunodeficiency virus infection with saquinavir, zidovudine, and zalcitabine. AIDS Clinical Trials Group.** *N. Engl. J. Med.* 1996, **334:**1011-1017.
137. D'Aquila RT, Hughes MD, Johnson VA, Fischl MA, Sommadossi JP, Liou SH, Timpone J, Myers M, Basgoz N, Niu M, Hirsch MS: **Nevirapine, zidovudine, and didanosine compared with zidovudine and didanosine in patients with HIV-1 infection. A randomized, double-blind, placebo-controlled trial. National Institute of Allergy and Infectious Diseases AIDS Clinical Trials Group Protocol 241 Investigators.** *Ann Intern Med* 1996, **124:**1019-1030.
138. Autran B, Carcelain G, Li TS, Blanc C, Mathez D, Tubiana R, Katlama C, Debre P, Leibowitch J: **Positive effects of combined antiretroviral therapy on CD4+ T cell homeostasis and function in advanced HIV disease.** *Science* 1997, **277:**112-116.
139. Lederman MM, Connick E, Landay A, Kuritzkes DR, Spritzler J, St Clair M, Kotzin BL, Fox L, Chiozzi MH, Leonard JM, et al: **Immunologic responses associated with 12 weeks**

of combination antiretroviral therapy consisting of zidovudine, lamivudine, and ritonavir: results of AIDS Clinical Trials Group Protocol 315. *J. Infect. Dis.* 1998, **178:**70-79.

140. Fischl MA, Richman DD, Grieco MH, Gottlieb MS, Volberding PA, Laskin OL, Leedom JM, Groopman JE, Mildvan D, Schooley RT, et al.: **The efficacy of azidothymidine (AZT) in the treatment of patients with AIDS and AIDS-related complex. A double-blind, placebo-controlled trial.** *N. Engl. J. Med.* 1987, **317:**185-191.

141. Cheng YC, Dutschman GE, Bastow KF, Sarngadharan MG, Ting RY: **Human immunodeficiency virus reverse transcriptase. General properties and its interactions with nucleoside triphosphate analogs.** *J. Biol. Chem.* 1987, **262:**2187-2189.

142. Balzarini J, Herdewijn P, De Clercq E: **Differential patterns of intracellular metabolism of 2',3'-didehydro-2',3'-dideoxythymidine and 3'-azido-2',3'-dideoxythymidine, two potent anti-human immunodeficiency virus compounds.** *J. Biol. Chem.* 1989, **264:**6127-6133.

143. Richman DD: **HIV chemotherapy.** *Nature* 2001, **410:**995-1001.

144. Hart GJ, Orr DC, Penn CR, Figueiredo HT, Gray NM, Boehme RE, Cameron JM: **Effects of (-)-2'-deoxy-3'-thiacytidine (3TC) 5'-triphosphate on human immunodeficiency virus reverse transcriptase and mammalian DNA polymerases alpha, beta, and gamma.** *Antimicrobial agents and chemotherapy* 1992, **36:**1688-1694.

145. Larder BA, Kemp SD: **Multiple mutations in HIV-1 reverse transcriptase confer high-level resistance to zidovudine (AZT).** *Science* 1989, **246:**1155-1158.

146. Marcelin AG, Delaugerre C, Wirden M, Viegas P, Simon A, Katlama C, Calvez V: **Thymidine analogue reverse transcriptase inhibitors resistance mutations profiles and association to other nucleoside reverse transcriptase inhibitors resistance mutations observed in the context of virological failure.** *J. Med. Virol.* 2004, **72:**162-165.

147. Meyer PR, Matsuura SE, Mian AM, So AG, Scott WA: **A mechanism of AZT resistance: an increase in nucleotide-dependent primer unblocking by mutant HIV-1 reverse transcriptase.** *Mol. Cell.* 1999, **4:**35-43.

148. Boyer PL, Sarafianos SG, Arnold E, Hughes SH: **Selective excision of AZTMP by drug-resistant human immunodeficiency virus reverse transcriptase.** *J. Virol.* 2001, **75:**4832-4842.

149. Schinazi RF, Lloyd RM, Jr., Nguyen MH, Cannon DL, McMillan A, Ilksoy N, Chu CK, Liotta DC, Bazmi HZ, Mellors JW: **Characterization of human immunodeficiency viruses resistant to oxathiolane-cytosine nucleosides.** *Antimicrobial agents and chemotherapy* 1993, **37:**875-881.

150. Quan Y, Gu Z, Li X, Li Z, Morrow CD, Wainberg MA: **Endogenous reverse transcription assays reveal high-level resistance to the triphosphate of (-)2'-dideoxy-3'-thiacytidine by mutated M184V human immunodeficiency virus type 1.** *J. Virol.* 1996, **70:**5642-5645.

151. Wainberg MA, Miller MD, Quan Y, Salomon H, Mulato AS, Lamy PD, Margot NA, Anton KE, Cherrington JM: **In vitro selection and characterization of HIV-1 with reduced susceptibility to PMPA.** *Antivir. Ther.* 1999, **4:**87-94.

152. Margot NA, Isaacson E, McGowan I, Cheng AK, Schooley RT, Miller MD: **Genotypic and phenotypic analyses of HIV-1 in antiretroviral-experienced patients treated with tenofovir DF.** *AIDS* 2002, **16:**1227-1235.

153. Colson P, Henry M, Tivoli N, Gallais H, Gastaut JA, Moreau J, Tamalet C: **Polymorphism and drug-selected mutations in the reverse transcriptase gene of HIV-2 from patients living in southeastern France.** *J. Med. Virol.* 2005, **75:**381-390.

154. Descamps D, Damond F, Matheron S, Collin G, Campa P, Delarue S, Pueyo S, Chene G, Brun-Vezinet F: **High frequency of selection of K65R and Q151M mutations in HIV-2 infected patients receiving nucleoside reverse transcriptase inhibitors containing regimen.** *J. Med. Virol.* 2004, **74:**197-201.

155. Andreatta K, Miller MD, White KL: **HIV-2 antiviral potency and selection of drug resistance mutations by the integrase strand transfer inhibitor elvitegravir and NRTIs emtricitabine and tenofovir in vitro.** *J. Acquir. Immune Defic. Syndr.* 2013, **62:**367-374.

156. Tantillo C, Ding J, Jacobo-Molina A, Nanni RG, Boyer PL, Hughes SH, Pauwels R, Andries K, Janssen PA, Arnold E: **Locations of anti-AIDS drug binding sites and resistance mutations in the three-dimensional structure of HIV-1 reverse transcriptase. Implications for mechanisms of drug inhibition and resistance.** *J. Mol. Biol.* 1994, **243:**369-387.

157. Parkin NT, Schapiro JM: **Antiretroviral drug resistance in non-subtype B HIV-1, HIV-2 and SIV.** *Antivir. Ther.* 2004, **9:**3-12.

158. Rodgers DW, Gamblin SJ, Harris BA, Ray S, Culp JS, Hellmig B, Woolf DJ, Debouck C, Harrison SC: **The structure of unliganded reverse transcriptase from the human immunodeficiency virus type 1.** *Proc. Natl. Acad. Sci. U. S. A.* 1995, **92:**1222-1226.

159. Hsiou Y, Ding J, Das K, Clark AD, Jr., Hughes SH, Arnold E: **Structure of unliganded HIV-1 reverse transcriptase at 2.7 A resolution: implications of conformational changes for polymerization and inhibition mechanisms.** *Structure* 1996, **4:**853-860.

160. Bacheler L, Jeffrey S, Hanna G, D'Aquila R, Wallace L, Logue K, Cordova B, Hertogs K, Larder B, Buckery R, et al: **Genotypic correlates of phenotypic resistance to efavirenz in virus isolates from patients failing nonnucleoside reverse transcriptase inhibitor therapy.** *J. Virol.* 2001, **75:**4999-5008.

161. Dykes C, Fox K, Lloyd A, Chiulli M, Morse E, Demeter LM: **Impact of clinical reverse transcriptase sequences on the replication capacity of HIV-1 drug-resistant mutants.** *Virology* 2001, **285:**193-203.

162. Deeks SG: **International perspectives on antiretroviral resistance. Nonnucleoside reverse transcriptase inhibitor resistance.** *J. Acquir. Immune. Defic. Syndr.* 2001, **26 Suppl 1:**S25-33.

163. Imamichi T, Murphy MA, Imamichi H, Lane HC: **Amino acid deletion at codon 67 and Thr-to-Gly change at codon 69 of human immunodeficiency virus type 1 reverse transcriptase confer novel drug resistance profiles.** *J. Virol.* 2001, **75:**3988-3992.

164. Grobler JA, Stillmock K, Hu B, Witmer M, Felock P, Espeseth AS, Wolfe A, Egbertson M, Bourgeois M, Melamed J, et al: **Diketo acid inhibitor mechanism and HIV-1 integrase: implications for metal binding in the active site of phosphotransferase enzymes.** *Proc. Natl. Acad. Sci. U. S. A.* 2002, **99:**6661-6666.

165. Damond F, Lariven S, Roquebert B, Males S, Peytavin G, Morau G, Toledano D, Descamps D, Brun-Vezinet F, Matheron S: **Virological and immunological response to HAART regimen containing integrase inhibitors in HIV-2-infected patients.** *AIDS* 2008, **22:**665-666.

166. Garrido C, Geretti AM, Zahonero N, Booth C, Strang A, Soriano V, De Mendoza C: **Integrase variability and susceptibility to HIV integrase inhibitors: impact of subtypes, antiretroviral experience and duration of HIV infection.** *J. Antimicrob. Chemother.* 2010, **65:**320-326.
167. Singh IR, Gorzynski JE, Drobysheva D, Bassit L, Schinazi RF: **Raltegravir is a potent inhibitor of XMRV, a virus implicated in prostate cancer and chronic fatigue syndrome.** *PloS One* 2010, **5:**e9948.
168. Quercia R, Dam E, Perez-Bercoff D, Clavel F: **Selective-advantage profile of human immunodeficiency virus type 1 integrase mutants explains in vivo evolution of raltegravir resistance genotypes.** *J Virol* 2009, **83:**10245-10249.
169. Fransen S, Gupta S, Danovich R, Hazuda D, Miller M, Witmer M, Petropoulos CJ, Huang W: **Loss of raltegravir susceptibility by human immunodeficiency virus type 1 is conferred via multiple nonoverlapping genetic pathways.** *J Virol* 2009, **83:**11440-11446.
170. Desbois D, Roquebert B, Peytavin G, Damond F, Collin G, Benard A, Campa P, Matheron S, Chene G, Brun-Vezinet F, Descamps D: **In vitro phenotypic susceptibility of human immunodeficiency virus type 2 clinical isolates to protease inhibitors.** *Antimicrobial agents and chemotherapy* 2008, **52:**1545-1548.
171. Brower ET, Bacha UM, Kawasaki Y, Freire E: **Inhibition of HIV-2 protease by HIV-1 protease inhibitors in clinical use.** *Chem. Biol. Drug Des* 2008, **71:**298-305.
172. Rodes B, Sheldon J, Toro C, Jimenez V, Alvarez MA, Soriano V: **Susceptibility to protease inhibitors in HIV-2 primary isolates from patients failing antiretroviral therapy.** *J. Antimicrob. Chemother.* 2006, **57:**709-713.
173. Quinones-Mateu ME, Arts EJ: **Fitness of drug resistant HIV-1: methodology and clinical implications.** *Drug Resist. Updat.* 2002, **5:**224-233.
174. Nijhuis M, Deeks S, Boucher C: **Implications of antiretroviral resistance on viral fitness.** *Curr. Opin. Infect. Dis.* 2001, **14:**23-28.
175. Lalezari JP, Henry K, O'Hearn M, Montaner JS, Piliero PJ, Trottier B, Walmsley S, Cohen C, Kuritzkes DR, Eron JJ, Jr., et al: **Enfuvirtide, an HIV-1 fusion inhibitor, for drug-resistant HIV infection in North and South America.** *N. Engl. J. Med.* 2003, **348:**2175-2185.
176. Poveda E, Rodes B, Toro C, Soriano V: **Are fusion inhibitors active against all HIV variants?** *AIDS Res Hum Retroviruses* 2004, **20:**347-348.
177. Reeves JD, Miamidian JL, Biscone MJ, Lee FH, Ahmad N, Pierson TC, Doms RW: **Impact of mutations in the coreceptor binding site on human immunodeficiency virus type 1 fusion, infection, and entry inhibitor sensitivity.** *J. Virol.* 2004, **78:**5476-5485.
178. Baldwin CE, Sanders RW, Deng Y, Jurriaans S, Lange JM, Lu M, Berkhout B: **Emergence of a drug-dependent human immunodeficiency virus type 1 variant during therapy with the T20 fusion inhibitor.** *J. Virol.* 2004, **78:**12428-12437.
179. Tremblay CL, Kollmann C, Giguel F, Chou TC, Hirsch MS: **Strong in vitro synergy between the fusion inhibitor T-20 and the CXCR4 blocker AMD-3100.** *J. Acquir. Immune Defic. Syndr.* 2000, **25:**99-102.
180. Dragic T, Trkola A, Thompson DA, Cormier EG, Kajumo FA, Maxwell E, Lin SW, Ying W, Smith SO, Sakmar TP, Moore JP: **A binding pocket for a small molecule inhibitor of HIV-1 entry within the transmembrane helices of CCR5.** *Proc. Natl. Acad. Sci. U. S. A.* 2000, **97:**5639-5644.

181. Visseaux B, Charpentier C, Hurtado-Nedelec M, Storto A, Antoine R, Peytavin G, Damond F, Matheron S, Brun-Vezinet F, Descamps D: **In vitro phenotypic susceptibility of HIV-2 clinical isolates to CCR5 inhibitors.** *Antimicrobial agents and chemotherapy* 2012, **56:**137-139.

182. Lobritz MA, Marozsan AJ, Troyer RM, Arts EJ: **Natural variation in the V3 crown of human immunodeficiency virus type 1 affects replicative fitness and entry inhibitor sensitivity.** *J. Virol.* 2007, **81:**8258-8269.

183. Dorr P, Westby M, Dobbs S, Griffin P, Irvine B, Macartney M, Mori J, Rickett G, Smith-Burchnell C, Napier C, et al: **Maraviroc (UK-427,857), a potent, orally bioavailable, and selective small-molecule inhibitor of chemokine receptor CCR5 with broad-spectrum anti-human immunodeficiency virus type 1 activity.** *Antimicrobial agents and chemotherapy* 2005, **49:**4721-4732.

184. Westby M, Lewis M, Whitcomb J, Youle M, Pozniak AL, James IT, Jenkins TM, Perros M, van der Ryst E: **Emergence of CXCR4-using human immunodeficiency virus type 1 (HIV-1) variants in a minority of HIV-1-infected patients following treatment with the CCR5 antagonist maraviroc is from a pretreatment CXCR4-using virus reservoir.** *J. Virol.* 2006, **80:**4909-4920.

185. Finzi D, Hermankova M, Pierson T, Carruth LM, Buck C, Chaisson RE, Quinn TC, Chadwick K, Margolick J, Brookmeyer R, et al: **Identification of a reservoir for HIV-1 in patients on highly active antiretroviral therapy.** *Science* 1997, **278:**1295-1300.

186. Chun TW, Carruth L, Finzi D, Shen X, DiGiuseppe JA, Taylor H, Hermankova M, Chadwick K, Margolick J, Quinn TC, et al: **Quantification of latent tissue reservoirs and total body viral load in HIV-1 infection.** *Nature* 1997, **387:**183-188.

187. Cheung MC, Pantanowitz L, Dezube BJ: **AIDS-related malignancies: emerging challenges in the era of highly active antiretroviral therapy.** *Oncologist* 2005, **10:**412-426.

188. Xia C, Luo D, Yu X, Jiang S, Liu S: **HIV-associated dementia in the era of highly active antiretroviral therapy (HAART).** *Microbes Infect.* 2011, **13:**419-425.

189. Nunez M: **Clinical syndromes and consequences of antiretroviral-related hepatotoxicity.** *Hepatology* 2010, **52:**1143-1155.

190. Sungkanuparph S, Anekthananon, T., Hiransuthikul, N., Supparatpinyo, K., Mootsikapun, P., Chetchotisakd, P., Kiertiburanakul, S., Tansuphaswadikul, S., Buppanharun, W. & Techasathit, W: **Guidelines for antiretroviral therapy in HIV-1 infected adults and adolescents: the recommendations of the Thai AIDS Society (TAS).** *J. Med. Assoc. Thai.* 2008, **91:**1925 - 1936.

191. Granich RM, Gilks CF, Dye C, De Cock KM, Williams BG: **Universal voluntary HIV testing with immediate antiretroviral therapy as a strategy for elimination of HIV transmission: a mathematical model.** *Lancet* 2009, **373:**48-57.

192. Woffendin C, Ranga U, Yang Z, Xu L, Nabel GJ: **Expression of a protective gene-prolongs survival of T cells in human immunodeficiency virus-infected patients.** *Proc. Natl. Acad. Sci. U. S. A.* 1996, **93:**2889-2894.

193. Wheeler YY, Chen SY, Sane DC: **Intrabody and intrakine strategies for molecular therapy.** *Mol. Ther.* 2003, **8:**355-366.

194. Schroers R, Davis CM, Wagner HJ, Chen SY: **Lentiviral transduction of human T-lymphocytes with a RANTES intrakine inhibits human immunodeficiency virus type 1 infection.** *Gene Ther.* 2002, **9:**889-897.

195. Marasco WA, Haseltine WA, Chen SY: **Design, intracellular expression, and activity of a human anti-human immunodeficiency virus type 1 gp120 single-chain antibody.** *Proc. Natl. Acad. Sci. U. S. A.* 1993, **90:**7889-7893.

196. Mhashilkar AM, Bagley J, Chen SY, Szilvay AM, Helland DG, Marasco WA: **Inhibition of HIV-1 Tat-mediated LTR transactivation and HIV-1 infection by anti-Tat single chain intrabodies.** *Embo J.* 1995, **14:**1542-1551.

197. Wu Y, Duan L, Zhu M, Hu B, Kubota S, Bagasra O, Pomerantz RJ: **Binding of intracellular anti-Rev single chain variable fragments to different epitopes of human immunodeficiency virus type 1 rev: variations in viral inhibition.** *J. Virol.* 1996, **70:**3290-3297.

198. Yap MW, Nisole S, Stoye JP: **A single amino acid change in the SPRY domain of human Trim5alpha leads to HIV-1 restriction.** *Curr. Biol.* 2005, **15:**73-78.

199. Levine BL, Humeau LM, Boyer J, MacGregor RR, Rebello T, Lu X, Binder GK, Slepushkin V, Lemiale F, Mascola JR, et al: **Gene transfer in humans using a conditionally replicating lentiviral vector.** *Proc. Natl. Acad. Sci. U. S. A.* 2006, **103:**17372-17377.

200. Tebas P, Stein D, Binder-Scholl G, Mukherjee R, Brady T, Rebello T, Humeau L, Kalos M, Papasavvas E, Montaner LJ, et al: **Antiviral effects of autologous CD4 T cells genetically modified with a conditionally replicating lentiviral vector expressing long antisense to HIV.** *Blood* 2013, **121:**1524-1533.

201. Bohjanen PR, Liu Y, Garcia-Blanco MA: **TAR RNA decoys inhibit tat-activated HIV-1 transcription after preinitiation complex formation.** *Nucleic Acids Res.* 1997, **25:**4481-4486.

202. Lee SW, Gallardo HF, Gilboa E, Smith C: **Inhibition of human immunodeficiency virus type 1 in human T cells by a potent Rev response element decoy consisting of the 13-nucleotide minimal Rev-binding domain.** *J. Virol.* 1994, **68:**8254-8264.

203. Kohn DB, Bauer G, Rice CR, Rothschild JC, Carbonaro DA, Valdez P, Hao Q, Zhou C, Bahner I, Kearns K, et al: **A clinical trial of retroviral-mediated transfer of a rev-responsive element decoy gene into CD34(+) cells from the bone marrow of human immunodeficiency virus-1-infected children.** *Blood* 1999, **94:**368-371.

204. Mitsuyasu RT, Anton PA, Deeks SG, Scadden DT, Connick E, Downs MT, Bakker A, Roberts MR, June CH, Jalali S, et al: **Prolonged survival and tissue trafficking following adoptive transfer of CD4zeta gene-modified autologous CD4(+) and CD8(+) T cells in human immunodeficiency virus-infected subjects.** *Blood* 2000, **96:**785-793.

205. DiGiusto DL, Krishnan A, Li L, Li H, Li S, Rao A, Mi S, Yam P, Stinson S, Kalos M, et al: **RNA-based gene therapy for HIV with lentiviral vector-modified CD34(+) cells in patients undergoing transplantation for AIDS-related lymphoma.** *Science translational medicine* 2010, **2:**36ra43.

206. Rossi JJ, June CH, Kohn DB: **Genetic therapies against HIV.** *Nat. Biotechnol.* 2007, **25:**1444-1454.

207. Jaeger J, Restle T, Steitz TA: **The structure of HIV-1 reverse transcriptase complexed with an RNA pseudoknot inhibitor.** *The EMBO Journal* 1998, **17:**4535-4542.

208. Mosing RK, Mendonsa SD, Bowser MT: **Capillary electrophoresis-SELEX selection of aptamers with affinity for HIV-1 reverse transcriptase.** *Anal. Chem.* 2005, **77:**6107-6112.

209. Schneider DJ, Feigon J, Hostomsky Z, Gold L: **High-affinity ssDNA inhibitors of the reverse transcriptase of type 1 human immunodeficiency virus.** *Biochemistry* 1995, **34:**9599-9610.

210. DeStefano JJ, Cristofaro JV: **Selection of primer-template sequences that bind human immunodeficiency virus reverse transcriptase with high affinity.** *Nucleic Acids Res.* 2006, **34:**130-139.

211. DeStefano JJ, Nair GR: **Novel aptamer inhibitors of human immunodeficiency virus reverse transcriptase.** *Oligonucleotides* 2008, **18:**133-144.

212. Lai YT, DeStefano JJ: **DNA aptamers to human immunodeficiency virus reverse transcriptase selected by a primer-free SELEX method: characterization and comparison with other aptamers.** *Nucleic Acid Ther.* 2012, **22:**162-176.

213. Samson M, Libert F, Doranz BJ, Rucker J, Liesnard C, Farber CM, Saragosti S, Lapoumeroulie C, Cognaux J, Forceille C, et al: **Resistance to HIV-1 infection in caucasian individuals bearing mutant alleles of the CCR-5 chemokine receptor gene.** *Nature* 1996, **382:**722-725.

214. Anderson J, Akkina R: **HIV-1 resistance conferred by siRNA cosuppression of CXCR4 and CCR5 coreceptors by a bispecific lentiviral vector.** *AIDS Res. Ther.* 2005, **2:**1.

215. Cordelier P, Kulkowsky JW, Ko C, Matskevitch AA, McKee HJ, Rossi JJ, Bouhamdan M, Pomerantz RJ, Kari G, Strayer DS: **Protecting from R5-tropic HIV: individual and combined effectiveness of a hammerhead ribozyme and a single-chain Fv antibody that targets CCR5.** *Gene Ther.* 2004, **11:**1627-1637.

216. Yang AG, Bai X, Huang XF, Yao C, Chen S: **Phenotypic knockout of HIV type 1 chemokine coreceptor CCR-5 by intrakines as potential therapeutic approach for HIV-1 infection.** *Proc. Natl. Acad. Sci. U. S. A.* 1997, **94:**11567-11572.

217. Liang M, Kamata M, Chen KN, Pariente N, An DS, Chen IS: **Inhibition of HIV-1 infection by a unique short hairpin RNA to chemokine receptor 5 delivered into macrophages through hematopoietic progenitor cell transduction.** *J Gene Med* 2010, **12:**255-265.

218. Shimizu S, Hong P, Arumugam B, Pokomo L, Boyer J, Koizumi N, Kittipongdaja P, Chen A, Bristol G, Galic Z, et al: **A highly efficient short hairpin RNA potently down-regulates CCR5 expression in systemic lymphoid organs in the hu-BLT mouse model.** *Blood* 2010, **115:**1534-1544.

219. Wilen CB, Wang J, Tilton JC, Miller JC, Kim KA, Rebar EJ, Sherrill-Mix SA, Patro SC, Secreto AJ, Jordan AP, et al: **Engineering HIV-resistant human CD4+ T cells with CXCR4-specific zinc-finger nucleases.** *PLoS Pathog.* 2011, **7:**e1002020.

220. Perez EE, Wang J, Miller JC, Jouvenot Y, Kim KA, Liu O, Wang N, Lee G, Bartsevich VV, Lee YL, et al: **Establishment of HIV-1 resistance in CD4+ T cells by genome editing using zinc-finger nucleases.** *Nat. Biotechnol.* 2008, **26:**808-816.

221. Holt N, Wang J, Kim K, Friedman G, Wang X, Taupin V, Crooks GM, Kohn DB, Gregory PD, Holmes MC, Cannon PM: **Human hematopoietic stem/progenitor cells modified by zinc-finger nucleases targeted to CCR5 control HIV-1 in vivo.** *Nat. Biotechnol.* 2010, **28:**839-847.

222. Kang H, Minder P, Park MA, Mesquitta WT, Torbett BE, Slukvin, II: **CCR5 Disruption in Induced Pluripotent Stem Cells Using CRISPR/Cas9 Provides Selective Resistance of Immune Cells to CCR5-tropic HIV-1 Virus.** *Mol. Ther. Nucleic Acids* 2015, **4:**e268.

223. Mussolino C, Morbitzer R, Lutge F, Dannemann N, Lahaye T, Cathomen T: **A novel TALE nuclease scaffold enables high genome editing activity in combination with low toxicity.** *Nucleic Acids Res.* 2011, **39:**9283-9293.

224. Holkers M, Maggio I, Liu J, Janssen JM, Miselli F, Mussolino C, Recchia A, Cathomen T, Goncalves MA: **Differential integrity of TALE nuclease genes following adenoviral and lentiviral vector gene transfer into human cells.** *Nucleic Acids Res.* 2013, **41:**e63.

225. Mock U, Machowicz R, Hauber I, Horn S, Abramowski P, Berdien B, Hauber J, Fehse B: **mRNA transfection of a novel TAL effector nuclease (TALEN) facilitates efficient knockout of HIV co-receptor CCR5.** *Nucleic Acids Res.* 2015, **43:**5560-5571.

226. Siliciano JD, Lai J, Callender M, Pitt E, Zhang H, Margolick JB, Gallant JE, Cofrancesco J, Jr., Moore RD, Gange SJ, Siliciano RF: **Stability of the latent reservoir for HIV-1 in patients receiving valproic acid.** *J. Infect. Dis.* 2007, **195:**833-836.

227. Laird GM, Bullen CK, Rosenbloom DI, Martin AR, Hill AL, Durand CM, Siliciano JD, Siliciano RF: **Ex vivo analysis identifies effective HIV-1 latency-reversing drug combinations.** *J. Clin. Invest.* 2015, **125:**1901-1912.

228. Hutter G, Nowak D, Mossner M, Ganepola S, Mussig A, Allers K, Schneider T, Hofmann J, Kucherer C, Blau O, et al: **Long-term control of HIV by CCR5 Delta32/Delta32 stem-cell transplantation.** *N. Engl. J. Med.* 2009, **360:**692-698.

229. Hutter G, Thiel E: **Allogeneic transplantation of CCR5-deficient progenitor cells in a patient with HIV infection: an update after 3 years and the search for patient no. 2.** *AIDS* 2011, **25:**273-274.

230. Shiver JW, Fu TM, Chen L, Casimiro DR, Davies ME, Evans RK, Zhang ZQ, Simon AJ, Trigona WL, Dubey SA, et al: **Replication-incompetent adenoviral vaccine vector elicits effective anti-immunodeficiency-virus immunity.** *Nature* 2002, **415:**331-335.

231. Shiver JW, Emini EA: **Recent advances in the development of HIV-1 vaccines using replication-incompetent adenovirus vectors.** *Annu. Rev. Med.* 2004, **55:**355-372.

232. Tomaras GD, Binley JM, Gray ES, Crooks ET, Osawa K, Moore PL, Tumba N, Tong T, Shen X, Yates NL, et al: **Polyclonal B cell responses to conserved neutralization epitopes in a subset of HIV-1-infected individuals.** *J. Virol.* 2011, **85:**11502-11519.

233. Mascola JR, Haynes BF: **HIV-1 neutralizing antibodies: understanding nature's pathways.** *Immunol Rev.* 2013, **254:**225-244.

234. Hansen SG, Sacha JB, Hughes CM, Ford JC, Burwitz BJ, Scholz I, Gilbride RM, Lewis MS, Gilliam AN, Ventura AB, et al: **Cytomegalovirus vectors violate CD8+ T cell epitope recognition paradigms.** *Science* 2013, **340:**1237874.

235. Haynes BF: **New approaches to HIV vaccine development.** *Curr. Opin. Immunol.* 2015, **35:**39-47.

236. Bonsignori M, Pollara J, Moody MA, Alpert MD, Chen X, Hwang KK, Gilbert PB, Huang Y, Gurley TC, Kozink DM, et al: **Antibody-dependent cellular cytotoxicity-mediating antibodies from an HIV-1 vaccine efficacy trial target multiple epitopes and preferentially use the VH1 gene family.** *J. Virol.* 2012, **86:**11521-11532.

237. Burton DR, Mascola JR: **Antibody responses to envelope glycoproteins in HIV-1 infection.** *Nat. Immunol.* 2015, **16:**571-576.

238. Chen Y, Zhang J, Hwang KK, Bouton-Verville H, Xia SM, Newman A, Ouyang YB, Haynes BF, Verkoczy L: **Common tolerance mechanisms, but distinct cross-reactivities associated with gp41 and lipids, limit production of HIV-1 broad neutralizing antibodies 2F5 and 4E10.** *J. Immunol.* 2013, **191:**1260-1275.

239. Barouch DH, Stephenson KE, Borducchi EN, Smith K, Stanley K, McNally AG, Liu J, Abbink P, Maxfield LF, Seaman MS, et al: **Protective efficacy of a global HIV-1 mosaic vaccine against heterologous SHIV challenges in rhesus monkeys.** *Cell* 2013, **155:**531-539.

240. Borthwick N, Ahmed T, Ondondo B, Hayes P, Rose A, Ebrahimsa U, Hayton EJ, Black A, Bridgeman A, Rosario M, et al: **Vaccine-elicited human T cells recognizing conserved protein regions inhibit HIV-1.** *Mol. Ther.* 2014, **22:**464-475.

241. Mothe B, Hu X, Llano A, Rosati M, Olvera A, Kulkarni V, Valentin A, Alicea C, Pilkington GR, Sardesai NY, et al: **A human immune data-informed vaccine concept elicits strong and broad T-cell specificities associated with HIV-1 control in mice and macaques.** *J. Transl. Med.* 2015, **13:**60.

242. Barouch DH, Liu J, Peter L, Abbink P, Iampietro MJ, Cheung A, Alter G, Chung A, Dugast AS, Frahm N, et al: **Characterization of humoral and cellular immune responses elicited by a recombinant adenovirus serotype 26 HIV-1 Env vaccine in healthy adults (IPCAVD 001).** *J. Infect. Dis.* 2013, **207:**248-256.

243. Baba TW, Liska V, Hofmann-Lehmann R, Vlasak J, Xu W, Ayehunie S, Cavacini LA, Posner MR, Katinger H, Stiegler G, et al: **Human neutralizing monoclonal antibodies of the IgG1 subtype protect against mucosal simian-human immunodeficiency virus infection.** *Nat. Med.* 2000, **6:**200-206.

244. Mascola JR, Stiegler G, VanCott TC, Katinger H, Carpenter CB, Hanson CE, Beary H, Hayes D, Frankel SS, Birx DL, Lewis MG: **Protection of macaques against vaginal transmission of a pathogenic HIV-1/SIV chimeric virus by passive infusion of neutralizing antibodies.** *Nat. Med.* 2000, **6:**207-210.

245. Parren PW, Marx PA, Hessell AJ, Luckay A, Harouse J, Cheng-Mayer C, Moore JP, Burton DR: **Antibody protects macaques against vaginal challenge with a pathogenic R5 simian/human immunodeficiency virus at serum levels giving complete neutralization in vitro.** *J. Virol.* 2001, **75:**8340-8347.

246. Moldt B, Rakasz EG, Schultz N, Chan-Hui PY, Swiderek K, Weisgrau KL, Piaskowski SM, Bergman Z, Watkins DI, Poignard P, Burton DR: **Highly potent HIV-specific antibody neutralization in vitro translates into effective protection against mucosal SHIV challenge in vivo.** *Proc. Natl. Acad. Sci. U. S. A.* 2012, **109:**18921-18925.

247. Schnepp BC, Johnson PR: **Adeno-associated virus delivery of broadly neutralizing antibodies.** *Curr. Opin. HIV AIDS* 2014, **9:**250-256.

248. Balazs AB, Chen J, Hong CM, Rao DS, Yang L, Baltimore D: **Antibody-based protection against HIV infection by vectored immunoprophylaxis.** *Nature* 2012, **481:**81-84.

249. Goff SP: **Retroviral reverse transcriptase: synthesis, structure, and function.** *J. Acquir. Immune Defic. Syndr.* 1990, **3:**817-831.

250. Filler AG, Lever AM: **Effects of cation substitutions on reverse transcriptase and on human immunodeficiency virus production.** *AIDS Res. Hum. Retroviruses* 1997, **13:**291-299.

251. Cousins RJ, Liuzzi JP, Lichten LA: **Mammalian zinc transport, trafficking, and signals.** *J. Biol. Chem.* 2006, **281:**24085-24089.

252. Warren K, Warrilow D, Meredith L, Harrich D: **Reverse Transcriptase and Cellular Factors: Regulators of HIV-1 Reverse Transcription.** *Viruses* 2009, **1:**873-894.

253. Bushman FD, Malani N, Fernandes J, D'Orso I, Cagney G, Diamond TL, Zhou H, Hazuda DJ, Espeseth AS, Konig R, et al: **Host cell factors in HIV replication: meta-analysis of genome-wide studies.** *PLoS Pathog.* 2009, **5:**e1000437.

254. Konig R, Zhou Y, Elleder D, Diamond TL, Bonamy GM, Irelan JT, Chiang CY, Tu BP, De Jesus PD, Lilley CE, et al: **Global analysis of host-pathogen interactions that regulate early-stage HIV-1 replication.** *Cell* 2008, **135:**49-60.

255. Jiang Y, Zheng W, Long L, Zhao W, Li X, Mo X, Lu J, Fu X, Li W, Liu S, et al: **Brain magnetic resonance imaging and manganese concentrations in red blood cells of smelting workers: search for biomarkers of manganese exposure.** *Neurotoxicology* 2007, **28:**126-135.

256. Choi Y, Park JK, Park NH, Shin JW, Yoo CI, Lee CR, Lee H, Kim HK, Kim SR, Jung TH, et al: **Whole blood and red blood cell manganese reflected signal intensities of T1-weighted magnetic resonance images better than plasma manganese in liver cirrhotics.** *J. Occup. Health* 2005, **47:**68-73.

257. De Smet K, De Haan R, Calistri A, Campbell PA, Ebramzadeh E, Pattyn C, Gill HS: **Metal ion measurement as a diagnostic tool to identify problems with metal-on-metal hip resurfacing.** *J. Bone Joint Surg. Am.* 2008, **90 Suppl 4:**202-208.

258. Outten CE, O'Halloran TV: **Femtomolar sensitivity of metalloregulatory proteins controlling zinc homeostasis.** *Science* 2001, **292:**2488-2492.

259. Finney LA, O'Halloran TV: **Transition metal speciation in the cell: insights from the chemistry of metal ion receptors.** *Science* 2003, **300:**931-936.

260. Levinson W, Faras A, Woodson B, Jackson J, Bishop JM: **Inhibition of RNA-dependent DNA polymerase of Rous sarcoma virus by thiosemicarbazones and several cations.** *Proc. Natl. Acad. Sci. U. S. A.* 1973, **70:**164-168.

261. Palan PR, Eidinoff ML: **Specific effect of zinc ions on DNA polymerase activity of avian myeloblastosis virus.** *Mol Cell Biochem.* 1978, **21:**67-69.

262. Brewer GJ, Aster JC, Knutsen CA, Kruckeberg WC: **Zinc inhibition of calmodulin: a proposed molecular mechanism of zinc action on cellular functions.** *Am. J. Hematol.* 1979, **7:**53-60.

263. Fridlender B, Chejanovsky N, Becker Y: **Selective inhibition of herpes simplex virus type 1 DNA polymerase by zinc ions.** *Virology* 1978, **84:**551-554.

264. te Velthuis AJ, van den Worm SH, Sims AC, Baric RS, Snijder EJ, van Hemert MJ: **Zn(2+) inhibits coronavirus and arterivirus RNA polymerase activity in vitro and zinc ionophores block the replication of these viruses in cell culture.** *PLoS Pathog.* 2010, **6:**e1001176.

265. Siberry GK, Ruff AJ, Black R: **Zinc and human immunodeficiency virus infection.** *Nutritional Res.* 2002, **22:**527-538.

266. Fenstermacher KJ, DeStefano JJ: **Mechanism of HIV reverse transcriptase inhibition by zinc: formation of a highly stable enzyme-(primer-template) complex with profoundly diminished catalytic activity.** *J. Biol. Chem.* 2011, **286:**40433-40442.

267. Bolton EC, Mildvan AS, Boeke JD: **Inhibition of reverse transcription in vivo by elevated manganese ion concentration.** *Mol. Cell* 2002, **9:**879-889.

268. Hsu M, Aravantinou M, Menon R, Seidor S, Goldman D, Kenney J, Derby N, Gettie A, Blanchard J, Piatak M, Jr., et al: **A combination microbicide gel protects macaques against vaginal simian human immunodeficiency virus-reverse transcriptase**

infection, but only partially reduces herpes simplex virus-2 infection after a single high-dose cochallenge. *AIDS Research and Human Retroviruses* 2014, **30:**174-183.

269. Kenney J, Rodriguez A, Kizima L, Seidor S, Menon R, Jean-Pierre N, Pugach P, Levendosky K, Derby N, Gettie A, et al: **A modified zinc acetate gel, a potential nonantiretroviral microbicide, is safe and effective against simian-human immunodeficiency virus and herpes simplex virus 2 infection in vivo.** *Antimicrobial agents and chemotherapy* 2013, **57:**4001-4009.

270. Singer R, Mawson P, Derby N, Rodriguez A, Kizima L, Menon R, Goldman D, Kenney J, Aravantinou M, Seidor S, et al: **An intravaginal ring that releases the NNRTI MIV-150 reduces SHIV transmission in macaques.** *Science translational medicine* 2012, **4:**150ra123.

271. Kenney J, Singer R, Derby N, Aravantinou M, Abraham CJ, Menon R, Seidor S, Zhang S, Gettie A, Blanchard J, et al: **A single dose of a MIV-150/Zinc acetate gel provides 24 h of protection against vaginal simian human immunodeficiency virus reverse transcriptase infection, with more limited protection rectally 8-24 h after gel use.** *AIDS Research and Human Retroviruses* 2012, **28:**1476-1484.

272. Kenney J, Aravantinou M, Singer R, Hsu M, Rodriguez A, Kizima L, Abraham CJ, Menon R, Seidor S, Chudolij A, et al: **An antiretroviral/zinc combination gel provides 24 hours of complete protection against vaginal SHIV infection in macaques.** *PloS One* 2011, **6:**e15835.

273. Haraguchi Y, Sakurai H, Hussain S, Anner BM, Hoshino H: **Inhibition of HIV-1 infection by zinc group metal compounds.** *Antiviral Research* 1999, **43:**123-133.

274. Kumel G, Schrader S, Zentgraf H, Daus H, Brendel M: **The mechanism of the antiherpetic activity of zinc sulphate.** *J. Gen. Virol.* 1990, **71 (Pt 12):**2989-2997.

275. Kumel G, Turley H, Brendel M: **[Zinc sulfate and heparin for local therapy of herpes. Antiherpetic drugs, not leading to selection of HSV variants].** *Fortschr. Med.* 1995, **113:**235-238.

276. Arens M, Travis S: **Zinc salts inactivate clinical isolates of herpes simplex virus in vitro.** *J. Clin. Microbiol* 2000, **38:**1758-1762.

277. **Lipactin Gel** [Taken from http://www.louis-widmer.ch/en_CH/our-products/dermatologica/herpes-simplex/rlipactin-gel/]

278. Bourne N, Stegall R, Montano R, Meador M, Stanberry LR, Milligan GN: **Efficacy and toxicity of zinc salts as candidate topical microbicides against vaginal herpes simplex virus type 2 infection.** *Antimicrobial agents and chemotherapy* 2005, **49:**1181-1183.

279. Fernandez-Romero JA, Abraham CJ, Rodriguez A, Kizima L, Jean-Pierre N, Menon R, Begay O, Seidor S, Ford BE, Gil PI, et al: **Zinc acetate/carrageenan gels exhibit potent activity in vivo against high-dose herpes simplex virus 2 vaginal and rectal challenge.** *Antimicrobial agents and chemotherapy* 2012, **56:**358-368.

280. Julias JG, Pathak VK: **Deoxyribonucleoside triphosphate pool imbalances in vivo are associated with an increased retroviral mutation rate.** *J. Virol.* 1998, **72:**7941-7949.

281. Farrell NP: **Introduction.** In *Uses of inorganic chemistry in medicine.* Edited by Farrell NP: The Royal Society of Chemistry; 1999: 1-10

282. Vallee BL, Falchuk KH: **The biochemical basis of zinc physiology.** *Physiol. Rev.* 1993, **73:**79-118.

283. Sirover MA, Loeb LA: **Metal-induced infidelity during DNA synthesis.** *Proc. Natl. Acad. Sci. U. S. A.* 1976, **73:**2331-2335.

284. Sirover MA, Loeb LA: **Metal activation of DNA synthesis.** *Biochem. Biophys. Res. Commun.* 1976, **70:**812-817.

285. Kunkel TA, Loeb LA: **On the fidelity of DNA replication. Effect of divalent metal ion activators and deoxyrionucleoside triphosphate pools on in vitro mutagenesis.** *J. Biol. Chem.* 1979, **254:**5718-5725.

286. Sirover MA, Loeb LA: **On the fidelity of DNA replication. Effect of metal activators during synthesis with avian myeloblastosis virus DNA polymerase.** *J. Biol. Chem.* 1977, **252:**3605-3610.

287. Aggarwal S, Bradel-Tretheway B, Takimoto T, Dewhurst S, Kim B: **Biochemical characterization of enzyme fidelity of influenza A virus RNA polymerase complex.** *PloS One* 2010, **5:**e10372.

288. Sirover MA, Dube DK, Loeb LA: **On the fidelity of DNA replication. Metal activation of Escherichia coli DNA polymerase I.** *J. Biol. Chem.* 1979, **254:**107-111.

289. Cases-Gonzalez CE, Gutierrez-Rivas M, Menendez-Arias L: **Coupling ribose selection to fidelity of DNA synthesis. The role of Tyr-115 of human immunodeficiency virus type 1 reverse transcriptase.** *J. Biol. Chem.* 2000, **275:**19759-19767.

290. Miyaki M, Murata I, Osabe M, Ono T: **Effect of metal cations on misincorporation by E. coli DNA polymerases.** *Biochem. Biophys. Res. Commun.* 1977, **77:**854-860.

291. Hall ZW, Lehman IR: **An in vitro transversion by a mutationally altered T4-induced DNA polymerase.** *J. Mol. Biol.* 1968, **36:**321-333.

292. Seal G, Shearman CW, Loeb LA: **On the fidelity of DNA replication. Studies with human placenta DNA polymerases.** *J. Biol. Chem.* 1979, **254:**5229-5237.

293. Fromant M, Blanquet S, Plateau P: **Direct random mutagenesis of gene-sized DNA fragments using polymerase chain reaction.** *Anal. Biochem.* 1995, **224:**347-353.

294. Hou EW, Prasad R, Beard WA, Wilson SH: **High-level expression and purification of untagged and histidine-tagged HIV-1 reverse transcriptase.** *Protein Expr. Purif.* 2004, **34:**75-86.

295. Sambrook J, Russell DW: *Molecular Cloning: A Laboratory Manual.* 3rd edn. Cold Spring Harbor, NY: Cold Spring Harbor Laboratory Press; 2001.

296. DeStefano JJ: **Effect of reaction conditions and 3AB on the mutation rate of poliovirus RNA-dependent RNA polymerase in a alpha-complementation assay.** *Virus Res.* 2010, **147:**53-59.

297. Keith BJ, Jozwiakowski SK, Connolly BA: **A plasmid-based lacZalpha gene assay for DNA polymerase fidelity measurement.** *Anal. Biochem.* 2013, **433:**153-161.

298. Yu H, Goodman MF: **Comparison of HIV-1 and Avian Myelblastosis Virus Reverse Transcriptase Fidelity on RNA and DNA Templates.** *J. Biol. Chem.* 1992, **267:**10888-10896.

299. Goldschmidt V, Didierjean J, Ehresmann B, Ehresmann C, Isel C, Marquet R: **Mg2+ dependency of HIV-1 reverse transcription, inhibition by nucleoside analogues and resistance.** *Nucleic Acids Res.* 2006, **34:**42-52.

300. Mendelman LV, Petruska J, Goodman MF: **Base mispair extension kinetics. Comparison of DNA polymerase alpha and reverse transcriptase.** *J. Biol. Chem.* 1990, **265:**2338-2346.

301. Liesch GR, DeStefano JJ: **Analysis of mutations made during active synthesis or extension of mismatched substrates further define the mechanism of HIV-RT mutagenesis.** *Biochemistry* 2003, **42:**5925-5936.

302. Wells VR, Plotch SJ, DeStefano JJ: **Determination of the mutation rate of poliovirus RNA-dependent RNA polymerase.** *Virus Res* 2001, **74:**119-132.

303. Zakour RA, Kunkel TA, Loeb LA: **Metal-induced infidelity of DNA synthesis.** *Environ. Health Perspect.* 1981, **40:**197-205.

304. Rezende LF, Prasad VR: **Nucleoside-analog resistance mutations in HIV-1 reverse transcriptase and their influence on polymerase fidelity and viral mutation rates.** *Int J. Biochem. Cell Biol.* 2004, **36:**1716-1734.

305. Svarovskaia ES, Cheslock SR, Zhang WH, Hu WS, Pathak VK: **Retroviral mutation rates and reverse transcriptase fidelity.** *Front. Biosci.* 2003, **8:**d117-134.

306. Mangani S, Hakansson K: **Crystallographic studies of the binding of protonated and unprotonated inhibitors to carbonic anhydrase using hydrogen sulphide and nitrate anions.** *Eur. J. Biochem.* 1992, **210:**867-871.

307. Kitagawa Y, Tanaka N, Hata Y, Kusunoki M, Lee GP, Katsube Y, Asada K, Aibara S, Morita Y: **Three-dimensional structure of Cu,Zn-superoxide dismutase from spinach at 2.0 A resolution.** *J. Biochem.* 1991, **109:**477-485.

308. Beckman RA, Mildvan AS, Loeb LA: **On the fidelity of DNA replication: manganese mutagenesis in vitro.** *Biochemistry* 1985, **24:**5810-5817.

309. Mullen GP, Serpersu EH, Ferrin LJ, Loeb LA, Mildvan AS: **Metal binding to DNA polymerase I, its large fragment, and two 3',5'-exonuclease mutants of the large fragment.** *J. Biol. Chem.* 1990, **265:**14327-14334.

310. El-Deiry WS, Downey KM, So AG: **Molecular mechanisms of manganese mutagenesis.** *Proc. Natl. Acad. Sci. U. S. A.* 1984, **81:**7378-7382.

311. Kirmizialtin S, Pabit SA, Meisburger SP, Pollack L, Elber R: **RNA and its ionic cloud: solution scattering experiments and atomically detailed simulations.** *Biophys. J.* 2012, **102:**819-828.

312. Achuthan V, DeStefano JJ: **Alternative divalent cations (Zn(2)(+), Co(2)(+), and Mn(2)(+)) are not mutagenic at conditions optimal for HIV-1 reverse transcriptase activity.** *BMC Biochem.* 2015, **16:**12.

313. Arts EJ, Hazuda DJ: **HIV-1 antiretroviral drug therapy.** In *HIV From Biology to Prevention and Treatment.* Edited by Bushman FD, Nabel GJ, Swanstrom R. Cold Spring Harbor: Cold Spring Harbor Laboratory Press; 2012: 321-343

314. Cowan JA, Ohyama T, Howard K, Rausch JW, Cowan SM, Le Grice SF: **Metal-ion stoichiometry of the HIV-1 RT ribonuclease H domain: evidence for two mutually exclusive sites leads to new mechanistic insights on metal-mediated hydrolysis in nucleic acid biochemistry.** *J. Biol. Inorg. Chem.* 2000, **5:**67-74.

315. Joyce CM, Steitz TA: **Function and structure relationships in DNA polymerases.** *Annu. Rev. Biochem.* 1994, **63:**777-822.

316. Nakamura H, Katayanagi K, Morikawa K, Ikehara M: **Structural models of ribonuclease H domains in reverse transcriptases from retroviruses.** *Nucleic Acids Res.* 1991, **19:**1817-1823.

317. Yang W, Steitz TA: **Recombining the structures of HIV integrase, RuvC and RNase H.** *Structure* 1995, **3:**131-134.

318. Oda Y, Nakamura H, Kanaya S, Ikehara M: **Binding of metal ions to E. coli RNase HI observed by 1H-15N heteronuclear 2D NMR.** *J. Biomol. NMR* 1991, **1:**247-255.

319. Maguire ME, Cowan JA: **Magnesium chemistry and biochemistry.** *Biometals* 2002, **15:**203-210.

320. Moomaw AS, Maguire ME: **The unique nature of mg2+ channels.** *Physiology (Bethesda)* 2008, **23:**275-285.

321. Traut TW: **Physiological concentrations of purines and pyrimidines.** *Mol. Cell Biochem.* 1994, **140:**1-22.

322. Delva P, Pastori C, Degan M, Montesi G, Lechi A: **Catecholamine-induced regulation in vitro and ex vivo of intralymphocyte ionized magnesium.** *J. Membr. Biol.* 2004, **199:**163-171.

323. Wang S, McDonnell EH, Sedor FA, Toffaletti JG: **pH effects on measurements of ionized calcium and ionized magnesium in blood.** *Arch. Pathol. Lab Med.* 2002, **126:**947-950.

324. Gee JB, 2nd, Corbett RJ, Perlman JM, Laptook AR: **Hypermagnesemia does not increase brain intracellular magnesium in newborn swine.** *Pediatr. Neurol.* 2001, **25:**304-308.

325. Delva P, Pastori C, Degan M, Montesi G, Lechi A: **Intralymphocyte free magnesium and plasma triglycerides.** *Life Sci* 1998, **62:**2231-2240.

326. Diamond TL, Roshal M, Jamburuthugoda VK, Reynolds HM, Merriam AR, Lee KY, Balakrishnan M, Bambara RA, Planelles V, Dewhurst S, Kim B: **Macrophage tropism of HIV-1 depends on efficient cellular dNTP utilization by reverse transcriptase.** *J Biol Chem* 2004, **279:**51545-51553.

327. Gao WY, Cara A, Gallo RC, Lori F: **Low levels of deoxynucleotides in peripheral blood lymphocytes: a strategy to inhibit human immunodeficiency virus type 1 replication.** *Proc Natl Acad Sci U S A* 1993, **90:**8925-8928.

328. Roberts JD, Bebenek K, Kunkel TA: **The accuracy of reverse transcriptase from HIV-1.** *Science* 1988, **242:**1171-1173.

329. Rezende LF, Drosopoulos WC, Prasad VR: **The influence of 3TC resistance mutation M184I on the fidelity and error specificity of human immunodeficiency virus type 1 reverse transcriptase.** *Nucleic Acids Res.* 1998, **26:**3066-3072.

330. Rezende LF, Kew Y, Prasad VR: **The effect of increased processivity on overall fidelity of human immunodeficiency virus type 1 reverse transcriptase.** *Journal of Biomedical Science* 2001, **8:**197-205.

331. Boyer PL, Hughes SH: **Effects of amino acid substitutions at position 115 on the fidelity of human immunodeficiency virus type 1 reverse transcriptase.** *J. Virol.* 2000, **74:**6494-6500.

332. Ji J, Loeb LA: **Fidelity of HIV-1 reverse transcriptase copying a hypervariable region of the HIV-1 env gene.** *Virology* 1994, **199:**323-330.

333. Weiss KK, Chen R, Skasko M, Reynolds HM, Lee K, Bambara RA, Mansky LM, Kim B: **A role for dNTP binding of human immunodeficiency virus type 1 reverse transcriptase in viral mutagenesis.** *Biochemistry* 2004, **43:**4490-4500.

334. Mansky LM: **The mutation rate of human immunodeficiency virus type 1 is influenced by the vpr gene.** *Virology* 1996, **222:**391-400.

335. Curr K, Tripathi S, Lennerstrand J, Larder BA, Prasad VR: **Influence of naturally occurring insertions in the fingers subdomain of human immunodeficiency virus type 1 reverse transcriptase on polymerase fidelity and mutation frequencies in vitro.** *J Gen Virol* 2006, **87:**419-428.

336. Fisher TS, Prasad VR: **Substitutions of Phe61 located in the vicinity of template 5'-overhang influence polymerase fidelity and nucleoside analog sensitivity of HIV-1 reverse transcriptase.** *J. Biol. Chem.* 2002, **277:**22345-22352.

337. Cline J, Braman JC, Hogrefe HH: **PCR fidelity of pfu DNA polymerase and other thermostable DNA polymerases.** *Nucleic Acids Res.* 1996, **24:**3546-3551.

338. Bebenek K, Abbotts J, Roberts JD, Wilson SH, Kunkel TA: **Specificity and mechanism of error prone replication by human immunodeficiency virus 1 reverse transcriptase.** *Journal of Biological Chemistry* 1989, **264:**16948-16956.

339. Ji J, Hoffmann JS, Loeb L: **Mutagenicity and pausing of HIV reverse transcriptase during HIV plus- strand DNA synthesis.** *Nucleic Acids Res.* 1994, **22:**47-52.

340. Weber J, Grosse F: **Fidelity of human immunodeficiency virus type I reverse transcriptase in copying natural DNA.** *Nucleic Acids Res.* 1989, **17:**1379-1393.

341. Mendelman LV, Boosalis MS, Petruska J, Goodman MF: **Nearest neighbor influences on DNA polymerase insertion fidelity.** *J Biol Chem* 1989, **264:**14415-14423.

342. Eckert KA, Kunkel TA: **High fidelity DNA synthesis by the Thermus aquaticus DNA polymerase.** *Nucleic Acids Res* 1990, **18:**3739-3744.

343. Eckert KA, Kunkel TA: **Fidelity of DNA synthesis catalyzed by human DNA polymerase alpha and HIV-1 reverse transcriptase: effect of reaction pH.** *Nucleic Acids Res.* 1993, **21:**5212-5220.

344. Eckert KA, Kunkel TA: **Effect of reaction pH on the fidelity and processivity of exonuclease-deficient Klenow polymerase.** *J. Biol. Chem.* 1993, **268:**13462-13471.

345. Yarrington RM, Chen J, Bolton EC, Boeke JD: **Mn2+ suppressor mutations and biochemical communication between Ty1 reverse transcriptase and RNase H domains.** *J. Virol.* 2007, **81:**9004-9012.

346. Cristofaro JV, Rausch JW, Le Grice SF, DeStefano JJ: **Mutations in the ribonuclease H active site of HIV-RT reveal a role for this site in stabilizing enzyme-primer-template binding.** *Biochemistry* 2002, **41:**10968-10975.

347. Álvarez M, Barrioluengo V, Afonso-Lehmann RN, Menéndez-Arias L: **Altered error specificity of RNase H-deficient HIV-1 reverse transcriptases during DNA-dependent DNA synthesis.** *Nucleic Acids Research* 2013, **41:**4601-4612.

348. Holtz CM, Mansky LM: **Variation of HIV-1 mutation spectra among cell types.** *Journal of Virology* 2013, **87:**5296-5299.

349. Gotte M: **Inhibition of HIV-1 reverse transcription: basic principles of drug action and resistance.** *Expert Rev. Anti Infect. Ther.* 2004, **2:**707-716.

350. Gallant JE, Gerondelis PZ, Wainberg MA, Shulman NS, Haubrich RH, St Clair M, Lanier ER, Hellmann NS, Richman DD: **Nucleoside and nucleotide analogue reverse transcriptase inhibitors: a clinical review of antiretroviral resistance.** *Antivir. Ther.* 2003, **8:**489-506.

351. Wondrak EM, Lower J, Kurth R: **Functional purification and enzymic characterization of the RNA-dependent DNA polymerase of human immunodeficiency virus.** *J. Gen. Virol.* 1986, **67 (Pt 12):**2791-2797.

352. Hoffman AD, Banapour B, Levy JA: **Characterization of the AIDS-associated retrovirus reverse transcriptase and optimal conditions for its detection in virions.** *Virology* 1985, **147:**326-335.

353. Rey MA, Spire B, Dormont D, Barre-Sinoussi F, Montagnier L, Chermann JC: **Characterization of the RNA dependent DNA polymerase of a new human T-lymphotropic retrovirus (lymphadenopathy associated virus).** *Biochem. Biophys. Res. Commun.* 1984, **121:**126-133.

354. Starnes MC, Cheng YC: **Human immunodeficiency virus reverse transcriptase-associated RNase H activity.** *J. Biol. Chem.* 1989, **264:**7073-7077.

355. Schauer GD, Huber KD, Leuba SH, Sluis-Cremer N: **Mechanism of allosteric inhibition of HIV-1 reverse transcriptase revealed by single-molecule and ensemble fluorescence.** *Nucleic Acids Res.* 2014, **42:**11687-11696.

356. Zhang Z, Walker M, Xu W, Shim JH, Girardet JL, Hamatake RK, Hong Z: **Novel nonnucleoside inhibitors that select nucleoside inhibitor resistance mutations in human immunodeficiency virus type 1 reverse transcriptase.** *Antimicrobial agents and chemotherapy* 2006, **50:**2772-2781.

357. Munshi V, Lu M, Felock P, Barnard RJ, Hazuda DJ, Miller MD, Lai MT: **Monitoring the development of non-nucleoside reverse transcriptase inhibitor-associated resistant HIV-1 using an electrochemiluminescence-based reverse transcriptase polymerase assay.** *Anal. Biochem.* 2008, **374:**121-132.

358. Maga G, Amacker M, Ruel N, Hubscher U, Spadari S: **Resistance to nevirapine of HIV-1 reverse transcriptase mutants: loss of stabilizing interactions and thermodynamic or steric barriers are induced by different single amino acid substitutions.** *J. Mol. Biol.* 1997, **274:**738-747.

359. Boyer PL, Sarafianos SG, Clark PK, Arnold E, Hughes SH: **Why do HIV-1 and HIV-2 use different pathways to develop AZT resistance?** *PLoS Pathog.* 2006, **2:**e10.

360. Meyer PR, Matsuura SE, So AG, Scott WA: **Unblocking of chain-terminated primer by HIV-1 reverse transcriptase through a nucleotide-dependent mechanism.** *Proc. Natl. Acad. Sci. U. S. A.* 1998, **95:**13471-13476.

361. Beach LB, Rawson JM, Kim B, Patterson SE, Mansky LM: **Novel inhibitors of human immunodeficiency virus type 2 infectivity.** *J. Gen. Virol.* 2014, **95:**2778-2783.

362. Menendez-Arias L, Alvarez M: **Antiretroviral therapy and drug resistance in human immunodeficiency virus type 2 infection.** *Antiviral Research* 2014, **102:**70-86.

363. Fletcher RS, Holleschak G, Nagy E, Arion D, Borkow G, Gu Z, Wainberg MA, Parniak MA: **Single-step purification of recombinant wild-type and mutant HIV-1 reverse transcriptase.** *Protein Expr. Purif.* 1996, **7:**27-32.

364. Gu Z, Fletcher RS, Arts EJ, Wainberg MA, Parniak MA: **The K65R mutant reverse transcriptase of HIV-1 cross-resistant to 2', 3'-dideoxycytidine, 2',3'-dideoxy-3'-thiacytidine, and 2',3'-dideoxyinosine shows reduced sensitivity to specific dideoxynucleoside triphosphate inhibitors in vitro.** *J. Biol. Chem.* 1994, **269:**28118-28122.

365. Boyer PL, Clark PK, Hughes SH: **HIV-1 and HIV-2 reverse transcriptases: different mechanisms of resistance to nucleoside reverse transcriptase inhibitors.** *J. Virol.* 2012, **86:**5885-5894.

366. Xu HT, Quan Y, Schader SM, Oliveira M, Bar-Magen T, Wainberg MA: **The M230L nonnucleoside reverse transcriptase inhibitor resistance mutation in HIV-1 reverse transcriptase impairs enzymatic function and viral replicative capacity.** *Antimicrobial agents and chemotherapy* 2010, **54:**2401-2408.

367. De Clercq E: **Anti-HIV drugs: 25 compounds approved within 25 years after the discovery of HIV.** *Int. J. Antimicrob. Agents* 2009, **33:**307-320.

368. Kirby KA, Michailidis E, Fetterly TL, Steinbach MA, Singh K, Marchand B, Leslie MD, Hagedorn AN, Kodama EN, Marquez VE, et al: **Effects of substitutions at the 4' and 2**

positions on the bioactivity of 4'-ethynyl-2-fluoro-2'-deoxyadenosine. *Antimicrobial agents and chemotherapy* 2013, **57:**6254-6264.

369.   Michailidis E, Huber AD, Ryan EM, Ong YT, Leslie MD, Matzek KB, Singh K, Marchand B, Hagedorn AN, Kirby KA, et al: **4'-Ethynyl-2-fluoro-2'-deoxyadenosine (EFdA) inhibits HIV-1 reverse transcriptase with multiple mechanisms.** *J. Biol. Chem.* 2014, **289:**24533-24548.

370.   Stoddart CA, Galkina SA, Joshi P, Kosikova G, Moreno ME, Rivera JM, Sloan B, Reeve AB, Sarafianos SG, Murphey-Corb M, Parniak MA: **Oral administration of the nucleoside EFdA (4'-ethynyl-2-fluoro-2'-deoxyadenosine) provides rapid suppression of HIV viremia in humanized mice and favorable pharmacokinetic properties in mice and the rhesus macaque.** *Antimicrobial agents and chemotherapy* 2015, **59:**4190-4198.

371.   Michailidis E, Marchand B, Kodama EN, Singh K, Matsuoka M, Kirby KA, Ryan EM, Sawani AM, Nagy E, Ashida N, et al: **Mechanism of inhibition of HIV-1 reverse transcriptase by 4'-Ethynyl-2-fluoro-2'-deoxyadenosine triphosphate, a translocation-defective reverse transcriptase inhibitor.** *J. Biol. Chem.* 2009, **284:**35681-35691.

372.   Sevilya Z, Loya S, Hughes SH, Hizi A: **The ribonuclease H activity of the reverse transcriptases of human immunodeficiency viruses type 1 and type 2 is affected by the thumb subdomain of the small protein subunits.** *J. Mol. Biol.* 2001, **311:**957-971.

373.   Post K, Guo J, Howard KJ, Powell MD, Miller JT, Hizi A, Le Grice SF, Levin JG: **Human immunodeficiency virus type 2 reverse transcriptase activity in model systems that mimic steps in reverse transcription.** *J. Virol.* 2003, **77:**7623-7634.

374.   MacNeil A, Sarr AD, Sankale JL, Meloni ST, Mboup S, Kanki P: **Direct evidence of lower viral replication rates in vivo in human immunodeficiency virus type 2 (HIV-2) infection than in HIV-1 infection.** *J. Virol.* 2007, **81:**5325-5330.

375.   Reid P, MacInnes H, Cong ME, Heneine W, Garcia-Lerma JG: **Natural resistance of human immunodeficiency virus type 2 to zidovudine.** *Virology* 2005, **336:**251-264.

376.   Witvrouw M, Pannecouque C, Switzer WM, Folks TM, De Clercq E, Heneine W: **Susceptibility of HIV-2, SIV and SHIV to various anti-HIV-1 compounds: implications for treatment and postexposure prophylaxis.** *Antivir. Ther.* 2004, **9:**57-65.

377.   Sarafianos SG, Das K, Hughes SH, Arnold E: **Taking aim at a moving target: designing drugs to inhibit drug-resistant HIV-1 reverse transcriptases.** *Curr. Opin. Struct. Biol.* 2004, **14:**716-730.

378.   Arion D, Kaushik N, McCormick S, Borkow G, Parniak MA: **Phenotypic mechanism of HIV-1 resistance to 3'-azido-3'-deoxythymidine (AZT): increased polymerization processivity and enhanced sensitivity to pyrophosphate of the mutant viral reverse transcriptase.** *Biochemistry* 1998, **37:**15908-15917.

379.   Tambuyzer L, Azijn H, Rimsky LT, Vingerhoets J, Lecocq P, Kraus G, Picchio G, de Bethune MP: **Compilation and prevalence of mutations associated with resistance to non-nucleoside reverse transcriptase inhibitors.** *Antivir Ther* 2009, **14:**103-109.

380.   De Clercq E: **Non-nucleoside reverse transcriptase inhibitors (NNRTIs): past, present, and future.** *Chem. Biodivers.* 2004, **1:**44-64.

381.   Spence RA, Kati WM, Anderson KS, Johnson KA: **Mechanism of inhibition of HIV-1 reverse transcriptase by nonnucleoside inhibitors.** *Science* 1995, **267:**988-993.

382.   Ghosn J, Chaix ML, Delaugerre C: **HIV-1 resistance to first- and second-generation non-nucleoside reverse transcriptase inhibitors.** *AIDS Rev* 2009, **11:**165-173.

383. Gu Z, Gao Q, Fang H, Salomon H, Parniak MA, Goldberg E, Cameron J, Wainberg MA: **Identification of a mutation at codon 65 in the IKKK motif of reverse transcriptase that encodes human immunodeficiency virus resistance to 2',3'-dideoxycytidine and 2',3'-dideoxy-3'-thiacytidine.** *Antimicrobial agents and chemotherapy* 1994, **38:**275-281.
384. Johnson VA, Calvez V, Gunthard HF, Paredes R, Pillay D, Shafer R, Wensing AM, Richman DD: **2011 update of the drug resistance mutations in HIV-1.** *Top Antivir. Med.* 2011, **19:**156-164.
385. Stone C, Ait-Khaled M, Craig C, Griffin P, Tisdale M: **Human immunodeficiency virus type 1 reverse transcriptase mutation selection during in vitro exposure to tenofovir alone or combined with abacavir or lamivudine.** *Antimicrobial agents and chemotherapy* 2004, **48:**1413-1415.
386. Winters MA, Shafer RW, Jellinger RA, Mamtora G, Gingeras T, Merigan TC: **Human immunodeficiency virus type 1 reverse transcriptase genotype and drug susceptibility changes in infected individuals receiving dideoxyinosine monotherapy for 1 to 2 years.** *Antimicrobial agents and chemotherapy* 1997, **41:**757-762.
387. De Clercq E: **The role of non-nucleoside reverse transcriptase inhibitors (NNRTIs) in the therapy of HIV-1 infection.** *Antiviral Research* 1998, **38:**153-179.
388. Richman DD: **Resistance of clinical isolates of human immunodeficiency virus to antiretroviral agents.** *Antimicrobial agents and chemotherapy* 1993, **37:**1207-1213.
389. Rubsamen-Waigmann H, Huguenel E, Shah A, Paessens A, Ruoff HJ, von Briesen H, Immelmann A, Dietrich U, Wainberg MA: **Resistance mutations selected in vivo under therapy with anti-HIV drug HBY 097 differ from resistance pattern selected in vitro.** *Antiviral Research* 1999, **42:**15-24.
390. Huang P, Farquhar D, Plunkett W: **Selective action of 3'-azido-3'-deoxythymidine 5'-triphosphate on viral reverse transcriptases and human DNA polymerases.** *J. Biol. Chem.* 1990, **265:**11914-11918.
391. Huang H, Chopra R, Verdine GL, Harrison SC: **Structure of a covalently trapped catalytic complex of HIV-1 reverse transcriptase: implications for drug resistance.** *Science* 1998, **282:**1669-1675.
392. Esnouf R, Ren J, Ross C, Jones Y, Stammers D, Stuart D: **Mechanism of inhibition of HIV-1 reverse transcriptase by non-nucleoside inhibitors.** *Nat. Struct. Biol.* 1995, **2:**303-308.
393. Santos LH, Ferreira RS, Caffarena ER: **Computational drug design strategies applied to the modelling of human immunodeficiency virus-1 reverse transcriptase inhibitors.** *Mem. Inst. Oswaldo Cruz.* 2015, **110:**847-864.
394. Eide DJ: **Zinc transporters and the cellular trafficking of zinc.** *Biochim. Biophys. Acta.* 2006, **1763:**711-722.
395. Coleman JE: **Zinc proteins: enzymes, storage proteins, transcription factors, and replication proteins.** *Annu Rev Biochem* 1992, **61:**897-946.
396. Dubben S, Honscheid A, Winkler K, Rink L, Haase H: **Cellular zinc homeostasis is a regulator in monocyte differentiation of HL-60 cells by 1 alpha,25-dihydroxyvitamin D3.** *J. Leukoc. Biol.* 2010, **87:**833-844.
397. Honscheid A, Dubben S, Rink L, Haase H: **Zinc differentially regulates mitogen-activated protein kinases in human T cells.** *J. Nutr. Biochem.* 2011.
398. Tripathi K, Balagam R, Vishnoi NK, Dixit NM: **Stochastic simulations suggest that HIV-1 survives close to its error threshold.** *PLoS Computational Biology* 2012, **8:**e1002684.

399. Dapp MJ, Holtz CM, Mansky LM: **Concomitant lethal mutagenesis of human immunodeficiency virus type 1.** *Journal of Molecular Biology* 2012, **419:**158-170.

400. Summers J, Litwin S: **Examining the theory of error catastrophe.** *J. Virol.* 2006, **80:**20-26.

401. Smith RA, Loeb LA, Preston BD: **Lethal mutagenesis of HIV.** *Virus Research* 2005, **107:**215-228.

402. Anderson JP, Daifuku R, Loeb LA: **Viral error catastrophe by mutagenic nucleosides.** *Annual Review of Microbiology* 2004, **58:**183-205.

403. Clementi M: **Can modulation of viral fitness represent a target for anti-HIV-1 strategies?** *The new microbiologica* 2004, **27:**207-214.

404. Graci JD, Cameron CE: **Challenges for the development of ribonucleoside analogues as inducers of error catastrophe.** *Antiviral Chemistry & Chemotherapy* 2004, **15:**1-13.

405. Eigen M: **Error catastrophe and antiviral strategy.** *Proceedings of the National Academy of Sciences of the United States of America* 2002, **99:**13374-13376.

406. Graci JD, Cameron CE: **Quasispecies, error catastrophe, and the antiviral activity of ribavirin.** *Virology* 2002, **298:**175-180.

407. Domingo E, Mas A, Yuste E, Pariente N, Sierra S, Gutierrez-Riva M, Menendez-Arias L: **Virus population dynamics, fitness variations and the control of viral disease: an update.** *Progress in drug research Fortschritte der Arzneimittelforschung Progres des recherches pharmaceutiques* 2001, **57:**77-115.

408. Crotty S, Cameron CE, Andino R: **RNA virus error catastrophe: direct molecular test by using ribavirin.** *Proc. Natl. Acad. Sci. U. S. A.* 2001, **98:**6895-6900.

409. Rawson JM, Heineman RH, Beach LB, Martin JL, S1chnettler EK, Dapp MJ, Patterson SE, Mansky LM: **5,6-Dihydro-5-aza-2'-deoxycytidine potentiates the anti-HIV-1 activity of ribonucleotide reductase inhibitors.** *Bioorganic & medicinal chemistry* 2013, **21:**7222-7228.

410. Dapp MJ, Patterson SE, Mansky LM: **Back to the future: revisiting HIV-1 lethal mutagenesis.** *Trends in Microbiology* 2013, **21:**56-62.

411. Esposito F, Corona A, Tramontano E: **HIV-1 Reverse Transcriptase Still Remains a New Drug Target: Structure, Function, Classical Inhibitors, and New Inhibitors with Innovative Mechanisms of Actions.** *Molecular Biology International* 2012, **2012:**586401.

412. Clementi M: **Perspectives and opportunities for novel antiviral treatments targeting virus fitness.** *Clinical microbiology and infection : the official publication of the European Society of Clinical Microbiology and Infectious Diseases* 2008, **14:**629-631.

413. Loeb LA, Mullins JI: **Lethal mutagenesis of HIV by mutagenic ribonucleoside analogs.** *AIDS Research and Human Retroviruses* 2000, **16:**1-3.

414. Touyz RM, Yao G: **Modulation of vascular smooth muscle cell growth by magnesium-role of mitogen-activated protein kinases.** *Journal of cellular physiology* 2003, **197:**326-335.

415. Abram ME, Ferris AL, Das K, Quinones O, Shao W, Tuske S, Alvord WG, Arnold E, Hughes SH: **Mutations in HIV-1 RT Affect the Errors Made in a Single Cycle of Viral Replication.** *Journal of Virology* 2014.

416. Mattapallil JJ, Douek DC, Hill B, Nishimura Y, Martin M, Roederer M: **Massive infection and loss of memory CD4+ T cells in multiple tissues during acute SIV infection.** *Nature* 2005, **434:**1093-1097.

417. Castellino F, Huang AY, Altan-Bonnet G, Stoll S, Scheinecker C, Germain RN: **Chemokines enhance immunity by guiding naive CD8+ T cells to sites of CD4+ T cell-dendritic cell interaction.** *Nature* 2006, **440:**890-895.

418. Williams MA, Tyznik AJ, Bevan MJ: **Interleukin-2 signals during priming are required for secondary expansion of CD8+ memory T cells.** *Nature* 2006, **441:**890-893.

419. Bachmann MF, Wolint P, Walton S, Schwarz K, Oxenius A: **Differential role of IL-2R signaling for CD8+ T cell responses in acute and chronic viral infections.** *Eur. J. Immunol.* 2007, **37:**1502-1512.

420. Williams MA, Holmes BJ, Sun JC, Bevan MJ: **Developing and maintaining protective CD8+ memory T cells.** *Immunol. Rev.* 2006, **211:**146-153.

421. Boni C, Fisicaro P, Valdatta C, Amadei B, Di Vincenzo P, Giuberti T, Laccabue D, Zerbini A, Cavalli A, Missale G, et al: **Characterization of hepatitis B virus (HBV)-specific T-cell dysfunction in chronic HBV infection.** *J. Virol.* 2007, **81:**4215-4225.

422. Brooks DG, McGavern DB, Oldstone MB: **Reprogramming of antiviral T cells prevents inactivation and restores T cell activity during persistent viral infection.** *J. Clin. Invest.* 2006, **116:**1675-1685.

423. Bevan MJ: **Helping the CD8(+) T-cell response.** *Nat. Rev. Immunol.* 2004, **4:**595-602.

424. Zhou X, Ramachandran S, Mann M, Popkin DL: **Role of lymphocytic choriomeningitis virus (LCMV) in understanding viral immunology: past, present and future.** *Viruses* 2012, **4:**2650-2669.

425. Welsh RM, Seedhom MO: **Lymphocytic choriomeningitis virus (LCMV): propagation, quantitation, and storage.** *Curr. Protoc. Microbiol.* 2008, **Chapter 15:**Unit 15A 11.